Evaluation of Lanthanum/Iron Oxide Amended Formable Biochar for Phosphorous and Nitrogen Removal in Wastewater: Preparation, Mechanism, and Application

by

Enhui Sun

Submitted in fulfilment of the academic requirements of

Doctor of Ecological Science

In the School of Life Sciences

College of Agriculture, Engineering and Science

University of KwaZulu-Natal

Pietermaritzburg

South Africa

December 2022

PREFACE

The research contained in this thesis was completed by the candidate while registered in the School of Life Science, College of Agriculture, Engineering and Science, University of KwaZulu-Natal, Pietermaritzburg campus, South Africa, from January 2019 to December 2022, under the supervision of Dr Charles Hunter and Co-supervision of Prof. Linzhang Yang. The research was financially supported by L. Z. Yang through the Special Fund for Agro-scientific Research in the Public Interest (2100012); Y. F. Feng through the National Natural Science Foundation of China (41877090), and the National Key Research and Development Program of China (2021YFD1700805); E. H. Sun through the National Natural Science Foundation of China (41807132) and the National Key Technology R & D Program of China (2018YFC1903204-02); H. Y. Huang through the Jiangsu Province Agricultural Independent Innovation Fund (CX(19)2003); Q. B. Xiao through the National Natural Science Foundation of China (22078136).

The contents of this work have not been submitted in any form to another university and, except where the work of others is acknowledged in the text, the results reported are due to investigations by the candidate.

As the candidate's supervisors, we have approved this thesis for submission.

Dr C Hunter

Signed: Dr Charles Hunter (Supervisor)

Date: Nov. 20, 2022

Signed: Prof. Lingzhang Yang (Co-Supervisor)

Date: Nov. 20, 2022

DECLARATION 1: PLAGIARISM

I, Enhui Sun, declare that:

(i) the research reported in this thesis, except where otherwise indicated or acknowledged, is my original work;

(ii) this thesis has not been submitted in full or in part for any degree or examination to any other university;

(iii) this thesis does not contain other persons' data, pictures, graphs, or other information unless specifically acknowledged as being sourced from other persons;

(iv) this thesis does not contain other persons' writing, unless specifically acknowledged as being sourced from other researchers. Where other written sources have been quoted, then:

a) their words have been re-written but the general information attributed to them has been referenced;

b) where their exact words have been used, their writing has been placed inside quotation marks and referenced.

(v) where I have used material for which publications followed, I have indicated in detail my role in the work;

(vi) this thesis is primarily a collection of material, prepared by myself, published as journal articles or presented as a poster and oral presentations at conferences. In some cases, additional material has been included;

(vii) this thesis does not contain text, graphics or tables copied and pasted from the Internet, unless specifically acknowledged, and the source being detailed in the thesis and in the References sections.

Signed: Enhui Sun

Date: Nov. 20, 2022

DECLARATION 2: PUBLICATIONS, PATENT AND CONFERENCES

In each of the listed publications I, **Enhui Sun** was the principal investigator and author of each paper, patent, and conference. The [*] indicates the corresponding author.

✚ **Publication/Under Review**

1. <u>***Sun EH***</u>[*], Zhang YY, Xiao QB, Li HY, Qu P, Yong C, Wang BY, Feng YF[*], Huang HY, Yang LZ, Hunter C, 2022. Formable porous biochar loaded with La-Fe(hydr)oxides/montmorillonite for efficient removal of phosphorus in wastewater: Process and mechanisms. ***Biochar***, **4: 53. Published (Q1, IF = 11.452),** <u>**CHAPTER 3**</u>.

   Author's contributions: ES: Conceptualization, Methodology, Data management, Writing – original draft. YZ: Methodology, Data curation, Review & editing. QX: Investigation, and Funding acquisition. HL: Review. PQ: Methodology, Data curation. CY: Methodology and Data curation. BW: Review & editing, mathematical model validation. YF: Methodology, Validation, Data curation, Review & editing, Funding acquisition. HH: Validation, Review & editing. CH and LY: Supervision and Co-supervision, Formal analysis, Validation, Data curation, Review & editing, and Resources.

2. <u>***Sun EH***</u>, Peng K, He L, Yong C, Feng YF[*], Huang HY[*], Hunter C, Yang LZ, Wang HL, **2022**. A scientometric analysis review of progress and emerging trends in biochar application for wastewater remediation. ***Critical Reviews in Environmental Science and Technology***. **Submitted,** <u>**CHAPTER 2**</u>.

   Author's contributions: ES: Conceptualization, Formal analysis, Investigation, Writing – original draft, Writing – review & editing, Project administration, Funding acquisition. KP: Investigation, Data collection. LH and CY: Investigation, Data check, and Formal analysis. YF: Conceptualization, Formal analysis, Investigation. HH: Project administration, Validation, Funding acquisition. CH and LY: Conceptualization, Supervision and Co-Supervision, Review & editing. HW: Validation, Review & editing.

3. <u>***Sun EH***</u>, Sun SJ, Zhang J, Yong C, Huang HY[*], Hunter C[*], Yang LZ. Immobilization of p-accumulating bacteria on formed-biochar supported lanthanum-iron oxide nanoparticles: Synergistic removal of phosphorus. ***Colloids and Surfaces A: Physicochemical and Engineering Aspects***. **Submitted,** <u>**CHAPTER 4**</u>.

Authorship contribution statement: SE: Project administration, Conceptualization, Writing-original draft, Writing-review & editing, Funding acquisition, Methodology, Resources. SE and SS: Designed and Conducted the Experiments. ZJ and YC: Review & Editing. HH: Project administration, Conceptualization, Funding acquisition. HC and YL: Conceptualization, Supervision, Co-supervision, Methodology.

➕ Patent

1. ***Sun EH***, Cheng L, Huang HY, Zhang J, Qu P, Yong C, Xu YD. Preparation method and application of porous biochar enhanced microbial membrane carrier material. ***China Patent***, Application date: 07/31/2020 (**Authorized No. ZL 202010761279.0**).

2. ***Sun EH***, Huang HY, Qu P, Yong C, Zeng FM, Xu YD. Preparation and application of lanthanum and iron oxide modified straw porous biochar. ***China Patent***, Application date: 04/03/2021 (**Authorized No. ZL 202010258645.0**).

3. ***Sun EH***, Zeng FM, Huang HY, Qu P, Yong C, Xu YD. Fe/silicate modified porous carbon and application thereof in wastewater pollutant adsorption. ***China Patent***, Application date: 16/04/2021 (**Applied No. CN202110410095.4**).

4. ***Sun EH***, Huang HY, Jin HM, Wu GF, Chang ZZ, Ye XM, Xu YD, Yong C. Preparation method for combined modified straw active particulate carbon adsorption material and use of same. PCT, ***USA Patent***, Publication Date: 24/09/2020 (**Authorized No. 16/621,621**).

5. Jin HM, Zhu N, Xi YL, ***Sun EH***, Du J, Huang HY, Ye XM, Zheng MJ, Li DY. Malic acid and $KMnO_4$ -based composite and modified cow dung biogas residue hydrochar preparation method. PCT, ***USA Patent***, Publication Date: 02/12/2021 (**Applied No. US 11,235,305 B2, authorized**).

➕ Conference Presentations or Posters

1. ***Sun EH***. BIO Africa Convention 2022, Durban, August 27 - 31, 2022, Registration ID 2884031. https://app.glueup.com/event/bio-africa-convention-2022-59267/.

2. ***Sun EH***, Zeng FM. First Session of Biology International Symposium on Carbon Research and Applications, Shenyang Agricultural University, Shenyang, Poster, 2019/09/20~2019/09/23.

3. **_Sun EH_**. Third iron Environmental Chemistry and Pollution Control Technical Seminar, College of Environment, Zhejiang Gongshang University, Hangzhou, 2020/10/09~2020/10/11.
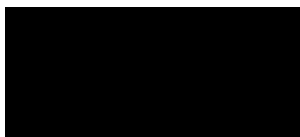
Signed: Enhui Sun

Date: Nov. 29, 2022

ABSTRACT

Globally, phosphorus (P) and nitrogen (N) pollution levels are a major challenge, resulting in an urgent need for N and P emission reduction and remediation. High concentrations of N and P nutrient salts flow into farmland ditches via rainwater run-off, migrating into downstream waterbodies and driving eutrophication in aquatic environments. Therefore, methods are required to remove N and P during the treatment of wastewater to reduce their impact on receiving water bodies. Formable methods can significantly increase the size of biochar to a granular scale, which improves its hydraulic properties, and enhances its amenability for separation, recovery, and reuse. A novel formable porous particle biochar adsorbent (LaFe/MB) with high efficiency for phosphorus removal from wastewater was prepared by in-situ impregnation and granulation of lanthanum/ferric oxide (hydroxide) on the surface of biochar/nano-montmorillonite. The aims of the study were to 1) characterize the LaFe/MB biochar composite material and determine the mechanisms associated with P adsorption, for providing a novel and more comprehensive perspective of the phosphorus removal process; 2) explore the synergistic phosphorus removal effect of microorganisms immobilized on the novel biochar; and, 3) evaluate the ability of this novel biochar to treat high nitrogen and phosphorus concentration wastewater and determine the impact on associated microbiota. The major results of the study are summarised as follows:

The development of biochar-based granule-like adsorbents suitable for scaled-up applications has been attracting increasing attention in the field of water treatment. Herein, a new formable porous granulated biochar loaded with La-Fe(hydr)oxides/montmorillonite (LaFe/MB) was fabricated via a granulation and pyrolysis process for enhanced phosphorus (P) removal from wastewater. Montmorillonite acted as a binder that increased the size of the granulated biochar, while the use of Fe promoted the surface charge and facilitated the dispersion of La, which was responsible for selective phosphate removal. LaFe/MB exhibited rapid phosphate adsorption kinetics and high maximum adsorption capacity (Langmuir model, 52.12 mg P/g), which are better than that of many existing granulated materials. The desorption and recyclability experiments showed that LaFe/MB could be regenerated, and maintained 76.7% of its initial phosphate adsorption capacity after four adsorption cycles. The high hydraulic endurance strength retention rate of the developed material (91.6%) suggested high practical applicability in actual wastewater. Electrostatic attraction, surface precipitation, and

inner-sphere complexation via ligand exchange were found to be involved in selective P removal over a wide pH range of 3 to 9. The thermodynamic parameters were determined, which revealed the feasibility and spontaneity of adsorption. Based on approximate site energy distribution analyses, high distribution frequency contributed to efficient P removal. The research results provide new insight that LaFe/MB shows great application prospects for advanced phosphate removal from wastewater.

A stable, high-efficiency phosphorus removal system was established using a phosphorus accumulating bacteria (PAB) consortium in conjunction with formable-biochar-supported lanthanum-iron oxide nanoparticles (FBO) to form a colonized Bio-FBO composite. A preliminary colonization study demonstrated that a 1:10 dilution of PAB inoculum resulted in the highest level of biofilm development on FBO nanoparticles. PAB was immobilized on the external and internal surfaces of FBO via physical adsorption. Abundant oxygen-containing functional groups on the surface of FBO facilitate the attachment of microorganisms. P uptake by Bio-FBO reached ca. 100% after 60 h when an initial P concentration of 10 mg P/L was used. Adsorption kinetics data demonstrated that P removal from wastewater using Bio-FBO fitted well with the Pseudo-second order kinetic model. Microbial analysis showed that *Acinetobacter* was the most dominant group in the bio-system, and were considered important contributors to phosphorous removal. The above results demonstrated that the effective removal of phosphorus in this process was due to the synergistic effect of FBO and PAB. Hence, the excellent porosity, active groups, and microbial attachment of Bio-FBO carbon-based bio-sorbents made it a potential candidate for phosphorus removal, especially in phosphorus-rich wastewater treatment.

Ammonia volatilization is the main N-loss pathway that occurs during urine storage and transportation. The impact of using functionalized formed-biochar (BMt) in conjunction with urease inhibitor (NBPT) on nitrogen loss, nutrient transformation, and bacterial community composition during urine storage was investigated. Results showed that BMt can limit the conversion of total nitrogen to ammonia during the early stages of storage and was also able to immobilize ammonium ions from solution by adsorption. The addition of 2 g/L BMt to urine samples reduced gaseous NH_3 emission by 40.7%. Further, when urease inhibitor-mediated porous formed-biochar doped metal oxide (0.1% w/w) was used, the conversion of urea to ammonia nitrogen was significantly inhibited, with an 89.7% reduction of NH_3 emission being

achieved. The BMt_NBPT treatment was also found to reduce the level of phosphorous precipitation. Additionally, alpha analysis of 16s rRNA gene sequence data from each treatment revealed that the BMt and BMT_NBPT treatments both supported greater levels of microbial diversity compared to the untreated control. The relative abundance of taxonomic groups associated with pathogenic traits were reduced compared to the unamended control. The current study demonstrates that a BMt_NBPT treatment of urine has the potential as a novel alternative to the traditional acidification method used to inhibit urea hydrolysis.

In summary, the formable porous particle biochar adsorbent can effectively adsorb inorganic N and P in wastewater. This novel biochar composite offers new approaches to removing and recycling environmental pollutants from wastewater and is of great significance for practical engineering applications. Based on the results, the environmental effect, cost analysis, renewability, and life cycle of this new type of formable porous granulated biochar material in real wastewater will be evaluated in future studies.

ACKNOWLEDGMENTS

TABLE OF CONTENTS

LIST OF TABLES

LIST OF FIGURES

LIST OF IMPORTANT ABBREVIATIONS

- ACB — Activated Carbon Biochar
- ARGs — Antibiotic Resistance Genes
- B — Biochar
- Bio-FBO — Immobilization of PAB on FBO
- BMt — Functionalized Formed-Biochar
- CWs — Constructed Wetlands
- ECs — Emerging Contaminants
- EDS — Energy Dispersive X-ray Spectroscopy
- EWFD — European Water Framework Directive
- FBO — Formed-Biochar/Nanoscale Lanthanum-Iron Oxide Composite
- Fe — Iron
- FTIR — Fourier Transform Infrared Spectroscopy
- GES — Good Ecological Status
- HMs — Heavy Metals
- HTC — Hydrothermal Carbonization
- La — Lanthanum
- LaFe/MB — Formable Porous Granulated Biochar Loaded with La-Fe(hydr)oxides/Montmorillonite
- LCA — Life Cycle Assessment
- MB — Biochar/Montmorillonite
- MPs — Microplastics
- MSFD — Marine Strategy Framework Directive
- N — Nitrogen
- NBPT — N-(n-butyl) Thiophosphoric Triamide
- NEA — North-East Atlantic
- P — Phosphorus
- PAB — Phosphorus Accumulating Bacteria
- PAHs — Polycyclic aromatic Hydrocarbons
- PFRs — Persistent Free Radicals
- PHB — Poly-β-hydroxybutyrate
- ROS — Reactive Oxygen Species

- ❏ SDG — Sustainable Development Goals
- ❏ SED — Site Energy Distribution
- ❏ SEM — Scanning Electron Microscopy
- ❏ SSA — Specific Surface Area
- ❏ WoS — Web of Science
- ❏ XPS — X-Ray Photoelectron Spectroscopy
- ❏ XRD — X-Ray Diffraction
- ❏ ΔS^0 — Entropy Change
- ❏ ΔH^0 — Free Enthalpy Change
- ❏ ΔG^0 — Energy Change

CHAPTER *1*

INTRODUCTION

CHAPTER 1: INTRODUCTION

1.1 Background overview

With growing global populations and expanding agricultural-based economies, more and more nutritive elements are being discharged into closed or semi-closed water bodies such as lakes and reservoirs, raising concerns of their negative impact on water quality (Venkatesan et al., 2018). The eutrophication of water leads to the rapid proliferation of algae, a reduction of dissolved oxygen in water, and even the production of H_2S in anaerobic environments, which aggravates the deterioration of water quality (Hein, 2006). Many studies have shown that nitrogen (N) and phosphorus (P) are the main causes of eutrophication in water bodies (Dai et al., 2020; Menesguen et al., 2018). It is generally believed that freshwater ecosystems are primarily P limited, while marine ecosystems are primarily N limited and when inorganic nitrogen exceeds 3.0 mg/L and total phosphorus exceeds 0.02 mg/L in natural water bodies, eutrophication can occur. (Paerl et al., 2016).

Phosphorus exists in natural water in the form of orthophosphate and polymeric phosphate, most of which comes from industrial and agricultural wastewater and domestic sewage. There are dissolved, suspended, and colloidal forms of phosphorus in water, there are orthophosphate, polymeric phosphate, and organophosphate (Chu et al., 2018). There is less organic phosphorus in the water than other forms. Through biochemical action, polymerized phosphate and organic phosphorus can be converted into orthophosphate (Jin et al., 2019; Santiviago Petzoldt et al., 2020).

Both future conservation and management of phosphorus (P) load to the environment require an understanding of the biogeochemical cycle of P, which requires analytical techniques for the precise speciation and measurement of P and its various forms and species (Venkatesan et al., 2018). The prevalence of different forms or species of phosphorus depends on the source of wastewater (Xie et al., 2021). Natural and biological oxidation processes usually convert complex phosphorus in water to orthophosphate. More than 90% of phosphorus in conventional secondary biological treatment water is orthophosphate. Therefore, orthophosphate is the main removal object in the field of sewage treatment. Phosphorus ion morphology is affected by the pH value of the medium (Fig. 1.1), which mainly includes the following four types H_3PO_4,

$H_2PO_4^-$, HPO_4^{2-} and PO_4^{3-}. Orthophosphate is a triprotic acid with dissociation constants of $pK_1=2.12$, $pK_2=7.21$, and $pK_3=12.31$, that correspond to H_3PO_4, $H_2PO_4^-$ and HPO_4^{2-} respectively (Mi et al., 2022). The dissociation constants can be used to calculate the function of pH value on phosphate species and the function diagram of a mass fraction on pH value. It mainly exists in the form of H_3PO_4 and $H_2PO_4^-$ under acidic, $H_2PO_4^-$ and HPO_4^{2-} under neutral, and HPO_4^{2-}, and PO_4^{3-} under alkaline conditions (Koh et al., 2020). Therefore, the pH environment of sewage has an important influence on phosphorus removal by adsorption.
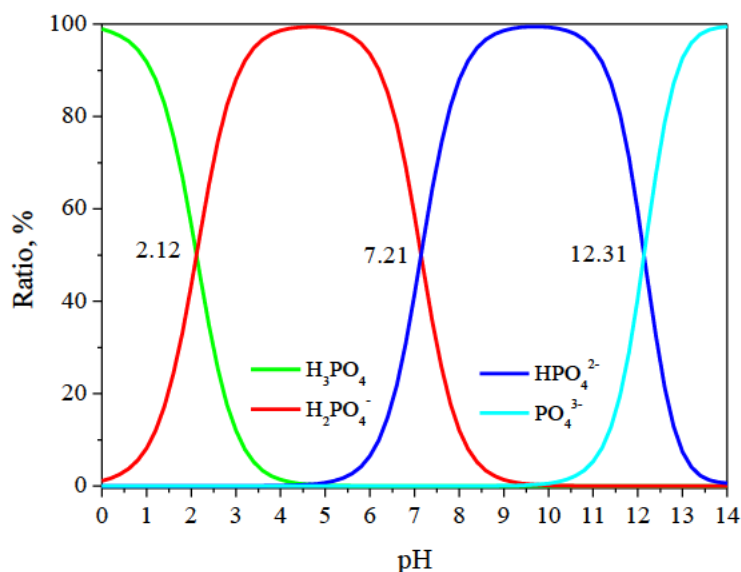
Figure 1.1 Distribution of phosphate species at different pH values.

Since 1950, an increase in nitrogen (N) and P river loadings in the North-East Atlantic (NEA) continental seas has induced a deep change in the marine coastal ecosystems, leading to eutrophication symptoms in some areas. To recover a Good Ecological Status (GES) in the NEA, as required by European Water Framework Directive (EWFD) and Marine Strategy Framework Directive (MSFD), reductions in N- and P-river loadings are necessary (Menesguen et al., 2018).

Industrial and agricultural activities have caused a serious imbalance in the phosphorus cycle, resulting in eutrophication pollution which has become a major environmental problem all over the world (Menesguen et al., 2018). Phosphorus is an essential element for life composition and one of the main factors leading to the eutrophication of water bodies. Recent surveys indicate that 37.6% of China's lakes are in a eutrophication state (Fig. 1.2 and Fig. 1.3) (Beijing: Ministry of Ecology and Environment, 2020). Monitoring results of centralized

drinking water sources, groundwater, inland fishery waters, and maritime areas under the jurisdiction of prefecture-level and above cities in China have shown that the total phosphorus or active phosphate index exceeded the standard in these water sources (Beijing: Ministry of Ecology and Environment, 2020).
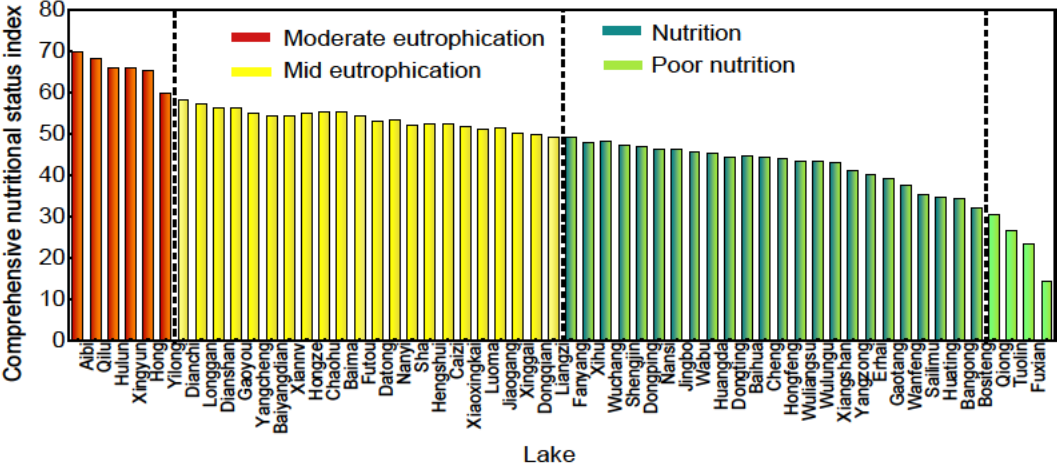
Figure 1.2 Comparison of eutrophication status of major lakes in 2019.
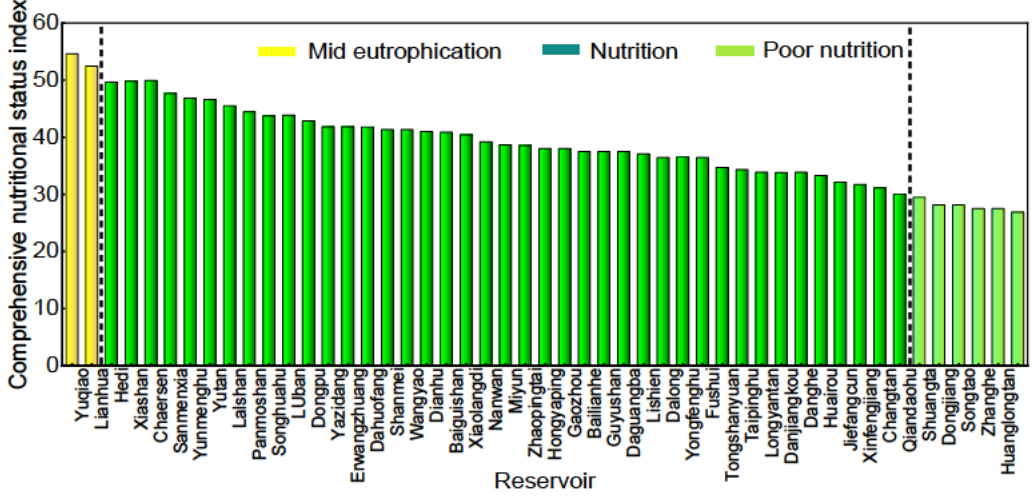
Figure 1.3 Comparison of nutrient status of major reservoirs in 2019.

According to the investigation and analysis of the main eutrophic lakes in China, the main source of phosphorus pollution is domestic wastewater, accounting for 61.6% of the total input of phosphorus, and human phosphorus emission accounts for 54.3% of the total input. The data show that the average annual phosphorus output in China is about 0.5 kg per person, and the average annual phosphorus output of washing powder is about 0.175 kg per person. The second is agricultural non-point source pollution, of which 20.5% is from livestock and poultry

breeding and aquaculture, and 16.51% is from surface runoff. The application of inorganic fertilizers and chemical pesticides are the main reasons for the source of surface runoff phosphorus (Deng, 2015).

Nitrogen compounds in water can be divided into inorganic (e.g. ammonium, ammonia nitrogen, nitrite nitrogen, and nitrate nitrogen) and organic nitrogen (e.g. urea, amino acids, proteins, etc.) (Sharma et al., 2022). Under biochemical action ammonia nitrogen, nitrite and nitrate nitrogen can constitute a cycle of mutual conversion. Among them, ammonia nitrogen belongs to the transition state in the nitrogen cycle, which accounts for the most serious harm to water quality (Ding et al. 2022). Although urine only accounts for 1% of sewage, it has a complex composition, high nutrient, and organic content, and is the main contributor of N and P in sewage. It is also a potential recyclable resource. It has become a research hotspot to realize the separate collection and resource utilization of urine wastewater from the source (Lienert et al., 2010; Maurer et al., 2006). The key point is that urine wastewater is prone to the transformation of nitrogen into unstable states and ammonia volatilization in the storage process, which not only causes the waste of nutrient resources but also further aggravates the eutrophication of water if incorrectly processed.

As is well known, the discharge of phosphorus and nitrogen-laden wastewater not only results in the loss of non-renewable P and N resources but also causes the eutrophication of natural water sources (Nageshwari and Balasubramanian, 2022), which has become a serious environmental problem worldwide (Dai et al., 2020). Thus, recovering P and N from wastewater for reuse as fertilizer in agriculture provides a "double benefit", i.e., recycling the non-renewable phosphorus resource from wastewater and protecting closed water bodies such as lakes, ponds, and reservoirs from eutrophication by reducing the input of phosphorus (Jiao et al., 2021).

Biochar is made from different feedstocks, including wood, crop waste residues and various other forms of organic materials and is produced through thermal cracking in the absence of oxygen (Amalina et al., 2022). The process is simple, and biochar is considered to be a stable, highly aromatic product, which is rich in carbon (Xie et al., 2022). In recent years, biochar has become a research hotspot in environmental science due to its excellent surface properties and ecological effect (Jiao et al., 2021). Due to its outstanding surface porosity, relatively large

specific surface area, and surface energy, as well as typical structural features such as carboxyl, phenolic hydroxyl, hydroxyl, and aliphatic double bond functional groups, biochar has a very strong adsorption capacity. It has been widely used in removing phosphorus pollutants from wastewater (Ahmad et al., 2014). Since the successful usage of biochar, screening and preparation of adsorbents has been a prominent research area in environmental science. However, biochar research has mainly focused on surface activation, including physical, chemical, and biological activation. Unfortunately, traditional biochar is very difficult to recycle because of powder features, and easy runoff into the downstream waters (Ahmad et al., 2014). Novel functional adsorbents urgently need to be generated. The phosphorus reduction mechanism of functional adsorbent is not clear, but it is currently considered that removing phosphorus in farmland ecological ditch is pivotal and firstly required for improving surface charge, reactive group, and specific surface area of biochar (Kambo and Dutta, 2015; Sadhu et al., 2021; Wang et al., 2018).

Montmorillonite is a silicate mineral with nano-scale sheet structure, unique layered molecular structure, and irregular crystal defects, which makes it have a good adsorption effect on pollutants in water (Viglasova et al., 2018). Although montmorillonite has a net negative charge it contains a large number of metal elements, such as magnesium and calcium, which can form bonds with phosphorus and reduce phosphorus concentrations in water. Further, chemical impregnation of montmorillonite with lanthanum significantly improves anionic phosphate adsorption (Arif et al., 2021). Lanthanide compounds show strong ligand adsorption for phosphate due to their strong Lewis acidity and multi-point coordination ability. The adsorption performance of biochar can be effectively improved by using montmorillonite material as a solid acidic catalyst in biochar due to the huge surface area and high surface activity (Chen et al., 2017). Studies have shown that biochar appeared to be conducive to the enrichment of microorganisms (He et al., 2017). More importantly, its enhanced adsorption properties will be harnessed in this research. We aim to optimize the structure of formable porous biochar loaded with La-Fe(hydr)oxides/montmorillonite and determine its structural characteristics, stability, and its effect/mechanism on phosphorus emission reduction.

At present, studies on the adsorption of pollutants in water with biochar treated by various modification methods are increasing. One reason for choosing biochar is that it is cheap and readily available. Biological pre-treatment technology is a relatively new concept that utilizes

biological processes to improve biomass feedstock for engineered biochar production (Kazemi Shariat Panahi et al., 2020). The biological modification involves fixing microorganisms on the surface of biochar through colonization and biofilm generation. This would lead to improving the desirable properties and the removal ability of pollutants in water via a combined adsorption and biodegradation process (Bouabidi et al., 2018). In the literature, the anaerobic digestion pre-treatment would increase the specific surface area (SSA) of biochar resulting in enhanced adsorption performance (Inyang et al., 2010; Yao et al., 2011). Additionally, Su et al. (2020) found that a high BET-specific surface area to volume ratio in the formable biochar can enhance microbial growth, resulting in higher biofilm mass (14 wt.%) and removal of total suspended solids (68%) (Su et al., 2020). Since most microorganisms are ≥ 1-2 μm in size, they cannot directly enter the micro, meso, and macropores (2~200 nm) that exist in biochar. However, the adsorption of nutrients or pollutants in the micro and mesopores can improve enrichment conditions for microbial colonization on adjacent macropores and intergranular surfaces (Jayakumar et al., 2021). An additional advantage of microbial modification is that functional bacteria could degrade the adsorbate (NH_4^+-N, TP, and COD) adsorbed by the biochar and also achieve biological regeneration of biochar as well (Liao et al., 2022). More importantly, biochar is usually in powder form and, even if it can be biologically regenerated, is easily lost and difficult to recycle. Thus, we highlight the need to correlate biochar properties (especially the dimensions and specifications) to biofilm development, which can eventually determine adsorption efficiency and sustainability.
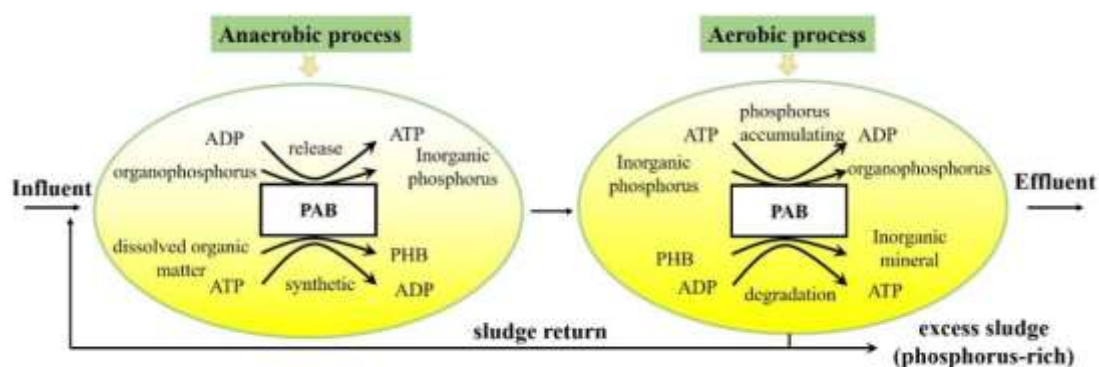
Figure 1.4 Diagram of action mechanism of phosphorus-accumulating bacteria in an anaerobic-aerobic environment.

Phosphorus removal by biological means primarily involves the use of a class of microorganisms known as phosphorus-accumulating bacteria that can sequester more

phosphorus than their physiological needs, from the external environment. Polymerized phosphorus is stored in the bacteria to form a high phosphorus sludge, which can be then removed from the system, to achieve the effect of phosphorus removal from water (Islam et al., 2017). A schematic diagram of the phosphorus removal mechanism of phosphorus-accumulating bacteria is shown in Fig.1.4. The main advantages of biological phosphorus removal are low operating costs and its ability to remove N and P nutrients from water without the use of other chemical reagents (Sales and Lee, 2015).

In this study a novel large porous particle straw biochar (LaFe/MB) was developed by formulating chemical-impregnated treatments of biochar and montmorillonite, with the incorporation of iron and lanthanum salts that serve as active agents to form nanoparticles on the biochar surface. Compared with conventional biochar, the preparation of large-size structural biochar materials not only improves the adsorption capacity but also, more importantly, increases the strength of the biochar, helping to solve the problems such as solid-liquid separation of biochar, difficulty in recovery, reuse, and dust pollution. The main objective of this work is to introduce a simple method to prepare novel formable porous granular biochar composites for environmental water purification applications. The physical and chemical properties of these functional biochar materials were characterized. Meanwhile, the potential application value of functional biochar materials in the water purification field was evaluated by measuring the adsorption characteristics of phosphate in wastewater, which has long been used as a model compound to evaluate the eutrophication of water. The contribution of biofilm formation on granular biochar composites, to the P removal process, was also assessed lastly, the application of using functionalized formed-biochar in conjunction with a urease inhibitor to prevent ammonia volatilization in source-separated urine was also evaluated.

1.2 Hypotheses to be tested

❑ It was hypothesized that the pore structure of LaFe/MB biochar granules changed compared to unmodified biochar. The carbon skeleton after calcining biomass-based can provide enough reaction space for adsorbents, ensure sufficient contact between adsorbents and pollutants, and the surface is rich in a variety of active functional groups.

☐ Activation effect of metal colloidal oxide. Biochar surfaces impregnated with small amounts of iron, calcium, magnesium, and other oxides, activated by lanthanide iron salt, may form a more positively charged metal ionic colloid, which improves its phosphate adsorption characteristics through the complex reaction with phosphate plays a role in the fixation.

☐ Surface charge enrichment. The nano-montmorillonite particles are more evenly dispersed on the inner surface of the carbon skeleton, which is stripped and dispersed into thinner single wafers, which may lead to inter-layer structure changes.

☐ That the surface properties of the LaFe/MB biochar granules are amenable to the immobilization of microorganisms and that these biofilms can enhance the removal of phosphorus and nitrogen from aqueous solutions.

1.3 Aims and objectives

☐ To achieve uniform colloidal oxide distribution on LaFe/MB by vacuum pressure impregnation in order to facilitate directional adsorption of targeted pollutants.

☐ To determine the contribution of phosphorus combination forms to the process of phosphorus adsorption to LaFe/MB and to elucidate the main mechanism of phosphorus removal by LaFe/MB.

☐ To enhance the abundance of PABs by acclimating a consortium of phosphorus accumulating bacteria with sludge, and to detect the distribution of PABs on LaFe/MB surface.

☐ To analyse the phosphorus binding morphology of LaFe/MB during phosphorus adsorption by structural characterization, and determining the phosphorus removal mechanism in reduction of phosphorus in actual nitrogen and phosphorus pollution source water with synergy effects of PABs by adsorption kinetics and thermodynamics.

❑ To reduce the loss of nitrogen and phosphorous resources from high concentration nitrogen and phosphorus sources (i.e. source separated urine) using functionalized formed-biochar in conjunction with a urease inhibitor.

1.4 Key questions to be answered

❑ Does the in-situ formed metal colloidal oxide play a key role in the removal of phosphorus?

❑ Do LaFe/MB biochar granules support biofilm formation of phosphorous accumulating bacteria (PABs) communities and can this association result in enhanced or synergistic phosphorus removal?

❑ What is the influence of LaFe/MB biochar granules on nitrogen and phosphorus resources in high-concentration wastewater (viz., source-separated urine)?

1.5 The innovation of this thesis

According to the previous discussion, the innovations of this study are as follows:

❑ A novel functionalized adsorbent based on porous granulated biochar specifically formulated and modified to promote phosphorus removal was prepared and evaluated.

❑ Furthermore, the use of LaFe/MB not only effectively enhances the relief of P eutrophication, but also realizes the efficient immobilization and recovery of P resources. Meanwhile, in terms of a possible shortage of phosphate ore, immobilizing and recovering the formed-biochar from the wastewater systems can be a promising way to supply secondary sourced phosphorus to the market and thereby promote the blue economy.

❑ Large-size LaFe/MB also facilitates topological loading with microbial biofilms, which may enhance the control effect at high concentrations of nitrogen and phosphorus.

1.6 Outline of thesis structure

This thesis consists of six chapters, which are outlined below. The referencing system used in this thesis is based on the referencing style of the Journal of "Biochar". The thesis is presented in the form of discrete research chapters and each experimental chapter follows the format of a stand-alone research paper. This is the preferred thesis format adopted by the University of KwaZulu-Natal. Thus, there may be some unavoidable repetition of references and introductory information between chapters.

- ❑ Chapter 1 - This introductory chapter summarizes the present situation of phosphorus pollution in wastewater and details the research objectives and hypotheses of the study undertaken.

- ❑ Chapter 2 - This chapter provides a literature review detailing the application of biochar to remove wastewater contaminants. The chapter also includes a scientometric analysis of progress and emerging trends in biochar application for wastewater remediation based on CiteSpace visualization.

- ❑ Chapter 3 - This experimental chapter describes the process and mechanism of formable porous biochar loaded with La-Fe (hydr)oxides/montmorillonite for the efficient removal of phosphorus in wastewater.

- ❑ Chapter 4 - This chapter focuses on the enhanced removal of phosphate by p-accumulating bacteria immobilized on biochar-formed/nanoscale lanthanum-iron oxide composite.

- ❑ Chapter 5 - Chapter five investigates the effects of biochar used in combination with urease inhibitors, on nitrogen conversion and ammonia emission during urine storage with high nitrogen content.

- ❑ Chapter 6 - The final chapter, integrates the work presented, provides conclusions, and discusses the contributions of this biochar research. Future research areas, relevant to the study undertaken are also identified.

References

Ahmad M, Rajapaksha A U, Lim J E, et al. (2014). Biochar as a sorbent for contaminant management in soil and water: a review. Chemosphere 99: 19.

Arif M, Liu G, Yousaf B, et al. (2021). Synthesis, characteristics and mechanistic insight into the clays and clay minerals-biochar surface interactions for contaminants removal-A review. Journal of Cleaner Production 310: 127548.

Bouabidi Z B, El-Naas M H, Zhang Z E, (2018). Immobilization of microbial cells for the biotreatment of wastewater: A review. Environmental Chemistry Letters 17: 241.

Chen L, Chen X L, Zhou C H, et al. (2017). Environmental-friendly montmorillonite-biochar composites: Facile production and tuneable adsorption-release of ammonium and phosphate. Journal of Cleaner Production 156: 648.

Chu Y B, Li M, Liu J W, et al. (2018). Molecular insights into the mechanism and the efficiency-structure relationship of phosphorus removal by coagulation. Water Research 147: 195.

Dai Y J, Wang W S, Lu L, et al. (2020). Utilization of biochar for the removal of nitrogen and phosphorus. Journal of Cleaner Production 257: 120573.

Deng L. Study on removal of chromium(Ⅵ) and phosphate from aqueous solution using Mg-Al hydrotalcite-based composites[D]. Hunan University, 2015.

Ding S, Dan S F, Liu Y, et al. (2022). Importance of ammonia nitrogen potentially released from sediments to the development of eutrophication in a plateau lake. Environmental Pollution 305: 119275.

He S Y, Zhong L H, Duan J J, et al. (2017). Bioremediation of Wastewater by Iron Oxide-Biochar Nanocomposites Loaded with Photosynthetic Bacteria. Front Microbiol 8: 823.

Hein L, (2006). Cost-efficient eutrophication control in a shallow lake ecosystem subject to two steady states. Ecological Economics 59: 429.

Inyang M, Gao B, Pullammanappallil P, et al. (2010). Biochar from anaerobically digested sugarcane bagasse. Bioresour Technol 101: 8868.

Islam M S, Zhang Y, Dong S M, et al. (2017). Dynamics of microbial community structure and nutrient removal from an innovative side-stream enhanced biological phosphorus removal process. Journal of Environmental Management 198: 300.

Jayakumar A, Wurzer C, Soldatou S, et al. (2021). New directions and challenges in engineering biologically-enhanced biochar for biological water treatment. Science of the Total Environment 796: 148977.

Jiao Y X, Li D Y, Wang M, et al. (2021). A scientometric review of biochar preparation research from 2006 to 2019. Biochar 3: 283.

Jin X, Rong N, Zhang W Q, et al. (2019). Bioavailability of organic phosphorus in an eutrophic lake: Insights from an in-situ experiment. Ecological Indicators 107: 105622.

Kambo H S, Dutta A, (2015). A comparative review of biochar and hydrochar in terms of production, physico-chemical properties and applications. Renewable and Sustainable Energy Reviews 45: 359.

Kazemi S P H, Dehhaghi M, Ok Y S, et al. (2020). A comprehensive review of engineered biochar: Production, characteristics, and environmental applications. Journal of Cleaner Production 270: 122462.

Koh K Y, Zhang S, Paul Chen J, (2020). Hydrothermally synthesized lanthanum carbonate nanorod for adsorption of phosphorus: Material synthesis and optimization, and demonstration of excellent performance. Chemical Engineering Journal 380: 122153.

Liao Y, Jiang L, Cao X K, et al. (2022). Efficient removal mechanism and microbial characteristics of tidal flow constructed wetland based on in-situ biochar regeneration (BR-TFCW) for rural grey water. Chemical Engineering Journal 431: 134185.

Maurer M, Pronk W, Larsen T A, (2006). Treatment processes for source-separated urine. Water Research 40: 3151.

Menesguen A, Desmit X, Duliere V, et al. (2018). How to avoid eutrophication in coastal seas? A new approach to derive river-specific combined nitrate and phosphate maximum concentrations. Science of the Total Environment 628-629: 400.

Mi X, Yu F, Zhang H N, et al. (2022). Lanthanum activated palygorskite for selective phosphate separation from aqueous media: Comprehensive understanding of adsorptive behavior and mechanism affected by interfering substances. Chemical Engineering Journal 443, 1: 136423.

Nageshwari K, Balasubramanian P, (2022). Evolution of struvite research and the way forward in resource recovery of phosphates through scientometric analysis. Journal of Cleaner Production 357: 131737.

Paerl H P, Scott J T, McCarthy M J, et al. (2016). It takes two to tango: When and where dual nutrient (N & P) reductions are needed to protect lakes and downstream ecosystems. Environmental Science & Technology 50, 20: 10805-10813.

Sadhu M, Bhattacharya P, Vithanage M, et al. (2021). Adsorptive removal of fluoride using biochar – A potential application in drinking water treatment. Separation and Purification Technology 278: 119106.

Sales C M, Lee P K H, (2015). Resource recovery from wastewater: application of meta-omics to phosphorus and carbon management. Current Opinion in Biotechnology 33: 260.

Santiviago Petzoldt C, Peralta Lezcano J, López Moreda I, (2020). Removal of orthophosphate and dissolved organic phosphorus from synthetic wastewater in a combined struvite precipitation-adsorption system. Journal of Environmental Chemical Engineering 8: 103923.

Sharma V K, Manoli K, Ma X M, (2022). Reactivity of nitrogen species with inorganic and organic compounds in water. Chemosphere 302: 134911.

Su M H, Azwar E, Yang Y F, et al. (2020). Simultaneous removal of toxic ammonia and lettuce cultivation in aquaponic system using microwave pyrolysis biochar. Journal of Hazardous Materials 396: 122610.

Sun E H, Zhang Y, Xiao Q B, et al. (2022). Formable porous biochar loaded with La-Fe(hydr)oxides/montmorillonite for efficient removal of phosphorus in wastewater: process and mechanisms. Biochar 4: 53.

Viglasova E, Galambos M, Dankova Z, et al. (2018). Production, characterization and adsorption studies of bamboo-based biochar/montmorillonite composite for nitrate removal. Waste Management 79: 385.

Venkatesan A K, Gan W H, Ashani H, et al. (2018). Size exclusion chromatography with online ICP-MS enables molecular weight fractionation of dissolved phosphorus species in water samples. Water Research 133: 264.

Wang T F, Zhai Y B, Zhu Y, et al. (2018). A review of the hydrothermal carbonization of biomass waste for hydrochar formation: Process conditions, fundamentals, and physicochemical properties. Renewable and Sustainable Energy Reviews 90: 223.

Xie E, Su Y P, Deng S Q, et al. (2021). Significant influence of phosphorus resources on the growth and alkaline phosphatase activities of Microcystis aeruginosa. Environmental Pollution 268: 115807.

Xie Y Q, Wang L, Li H L, et al. (2022). A critical review on production, modification and utilization of biochar. Journal of Analytical and Applied Pyrolysis 161: 105405.

Yao Y, Gao B, Inyang M, et al. (2011). Biochar derived from anaerobically digested sugar beet tailings: characterization and phosphate removal potential. Bioresource Technology 102: 6273.

Ministry of Ecology and Environment of the People's Republic of China. 2019 China Marine Ecological Environment Bulletin [R]. Beijing: Ministry of Ecology and Environment, 2020.

CHAPTER *2*

A SCIENTOMETRIC ANALYSIS REVIEW OF PROGRESS AND EMERGING TRENDS IN BIOCHAR APPLICATION FOR WASTEWATER REMEDIATION

CHAPTER 2: A SCIENTOMETRIC ANALYSIS REVIEW OF PROGRESS AND EMERGING TRENDS IN BIOCHAR APPLICATION FOR WASTEWATER REMEDIATION

Graphical Abstract
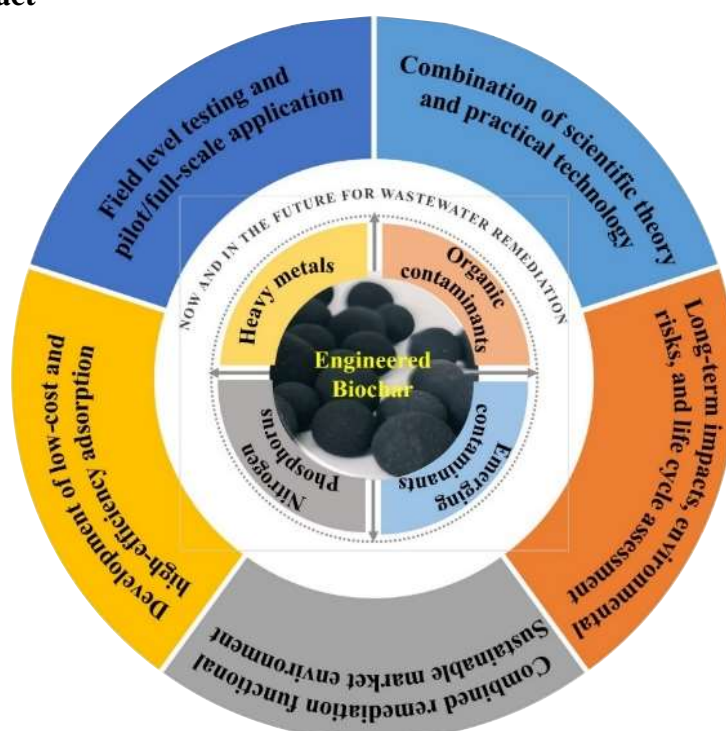
Abstract

The rapid recent development of the application of biochar for the treatment of wastewater contaminants such as heavy metals, organic, inorganic, or emerging pollutants; a scientometric review is required to guide future studies. Here, a bibliometric analysis strategy was applied to mine the key findings of massive published data as a way to assess the existing challenges and research gaps, and bring unique insights for future research prospects. The number of scientific developments associated with biochar applications has accelerated considerably since 2016. Currently, the analysis reveals that multidisciplinary collaborations are now being fostered among researchers worldwide. The research frontier identification revealed the potential for

future promising research in the areas of sewage treatment, efficient removal, regeneration disposal, and functional composite materials. There has been growing interest in studies on the disposal and leaching of toxic substances, stability, long-term effects, life cycle assessment (LCA), and the energy and emission reduction of biochar. Advances in these areas will facilitate the transfer of the technologies from laboratory and pilot scales to the larger scale required for actual engineering applications with controllable economic costs. The findings can provide researchers with a deeper understanding of the development of biochar applications in wastewater remediation.

Keywords

Engineered biochar, Wastewater treatment, Emerging contaminants, Adsorption, Bibliometric analysis, CiteSpace

2.1 Introduction

Remediation of contaminated wastewater is one of the major challenges of the 21st century (Malyan et al., 2021). With continued rapid urbanization and industrialization, there is increasing environmental pollution, and water pollution specifically, is a significant current concern worldwide (Mollick et al., 2020). Significant environmental damage has occurred, involving waters contaminated with heavy metals (HMs), chemical dyes (Kishor et al., 2021), nutrients (e.g., N and P), agrochemicals (e.g., pesticides), veterinary residues and pharmaceutical effluents (e.g., antibiotics, hormones, and drug residues) (Khasawneh and Palaniandy, 2021). According to the World Health Organization, 80% of global diseases are linked to water pollution (Malyan et al., 2021). Overall, there is a critical need for the removal of wastewater-borne contaminants before wastewater streams can be reused for any purpose.

With the continuous expansion of the types and scale of biomass production, biochar-based adsorbents have attracted extensive attention as green and sustainable materials that can be used to counter water pollution. This is attributed to their high specific surface area, porosity, reactive surface functional groups, inexpensive nature, and tuneable physicochemical properties (Xiao et al., 2018). Biochar can be produced from numerous types of biomass, such as a kitchen (Patra et al., 2021), municipal (Ramola et al., 2020), agricultural (Younis et al., 2020), and forestry

(Yoon et al., 2021) waste material. It can be prepared under artificially controlled pyrolysis or hydrothermal conditions, which are mainly accomplished by adjusting pyrolysis temperature and residence time (Jiao et al., 2021). The widespread use of biochar for issues related to the hydrosphere (wastewater pollution), the lithosphere (soil health management), and the atmosphere (greenhouse gases mitigation) has led to a growing global interest in its application to solve environmental problems (Malyan et al., 2021). For instance, biochar has been used for the treatment of stormwater, urban, agricultural, and industrial effluents (Ahmad et al., 2014). A recent review by He et al. (2022a), has highlighted the role that "Biochar" technologies and applications can play in achieving carbon neutrality by 2050; and has advocated that biochar applications should be integrated into treatment strategies for municipal wastewater, industrial wastewater, and stormwater. For example, in greywater treatment, wetland construction has been used as a sustainable treatment technology, thereby reducing the carbon footprint and new water demand. Biochar has been utilized as a filter media in such systems and shown to promote the removal of organic and inorganic water pollutants (Quispe et al., 2022). A number of reviews focusing on contaminant removal using biochar materials have been covered from the perspective of different disciplines (Ghodszad et al., 2021; Rangabhashiyam and Balasubramanian, 2019). However, the general nature of many of these reviews does not allow for a quick grasp of research 'hotspots' or provide insights into changes in research direction. There has been little data-driven bibliometric and survey-based analysis of recent biochar literature. Given the importance of this topic, rigorous quantitative and statistical analysis is required.

Bibliometric analysis is a data and information visualization analysis tool that can explore important changes and development trends within a specific research field (Boraah et al., 2022). Bibliometrics involves accessing literature as a database for quantitative research using mathematical econometric methods to analyse development trends and 'hotspots' (He et al., 2022b). Filtering and processing extensive information resources enable the identification of the knowledge association between publications, to explore the potential value of knowledge. Bibliometric analysis is underpinned by mathematics, statistics, and computer science foundations, which facilitates convenient and intuitive analysis of data, providing accurate insights into the progress of scientific research trends (Wu et al., 2021a). Both in theory and practice, the results of this approach can have important guiding significance for continued research.

To the best of our knowledge, there has not been a scientific analysis of actual engineering applications of biochar, and in particular, in-depth sustainability studies of biochar regeneration and disposal management. In this study, bibliometrics was used to analyse the research outputs associated with biochar publications from 2012 to 2021, with metrics that include the development trend, research field, main institution, principle researchers, levels, and impact (guiding significance and concern).

This review highlights the chronological development of biochar application in wastewater remediation research from its infancy to the latest studies; it identifies current research 'hotspots' and reveals research gaps to present a comprehensive overview of the removal of contaminants from wastewater using biochar. Knowledge of current research and future development trends can help guide practical engineering applications of biochar removal of water pollutants. This analysis also identifies avenues for future research in the engineering of biochar and provides a reference for the future development of strategies to enable the full-scale application of biochar-based adsorbents.

2.2 Data and methodology

To assess the biochar literature and determine its research bias in the remediation of contamination in water, agricultural and industrial effluents, a bibliometric study was conducted of articles published between 2012 and 2021. The data presented in this paper were obtained from the curated citation index Web of Science (WoS) Core Collection^{TM} (Clarivate Analytics, USA), which covers over 21,100 peer-reviewed, scholarly journals published worldwide. The WoS is considered comprehensive, inclusive, influential, and scientifically robust. A comprehensive search of literature relating to biochar removal of water pollution, published from 2012 to 2021 was undertaken. A total of 17 search terms were selected as keywords for the search engine, enabling the identification of publications containing these search terms in the title, abstract, or keywords. These keywords were selected according to terms frequently used in previous literature reviews; the combined keywords used in the pre-search mode of the WoS core set included: "Topic = ((biochar OR black carbon OR charcoal OR char OR carbon black OR bio-char OR biochar-based) AND (wastewater OR aqueous OR constructed wetland OR effluent) AND (adsorption OR sorption OR remove OR eliminate OR purify OR purification)). The collected documents were refined by: Document Types: (Article or Review).

A total of 6295 documents were found in the WoS database. After eliminating conference papers and manual screening, we ended up with 6149 valid articles that were downloaded on July 06, 2022.

Software OriginPro 9.0 (OriginLab Corp., Massachusetts, USA) was used to analyse the annual volume distribution, primary source journal distribution, country/region distribution, subject category distribution, and keywords. We used the visualization functions of CiteSpace software 5.7.R2 to identify research 'hotspots' and frontiers. CiteSpace is a Java application that is used for the visualization and analysis of trends and patterns in scientific literature. Visualization software can focus the research process in a research field on a web map, providing a clear picture of the research trends. The Journal Citation Reports collect the impact factor (IF) values for 2022.

2.3 Scientiometric findings

2.3.1 General analysis

2.3.1.1 Publication evolution

The annual and a cumulative number of published articles focusing on the application of biochar technology to remove pollutants from wastewater is depicted in Fig. 2.1. From 2012 to 2015, the number of bibliographic documents relating to this topic did not show much significant growth. Subsequently, from 2016 onwards there has been a rapid increase in the annual number of publications, with the cumulative number of published documents also demonstrating an increasing trend as well. This trend indicates the growing prominence of biochar-based research within the field of water pollution treatment. It is worth noting that the number of publications within this area of research is still exhibiting an upward trend.
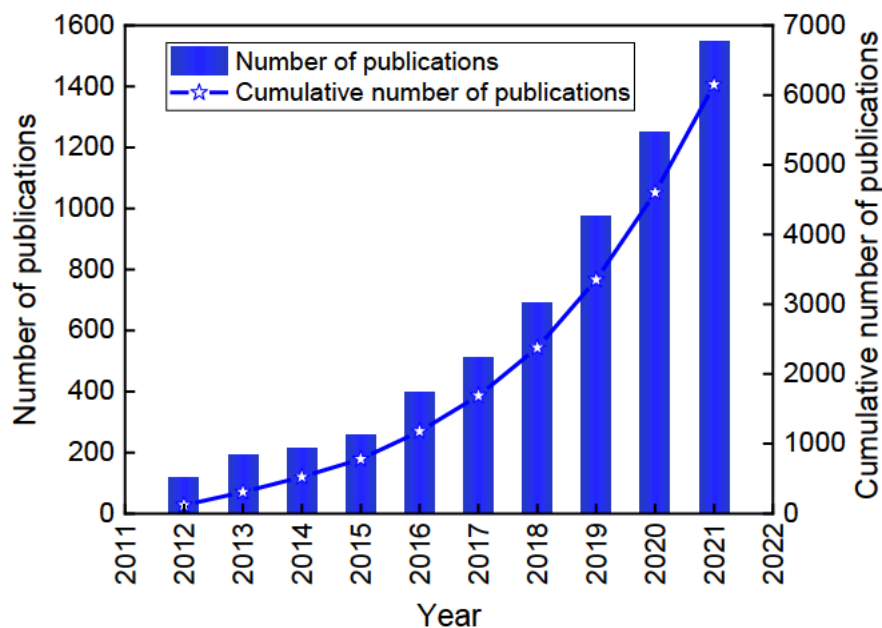
Figure 2.1 Annual and a cumulative number of published papers on the application of biochar technology to the removal of pollutants in wastewater.

2.3.1.2 Categories and cited journals analysis

Categories analysis sorts published scientific literature based on a specific topic (i.e. biochar removal of pollutants from wastewater) according to specific attributes, such as representative scientific fields analysed using the WoS database (Table 2.1). The most prominent category identified in this field being "Environmental Sciences", which accounted for 45.48% of the total publications. Moreover, "Engineering Chemical" accounted for 22.91%, followed by "Engineering Environmental" (21.76%), "Water Resources" (11.82%), "Chemistry Multidisciplinary" (10.47%), "Energy Fuels" (8.86%), "Chemistry Physical" (7.04%), "Biotechnology Applied Microbiology" (7.04%), "Green Sustainable Science Technology" (5.48%), and, "Agricultural Engineering" (5.25%). Analysing the distribution of literature is an effective method to understand the quality of core journals in this field.

Analysing the distribution of journals is an effective method to understand the quality of core journals in this field. According to the search results, the top 10 journals, including high-yielding journals with different specific publications, as well the proportion of journals and IF are listed in Table 2.2. Chemosphere had the most publications, accounting for 5.19% of the total articles, followed by Science of the Total Environment (4.91%), Bioresource Technology

(4.80%), Desalination and Water Treatment (4.26%), and Environmental Science and Pollution Research (4.15%). As can be seen, the most productive journals were also related to environmental science and engineering. In addition, it is noteworthy that the Journal of Hazardous Materials and Chemical Engineering Journal had a much lower total number of publications than the top-ranked of Chemosphere, but their IF (14.224 and 16.744) were higher than that of Chemosphere and most other journals. These results illustrated that the Journal of Hazardous Materials and Chemical Engineering Journal also had a significant impact on contaminants removal by the biochar research field.

Table 2.1 The top ten categories of published documents information obtained from WoS.

Rank	Categories	Count (No.)	Contribution (%)
1	Environmental Sciences	2797	45.48
2	Engineering Chemical	1409	22.91
3	Engineering Environmental	1338	21.76
4	Water Resources	727	11.82
5	Chemistry Multidisciplinary	644	10.47
6	Energy Fuels	545	8.86
7	Chemistry Physical	516	8.39
8	Biotechnology Applied Microbiology	433	7.04
9	Green Sustainable Science Technology	337	5.48
10	Agricultural Engineering	323	5.25

Table 2.2 Detailed information about the top ten most productive journals during 2012-2021, as well as information on the respective scientometric analysis parameters.

Published journal	Frequency	Percentage (%)	IF (2021)
Chemosphere	319	5.19	8.943
Science of the Total Environment	302	4.91	10.753
Bioresource Technology	295	4.80	11.888
Desalination and Water Treatment	262	4.26	1.273
Environmental Science and Pollution Research	255	4.15	5.190
Chemical Engineering Journal	198	3.22	16.744
Journal of Hazardous Materials	194	3.15	14.224
Journal of Cleaner Production	176	2.86	11.072
Journal of Environmental Chemical Engineering	163	2.65	7.968
Journal of Environmental Management	157	2.55	8.910

2.3.1.3 High citation papers

The number of citations reflect the influence and importance direction of a particular research field. The top 10 most cited papers in the review and article categories from 2012 to 2021 were analysed. The result showed that there was a good correlation between the journals with the highest number of publications in this field and highly cited papers (Table 2.3). Two journals, Chemosphere, and Bioresource Technology were prominent in terms of highly cited publications in this field. Among the top cited publications, two review articles were cited more than 1000 times each, with a further seven reviews being cited over 500 times, accounting for >70% of all review citations. The average number of citations per research article was 410. The most cited reference was still from the journal Chemosphere. The rapid accumulation of highly cited publications covering contaminant removal by biochar indicates that this field of research has increasingly become a research focal point. It also shows that the two journals of Chemosphere and Bioresource Technology have a high influence in this field. In addition, China and South Korea had three articles, and the rest of the countries had only one article. The results indicate that research groups from China and South Korea have recognized the importance and significance of biochar-related research and are contributing meaningfully to the growing body of literature that advocates the use of biochar-based technologies to remove contaminants from wastewater.

Table 2.3 The rank of citation frequency in the research areas related to the removal of pollutants from wastewater by biochar during 2012-2021.

Category	Corresponding author	Title	Year	Journal	Total citations	Country
Review	Ok, Yong Sik	Biochar as a sorbent for contaminant management in soil and water: A review	2014	Chemosphere	2312	South Korea
	Mohan, Dinesh	Organic and inorganic contaminants removal from water with biochar, a renewable, low cost and sustainable adsorbent - A critical review	2014	Bioresource Technology	1350	Indian
	Liu, Yunguo	Application of biochar for the removal of pollutants from aqueous solutions	2015	Chemosphere	956	China
	Chen, Yanshan and Ma, Lena Q.	Mechanisms of metal sorption by biochars: Biochar characteristics and modifications	2017	Chemosphere	751	China
	Gao, Bin	A review of biochar as a low-cost adsorbent for aqueous heavy metal removal	2015	Critical Reviews in Environmental Science and Technology	683	USA
	Tsang, Daniel C.W. and Ok, Yong Sik	Engineered/designer biochar for contaminant removal/immobilization from soil and water: Potential and implication of biochar modification	2016	Chemosphere	629	Sri Lanka
	Zhou, John L.	Adsorptive removal of antibiotics from water and wastewater: Progress and challenges	2015	Science of the Total Environment	589	South Korea

	Liu, Yunguo	Biochar-based nano-composites for the decontamination of wastewater: A review	2016	Bioresource Technology	424	China
	Gao, Bin	Surface functional groups of carbon-based adsorbents and their roles in the removal of heavy metals from aqueous solutions: A critical review	2019	Chemical Engineering Journal	383	China
	Zhou, John L.	Progress in the preparation and application of modified biochar for improved contaminant removal from water and wastewater	2016	Bioresource Technology	380	South Korea
Article	Gao, Bin	Removal of heavy metals from aqueous solution by biochars derived from anaerobically digested biomass	2012	Bioresource Technology	486	USA
	Wang, Li and Duan, Xiaoguang	Catalytic Removal of Aqueous Contaminants on N-Doped Graphitic Biochars: Inherent Roles of Adsorption and Nonradical Mechanisms	2018	Environmental Science & Technology	451	China
	Gao, Bin	Hydrogen peroxide modification enhances the ability of biochar (hydrochar) produced from hydrothermal carbonization of peanut hull to remove aqueous heavy metals: Batch and column tests	2012	Chemical Engineering Journal	446	China
	Gao, Bin	Engineered Biochar Reclaiming Phosphate from Aqueous Solutions: Mechanisms and Potential Application as a Slow-Release Fertilizer	2013	Environmental Science & Technology	400	China

Cao, Xinde	Removal of Cu, Zn, and Cd from aqueous solutions by the dairy manure-derived biochar	2013	Environmental Science and Pollution Research	398	China
Cho, Ju-Sik and Seo, Dong-Cheol	Competitive adsorption of heavy metals onto sesame straw biochar in aqueous solutions	2016	Chemosphere	389	South Korea
Kolodynska, Dorota	Kinetic and adsorptive characterization of biochar in metal ions removal	2012	Chemical Engineering Journal	388	Poland
Gao, Bin	Removal of arsenic by magnetic biochar prepared from pinewood and natural hematite	2015	Bioresource Technology	384	China
Jiang, Hong	Amino modification of biochar for enhanced adsorption of copper ions from synthetic wastewater	2014	Water Research	382	China
Jiang, Hong	Modification of bio-char derived from fast pyrolysis of biomass and its application in removal of tetracycline from aqueous solution	2012	Bioresource Technology	376	China

2.3.2 Contribution and collaboration analysis

2.3.2.1 Cited authors' analysis

According to this analysis, 17034 authors have been involved in biochar-related research focusing on the remediation of water pollution over the past 10 years. We counted the top 10 authors with the most published papers and showed the corresponding bibliometric indicators in Table 2.4. In terms of productivity, all the academics on the list had published at least twenty papers. According to statistics, Bin Gao from the University of Florida has contributed most of the publications, about 104 articles so far, indicating that he has been a prominent researcher in the relevant field. Ok, Yong Sik, who has published 101 articles, came in second-ranked with an H-index of 105, followed by Zeng, Guangming (68, H-index 160), Tsang, Daniel C.W. (59, H-index 84), and Liu, Yunguo (52, H-index 43). It is worth mentioning that Bin Gao was named as a highly cited author in the application of biochar and made great contributions to the development of contaminant removal by biochar technology.

Table 2.4 Top ten most productive authors for the application of biochar removal for water pollution and their respective scientometric analysis parameters during 2012-2021.

Author	Publications	H-index	Institute	Country
Gao, Bin	104	82	University of Florida	USA
Ok, Yong Sik	101	105	Korea University	Korea
Zeng, Guangming	68	160	Hunan University	China
Tsang, Daniel C.W.	59	84	Hong Kong Polytechnic University	China
Liu, Yunguo	52	43	Hunan University	China
Tan, Xiaofei	48	49	Hunan University	China
Wang, Hailong	44	59	Foshan University	China
Vithanage, Meththika	42	46	National Institute of Fundamental Studies	Sri Lanka
Cao, Xinde	36	56	Shanghai Jiao Tong University	China
Ngo, Hao H	28	76	University of Technology Sydney	Australia
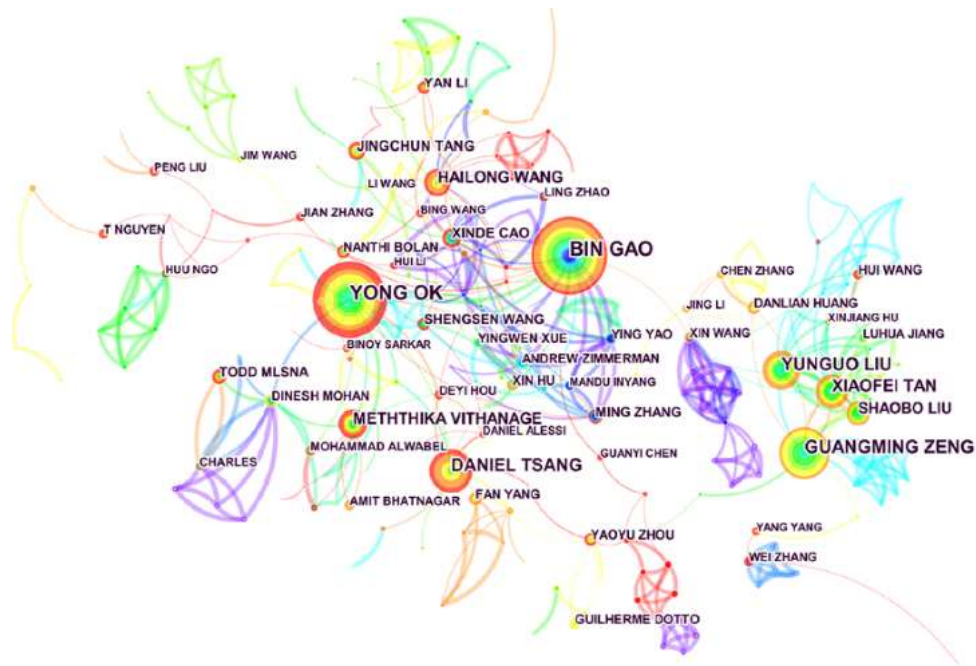
Figure 2.2 Author collaboration atlas in the production of scientific documents on biochar for removing pollutants from wastewater during 2012-2021.

Furthermore, a literature coupling network diagram (CiteSpace) illustrating author and co-authored knowledge domain maps can provide valuable information for analysing the authors' contributions and contacts in the field, and help to explore potential cooperative teams and partners in future biochar research (Fig. 2.2). Some clusters reveal closely collaborating authors with strong connections, such as Yong Sik Ok, Guangming Zeng, and Bin Gao, respectively at their cores. However, most collaborations occur primarily between authors of the same nationality and/or institutional background. Therefore, in the development process of biochar research, the role of cross-background, cross-institution, cross-country, and inter-discipline cooperation should be emphasized, which is conducive to the mutual learning between different teams, as well as the leapfrog and diversified development of the biochar field.

2.3.2.2 Influential geographical distribution and global collaboration

Analysis of major national/regional cooperation relationships, using CiteSpace software (Fig. 2.3) revealed the major contributors to biochar research focusing on the removal of contaminants from wastewater based on region and institution (Fig. 2.3). There are 112 countries/territories involved in research focusing on biochar removal from water pollution around the world. In terms of the research content, major countries showed similar main-stream

research distribution, mainly focusing on biochar preparation, mechanism exploration, and application analysis. China published 2906 papers, accounting for 47% of the total, higher than that of the USA (694) and India (588).
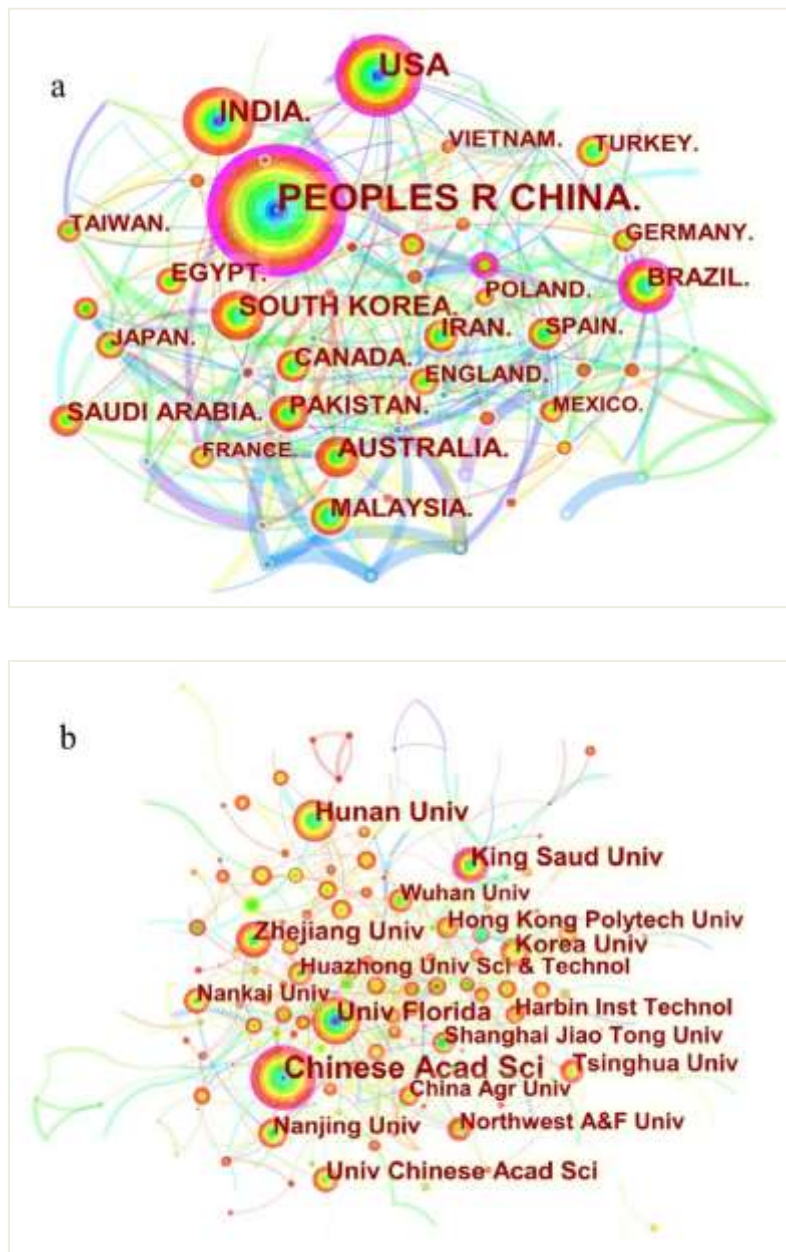
Figure 2.3 Contributions of countries around the world to the production of scientific documentation on biochar removal of contaminants from wastewater during 2012-2021 (a); Bibliographic coupling analysis of organizations in biochar-related field (b).

Table 2.5 Frequency and centrality of Countries/Institutions in the research of biochar removal for water pollution during 2012-2021.

Rank	Country	Frequency	Centrality	Institution	Frequency	Centrality
1	China	2906	0.23	Chinese Acad Sci	270	0.14
2	USA	694	0.15	Hunan Univ	129	0.04
3	India	588	0.03	Univ Florida	120	0.09
4	South Korea	368	0.04	Zhejiang Univ	101	0.06
5	Australia	263	0.04	King Saud Univ	95	0.11
6	Brazil	228	0.11	Korea Univ	88	0.07
7	Iran	224	0.04	Univ Chinese Acad Sci	77	0
8	Saudi Arabia	205	0.01	Nanjing Univ	70	0.06
9	Pakistan	193	0.07	Hong Kong Polytech Univ	70	0.08
10	Malaysia	176	0.04	Tsinghua Univ	68	0.05
11	Canada	168	0.03	Shanghai Jiao Tong Univ	60	0.09
12	Egypt	158	0.02	Nankai Univ	60	0.03
13	Turkey	145	0.01	Huazhong Univ Sci & Technol	59	0.04
14	England	142	0.10	Northwest A&F Univ	58	0.02
15	Spain	139	0.06	Harbin Inst Technol	56	0.02
16	Japan	119	0.04	Wuhan Univ	54	0.05
17	Taiwan	116	0.04	China Agr Univ	50	0.02
18	Germany	115	0.10	Cent S Univ	48	0.01

Note: Countries with a frequency below 100 are not reported.

Notably, China has published the most articles, received the most citations, and has the highest international influence (indicated by centrality, 0.23), higher than any other country/region, such as the USA (0.15), Brazil (0.11), England (0.10), Germany (0.10), and Pakistan (0.07) (Table 2.5). This shows that the international cooperation network in the biochar field in China is quite developed and that China has reached a level of prominence in biochar-related research. This is the result of research initiatives that have been identified as being nationally/internationally important. Additionally, statistical analysis of the core publishing institutions in a certain research field can reveal the main research institutions and teams in the field, to better understand this research area. According to Table 2.5, we can see that the Chinese

Academy of Sciences published 270 articles ranking first, with the highest centrality 0.14, followed by Hunan University (129 publications), University of Florida (120 publications), Zhejiang University (101 publications) and King Saud University (95 publications). In Fig. 2.3, a cluster analysis is conducted on the research institutions of relevant literature, a total of 542 nodes (N=542) and 654 links (E=654) are obtained. It presented the collaborations of institutions with more than 49 articles, forming a cooperative network with the Chinese Academy of Sciences and the University of Florida as the core.
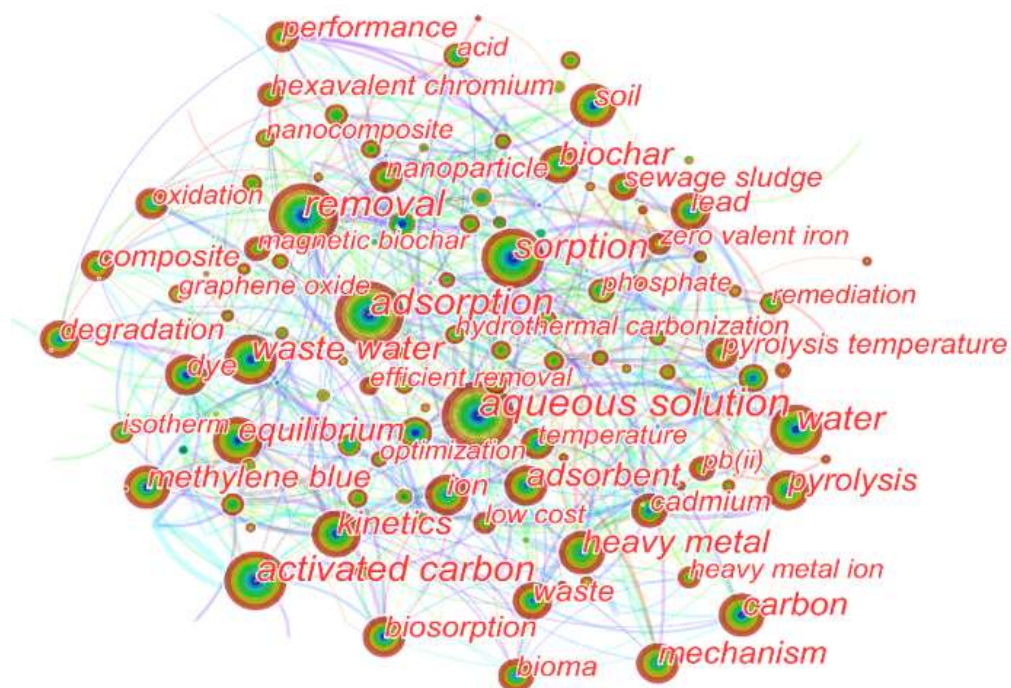
Figure 2.4 Co-keyword analysis of research terms related to biochar removal contaminants from wastewater during 2012-2021.

2.3.3 Research hotspots based on cluster analysis

2.3.3.1 Topic keywords map

According to the keyword statistics from 2012 to 2021, 198 keywords were retrieved, of which 100 appeared more than 50 times. Keyword co-occurrence analysis examines the co-occurrence of keywords in a large number of articles to describe the core content, structure, and research frontiers of a certain academic field. The time variation of keywords co-occurrence

map can reflect the evolution trend of biochar research hotspots. We obtained the keywords co-occurrence chart in the research stage in the past 10 years, as shown in Fig. 2.4.

The diameter of the circles associated with key terms indicates their level of centrality, and the width of connecting lines between nodes indicates co-occurrence intensity. The clustering phenomenon of 'hot' keywords indicates very concentrated research hotspots, indicating that the research emphasis on biochar was focused. Overall, there was greater attention to the field of contaminant removal from water by biochar.

2.3.3.2 Research frontier identification

To determine the current focus areas and development trends within the field of biochar research, we used the timeline function by CiteSpace (Kamali et al., 2020). The keyword timeline visualization of valid papers in the biochar-related field is shown in Fig. 2.5. The Y-axis is the keyword cluster, while the X-axis is the year of publication. All keywords are grouped into eight categories, each containing multiple keywords. In the year of the first occurrence of a keyword tag, the larger the intersection node, the higher the frequency of the keyword. Node links represent the cooperative association of keywords, where the higher centrality of nodes indicates that more links co-occur with other keywords. Hot keyword clustering results indicate very concentrated hotspots in the field. The collected studies were divided into seven clusters (kinetics, adsorption, performance, wastewater treatment, temperature, reduction, and composite).

Cluster #0 (kinetics): Kinetics and thermodynamics are important means to study the mechanism of pollutant removal behaviour of biochar adsorbents. The photocatalytic activity of functionalized biochar prepared by chemical activation is also widely used in antibiotic remediation (Kumar Patel et al., 2022). In particular, metal-composite modification significantly improved the catalytic performance of biochar. Since biochar antimicrobial properties do not affect biochar catalysis/adsorption, it may be a potential solution to remove antibiotics from aqueous environments (Ahmed et al., 2018). On the surface of biochar, carboxyl, ketone, nitro, and other major reactive groups act as electron-acceptors to generate π-π EDA, which interacts with antibiotic pollutants and carries out the adsorption process. Moreover, it was found that the sewage sludge-derived biochar was a promising material that can remove pollutants from water by adsorption and bring additional benefits for managing

large amounts of sewage (Rangabhashiyam et al., 2022), indicating that the study of sludge biochar has long been noticed by scholars. Sludge can be converted into harmless biochar materials with dual utilization value of adsorption and catalysis through pyrolysis, which is in line with the concept of sustainable development (Ji et al., 2022).

Cluster #1 (adsorption): This cluster mainly focuses on the keywords of "aqueous solution", "adsorption", and "removal". Among them, adsorption activity is an early hotspot, which can be seen from the evolution of cluster #1. However, it has fewer keywords and lines, indicating that the enthusiasm is fading in the new era, and the prelude to diversified research is being opened. Cluster #2 (performance): The most common keyword in this cluster are "performance", "phosphate", and "recovery". Studies on the removal of pollutants by biochar mainly focus on the activity and reactivity, with emphasis on the performance and mechanism of biochar modification. Among them, the removal of nitrogen, phosphorus, and, heavy metal ions by biochar composite materials has become a hot spot. Cluster #3 (wastewater treatment): This cluster mainly talks about how biochar removes pollutants from water, including pharmaceuticals, bisphenol A, organic contaminants, and persulfate removal. Persulfate activation and photocatalytic degradation of biochar are at the forefront of current scientific research, making the transformation of biochar mechanism research from activity to reactivity. Metal-organic framework-modified biochar materials have demonstrated huge potential for applications in pollutant treatment. Cluster #4 (temperature): The results show that the chemical properties of biochar are the most important factors affecting its environmental behaviour and effects, and the pyrolysis temperature is key to the preparation of biochar. Another keyword "hydrothermal carbonization" is a method for preparing biochar. Most biomass has high water content, and biochar preparation by pyrolysis requires drying of biomass to improve yield and reduce energy consumption, while hydrothermal carbonization (HTC) requires less energy and has a higher yield than pyrolysis. At the same time, it can also be seen that the research on the evolution of microbial community structure in biochar systems is also gradually emerging. Cluster #5 (reduction): The largest node in the cluster focuses on the term nanoparticle. It can be seen from the evolution of cluster #6 (composite) that the remediation of water by biochar composites modified with layered double hydroxides gradually became a hotspot field. A study of the preparation of high-performance and environmental protection of layered double hydroxides-ball milled biochar (LDH-BMBC), used in the solution and phosphate retention in the soil, as well as fine biochar of LDHs stripping support, provides valuable insights, expanded

the engineered ball milled biochars application in the environmental remediation (Li et al., 2022). The study of biochar composite formulated with different materials is also of profound significance.
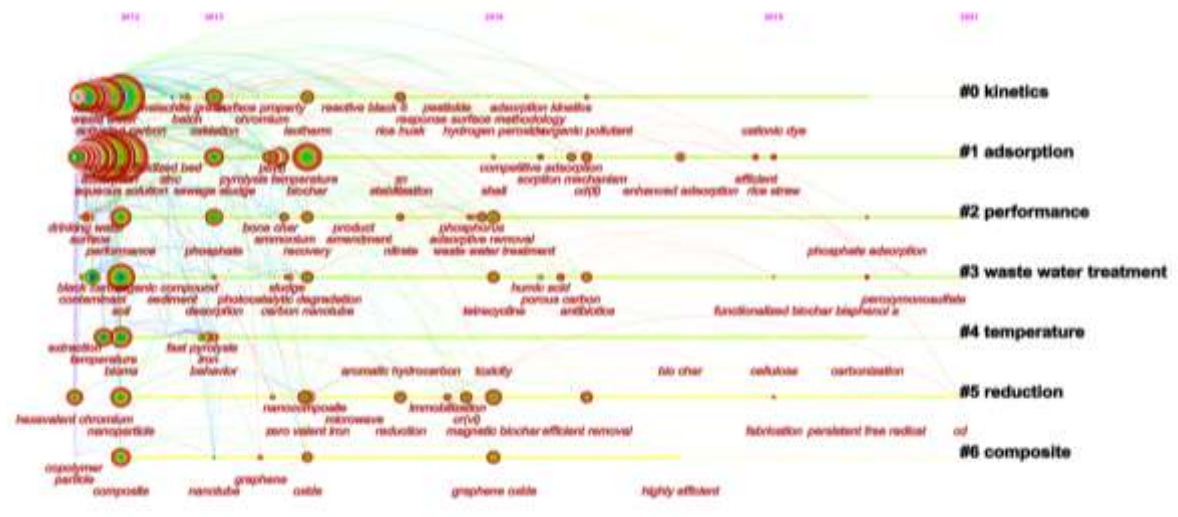
Figure 2.5 Timeline view of the evolution of keywords in the research of biochar removal for water pollution during 2012-2021.

Around 2017, the research on pollutant degradation and biochar removal mechanism began to increase rapidly (Ji et al., 2022a), with additional studies on biochar-based catalysts and catalytic activity (Rangarajan et al., 2022). Over the past decade, the application of biochar in water and the removal of pollutants has been a strong research focus area, while wastewater treatment, efficient removal of contaminants, and the development of functional composites are current popular research areas. Studies on the application of biochar in specific engineering applications (Zhang et al., 2021), and its use in environmental management practices are relatively new topics that indicate changes in the frontier of the biochar field (Zhang et al., 2019a). Advances in these areas will eventually close the loop for an actual circular economy of biochar.

2.3.4 Preliminary evolution of the research hotspots

Keyword emergent analysis refers to the statistical analysis of words that appear more frequently or are used more frequently in a certain period. The results of this kind of analysis can help reveal the research development trend of biochar removal for water pollution in

different time stages and help identify specific articles in the area of interest (Nageshwari and Balasubramanian, 2022). Keyword breakout analysis was conducted in CiteSpace on remove contaminants by biochar from wastewater. The results are shown in Table 2.6, as a list of the top 25 breakout keywords from 2012 to 2021, their occurrence time, and duration.

The higher the abruptness of a keyword, the higher the attention paid to the keyword in the considered time interval, which to some extent represents the research frontier and hotspot of a discipline field. Early studies of water pollution removal focused on "black carbon," "metal ion," "char," "charcoal," and "low-cost adsorbent." During this period, the focus was on the adsorption behaviour of carbon materials to wastewater and related mechanisms. Later "fast pyrolysis" and "different pyrolytic temperature," terms related to the preparation of biochar, became hot keywords, indicating greater attention to the biochar preparation process.

In addition, the analysis revealed a phase of studying soil under different levels of heavy metal pollution (Lee et al., 2020a). As a promising amendment, biochar has a stable aromatic structure and can be used as a remediation agent for soil contaminated with diverse types of heavy metals (Ji et al., 2022b). Additionally, biochar can fix carbon components in soil for a long time, improving organic matter in barren soil and increasing the number of microorganisms for improved soil quality (Liu et al., 2022).

In recent years, there have been increased studies examining the removal of pollutants such as hexavalent chromium. Hexavalent chromium is mainly a water contaminant, with toxic effects on water organisms and the human body (Shakya et al., 2019). The use of chromium-containing wastewater to irrigate farmland can result in the accumulation of this chemical in the soil, resulting in the inhibition of crop growth and development (Tseng et al., 2019). Thus, there is a clear need for improved approaches to remove this pollutant.

There has also been significant interest in the application of biochar to remove phosphates from water/wastewater to reduce the risk of eutrophication in receiving water bodies (Rajapaksha et al., 2022). This field has branched out gradually to identify suitable modifications of magnetic-based biochar to facilitate the recovery and recycling of this material (Zhang et al., 2019b).

Table 2.6 The emergence of the top 25 most explosive keywords cited bursts in the field of biochar removal for water pollution.

Keywords	Year	Strength	Begin	End	2010-2021
Black carbon	2012	42.76	2012	2017	
Metal ion	2012	27.03	2012	2018	
Char	2012	22.46	2012	2018	
Charcoal	2012	17.66	2012	2015	
Low-cost adsorbent	2012	14.13	2012	2016	
Azo dye	2012	13.12	2012	2016	
Polycyclic aromatic Hydrocarbon	2012	12.75	2012	2015	
Bioavailability	2012	12.11	2012	2016	
Surface	2012	10.74	2012	2015	
Chemical activation	2012	8.11	2012	2014	
Fly ash	2012	7.97	2012	2015	
Fast pyrolysis	2012	18.72	2013	2017	
Nanotube	2012	14.61	2013	2016	
Reactive dye	2012	11.32	2013	2014	
Surface chemistry	2012	9.86	2013	2015	
Malachite green	2012	9.39	2013	2016	
Sludge	2012	8.04	2014	2015	
Drinking water	2012	16.5	2015	2018	
Rice husk	2012	16.01	2015	2017	
Carbon nanotube	2012	21.39	2016	2018	
Desorption	2012	9.24	2016	2017	
Competitive adsorption	2012	17.24	2017	2018	
Sorption mechanism	2012	14.28	2017	2018	
Different pyrolytic Temperature	2012	14.28	2017	2018	
Hexavalent chromium	2012	16.24	2018	2021	

2.4 Literature review

Guided by the findings of the scientometric analysi, a literature review was compiled to appraise recent developments and research trends of biochar applications used in wastewater pollutant removal.

2.4.1 Effects of preparation method and modification process on the properties of biochar

2.4.1.1 Preparation methods

As shown in Table 2.7, the source and carbonization process of biomass are the main factors affecting the physicochemical and adsorption properties of biochar. Carbonization methods include pyrolysis, hydrothermal, gasification, and microwave treatments, with pyrolysis and hydrothermal treatments being considered the most important (Jiao et al., 2021).
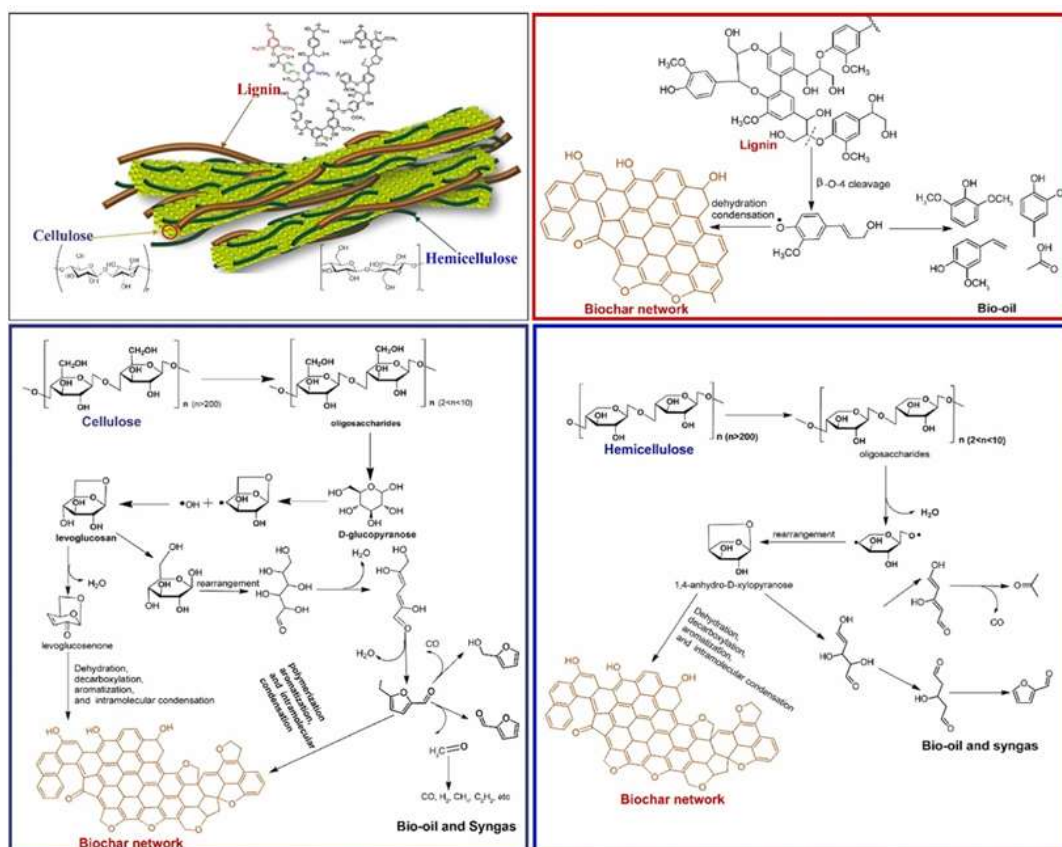
Figure 2.6 Schematic diagram of the mechanism associated with biochar formation by pyrolysis of lignocellulosic biomass (Shen et al., 2017).

As part of the comprehensive utilization of waste biomass, pyrolysis technology has been widely studied as an environmentally friendly and cost-effective method (Liu et al., 2021a). During pyrolysis, biomass is thermochemically degraded at 300 ~ 900 °C without oxygen to generate biochar, gaseous, and bio-oil products (Wan Mahari et al., 2022). Previous studies have explored the potential of agricultural wastes such as oil palm kernel shells (Lee et al., 2020b), woody biomass (Ding et al., 2019), and straw (Xu et al., 2022a), for conversion into engineered biochar (Fig. 2.6). Overall, the yield and physicochemical characteristics of biochar produced through pyrolysis are strongly influenced by both feedstock characteristics and operating conditions (Liu et al., 2021a). Dai et al. (2018) reported that biochar produced by pyrolysis of crab shell waste at 800 °C had a BET surface area of 81.57 m^2/g and a pore volume of 0.0861 mL/g (Dai et al., 2018). In another study, Liu (2021) reported co-pyrolysis of shrimp shells and corn straw, which greatly improved the thermal degradation characteristics. This hybrid biochar was used mainly for pollution control and resource recovery of wastewater from mining, metallurgy, and electroplating industries and is proving to be a promising adsorbent (Liu et al., 2021a).

Hydrothermal carbonization (HTC), also known as wet roasting, is a thermochemical process that converts organic raw materials into high-carbon-rich solid products at a temperature range of 175~300°C for 16 h (Rangabhashiyam and Balasubramanian, 2019). HTC skips the pre-drying step and converts organic feedstock with high water content into reaction media at relatively low temperatures and high pressures (Kim et al., 2020). This method has been used to prepare camellia shell biochar and exhibited stable energy and mass yield (Tu et al., 2018). In addition, the aromaticity of cherry pomace increased with the processing temperature (Wądrzyk et al., 2021). In environmental applications, the hydrochar surface presents a higher degree of aromatization and contains more oxygen-containing groups, which is conducive to improving its adsorption capacity (Wan Mahari et al., 2022). Activated biochar prepared from agricultural crop residues through HTC exhibited a maximum surface area of 1099 m^2/g and a maximum adsorption capacity of 400 mg/g; additionally, its modified oxygen-containing functional groups exhibit a three-dimensional carbon structure to attract incoming pollutants (Prasannamedha et al., 2021). However, the use and application of HTC biochar requires a large amount of water for a series of steps such as mechanical dewatering (compression), filtration, solar/thermal drying, and then use as an adsorbent for wastewater recovery. Hence, hydrochar produced using the HTC method may be more suitable for soil

remediation (Wang et al., 2021a). After thermochemical treatment, macro and micronutrients other than potassium and sodium were concentrated in hydrochar indicating that the material has great potential for agriculture applications (Castro et al., 2021).

2.4.1.2 Modification technologies

Unmodified biochars have been found to have limited decontamination applications due to their physicochemical properties, which may lack the sufficient adsorptive capacity to meet the desired remediation requirements (Chen et al., 2022). Several methods have been developed to modify the physicochemical properties of biochars to improve their adsorption capacity and effectiveness in removing environmental contaminants (Chen et al., 2022). The treatment process adopted and the biochar modification implemented will have a direct effect on the adsorption performance; examples of the adsorption characteristics of different modified biochar and their capacity to remove pollutants are outlined in Table 2.7. Currently, several modification methods can be applied to biochar depending on the application scenario; these include physical, chemical, and biological approaches to different activation and modification methods, which are summarized in Fig. 2.7 (Tan et al., 2017).

Physical modification usually involves heat treatment, such as steam and gas activation，allowing the improvement of surface area, pore structure, porosity, and pore volume (Sewu et al., 2019). For example, steam, NH_3, CO_2, and their combination were tested for biochar modifications (Kwak et al., 2019). Physical activation can also increase COOH, OH, and other oxygen-containing functional groups on the surface of biochar, thus improving overall pollutant adsorption efficiency (Sakhiya et al., 2021). Although physical activation is usually much cheaper than chemical activation methods, this approach typically results in much lower material porosity than chemical activation.

Chemical modification using either acid or alkali active agents, can improve the pore properties of biochar and increase the availability of binding sites by introducing different functional groups on the surface of biochar. Acid-modifying agents including HNO_3 (Imran et al., 2020), HCl (Wu et al., 2019), H_3PO_4 (Chen et al., 2018), and H_2SO_4 (Zhao et al., 2022) have been used, as have alkali agents such as NaOH and KOH (Ullah et al., 2022; Wang et al., 2022). Oxidants such as $KMnO_4$ and H_2O_2 can also be used to modify biochar (Xu et al., 2022a). The adsorption performance of biochar can also be improved by impregnation with metal salt

solutions (e.g. iron salt, magnesium salt, calcium salt, lanthanum salt, zinc salt) and/or the use of supported metal oxides (hydroxides) on the surface of adsorbents. Metal oxide-biochar composites have been used to remove organic and inorganic pollutants or heavy metals from wastewater treatment systems (Wang et al., 2018). Abundant persistent free radicals and oxygen-containing functional groups associated with iron-modified biochar demonstrate high electron shuttling capacities, and have demonstrated the potential to catalyse H_2O_2 to form hydroxyl radicals ($\cdot OH$) to remove organic pollutants in wastewater (Feng et al., 2021). Furthermore, introducing modifiers such as natural clay minerals can increase the porosity and cationic exchangeability of biochar-clay composites (Chen et al., 2022), and also improve the adsorption affinity for heavy metals, antibiotics, and polymers (Premarathna et al., 2019).
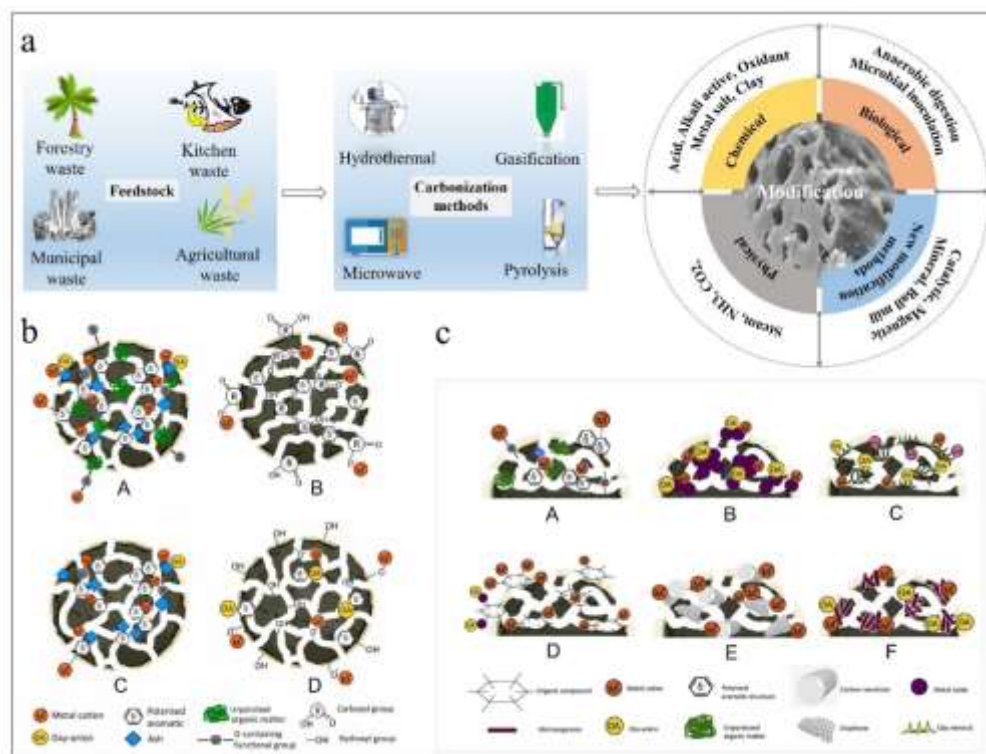
Figure 2.7 Possible modification methods for biochar with different raw materials prepared under varied carbonization processes (a); A comparison between different activation methods for engineering biochar concerning sorption characteristics. A) Pristine biochar; B) acid-treated biochar; C) gas/steam-activated biochar; and D) alkali-treated biochar (b). Adopted from (Sizmur et al., 2017). With permission from Elsevier. Copyright©2017; A comparison between different modification methods for engineering biochar concerning sorption characteristics. A) Pristine biochar; chemical impregnation/coating by B) metal oxides, C) clay minerals, D) organic compounds such as amino groups, polyethyleneimine,

chitosan or graphene oxide and E) carbon nanotubes; and F) microbial modification (c). Adopted from (Kazemi Shariat Panahi et al., 2020). With permission from Elsevier. Copyright©2020.

Biological pre-treatment technology is a relatively new approach that harnesses biological processes to modify engineered biochar products (Kazemi Shariat Panahi et al., 2020). Biochar derived from anaerobically digested biomass residues typically has high pH, strong ion exchange capacity, large surface area, and other excellent adsorption properties (Kumar et al., 2022). Moreover, microorganisms can be fixed on the surface of biochar through colonization and biofilm generation. The remediation performance of the biochar is improved via combined adsorption and biodegradation processes, which improve the overall removal of pollutants from wastewater (Bouabidi et al., 2018). Biologically modified biochars have been shown to exhibit superior removal efficiency for phosphate (Yao et al., 2011) and heavy metals (Ngambia et al., 2019). Yang et al. (2021) described the effects of bio-modification on rice straw biochar colonized by *Pseudomonas stutzeri* on the biodegradation of chloramphenicol, an antibiotic commonly used in aquaculture. The biodegradation efficiency achieved using *P. stutzeri* bio-modified biochar (90%) proved to be much higher than that of unmodified material (10%) or *P. stutzeri* alone (44%). The results indicated that biochar improved the biodegradation efficiency of chloramphenicol by promoting bacterial growth, changing fatty-acid composition, and increasing gene expression.

The rapid development of biochar applications, has resulted in a variety of new modification methods being tested, including catalytic (Goncalves et al., 2020), magnetic, mineral (Arif et al., 2021; Viglasova et al., 2018), and, ball mill (Kumar et al., 2020) modification. The appropriate modification method of biochar should be selected according to the characteristics of the pollutants to be removed for optimal adsorption.

2.4.2 Contaminant removal from wastewater using biochar

Biochar has been routinely used as an adsorption material to remove contaminants, namely heavy metals, organic contaminants, nitrogen and phosphorus, and other contaminants from wastewater (Tan et al., 2015). Heavy metals and organic contaminants are the main pollutants that have been targeted for adsorption removal by biochar (Mohan et al., 2014). Examples of

adsorption performance and pollutant removal mechanisms associated with biochar prepared with different raw materials and precursor types are shown in Table 2.7.

Table 2.7 Adsorption characteristics of contaminants removal using different biochars obtained with different materials and fabrication methods.

Preparation pathways	Precursor type	Raw material	Modification methods	Prepared conditions	Contaminants	Adsorption capacity (mg/g)	Mechanisms	References
Pyrolysis	Kitchen waste	Bone	$Fe(NO_3)_3/KMnO_4$	Pyrolysis at 300, 450, and 600°C, 2 h, N_2 protection	Cd (II), Cu(II) and Pb(II)	Cd(II) (151.3 ~163.4), Cu(II) (219.8~259.0) and Pb(II) (271.9 ~407.2)	Chemical complex, cation-π bonds, ion exchange and coprecipitation	(Xiao et al., 2020)
		Food waste, canola hull and oat hull	Impregnated with potassium hydroxide (KOH)	Variable temperatures (i.e., 700–900°C) and activation time (i.e., 60–120 min) under N_2 atmosphere	Dyes	Within 1–2 h of contact time at room temperature, whereas in case of rhodamine B only 91–94% removal was achieved.	Pore diffusion and surface diffusion	(Patra et al., 2021)
		Food waste	0.5 M $FeCl_3$	Pyrolyzed at 300, 450, and 600°C for 1.0, 2.5, and 4.0 h within a N_2 atmosphere	Phosphorus	27.24~31.801	Ligand exchange	(Kang et al., 2021)

Municipal waste	Fresh N. lappaceum peels	Dissolved in 250 mL of $FeSO_4 \cdot 7H_2O$ solution	Pyrolyzed at 350 W (228°C) for 30 min under N_2	Organochlorine pesticides	The removal of OCPs (2 mg L^{-1}) reached 96–99% within 120 min	π -π electron-donor-acceptor interaction and adsorption is facilitated by the hydrophobic sorption and pore filling.	(Batool et al., 2022)
	Spent waste	Bentonite and calcite	Pyrolyzed at various temperatures (300, 500 and 700°C) for 90 min	Lead (Pb)	544.37	Pore filling, electrostatic attraction	(Ramola et al., 2020)
	Sludge	KOH, $MgCl_2$ and $FeCl_3 \cdot 6H_2O$	Pyrolysis at 700°C for 2 h	Fluoroquinolone antibiotics, CIP, NOR, and OFL	49.9, 55.7 and 47.4	Pore filling, H-bonding, π-π conjugation and electrostatic	(Ma et al., 2022)
	Waste activated sludge	Co-precipitation of Fe^{3+}/Fe^{2+} or $FeCl_3$ impregnation	Pyrolyzed in 550°C and retained for 2 h under N_2 environment	Phosphate	110	Ligand exchange, ion exchange, electrostatic attraction	(Yang et al., 2018b)

	Sludge-based	A simple air roasting-oxidation modification	Carbonized with temperature from room to 600°C	U(VI)	490.2	Oxygen-containing functional groups and large specific surface area	(Sun et al., 2022b)
Agricultural waste	Corn stalks	Dissolved in FeSO$_4$·7H$_2$O and NaBH$_4$	Mixed with KHCO$_3$ and pyrolysis at 800°C for 2 h	Pb^{2+}, Cu^{2+}, Zn^{2+},	195.1, 161.9, and 109.7	Adsorption, precipitation, reduction and complexation	(Yang et al., 2018a)
	Peanut shell	0.2 mol/L MgCl$_2$ · 6H$_2$O solution	Pyrolyzed in a tubular pyrolytic furnace under limited oxygen condition from room temperature to 500°C with the heating rate of 5°C/min	Phosphate and ammonium	132.2 and 39.5	Struvite crystallization, ion exchange and Mg-P complexation formation.	(Xi et al., 2022)
	Rice straw	Mixed with FeCl$_3$·6H$_2$O and urea	One-pot pyrolysis method at 700°C	Tetracycline	156	Involved pore filling, hydrogen-bond interaction, surface complexation, and π-π interaction	(Mei et al., 2021)

Forestry waste	Rice straw	NaOH solution (10 M) under reflux at 85°C for 6 h	Thermally activated at 500°C under an inert atmosphere (N_2 gas (99%))	Ba(II)/Sr(II)	Remove Ba(II) and Sr(II) ions (97.5%) with pre-desalination (e.g., total salts reduction of 25.7% after 48 h)	Weak ion-exchange or pore-filling	(Younis et al., 2020)
	Hickory wood	$KMnO_4$ solution under ultrasonic irradiation for 2 h	Under N_2 flow at a Temperature of 600°C for 1 h	Pb(II), Cu(II), and Cd(II)	153.1, 34.2, and 28.1	Surface MnO_x particles and oxygen-containing groups.	(Wang et al., 2015a)
	Hickory wood	MgO particles were ball milled with 500 rpm for 12 h	Pyrolyzing at 600°C under N_2 atmo sphere	Methylene blue	460		(Zheng et al., 2020)
	Bamboo powder	With Mt in N_2 atmosphere	Pyrolyzing at 300-500°C	NH_4^+ and PO_4^{3-}	12.52, 105.28	The intercalation of NH_4^+ into the interlayer space of Mt, the adsorption of PO_4^{3-}, controlled by electrostatic attraction and ionic bonding (PO_4^{3-}).	(Chen et al., 2017)

	sawdust	Impregnation with Fe/Mg/Zn salts	Heated in a tube at 550°C for 2 h	Microplastics (MPs)	The removal efficiencies were 94.81%, 98.75%, and 99.46%, respectively	Electrostatic interaction and chemical bonding interaction	(Wang et al., 2021b)
	Grape pomace		Carbonized at 350, 550 and 750°C for 2 h under N_2 atmosphere.	Pesticide cymoxanil (CM)	161	Chemical sorption and multilayer formation on the heterogeneous surface of biochar	(Yoon et al., 2021)
Hydrothermal	Rice straw	Microwave assisted hydrothermal treatment	Process temperatures from 160°C to 200°C and reaction time was from 40 min to 70 min	Organics (Congo red, berberine hydrochloride and 2-naphthol) and two heavy metals (Zn^{2+} and Cu^{2+})	222.1, 174.0, 48.7, and 112.8, 144.9		(Li et al., 2019)
	Rice husk	7.5 M NaOH aqueous solution was mixed with	For the hydrothermal process, temperature was increased to	Malachite green	373.02	π - π interaction, H-bonding interaction.	(Tsai et al., 2022)

| Corn straws | 13.5 g of RHB, then placed in a Teflon container prior to keeping it in a high-pressure hydrothermal kettle. 2:1 mmol of $La(NO_3)_3 \cdot 6H_2O$ and $FeCl_3 \cdot 6H_2O$ dissolved in 60 mL of $(CH_2OH)_2$ under a sonication process. Then, 0.5 g of biochar, 3.6 g of CH_3COONa, | 130°C and held it for 5 h. Hydrothermal reactor and placed inside a muffle furnace for 12 h at 200°C | Phosphate | 330.86 | Electrostatic attraction and inner-sphere complexation via ligand exchange | (Qu et al., 2020) |

	0.5 g of urea and 1 g of PEG				
pitaya peel		Hydrothermal reaction temperature of 260°C for 3 h	Rare earth ions	108	Electrostatic attraction, ion exchange, surface complexation	(Feng et al., 2019)

2.4.2.1 Heavy metals

Industrial effluents can contain a variety of non-biodegradable heavy metals that present risks to human health and the environment. The accumulation of metals within the environment increases the severity of the threat. Examples of toxic metals occurring in wastewater effluents include lead, cadmium, hexavalent chromium, and mercury. In recent years, biochar has been evaluated as an adsorbent for metal removal (Islam et al., 2021). Given its favourable adsorptive properties and the structural components of colonized biomass, biochars can adsorb and precipitate heavy metals by interaction with a range of functional groups. To remove heavy metals from aqueous solutions, biochar can utilize several adsorption mechanisms including ion-exchange electrostatic interaction (chemisorption), surface complexation, inner-sphere complexation, co-precipitation, and physical adsorption (Othmani et al., 2021). Yan (2020) improved the adsorption of lead in wastewater by converting the skin of bean worms into phosphorus-rich biochar through pyrolysis. Pyrolysis significantly enhances the exposure of biochar surface active sites and reduces the Zeta potentials because biochar can strongly adsorb Pb(II) in solution through precipitation of hydroxyapatite, hydrocerite, and alamosite. Hydrogen peroxide-modified biochar derived from agricultural residues has been used to remove heavy metals in solution (Xue et al., 2012). An adsorption capacity of 22.82 mg/g was demonstrated, which is more than 20 times better that of untreated hydrochar; this was attributed mainly to additional oxygen-containing functional groups, especially carboxyl groups, on the surface of hydrochar as a result of the modification process (Xue et al., 2012). In another study, biochar prepared from sewage sludge underwent a carbon-supported Mg(II) modification via a simple precipitation-calcination synthesis route; subsequently, very favourable adsorption capacities of 2931.76 mg/g (Pb(II)) and 861.11 mg/g (Cd(II)) were achieved (Ngambia et al., 2019). The superior adsorption performance was attributed to ion exchange with Mg(II), coordination with surface and inner carboxylic or carbonyl functional groups, and co-precipitations of metal silicates.

Different pre-treatment conditions can also have a great impact on the adsorption performance of biochar. For example, the removal of soluble copper (Cu) and zinc (Zn) ions using biochar from soft and hard wood was improved by high pH conditions (Jiang et al., 2016). This is because the negative charge of biochar causes hydrolytic polymerization of metal ions; under saline conditions the surface charge of biochar results in competition between Na^+ and

exchangeable Ca^{2+} and/or heavy metal ions for negative charge sites. The presence of minerals in biochar also affects the adsorption of heavy metals, with decreased adsorption efficiency of biochar being experienced under demineralization conditions (Xu et al., 2013). In one study, manganese oxide was used to modify biochar to improve its adsorption capacity for copper (Song et al., 2014). A maximum adsorption capacity of 160 mg/g Cu^{2+} was achieved with MnO_x-loaded biochar, which is much higher than the original unmodified biochar. A schematic diagram summarising the major mechanisms of heavy metal removal by biochar is presented in Fig. 2.8.
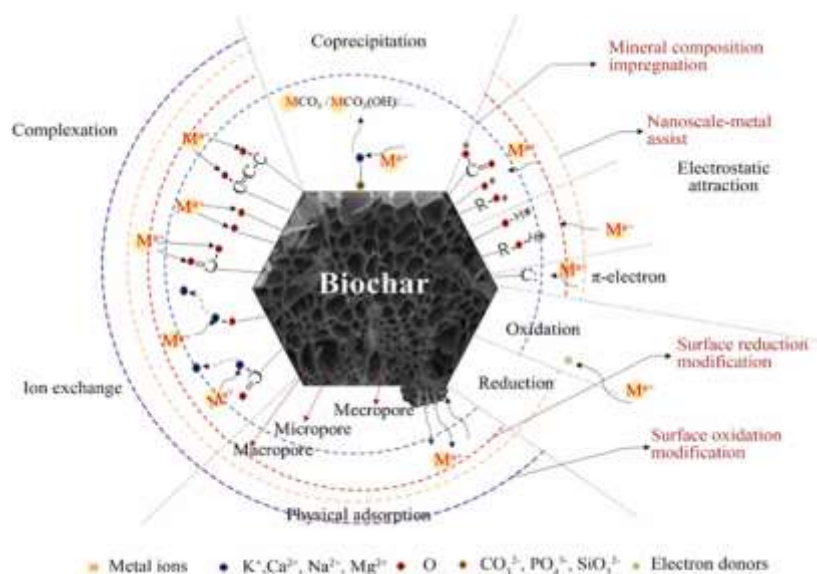
Figure 2.8 Schematic diagram of the mechanism of removal of heavy metals by biochar (Wang et al., 2019). With permission from Elsevier. Copyright©2019.

2.4.2.2 Organic contaminants

Organic contaminants commonly associated with wastewater include dyes, phenolics, pesticides, and polynuclear aromatics that are effectively removed by biochar adsorbents (Mohan et al., 2014). The surface properties of biochar play an important role in the adsorption of organic pollutants due to the merits of high microporous volumes, high aromaticity, abundant surface oxygen-containing functional groups, huge specific surface area as well as economic accessibility (Luo et al., 2022). In one study, biochar was prepared from weeds with nitric acid to effectively adsorb methylene blue from an aqueous solution, resulting in a material with a lower specific surface area, more oxygen-containing functional groups, and a lower maximum value of zero charge point (Güzel et al., 2017). The dye removal rate for this material was

highest at a pH value of 7.4 and temperature of 50 °C. Ates and Un (2013) investigated the effect of different pyrolysis temperatures (viz., 500, 600, 700, and 800 °C) on corner beam sawdust to prepare biochar material as an adsorbent for the treatment of dispersed Orange 30 dye. The dye removal reached 71% and the rate of removal increased with decreasing pH and initial concentration of dye present, which was achieved using the 800 °C char at a concentration of 2.4 g/L and a solution pH of 2.
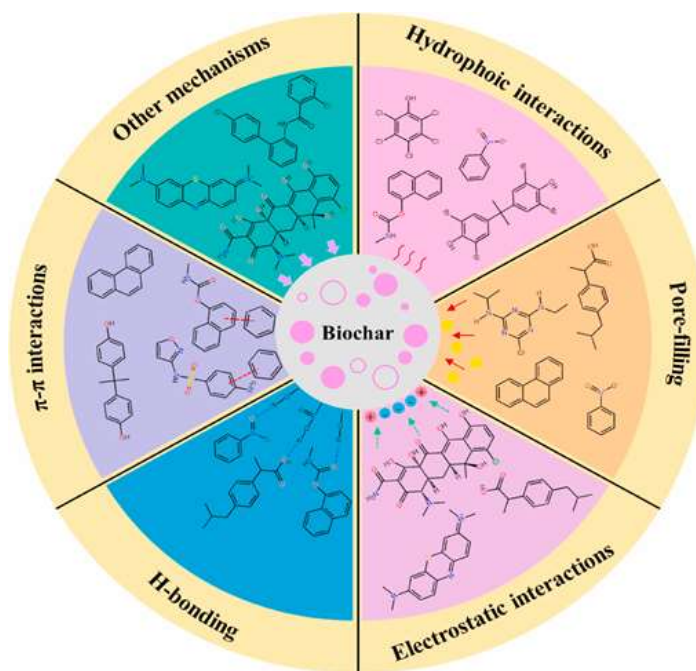
Figure 2.9 Mechanisms associated with biochar adsorption of organic pollutants (Li et al., 2022a).

There is significant interest in the removal of the important water pollutants of phenolic compounds, pesticides, and polycyclic aromatic hydrocarbons (PAHs). Activated carbon biochar (ACB) of wastewater sludge cake generated at 400 and 700°C have been used to remove organic pollutants such as carcinogenic PAHs, gasoline, and diesel from water (Sullivan et al., 2019). The use of ACBs can be tailored to meet the needs of specific applications, selecting materials based on available waste feedstock and synthesis conditions to provide targeted removal of selected chemicals (Sullivan et al., 2019). Advances in the use of customized biochar for the bioremediation of pesticides, antibiotics, and PAHs pollutants in aqueous and solid phases have been reviewed by Patel et al., (2022). Mn-modified biochar has achieved a removal rate of 4-chloro-3-methylphenol (CMP) close to 100% in a persulfate activation system; the enhanced catalytic activity was attributed to the generated $SO_4 \cdot^-$, $\cdot OH$, and $^1O_2$,

which contributed to the degradation of CMP (Liu et al., 2021b). A summary of the proposed mechanisms influencing biochar removal of organic pollutants is presented in Fig. 2.9.

2.4.2.3 Nitrogen and phosphorus

Excess nitrates and phosphates in water can negatively impact the biodiversity of aquatic life leading to serious problems, such as an overgrowth of algae and a depletion of available oxygen (Menesguen et al., 2018). Post-treatment of biochars has a significant effect on ammonium adsorption. The adsorption capacity of oxidized biochar produced from mixed maple was increased by 3.6 and 1.6 times, as compared to raw maple wood biochar when shorter residence times at lower high-temperature pyrolysis temperatures were used (Wang et al., 2016). Neutralizing oxygen-containing functional groups on the surface of oxidized biochar to pH 7 further increased ammonium adsorption three-fold at 500°C with a residence time of 5 min in the adsorption process. Moreover, pyrolysis temperature also affects adsorption capacity. Adsorption of NH_4^+ and NO_3^- was promoted by the production of biochars at low and high pyrolysis temperatures, respectively (Wang et al., 2015b). In general, unmodified biochars have a low adsorption capacity for NH_4^+–N, and an even lower affinity for NO_3^- resulting from electrostatic repulsion due to negative charge. Pre-treatment of raw materials can affect the adsorption of phosphorus and nitrogen. For example, a metal oxide modification of biochar has been shown to improve its ability to remove NH_4^+, NO_3^-, and PO_4^{3-} (Zhang et al., 2020). La-biochar from oak sawdust exhibited the maximum adsorption capacities for NH_4^+, NO_3^-, and PO_4^{3-} of 10.1, 100, and 142.7 mg/g, respectively (Wang et al., 2015b). The increased adsorption by La treatment is probably due to a large amount of acidic and basic functional groups on biochars, such as phenolic–OH and carboxyl C=O acidic function groups, which are capable of strongly binding to nitrogen and phosphorus. Biochar prepared by pyrolysis of crawfish waste exhibited a high yield of biochar (83%) with excellent content of carbon (9~30%) (Park et al., 2018). Under alkaline pH conditions, the maximum adsorption capacity of phosphate removal was 70.9 mg/g and adsorption occurred through the precipitation between PO_4^{3-} with calcium dissolved from CaO and Ca(OH)$_2$. Adsorption benefitted from the ion-exchange mechanism of $H_2PO_4^-$, and HPO_4^{2-} with the biochar surface (Park et al., 2018).
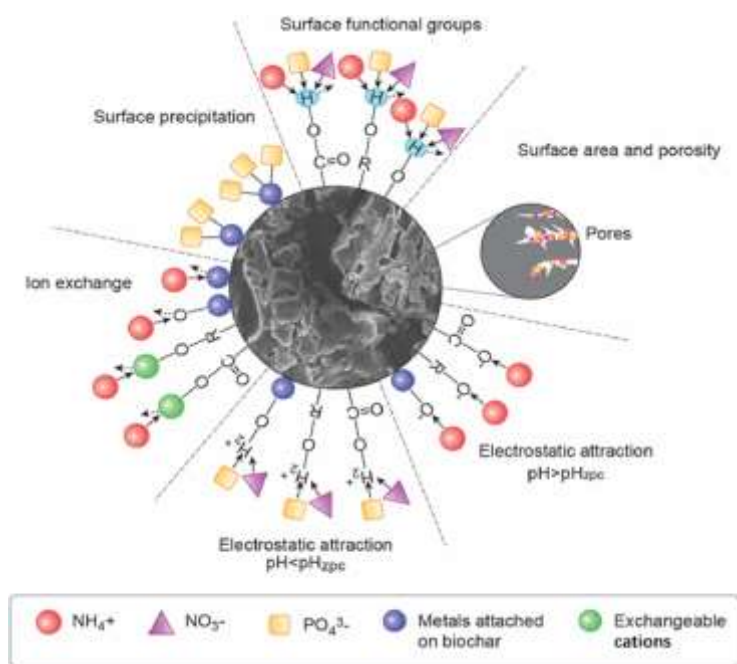
Figure 2.10 Proposed mechanisms associated with NH_4^+-N, NO_3^--N, and $PO_4^{3-}-P$ adsorption by biochar (Zhang et al., 2020).

Different solid adsorbent materials exhibit varying adsorption of P. Surface modification techniques have been developed to effectively remove P from water with adsorbents (Fang et al., 2018). In particular, biochar modified with lanthanum/iron oxide (hydroxide) has been successfully applied for the removal of phosphate pollutants. As reported by Fu et al. (2018), a novel lanthanum (La)-based magnetic adsorbent was used to remove phosphate from wastewater and reduced the phosphate concentration in real domestic wastewater to less than 0.02 mg/L from an initial phosphate concentration of 1.7 mg/L. The concentration of La/Fe, and the process used, were optimized to enhance phosphate sorption capacities and recovery; $La(OH)_3/Fe_3O_4$ efficiently reduced the PO_4^{3-} concentration to below 0.05 mg P/L (Wu et al., 2017). The iron-free release and good reusability of the utilized adsorbents support the large-scale applicability of the La/Fe composites (Singh et al., 2021). Although the adsorbent amended by La/Fe can remove PO_4^{3-} well and can be easily separated from aqueous solution using applied magnetic fields in wastewater (Wu et al., 2017), it is difficult to implement this separation technology for large-scale engineering applications. Overall, the performance of biochar needs to be further improved to overcome various challenges for wide-scale application in N and P removal. To demonstrate the effect of modified biochars on N and P removal, factors affecting the adsorption process, such as surface functional group interaction, ion exchange, surface area, and precipitation, are presented in Fig. 2.10.

2.4.2.4 Emerging contaminants (ECs)

The extensive presence of microplastics (MPs) and antibiotics in aquatic environments has recently been identified as a major global challenge (Li et al., 2022). However, the coexistence of polyethylene MPs and biochar can increase ammonium adsorption from an aqueous solution (Li et al., 2021). MPs are derived from plastic wastes and have attracted wide attention worldwide due to their wide distribution, easy transformation, and potential threats to living organisms (Wang et al., 2021b; Wu et al., 2021a). A recent study tested the removal of polystyrene microspheres (1 µm, 100 mg/mL) in an aqueous solution using magnetic biochar (MBC) and MBC modified with Mg or Zn; removal rates of 94.81%, 98.75%, and 99.46%, respectively were achieved (Wang et al., 2021b). Wang et al. (2020b) showed that biochar filters provide significant capacity for removal and immobilization of 10 µm diameter microplastic spheres (above 95%) which was much greater than that of a similar grain-sized sand filter.

Advances in engineering have further improved the remediation efficiency of biochar by developing novel interactions and binding capabilities with antibiotic contaminants, such as chemical/metal composite modifications that improve the catalytic activity of biochar (Kumar Patel et al., 2022). The overuse and misuse of antibiotics for disease treatment and growth enhancement in animal farming are major drivers of the occurrence, spread, and accumulation of antibiotic resistance genes (ARGs) in wastewater (Fu et al., 2022), hence, there is a growing need for materials to target removal of these harmful pollutants. With the increasingly widespread contamination of antibiotics, improving the catalytic degradation efficiency of antibiotics has become a key research direction (Li et al., 2022). Mei et al. (2021) prepared a Fe–N modified biochar following a one-pot pyrolysis method at 700°C, which demonstrated good adsorption of tetracycline (TC). The Fe–N modified biochar contained more functional groups, graphited-carbon structure, and magnetic components than the raw one which exhibited a maximum TC adsorption capacity of 156 mg/g. The relevant removal mechanisms include hydrogen bonding, pore filling, and surface complexation (Mei et al., 2021). Low pyrolysis temperature was found to have a great influence on TC removal. Magnetic porous biochars were prepared from tea waste pyrolyzed at different temperatures and tested for TC removal, and the results showed that the pyrolysis process significantly influenced the physicochemical properties of the materials. The optimal temperature (at 700°C) produced the material with the

highest surface area (1066 m^2/g) and pore volume (2.693 cm^3/g) (Li et al., 2022). The adsorption capacity of 333.22 mg/g, was explained by excellent surface area, pore-filling, pore-volume, π-π interaction, complexation, and hydrogen bonding properties (Li et al., 2022). In another study, a nitrogen and copper co-doped biochar (N-Cu/biochar) material was prepared, and persulfate activation for tetracycline degradation was proposed (Zhong et al., 2020). Additionally, Fe^{2+}, persistent free radicals (PFRs) on iron-modified biochar can be used as effective activators to generate reactive oxygen species (ROS) (e.g., ·OH, ^{1}O$_2$, and SO$_4$·$^-$), which can effectively degrade tetracycline and bisphenol A (Jiang et al., 2018). Through quenching and electron, paramagnetic resonance experiments verified the reaction pathway mechanisms was ·HO via PFRs in the system. The non-radical pathway of electron transfer between tetracycline and persulfate on the surface of the catalyst can lead to tetracycline degradation (Zhang and Wang, 2021).

Other water-borne pollutants, including radioactive contaminants (e.g. caesium, plutonium, strontium, uranium) (Sun et al., 2022b; Younis et al., 2020), inorganic acid salt (sulphate ion), fluoride, cyanide, and inorganic toxic chemicals can also be targeted by biochar (Sadhu et al., 2021). Younis et al. (2020) used biochar prepared from rice straw for the removal of barium/strontium from saline and found an enhanced ability to capture Sr(II)/Ba(II) ions with adsorption energies ranging from 0.61~0.89 kJ/mol. Oxidation modification can further improve the adsorption performance of biochar to U(VI) (Sun et al., 2022b). The increased formation of carbon-oxygen functional groups on the surface of oxidized biochar results in a maximum adsorption capacity of 490.2 mg/g for U(VI), higher than that of most reported adsorbent materials (Sun et al., 2022b). Sulphate ions are widely distributed in surface water, groundwater, and industrial wastewater. Although sulphate ions are generally considered non-toxic, they can cause harm to live organisms and the environment. A zirconium (Zr) oxide-modified biochar was synthesized to adsorb sulphate ions from an aqueous solution with a maximum sulphate adsorption capacity of 35.21 mg/g, with kinetic behaviour that was following the Langmuir model and pseudo-second-order rate equation (Ao et al., 2020). The potential application of biochar for fluoride removal during drinking water treatment has also been reported (Sadhu et al., 2021).

In summary, the ultimate goal is to apply contaminant removal strategies to realistic wastewater treatment conditions for optimal utilization of biochar (Jia et al., 2022).

2.4.3 Biochar application in wastewater treatment

Sustainable management of the environment and agriculture is essential to protect soil, water, and air in intensive agricultural practices and industrial activities (Kazemi Shariat Panahi et al., 2020). In recent work, biochar has been applied in constructed wetlands, paddy field wetlands, and sewage treatment plants.

2.4.3.1 Constructed wetlands

Biochar has been widely applied for wastewater treatment in constructed wetlands (CWs). One study systematically evaluated the impact of biochar addition on the sustainable operation of aerated CWs through the evaluation of typical pollutant removal, enzyme activity, and microbial secretion/structure analysis (Feng et al., 2022). The experimental results revealed a 92.63% removal rate of NH_4^+–N, 89.89% for TN, and > 95.0% reduction of heavy metals in aerated CWs with biochar addition, however, the efficacy of nitrogen removal (NH_4^+–N: 74.58%; TN: 58.52%) decreased significantly in the presence of Cr and Cu in the influent (Feng et al., 2022). Overall, efficient and stable removal of nutrients is required to meet more stringent emission standards for substances such as N and P. A bench-scale integrated flow constructed wetland (IFCWs) with different filling media was used to study the tertiary treatment of municipal sewage. The results showed the removal rates of NH_4^+–N, TN, and TP by biochar were 89.1±1.5%, 88.1±1.1%, and 75.9±4.5%, respectively. IFCWs constructed with zero-valent iron-biochar (86.4±1.5%, 88.3±0.7%, 91.6±3.8%) were better those of the control group (68.8±7.1%, 62.4±4.6%, 68.1±8.0%). This improvement was mainly because biochar increased the abundance of ammonia monooxygenase genes associated with ammonia-oxidizing bacteria (AOB-amoA), and zero-valent iron-biochar promoted the abundance of nitrate reductase genes (nirK, nirS), nitrous oxide reductase (nosZ), and hydrazine synthetase (hzsA) (Wu et al., 2022). Additional, principal component analysis (PCA) indicated that higher NH_4^+–N removal efficiency mainly resulted from the enhancement of microbial nitrification by biochar, and the improvement of NO_3^-–N removal efficiency was attributed to the enhanced denitrification and anammox by zero-valent iron (Wu et al., 2022). Biochar shows great potential in treating wetlands (TWs) for the reduction of various pesticides from agricultural runoff, such as chlorantraniliprole (CAP) (Abas et al., 2022). In a mesocosm experiment, the removal of CAP mass by biochar was 90 ~ 99% during the whole experiment, but the long-term efficiency remains to be explored.

2.4.3.2 Paddy field wetlands

Studies of the application of biochar in paddy field wetlands have mostly focused on soil quality improvement such as nutrient use efficiency (Zhang et al., 2022), the remediation of arsenic (As) or cadmium (Cd) contamination (El-Naggar et al., 2022), degradation of chlorinated organic contaminants (Song et al., 2017), mitigation of greenhouse gas emissions (CH_4 and N_2O) (Qin et al., 2016), and reduction of methylmercury uptake by rice grains in soil-rice ecosystems (Hu et al., 2021). Yuan et al. (2022) designed a novel ecological ditch system in the Chengdu Plain (Sichuan province, China), combining earth trenches and cemented channels with iron-containing biochar to reduce N and P losses from farmland. After two years of monitoring, the removal efficiencies of total N and P were 30.7% and 57.8%, respectively. Iron-containing biochar could remove N and P from the drainage system, especially at high concentrations; this effect is mainly attributed to the high adsorption of dissolved N and P components and the interception of particulate nutrients (Jin et al., 2022). However, there have been few studies on the environmental impact and evaluation of runoff water after biochar application in paddy field wetlands, suggesting this area could be the focus of future studies.

2.4.3.3 Sewage treatment

Phosphates in the tailwater of sewage treatment plants are becoming a global concern for sustainable environmental development and resource management (Cui et al., 2022). Phosphorus (P) is one of the most important non-metallic mineral resources on the earth (Cakmak et al., 2022). Current reserves could last until 2315 based on the UN median population projection for current per capita phosphate rock production rate, but only until 2170 if the UN high population estimate is used (Daneshgar et al., 2018). The potential for an imminent phosphorus crisis is of significant concern and considerable research attention has been devoted to the development of effective phosphorus recovery methods (Fu et al., 2018). Current phosphorus recovery and reuse processes are not sufficient to meet the needs of large-scale practical applications. Thus, the selection of the most suitable adsorbent materials for phosphate adsorption requires attention to determine adsorption potential, economic feasibility, local availability, and recycling efficiencies.

■ Batch and column experiments

In recent years, there have been advances in understanding the stability and engineering application of adsorbent composite materials for intermittent and columnar phosphorus removal. Various strategies have been reported to enhance phosphorus adsorption in batch and column tests. Modified biochar of different particle sizes has been prepared using surface-functionalized granulated and large-sized particles for column-based treatment. During granule production, fine particles of compressed powders collect and bind together to form granules. Granules of optimal size and porous shape allow the removal of the appropriate pollutants from water. For example, $MgFe_2O_4$-biochar-based lanthanum alginate microspheres were prepared by gelation via in-situ crosslinking of lanthanum alginate and calcination method and used for PO_4^{3-} removal from aqueous solution (Wang et al., 2020a). Kinetic adsorption comparison of powder and bead-type adsorbents verified favourable mass transfer performance (Wang et al., 2020a). Jung et al. (2016) prepared a granular *Laminaria japonica*-derived biochar via calcium-alginate beads encapsulation, and found this material suitable for column filtration due to its high hydraulic conductivity, making it attractive for use as an adsorbent.

Biochar derived from rice straw and clay, modified with lanthanum/iron-oxide, has been used in a particulate form for effective PO_4^{3-} removal (Sun et al., 2022a). Formable porous biochar loaded with La-Fe(hydr)oxides/montmorillonite has shown efficient removal of phosphorus in wastewater (Sun et al., 2022a); the preparation process of this adsorbent material has been reported by Sun et al. (2022a). Methods that utilize large formable porous biochar in combination with immobilized microorganisms for synergistic phosphorus removal technology may apply to large-scale practical engineering applications.

■ Immobilized microorganisms combined with biochar

Immobilized microbial technology is a new, reusable bioengineering approach that limits free microorganisms in specific areas by physical or chemical means, increasing the local density of microorganisms for high biological activity (Liu et al., 2012; Wu et al., 2021b). Different methods can be used to immobilize cells, including covalent coupling, physical entrapment, cross-linking, and the natural process of adhesion. Biofilm formation after adhesion can result in extremely high cell viability and biochemical activity (Zheng et al., 2009).

Recent advances have been made in the use of immobilized biochar with microbes for wastewater treatment (Pandey et al., 2020). As an immobilized carrier, biochar can adsorb high concentrations of substrates and gradually release them for microbial degradation, acting as a microbial buffer. The denitrification effect of immobilized cells is significantly improved, with total denitrification time being reduced from 24 h to 15 h compared to that of free cells (Liu et al., 2012). Biochar-immobilized microorganisms are synergistic with biochar, allowing improved adsorption and biodegradation. For inorganic substances, this may be due to physical adsorption, ion exchange, electrostatic attraction, precipitation, surface complexation of biochar as it is oxidized or reduced to a lower toxic valence state by microorganisms, precipitation removal, and intracellular accumulation. Du et al. (2016) studied the adsorption capacity and synergistic effect of corn straw biochar as a carrier to immobilize the 4-bromodiphenyl ether (BDE-3) degrading bacterium *Sphingomonas sp. DZ3*. The results showed that biochar had a protective effect on the strain and improved the tolerance of the strain to a higher concentration of BDE-3, with a maximum removal rate of 93%. BDE-3 removal occurs through the surface adsorption of biochar (π-π interaction) and microbial absorption and degradation (Du et al., 2016). The modified biochar has a higher specific surface area and more functional groups, which promotes the immobilization of microorganisms. A complex of modified biochar and *Pseudomonas stutzeri* strain XL-2 showed a good synergistic effect on ammonia nitrogen removal (Yu et al., 2019). A large number of irregular pores and hydrophilic functional groups promoted the immobilization of strain XL-2 on biochar, and the release of Mg^{2+} improved the ammonia oxygenase activity of this strain for NH_4^+–N removal (Yu et al., 2019). A novel Fe_3O_4 nanoparticles/biochar was synthesized and used to immobilize *Pseudomonas putida* bacteria for the removal of CCA, PO_4^{3-}, and NH_4^+ from pharmaceutical effluents, with corresponding removal rates of 82%, 95%, and 85%, respectively (Siddeeg et al., 2019). He et al. (2017) found that Fe_3O_4/biochar nanocomposites exhibited a high adsorption capacity for photosynthetic bacteria (PSB), with significantly enhanced nutrient removal capacities of PSB/Fe_3O_4/biochar agent of 87.5% for NH_4^+ and 92.1% of PO_4^{3-} from wastewater.

The contaminant removal efficiency of biochar-immobilized microorganisms depends largely on environmental factors (Abdel-Fattah et al., 2015), including the initial contaminant concentration, pH, temperature, and contact time. These factors can alter microbial growth or change the characteristics of biochar to influence the removal process. Compared with free-living microorganisms, biochar-immobilized microorganisms showed a stronger removal effect

under different initial pollutant concentrations (Chen et al., 2016). Modified biochar (MRHB) prepared by combining rice husk with magnetite promoted the denitrification performance of *Aquabacterium sp.* XL4 at a low C/N ratio, because MRHB enhances the electron transfer and membrane activity of this strain (Xu et al., 2022b).

As can be seen from the above-mentioned examples, microbial synergistic biochar has been applied for the treatment of the organic matter, heavy metals, ammonia nitrogen, and nitrate-nitrogen in wastewater. However, there have been limited studies on the coordinated removal of P using biochar-immobilized microorganisms, and there is a lack of economic evaluation or cost-benefit analysis for such engineering applications. Thus, it is imperative to develop a new high-efficiency adsorbent composite material for phosphorus removal as part of wastewater treatment technology. The ideal composite material can utilize previously characterized single components and then apply improved combinations of lanthanum/ferric oxide (for adsorption and catalysis) and phosphorus accumulating microorganisms (for bio-adsorption or take up and accumulate phosphorous as part of their biochemical processes, and biochar for adsorption) to prepare reusable materials with more efficient phosphorus resource recovery.

2.4.4 Regeneration and disposal of utilized biochar

2.4.4.1 Regeneration

To remove contaminants as part of a water treatment process, the economic costs of desorption/regeneration and the eventual disposal of adsorbents must be considered (Gupta et al., 2020). Traditional regeneration methods mainly include acid, alkali, and salt treatments, and recently developed regeneration methods include thermal desorption, magnetic separation, dissolution regeneration, advanced oxidation, microwave radiation, and microbial-assisted sorbent regeneration (Baskar et al., 2022). Each approach has advantages and disadvantages. Thermal regeneration is one of the most cost-effective approaches. The use of inorganic reagents for solvent regeneration is expensive although the process requires only mild regeneration conditions, the treatment time is long and the regeneration efficiency is low. Microwave radiation regeneration treatment time is short and the heating temperature is easier to control; there is no thermal inertia, and the porous structure of biochar can be maintained for energy conservation and reduced risk of secondary pollution. Supercritical regeneration is

suitable for the adsorption of highly volatile substances, and there is no solvent pollution problem when supercritical regeneration is performed using CO_2 and water as fluids.

2.4.4.2 Disposal

Although biochar is quite effective for the removal of heavy metals, toxic pollutants, and new pollutants, its post-use treatment is a particular concern, especially when the toxicity levels of new pollutants have not been determined (Hamid et al., 2022). Therefore, these pollutants require further scientific validation before being released into the environment (Shao et al., 2022). The key to improving the efficiency of pollutant desorption is to select appropriate regeneration technology. Factors such as type of adsorbent, pollutant, stability of adsorbent, the toxicity of spent adsorbent, and cost and energy requirements of regeneration process are important to assess the feasibility of industrial-scale applications. Biochar that has bound heavy metals (such as Cr (III), Cd (II), Cu (II), Pb (II), Nickel (II), Zinc (II), Mercury (II), Lead (II)) (Rangabhashiyam et al., 2022) or other emerging contaminants (e.g. sulphonamide antibiotics, ciprofloxacin, tetracycline, carbamazepine, and endocrine-disrupting chemicals) (Boraah et al., 2022) may be directly discharged into the environment, with potential serious harm for ecology and human health.

Although dumping waste adsorbents in landfills is a more traditional management method, the costs of this method should be evaluated, as proper treatment is required to prevent the seepage of toxic substances. The open dumping of waste biochar in developing countries remains a critical issue because of inadequate incineration and engineered landfills. Various factors such as environmental sustainability, carbon sequestration, secondary pollution, and the economic viability of these methods must be characterized for the disposal of used biochar adsorbents.

In many cases, biochar that has absorbed N and P can be reused as a slow-release fertilizer in the field to improve the soil. However, recycling waste biochar is not economically practical due to the huge amount of biochar produced, with high costs and low recovery rates. Some lost powdered biochar will cause secondary pollution to water bodies. Domestic attention to P resource recovery is increasing, but there is a lack of corresponding policy support and market environment, so research in this field remains in the academic research stage, with few engineering practical cases. Pilot-scale research is a key step towards practical application

(Zhang et al., 2021). In recent work, researchers used lanthanum-based polymeric nanocomposite La@201 to establish a pilot-scale adsorption system for P polishing removal with an average processing capacity of 10 m^3/day over 8 months (Zhang et al., 2021). The adsorption system effectively reduced the P concentration below the eutrophication limit (0.02 mg/L), for average removal rates of orthophosphate and total P of 91.23% and 78.51%, respectively. Another possibility is the use of nanoscale biochar, but although this material has high adsorption capacity, it is difficult to recover P resources (Kumar et al., 2020), and there may be environmental pollution effects caused by the entry of nanomaterials into the water, limiting prospects for sustainable development. Formed porous biochar can effectively avoid this phenomenon, and its recycling efficiency is relatively high. As a slow-release fertilizer, this kind of biochar can be directly applied to soil to improve soil aggregates, and pore structure, and as an excellent carrier of dominant microorganisms. Bioengineering biochar into large-scale profitable commodities (e.g., compound fertilizers) can reduce costs while promoting microbe, plant, soil, and environmental benefits (Kochanek et al., 2022).

In conclusion, there is a significant need for additional research into improved methods for the regeneration and recovery of biochar. Corresponding treatment methods need to be formulated to meet the needs of different pollutants targeted by adsorption. Also, developing low-cost technologies to recover contaminants from spent biochar and converting waste biochar into value-added products that can be recycled and reused is a reasonable way to reduce or eliminate the environmental hazards caused by waste biochar.

2.5 Conclusions and future perspectives

This study conducted a comprehensive scientometric review of the research status and development trend of biochar for the removal of pollutants from contaminated water from 2012 to 2021, and significant conclusions were drawn. Overall, there is growing scientific interest in this topic. The total number of biochar preparation-related papers showed a continuous growth trend, with 6149 articles published in 632 journals, covering 98 disciplines during the period. The journal Chemosphere published the most articles, with "Environmental Sciences" being the main discipline category. China has the largest number of publications in this field, with 2906, accounting for 47% of the total publications, indicating that China is at the forefront of this research. The Chinese Academy of Sciences and the University of Florida were identified

as core institutions of this research and played an important role in online dissemination. However, in terms of co-authoring, most work results from intra-institutional cooperation with greater emphasis required for cross-background, cross-institutional, cross-country cooperation, and cross-disciplines in biochar research, to promote mutual learning and diversified development among teams.

This article reviews current research trends using bibliometric analysis and identifies recent developments in understanding biochar adsorption of pollutants and other emerging contaminants from wastewater. There is a focus on strategies for phosphate removal or adsorption, and effective methods of phosphate removal and recovery using biochar and microorganisms are summarized. In addition, the processes of biochar recovery and reuse after the adsorption of water pollutants were compared, with a description of possible secondary environmental pollution. Our analysis suggests some potential research directions for future studies of biochar for the removal of pollutants from contaminated water, as listed below.

- Many low-cost adsorbents have been proposed, but the efficiencies of many sorbents have only been measured in the laboratory. Field-level testing and pilot-scale application are required for the implementation of strategies using biochar as an economical adsorbent for field application. Subsequently, engineering application scenarios of biochar should be compared to verify adsorption capacity with consideration of costs of recycling and regeneration.

- There have been many studies using biochar for the remediation of heavy metals and organic pollutants. In recent years, there has been growing research on emerging pollutants, but most work has focused on the adsorption effect, elemental morphology transformation, and removal mechanism. In the future, more attention should be paid to the combined remediation of heavy metals, organic pollutants, and emerging pollutants. Additionally, more work is required to develop effective disposal methods for waste biochar and monitor toxic and harmful substances throughout the lifetime of biochar.

- To date, global phosphorus resources are very limited, and phosphorus is one of the 20 most important minerals. The efficient management and control of P in natural environments, especially in water bodies, is essential for the balance and stability of

ecosystem both locally and globally. The focus has been on the development of low-cost adsorbents to solve environmental problems, while the full-scale application of biochar adsorbents requires greater insight into the reuse, mass production, pollutant/resource recovery, and management of spent-biochars. In addition, due to the sustainability of microorganisms, it seems that a feasible strategy to recover phosphorus resources is the development of biochar materials designed to effectively utilize microorganisms. Overall, establishing a sustainable market environment and incentive mechanisms with economic feasibility, legal compliance and policy support for phosphorus recycling is essential to explore the recycling of phosphorus resources.

- More in-depth studies are required to investigate the stability, long-term impacts, environmental risks, and life cycle assessment (LCA) of biochar. Advances in the methods and equipment for the preparation of biochar and, strategies to optimize energy use and reduce emissions during the production process are important priorities of current studies. Little work has focused on engineering applications of biochar, and it is necessary to strengthen the long-term combination of scientific theory and practical technology.

References

Abas K, Brisson J, Amyot M, et al. (2022). Effects of plants and biochar on the performance of treatment wetlands for removal of the pesticide chlorantraniliprole from agricultural runoff. Ecological Engineering 175: 106477.

Abdel-Fattah T M, Mahmoud M E, Ahmed S B, et al. (2015). Biochar from woody biomass for removing metal contaminants and carbon sequestration. Journal of Industrial and Engineering Chemistry 22: 103-109.

Ahmad M, Rajapaksha A U, Lim J E, et al. (2014). Biochar as a sorbent for contaminant management in soil and water: a review. Chemosphere 99: 19-33.

Ahmed M B, Zhou J L, Ngo H, et al. (2018). Sorption of hydrophobic organic contaminants on functionalized biochar: Protagonist role of pi-pi electron-donor-acceptor interactions and hydrogen bonds. Journal of Hazardous Materials 360: 270-278.

Ao H, Cao W, Hong Y, et al. (2020). Adsorption of sulphate ion from water by zirconium oxide-modified biochar derived from pomelo peel. Science of the Total Environment 708: 135092.

Arif M, Liu G, Yousaf B, et al. (2021). Synthesis, characteristics and mechanistic insight into the clays and clay minerals-biochar surface interactions for contaminants removal-A review. Journal of Cleaner Production 310: 127548.

Ates F, Tezcan Un U, (2013). Production of char from hornbeam sawdust and its performance evaluation in the dye removal. Journal of Analytical and Applied Pyrolysis 103: 159-166.

Baskar AV, Bolan N, Hoang S A, et al. (2022). Recovery, regeneration and sustainable management of spent adsorbents from wastewater treatment streams: A review. Science of the Total Environment 822: 153555.

Batool S, Shah A A, Abu Bakar A F, et al. (2022). Removal of organochlorine pesticides using zerovalent iron supported on biochar nanocomposite from Nephelium lappaceum (Rambutan) fruit peel waste. Chemosphere 289: 133011.

Boraah N, Chakma S, Kaushal P, (2022). Attributes of wood biochar as an efficient adsorbent for remediating heavy metals and emerging contaminants from water: A critical review and bibliometric analysis. Journal of Environmental Chemical Engineering 10: 107825.

Bouabidi Z B, El-Naas M H., Zhang Z, (2018). Immobilization of microbial cells for the biotreatment of wastewater: A review. Environmental Chemistry Letters 17: 241-257.

Cakmak E K, Hartl M, Kisser J, et al. (2022). Phosphorus mining from eutrophic marine environment towards a blue economy: The role of bio-based applications. Water Research 219: 118505.

Castro J S, Assemany P, Carneiro A C O, et al. (2021). Hydrothermal carbonization of microalgae biomass produced in agro-industrial effluent: Products, characterization and applications. Science of the Total Environment 768: 144480.

Chen H, Gao Y, Li J, et al. (2022). Engineered biochar for environmental decontamination in aquatic and soil systems: a review. Carbon Research 1:4.

Chen L, Chen X L, Zhou C H, et al. (2017). Environmental-friendly montmorillonite-biochar composites: Facile production and tuneable adsorption-release of ammonium and phosphate. Journal of Cleaner Production 156: 648-659.

Chen T, Luo L, Deng S, et al. (2018). Sorption of tetracycline on H_3PO_4 modified biochar derived from rice straw and swine manure. Bioresour Technol 267: 431-437.

Chen Y, Yu B, Lin J, et al. (2016). Simultaneous adsorption and biodegradation (SAB) of diesel oil using immobilized *Acinetobacter venetianus* on porous material. Chemical Engineering Journal 289: 463-470.

Cui J, Li J, Cui J W, et al. (2022). Removal effects of a biomass bottom ash composite on tailwater phosphate and its application in a rural sewage treatment plant. Science of the Total Environment 812: 152549.

Dai L, Zhu W, He L, et al. (2018). Calcium-rich biochar from crab shell: An unexpected super adsorbent for dye removal. Bioresour Technol 267: 510-516.

Daneshgar S, Callegari A, Capodaglio A G, et al. (2018). The Potential Phosphorus Crisis: Resource Conservation and Possible Escape Technologies: A Review. Resources 7: 37.

Ding Y, Zhang J, He Q, et al. (2019). The application and validity of various reaction kinetic models on woody biomass pyrolysis. Energy 179: 784-791.

El-Naggar A, Chen Z H, Jiang W T, et al. (2022). Biochar effectively remediates Cd contamination in acidic or coarse- and medium-textured soils: A global meta-analysis. Chemical Engineering Journal 442: 136225.

Fang L, Liu R, Li J, et al. (2018). Magnetite/Lanthanum hydroxide for phosphate sequestration and recovery from lake and the attenuation effects of sediment particles. Water Research 130: 243-254.

Feng L K, He S F, Zhao W X, et al. (2022). Can biochar addition improve the sustainability of intermittent aerated constructed wetlands for treating wastewater containing heavy metals? Chemical Engineering Journal 444: 136636.

Feng Y F, Sun H J, Han L F, et al. (2019). Fabrication of hydrochar based on food waste (FWHTC) and its application in aqueous solution rare earth ions adsorptive removal: Process, mechanisms and disposal methodology. Journal of Cleaner Production 212: 1423-1433.

Feng Z Q, Yuan R F, Wang F, et al. (2021). Preparation of magnetic biochar and its application in catalytic degradation of organic pollutants: A review. Science of the Total Environment 765: 142673.

Freeman A, Lilly M D, (1998). Effect of processing parameters on the feasibility and operational stability of immobilized viable microbial cells. Enzyme and Microbial Technology 23: 335-345.

Fu H Y, Yang Y X, Zhu R L, et al. (2018). Superior adsorption of phosphate by ferrihydrite-coated and lanthanum decorated magnetite. Journal of Colloid and Interface Science 530: 704-713.

Fu Y H, Wang F, Wang Z Q, et al. (2022). Application of magnetic biochar/quaternary phosphonium salt to combat the antibiotic resistome in livestock wastewater. Science of the Total Environment 811: 151386.

Ghodszad L, Reyhanitabar A, Maghsoodi M R, et al. (2021). Biochar affects the fate of phosphorus in soil and water: A critical review. Chemosphere 283: 131176.

Goncalves M G, da Silva Veiga P A, Fornari M R, et al. (2020). Relationship of the physicochemical properties of novel ZnO/biochar composites to their efficiencies in the degradation of sulfamethoxazole and methyl orange. Science of the Total Environment 748: 141381.

Gupta S, Sireesha S, Sreedhar I, et al. (2020). Latest trends in heavy metal removal from wastewater by biochar-based sorbents. Journal of Water Process Engineering 38: 101561.

Güzel F, Sayğılı H, Akkaya Sayğılı G, et al. (2017). Optimal oxidation with nitric acid of biochar derived from pyrolysis of weeds and its application in removal of hazardous dye methylene blue from aqueous solution. Journal of Cleaner Production 144: 260-265.

Hamid Y, Liu L, Usman M, et al. (2022). Functionalized biochars: synthesis, characterization, and applications for removing trace elements from water. Journal of Hazardous Materials 437: 129337.

He M J, Xu Z B, Hou D Y, et al. (2022a). Waste-derived biochar for water pollution control and sustainable development. Nature Reviews Earth & Environment 3: 444-460.

He S Y, Zhong L H, Duan J J, et al. (2017). Bioremediation of Wastewater by Iron Oxide-Biochar Nanocomposites Loaded with Photosynthetic Bacteria. Front Microbiol 8: 823.

He Y Q, Zhou Q X, Mo F, et al. (2022b). Bioelectrochemical degradation of petroleum hydrocarbons: A critical review and future perspectives. Environ Pollut 306: 119344.

Hu H L, Xi B D, Tan W B, (2021). Effects of sulphur-rich biochar amendment on microbial methylation of mercury in rhizosphere paddy soil and methylmercury accumulation in rice. Environ Pollut 286: 117290.

Imran M, Khan Z U H, Iqbal M M, et al. (2020). Effect of biochar modified with magnetite nanoparticles and HNO_3 for efficient removal of Cr(VI) from contaminated water: A batch and column scale study. Environ Pollut 261: 114231.

Islam M S, Kwak J H, Nzediegwu C, et al. (2021). Biochar heavy metal removal in aqueous solution depends on feedstock type and pyrolysis purging gas. Environ Pollut 281: 117094.

Ji J Q, Yuan X Z, Zhao Y L, et al. (2022a). Mechanistic insights of removing pollutant in adsorption and advanced oxidation processes by sludge biochar. Journal of Hazardous Materials 430: 128375.

Ji M Y, Wang X X, Usman M, et al. (2022b). Effects of different feedstocks-based biochar on soil remediation: A review. Environmental Pollution 294: 118655.

Jia Y Q, Sun S H, Wang S, et al. (2022). Phosphorus in water: A review on the speciation analysis and species-specific removal strategies. Critical Reviews in Environmental Science and Technology, 1-22.

Jiang S F, Ling L L, Chen W J, et al. (2018). Highly efficient removal of bisphenol A in a peroxymonosulfate/iron functionalized biochar system: mechanistic elucidation and quantification of the contributors. Chemical Engineering Journal 359: 572-583.

Jiang S, Huang L, Nguyen T A, et al. (2016). Copper and zinc adsorption by softwood and hardwood biochars under elevated sulphate-induced salinity and acidic pH conditions. Chemosphere 142: 64-71.

Jiao Y X, Li D Y, Wang M, et al. (2021). A scientometric review of biochar preparation research from 2006 to 2019. Biochar 3: 283-298.

Jin J Y, Tian X, Liu G L, et al. (2022). Novel ecological ditch system for nutrient removal from farmland drainage in plain area: Performance and mechanism. Journal of Environmental Management 318: 115638.

Jung K W, Jeong T U, Kang H J, et al. (2016). Characteristics of biochar derived from marine macroalgae and fabrication of granular biochar by entrapment in calcium-alginate beads for phosphate removal from aqueous solution. Bioresource Technology 211: 108-116.

Kamali M, Jahaninafard D, Mostafaie A, et al. (2020). Scientometric analysis and scientific trends on biochar application as soil amendment. Chemical Engineering Journal 395: 125128.

Kang J K, Seo E J., Lee C G, et al. (2021). Fe-loaded biochar obtained from food waste for enhanced phosphate adsorption and its adsorption mechanism study via spectroscopic and experimental approach. Journal of Environmental Chemical Engineering 9: 105751.

Kazemi Shariat Panahi H, Dehhaghi M, Ok Y S, et al. (2020). A comprehensive review of engineered biochar: Production, characteristics, and environmental applications. Journal of Cleaner Production 270: 122462.

Khasawneh O F S, Palaniandy P, (2021). Occurrence and removal of pharmaceuticals in wastewater treatment plants. Process Safety and Environmental Protection 150: 532-556.

Kim J Y, Oh S, Park Y K, (2020). Overview of biochar production from preservative-treated wood with detailed analysis of biochar characteristics, heavy metals behaviours, and their ecotoxicity. Journal of Hazardous Materials 384: 121356.

Kishor R, Purchase D, Saratale G D, et al. (2021). Ecotoxicological and health concerns of persistent colouring pollutants of textile industry wastewater and treatment approaches for environmental safety. Journal of Environmental Chemical Engineering 9: 105012.

Kochanek J, Soo R M, Martinez C, et al. (2022). Biochar for intensification of plant-related industries to meet productivity, sustainability and economic goals: A review. Resources, Conservation and Recycling 179: 106109.

Kumar A, Singh E, Mishra R, et al. (2022). Biochar as environmental armour and its diverse role towards protecting soil, water and air. Science of the Total Environment 806: 150444.

Kumar M, Xiong X N, Wan Z H, et al. (2020). Ball milling as a mechanochemical technology for fabrication of novel biochar nanomaterials. Bioresour Technol 312: 123613.

Kumar Patel A, Katiyar R, Chen C W, et al. (2022). Antibiotic bioremediation by new generation biochar: Recent updates. Bioresour Technol 358: 127384.

Kwak J H, Islam M S, Wang S, et al. (2019). Biochar properties and lead(II) adsorption capacity depend on feedstock type, pyrolysis temperature, and steam activation. Chemosphere 231: 393-404.

Lee P K, Kang M J, Jeong Y J, et al. (2020a). Lead isotopes combined with geochemical and mineralogical analyses for source identification of arsenic in agricultural soils surrounding a zinc smelter. Journal of Hazardous Materials 382: 121044.

Lee X J, Lee L Y, Hiew B Y Z, et al. (2020b). Valorisation of oil palm wastes into high yield and energy content biochars via slow pyrolysis: Multivariate process optimisation and combustion kinetic studies. Materials Science for Energy Technologies 3: 601-610.

Li B, Zhang Y, Xu J, et al. (2022). Facile preparation of magnetic porous biochars from tea waste for the removal of tetracycline from aqueous solutions: Effect of pyrolysis temperature. Chemosphere 291: 132713.

Li H, Luo Q P, Zhao S, et al. (2022). Watershed urbanization enhances the enrichment of pathogenic bacteria and antibiotic resistance genes on microplastics in the water environment. Environmental Pollution 313: 120185.

Li H Y, Cui S H, Tan Y, et al. (2022). Synergistic effects of ball-milled biochar-supported exfoliated LDHs on phosphate adsorption: Insights into role of fine biochar support. Environ Pollut 294: 118592.

Li X N, Jiang X, Song Y, et al. (2021). Coexistence of polyethylene microplastics and biochar increases ammonium sorption in an aqueous solution. Journal of Hazardous Materials 405: 124260.

Li, Y, Tsend N, Li T, et al. (2019). Microwave assisted hydrothermal preparation of rice straw hydrochars for adsorption of organics and heavy metals. Bioresour Technol 273: 136-143.

Liu J, Yang X Y, Liu H H, et al. (2021a). Mixed biochar obtained by the co-pyrolysis of shrimp shell with corn straw: Co-pyrolysis characteristics and its adsorption capability. Chemosphere 282: 131116.

Liu M Y, Zhu J, Yang X, et al. (2022). Biochar produced from the straw of common crops simultaneously stabilizes soil organic matter and heavy metals. Science of the Total Environment 828: 154494.

Liu T, Cui K P, Chen Y H, et al. (2021b). Removal of chlorophenols in the aquatic environment by activation of peroxymonosulfate with nMnO$_x$@Biochar hybrid composites: Performance and mechanism. Chemosphere 283: 131188.

Liu Y, Gan L, Chen Z L, et al. (2012). Removal of nitrate using *Paracoccus sp.* YF1 immobilized on bamboo carbon. Journal of Hazardous Materials 229-230: 419-425.

Luo Z R, Yao B, Yang X, et al. (2021). Novel insights into the adsorption of organic contaminants by biochar: A review. Chemosphere 287: 132113.

M. Siddeeg S, A. Tahoon, M, Ben Rebah F, 2019. Simultaneous removal of calconcarboxylic acid, NH$_4^+$ and PO$_4^{3-}$ from pharmaceutical effluent using iron oxide-biochar nanocomposite loaded with pseudomonas putida. Processes 7: 800.

Ma Y F, Lu T M, Yang L, et al. (2022). Efficient adsorptive removal of fluoroquinolone antibiotics from water by alkali and bimetallic salts co-hydrothermally modified sludge biochar. Environ Pollut 298: 118833.

Malyan S K, Kumar S S, Fagodiya R K, et al. (2021). Biochar for environmental sustainability in the energy-water-agroecosystem nexus. Renewable and Sustainable Energy Reviews 149: 111379.

Menesguen A, Desmit X, Duliere V, et al. (2018). How to avoid eutrophication in coastal seas? A new approach to derive river-specific combined nitrate and phosphate maximum concentrations. Science of the Total Environment 628-629: 400-414.

Mohan D, Sarswat A, Ok Y S, et al. (2014). Organic and inorganic contaminants removal from water with biochar, a renewable, low cost and sustainable adsorbent – A critical review. Bioresource Technology 160: 191-202.

Mollick S, Fajal S, Saurabh S, et al. (2020). Nanotrap grafted anion exchangeable hybrid materials for efficient removal of toxic oxyanions from water. ACS Cent Sci 6: 1534-1541.

Nageshwari K, Balasubramanian P, (2022). Evolution of struvite research and the way forward in resource recovery of phosphates through scientometric analysis. Journal of Cleaner Production 357: 131737.

Ngambia A, Ifthikar J, Shahib I, et al. (2019). Adsorptive purification of heavy metal contaminated wastewater with sewage sludge derived carbon-supported Mg(II) composite. Science of the Total Environment 691: 306-321.

Othmani A, John J, Rajendran H, et al. (2021). Biochar and activated carbon derivatives of lignocellulosic fibres towards adsorptive removal of pollutants from aqueous systems: Critical study and future insight. Separation and Purification Technology 274: 119062.

Pandey D, Daverey A, Arunachalam K, (2020). Biochar: Production, properties and emerging role as a support for enzyme immobilization. Journal of Cleaner Production 255: 120267.

Park J H, Wang J J, Xiao R, et al. (2018). Effect of pyrolysis temperature on phosphate adsorption characteristics and mechanisms of crawfish char. J Colloid Interface Sci 525: 143-151.

Patel A K, Singhania R R, Pal A, et al. (2022). Advances on tailored biochar for bioremediation of antibiotics, pesticides and polycyclic aromatic hydrocarbon pollutants from aqueous and solid phases. Science of the Total Environment 817: 153054.

Patra B R, Nanda S, Dalai A K, et al. (2021). Taguchi-based process optimization for activation of agro-food waste biochar and performance test for dye adsorption. Chemosphere 285: 131531.

Prasannamedha G, Kumar P S, Mehala R, et al. (2021). Enhanced adsorptive removal of sulfamethoxazole from water using biochar derived from hydrothermal carbonization of sugarcane bagasse. Journal of Hazardous Materials 407: 124825.

Premarathna K S D, Rajapaksha A U, Sarkar B, et al. (2019). Biochar-based engineered composites for sorptive decontamination of water: A review. Chemical Engineering Journal 372: 536-550.

Qin X B, Li Y, Wang H, et al. (2016). Long-term effect of biochar application on yield-scaled greenhouse gas emissions in a rice paddy cropping system: A four-year case study in south China. Science of the Total Environment 569-570: 1390-1401.

Quispe J I B, Campos L C, Mašek O, et al. (2022). Use of biochar-based column filtration systems for greywater treatment: A systematic literature review. Journal of Water Process Engineering 48: 102908.

Rajapaksha A U, Selvasembian R, Ashiq A, et al. (2022). A systematic review on adsorptive removal of hexavalent chromium from aqueous solutions: Recent advances. Science of the Total Environment 809: 152055.

Ramola S, Belwal T, Li C J, et al. (2020). Improved lead removal from aqueous solution using novel porous bentonite - and calcite-biochar composite. Science of the Total Environment 709: 136171.

Rangabhashiyam S, dos Santos Lins P, de Magalhães Oliveira L, et al. (2022). Sewage sludge-derived biochar for the adsorptive removal of wastewater pollutants: A critical review. Environ Pollut 293: 118581.

Rangarajan G, Jayaseelan A, Farnood R, (2022). Photocatalytic reactive oxygen species generation and their mechanisms of action in pollutant removal with biochar supported photocatalysts: A review. Journal of Cleaner Production 346: 131155.

Rangabhashiyam S, Balasubramanian P, (2019). The potential of lignocellulosic biomass precursors for biochar production: Performance, mechanism and wastewater application – A review. Industrial Crops and Products 128: 405-423.

Sadhu M, Bhattacharya P, Vithanage M, et al. (2021). Adsorptive removal of fluoride using biochar – A potential application in drinking water treatment. Separation and Purification Technology 278: 119106.

Sakhiya A K, Baghel P, Anand A, et al. (2021). A comparative study of physical and chemical activation of rice straw derived biochar to enhance Zn^{2+} adsorption. Bioresource Technology Reports 15: 100774.

Sewu D, Jung H, Kim S S, et al. (2019). Decolorization of cationic and anionic dye-laden wastewater by steam-activated biochar produced at an industrial-scale from spent mushroom substrate. Bioresour Technol 277: 77-86.

Shakya A, Nunez-Delgado A, Agarwal T, (2019). Biochar synthesis from sweet lime peel for hexavalent chromium remediation from aqueous solution. Journal of Environmental Management 251: 109570.

Shao B B, Liu Z F, Tang L, et al. (2022). The effects of biochar on antibiotic resistance genes (ARGs) removal during different environmental governance processes: A review. Journal of Hazardous Materials 435: 129067.

Shen Y F, Ma D C, Ge X L, (2017). CO_2-looping in biomass pyrolysis or gasification. Sustainable Energy & Fuels 1: 1700-1729.

Singh N, Khandelwal N, Ganie Z A, et al. (2021). Eco-friendly magnetic biochar: An effective trap for nanoplastics of varying surface functionality and size in the aqueous environment. Chemical Engineering Journal 418: 129405.

Song Y, Bian Y R, Wang F, et al. (2017). Effects of biochar on dechlorination of hexachlorobenzene and the bacterial community in paddy soil. Chemosphere 186: 116-123.

Song Z G, Lian F, Yu Z H, et al. (2014). Synthesis and characterization of a novel MnO_x-loaded biochar and its adsorption properties for Cu^{2+} in aqueous solution. Chemical Engineering Journal 242: 36-42.

Sullivan G L, Prigmore R M, Knight P, et al. (2019). Activated carbon biochar from municipal waste as a sorptive agent for the removal of polyaromatic hydrocarbons (PAHs), phenols and petroleum-based compounds in contaminated liquids. Journal of Environmental Management 251: 109551.

Sun E H, Zhang Y, Xiao Q B, et al. (2022a). Formable porous biochar loaded with La-Fe(hydr)oxides/montmorillonite for efficient removal of phosphorus in wastewater: process and mechanisms. Biochar 4: 53.

Sun Y W, Zeng B Y, Dai Y T, et al. (2022b). Modification of sludge-based biochar using air roasting-oxidation and its performance in adsorption of uranium(VI) from aqueous solutions. J Colloid Interface Sci 614: 547-555.

Tan X F, Liu Y G, Zeng G M, et al. (2015). Application of biochar for the removal of pollutants from aqueous solutions. Chemosphere 125: 70-85.

Tan X F, Liu S B, Liu Y G, et al. (2017). Biochar as potential sustainable precursors for activated carbon production: Multiple applications in environmental protection and energy storage. Bioresour Technol 227: 359-372.

Tsai C Y, Lin P Y, Hsieh S L, et al. (2022). Engineered mesoporous biochar derived from rice husk for efficient removal of malachite green from wastewaters. Bioresour Technol 347: 126749.

Tseng C H, Lee I H, Chen Y C, (2019). Evaluation of hexavalent chromium concentration in water and its health risk with a system dynamics model. Science of the Total Environment 669: 103-111.

Tu R, Jiang E C, Sun Y, et al. (2018). The pelletization and combustion properties of torrefied Camellia shell via dry and hydrothermal torrefaction: A comparative evaluation. Bioresour Technol 264: 78-89.

Ullah F, Ji G Z, Irfan M, et al. (2022). Adsorption performance and mechanism of cationic and anionic dyes by KOH activated biochar derived from medical waste pyrolysis. Environmental Pollution 314: 120271.

Viglasova E, Galambos M, Dankova Z, et al. (2018). Production, characterization and adsorption studies of bamboo-based biochar/montmorillonite composite for nitrate removal. Waste Management 79: 385-394.

Wądrzyk M, Grzywacz P, Janus R, et al. (2021). A two-stage processing of cherry pomace via hydrothermal treatment followed by biochar gasification. Renewable Energy 179: 248-261.

Wan Mahari W A, Waiho K, Azwar E, et al. (2022). A state-of-the-art review on producing engineered biochar from shellfish waste and its application in aquaculture wastewater treatment. Chemosphere 288: 132559.

Wang B Y, Fu H B, Han L F, et al. (2021a). Physicochemical properties of aged hydrochar in a rice-wheat rotation system: A 16-month observation. Environ Pollut 272: 116037.

Wang B, Lehmann J, Hanley K, et al. (2016). Ammonium retention by oxidized biochars produced at different pyrolysis temperatures and residence times. RSC Advances 6: 41907-41913.

Wang H Y, Gao B, Wang S S, et al. (2015a). Removal of Pb(II), Cu(II), and Cd(II) from aqueous solutions by biochar derived from $KMnO_4$ treated hickory wood. Bioresour Technol 197: 356-362.

Wang H B, Liu Y, Ifthikar J, et al. (2018). Towards a better understanding on mercury adsorption by magnetic bio-adsorbents with gamma-Fe_2O_3 from pinewood sawdust derived hydrochar: Influence of atmosphere in heat treatment. Bioresour Technol 256: 269-276.

Wang H X, Wang X Y, Teng H W, et al. (2022). Purification mechanism of city tail water by constructed wetland substrate with NaOH-modified corn straw biochar. Ecotoxicology and Environmental Safety 238: 113597.

Wang J, Sun C, Huang Q X, et al. (2021b). Adsorption and thermal degradation of microplastics from aqueous solutions by Mg/Zn modified magnetic biochars. Journal of Hazardous Materials 419: 126486.

Wang L, Wang J Y, Yan W, et al. (2020a). $MgFe_2O_4$-biochar based lanthanum alginate beads for advanced phosphate removal. Chemical Engineering Journal 387: 123305.

Wang L, Wang Y J, Ma F, et al. (2019). Mechanisms and reutilization of modified biochar used for removal of heavy metals from wastewater: A review. Science of the Total Environment 668: 1298-1309.

Wang Z H, Guo H Y, Shen F, et al. (2015b). Biochar produced from oak sawdust by Lanthanum (La)-involved pyrolysis for adsorption of ammonium (NH_4^+), nitrate (NO_3^-), and phosphate (PO_4^{3-}). Chemosphere 119: 646-653.

Wang Z H, Sedighi M, Lea-Langton A, (2020b). Filtration of microplastic spheres by biochar: removal efficiency and immobilisation mechanisms. Water Research 184: 116165.

Wu J W, Wang T, Zhang Y S, et al. (2019). The distribution of Pb(II)/Cd(II) adsorption mechanisms on biochars from aqueous solution: Considering the increased oxygen functional groups by HCl treatment. Bioresour Technol 291: 121859.

Wu J J, Zheng J J, Ma K, et al. (2022). Tertiary treatment of municipal wastewater by a novel flow constructed wetland integrated with biochar and zero-valent iron. Journal of Water Process Engineering 47: 102777.

Wu M, Jiang Y, Kwong R W M, et al. (2021a). How do humans recognize and face challenges of microplastic pollution in marine environments? A bibliometric analysis. Environ Pollut 280: 116959.

Wu P, Wang Z Y, Bhatnagar A, et al. (2021b). Microorganisms-carbonaceous materials immobilized complexes: Synthesis, adaptability and environmental applications. Journal of Hazardous Materials 416: 125915.

Xi H, Zhang X J, Zhang A H, et al. (2022). Concurrent removal of phosphate and ammonium from wastewater for utilization using Mg-doped biochar/bentonite composite beads. Separation and Purification Technology 285: 120399.

Xiao J, Hu R, Chen G C, et al. (2020). Facile synthesis of multifunctional bone biochar composites decorated with Fe/Mn oxide micro-nanoparticles: Physicochemical properties, heavy metals sorption behaviour and mechanism. Journal of Hazardous Materials 399: 123067.

Xiao L Z, Chen B L, Schnoor L J, et al. (2018). Insight into Multiple and Multilevel Structures of Biochars and Their Potential Environmental Applications: A Critical Review. Environmental Science & Technology 52: 5027-5047.

Xu J, Zhang Y, Li B, et al. (2022a). Improved adsorption properties of tetracycline on KOH/KMnO$_4$ modified biochar derived from wheat straw. Chemosphere 296: 133981.

Xu L, Su J F, Ali A, et al. (2022b). Magnetite-loaded rice husk biochar promoted the denitrification performance of *Aquabacterium sp.* XL4 under low carbon to nitrogen ratio: Optimization and mechanism. Bioresour Technol 348: 126802.

Xu X Y, Cao X D, Zhao L, 2013. Comparison of rice husk- and dairy manure-derived biochars for simultaneously removing heavy metals from aqueous solutions: Role of mineral components in biochars. Chemosphere 92: 955-961.

Xue Y W, Gao B, Yao Y, et al. (2012). Hydrogen peroxide modification enhances the ability of biochar (hydrochar) produced from hydrothermal carbonization of peanut hull to remove aqueous heavy metals: Batch and column tests. Chemical Engineering Journal 200-202: 673-680.

Yan Y B, Sarkar B, Zhou L, et al. (2020). Phosphorus-rich biochar produced through bean-worm skin waste pyrolysis enhances the adsorption of aqueous lead. Environ Pollut 266: 115177.

Yang F, Jian H X, Wang C P, et al. (2021). Effects of biochar on biodegradation of sulfamethoxazole and chloramphenicol by *Pseudomonas stutzeri* and *Shewanella putrefaciens*: Microbial growth, fatty acids, and the expression quantity of genes. Journal of Hazardous Materials 406: 124311.

Yang F, Zhang S S, Sun Y Q, et al. (2018a). Fabrication and characterization of hydrophilic corn stalk biochar-supported nanoscale zero-valent iron composites for efficient metal removal. Bioresour Technol 265: 490-497.

Yang Q, Wang X L, Luo W, et al. (2018b). Effectiveness and mechanisms of phosphate adsorption on iron-modified biochars derived from waste activated sludge. Bioresour Technol 247: 537-544.

Yao Y, Gao B, Inyang M, et al. (2011). Biochar derived from anaerobically digested sugar beet tailings: characterization and phosphate removal potential. Bioresour Technol 102: 6273-6278.

Yoon J Y, Kim J E, Song H J, et al. (2021). Assessment of adsorptive behaviours and properties of grape pomace-derived biochar as adsorbent for removal of cymoxanil pesticide. Environmental Technology & Innovation 21: 101242.

Younis S A, El-Salamony R A, Tsang Y F, et al. (2020). Use of rice straw-based biochar for batch sorption of barium/strontium from saline water: Protection against scale formation in petroleum/desalination industries. Journal of Cleaner Production 250: 119442.

Zhang C, Zeng G M, Huang D L, et al. (2019a). Biochar for environmental management: Mitigating greenhouse gas emissions, contaminant treatment, and potential negative impacts. Chemical Engineering Journal 373: 902-922.

Zhang M, Song G, Gelardi D L, et al. (2020). Evaluating biochar and its modifications for the removal of ammonium, nitrate, and phosphate in water. Water Research 186: 116303.

Zhang S, Lyu H, Tang J C, et al. (2019b). A novel biochar supported CMC stabilized nano zero-valent iron composite for hexavalent chromium removal from water. Chemosphere 217: 686-694.

Zhang S N, Wang J H, (2021). Removal of chlortetracycline from water by Bacillus cereus immobilized on Chinese medicine residues biochar. Environmental Technology & Innovation 24: 101930.

Zhang Y Y, Ahmed S, Zheng Z X, et al. (2021). Validation of pilot-scale phosphate polishing removal from surface water by lanthanum-based polymeric nanocomposite. Chemical Engineering Journal 412: 128630.

Zhang Y P, Zhao H, Hu W, et al. (2022). Understanding how reed-biochar application mitigates nitrogen losses in paddy soil: Insight into microbially-driven nitrogen dynamics. Chemosphere 295: 133904.

Zhao Y J, Liu X T, Li W H, et al. (2022). One-step synthesis of garlic peel derived biochar by concentrated sulfuric acid: Enhanced adsorption capacities for Enrofloxacin and interfacial interaction mechanisms. Chemosphere 290: 133263.

Zheng C L, Zhou J T, Wang J, et al. (2009). Aerobic degradation of nitrobenzene by immobilization of *Rhodotorula mucilaginosa* in polyurethane foam. Journal of Hazardous Materials 168: 298-303.

Zheng Y L, Wan Y S, Chen J J, et al. (2020). MgO modified biochar produced through ball milling: A dual-functional adsorbent for removal of different contaminants. Chemosphere 243: 125344.

Zhong Q F, Lin Q T, Huang R L, et al. (2020). Oxidative degradation of tetracycline using persulfate activated by N and Cu co-doped biochar. Chemical Engineering Journal 380: 122608.

CHAPTER *3*

FORMABLE POROUS BIOCHAR LOADED WITH LA-FE(HYDR)OXIDES/MONTMORILLONITE FOR EFFICIENT REMOVAL OF PHOSPHORUS IN WASTEWATER: PROCESS AND MECHANISMS

CHAPTER 3: FORMABLE POROUS BIOCHAR LOADED WITH LA-FE(HYDR)OXIDES/MONTMORILLONITE FOR EFFICIENT REMOVAL OF PHOSPHORUS IN WASTEWATER: PROCESS AND MECHANISMS

This chapter has been published with the title: Formable porous biochar loaded with La-Fe(hydr)oxides/montmorillonite for efficient removal of phosphorus in wastewater: Process and mechanisms in *Biochar (2022, 4, 53)*. https://doi.org/10.1007/s42773-022-00177-8. The published paper is presented in the following pages.

Graphical Abstract

Preparation technology and phosphorus removal mechanism of the functionalized adsorbent based on formable porous granulated biochar.
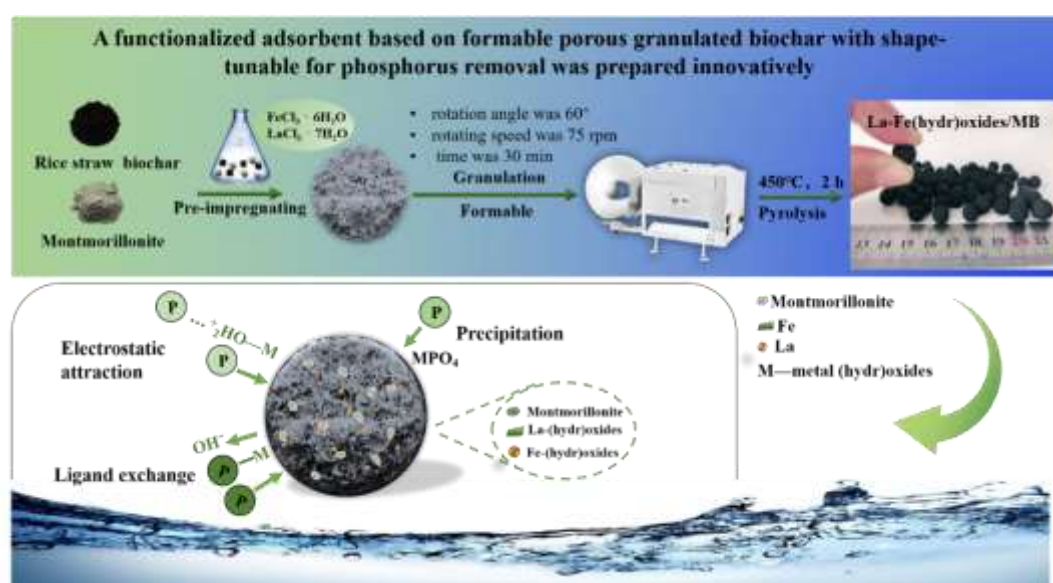
Highlights

✪ Novel formable porous functional biochar (LaFe/MB) was prepared for P removal.

✪ La/Fe oxide provides abundant sorption sites for P and almost no La/Fe leaching.

✪ LaFe/MB presented high compressive strength with high sorption capacity for P.

Abstract

The development of biochar-based granule-like adsorbents suitable for scaled-up application has been attracting increasing attention in the field of water treatment. Herein, a new formable porous granulated biochar loaded with La-Fe(hydr)oxides/montmorillonite (LaFe/MB) was fabricated via a granulation and pyrolysis process for enhanced phosphorus (P) removal from wastewater. Montmorillonite acted as a binder that increased the size of the granulated biochar, while the use of Fe promoted the surface charge and facilitated the dispersion of La, which was responsible for selective phosphate removal. LaFe/MB exhibited rapid phosphate adsorption kinetics and high maximum adsorption capacity (Langmuir model, 52.12 mg P g^{-1}), which are better than that of many existing granulated materials. The desorption and recyclability experiments showed that LaFe/MB could be regenerated, and maintained 76.7% of its initial phosphate adsorption capacity after four adsorption cycles. The high hydraulic endurance strength retention rate of the developed material (91.6%) suggested high practical applicability in actual wastewater. Electrostatic attraction, surface precipitation, inner-sphere complexation via ligand exchange and were found to be involved in selective P removal over a wide pH range of 3 to 9. The thermodynamic parameters were determined, which revealed the feasibility and spontaneity of adsorption. Based on approximate site energy distribution analyses, high distribution frequency contributed to efficient P removal. The research results provide new insight that LaFe/MB shows great application prospects for advanced phosphate removal from wastewater.

Keywords

Formable porous biochar, Montmorillonite, Metal (hydr)oxide, Wastewater phosphate removal, Adsorption mechanism

3.1 Introduction

Phosphorus (P) eutrophication is a growing concern globally (Cakmak et al., 2022). P is a key limiting nutrient for plant growth and essential for agricultural production (Ngatia et al., 2017); however, its contribution to underground water contamination and water bodies' eutrophication remains a major problem, which has been significantly accelerated by the intensification of agricultural activities (livestock production through faecal matter and urine;

fertilizer application for crop production; manure application for crop production) and the expansion of urbanization and industrialization (Zhang et al., 2021b). As reported, algae bloom occurred even at trace level (e.g. > 0.02 mg L^{-1}) (Banu et al., 2018).

Significant efforts have been made by scientists worldwide to find ways to lower the phosphate concentration in wastewater (Viglasova et al., 2018). Several techniques such as crystallization (Le Corre et al., 2009), membrane separation (Arola et al., 2021), chemical precipitation (Caravelli et al., 2012), biological (Islam et al., 2017), and adsorption (Melia et al., 2019) have been adopted to remove phosphate in wastewater. The control of phosphate levels using the adsorption method is receiving increasing attention due to its expected ability to realize P recovery and utilization through desorption to enhance P eutrophication mitigation (Bacelo et al., 2020). Meanwhile, in terms of possible shortage of phosphate ore, immobilizing from the wastewater systems can be a promising way to supply secondary sourced P to the market and thereby promoting the blue economy (Cakmak et al., 2022).

Biochar is the carbon-rich product obtained from the thermochemical conversion of biomass under oxygen-limited conditions (Wu et al., 2019), which has become a focal point of multidisciplinary research because of its unique characteristics, broad application, and promising development prospects (Chen et al., 2019; Kumar et al., 2020a). Biochar has been used for removal of heavy metals (Wang et al., 2020a), trace organic contaminants (Rong et al., 2019), ammonium ions (Zhang et al., 2020), and especially phosphate (Bacelo et al., 2020) from wastewater due to its high surface porosity, relatively large specific surface area, surface charge (Panahi et al., 2020; Tomczyk et al., 2020; Wu et al., 2020), and abundant functional groups (Mohan et al., 2014; Rajapaksha et al., 2016; Wang et al., 2017). However, pristine biochar usually has unsatisfactory sorption capability, and further modifications for advanced P removal of wastewater are needed (Huang et al., 2019; Viglasova et al., 2018). Researchers have demonstrated that La(OH)$_3$-modified canna biochar has a P removal rate of up to 99% in 37.37 mg P g^{-1} (Liu et al., 2022). A kind of lanthanum-based biochar from wheat stalks was used by Huang et al. (2022) for the removal of phosphate, exhibiting excellent adsorption capacities for P (64.3 mg g^{-1}). Feng et al. (2017) reported a novel nano-cerium oxide functionalized maize straw biochar (Ce-MSB), which decreased the total phosphorus concentration of surface water by 27.33%. It has also been reported that a nanocomposite porosity-enhanced MgO/biochar (PE-MgO/biochar) assembled by a novel combined electrochemical modification (CEM) method was able to achieve a maximum phosphate

adsorption capacity of more than 20 mg P g^{-1} (Jung and Ahn, 2016). However, biochars are usually present as ultra-fine powders, which cause blockage in adsorption columns and difficulty during recycling and reuse (Ai et al., 2019; Kumar et al., 2020b; Song et al., 2019; Xu et al., 2020a). Superior adsorption, ease of separation, and recyclability of adsorbent biochar materials are crucial for application in an actual engineering environment (Weber and Quicker, 2018).

Formable methods can significantly increase the size of the biochar to a granular scale, hence improving the hydraulic properties of biochar, so that they can be separated, recovered and reused. Recently, $MgFe_2O_4$-BM-La was synthesized via co-precipitation of iron and magnesium onto a reed biomass precursor, followed by crosslinking with lanthanum alginate. The resulting material showed the highest phosphate adsorption capacity, 2.5 times higher than that of BM-La and $MgFe_2O_4$-La. The capacity loss was only about 30% after three consecutive adsorption-regeneration cycles in the fixed bed column operation (Wang et al., 2020b). Jung et al. (2016) prepared granular biochar with calcium-alginate, which exhibited better performance than other powder adsorbents. In general, these granular biochar materials obtained by the formable method showed enhanced phosphate removal capability and hydraulic properties compared to their powder counterparts, making them promising candidates for column-based phosphate adsorption technology.

Clay minerals are also important materials for contaminant immobilization (An et al., 2020; Lazaratou et al., 2020). More importantly, the viscous montmorillonite can improve the diameter of biochar, which is beneficial to the recovery and separability of adsorbent (Vieira et al., 2018; Yao et al., 2014). Previous literature reported the preparation of montmorillonite-biochar composites (MBC) by the co-pyrolysis of montmorillonite and bamboo powder. MBC showed a maximum adsorption capacity of 34.72 mg P g^{-1} for PO_4^{3-} by the Langmuir model, which was attributed to the electrostatic attraction or ionic bonding between PO_4^{3-} and cations in the MBC samples such as Ca^{2+}, Mg^{2+}, Al^{3+}, and Fe^{3+} (Chen et al., 2017). Additionally, exchangeable cations in the interlayer of montmorillonite, including Fe^{2+}, Ca^{2+}, and Mg^{2+}, can balance the negative charges, thus effectively enhancing the active adsorption sites (Arif et al., 2021). In fact, a variety of surface-modified biochar-clay composites were synthesized using hematite as a modifier and granulated into ~4 mm grains by a mixer granulator for water treatment processes (Zhu et al., 2020). However, the efficient performance of adsorbents still presents significant challenges.

Oxides composed of multiple metals generally exhibit significantly superior physicochemical properties than single-component oxides. Several polymetallic oxides have been developed and used to improve phosphorus removal (Delaney et al., 2011; Shi et al., 2019). In recent years, various metal oxides or hydroxides, especially Fe^{2+}, La^{2+}, and Mg^{2+}, have been reported in-depth. In previous literature, it was found that magnetite/lanthanum hydroxide [M-La(OH)$_3$] hybrids adsorbed 52.7 mg P g^{-1} (Fang et al., 2018), while ferrihydrite-coated, lanthanum-decorated magnetite absorbed 44.8 mg P g^{-1} (Fu et al., 2018). In addition, lanthanide compounds showed strong ligand adsorption for phosphate even at trace levels due to their strong Lewis acidity and multi-point coordination ability (Qiu et al., 2017). Moreover, a study suggests that the introduction of iron can promote the uniform distribution of lanthanum iron bimetallic oxides in the Fe_3O_4/La(OH)$_3$ nanocomposite matrix (Ahmed and Lo, 2020). Based on the above background, lanthanum and iron can be co-loaded onto biochar to prepare low-cost composites with uniformly dispersed bimetallic oxides, which would be a promising phosphate removal adsorbent.

Pelletizing is a common technology to increase the particle size of powder adsorbent. Montmorillonite is a low-cost, non-toxic, and environmentally friendly viscous adsorbent material that not only provides metal oxides but also provides strong bonding and forming properties. Through impregnating the surfaces of biochar and montmorillonite with iron and lanthanum metal ions, the content of metal colloidal oxides and active adsorption sites on the surface of the mixed adsorption material can be increased. This can further improve the adsorption capacity of phosphorus as well as the granulation of biochar.

Herein, a method was developed for preparing a novel formable porous granulated straw biochar-loaded La-Fe (hydr)oxides/montmorillonite (LaFe/MB) adsorbent, in which iron and lanthanum bimetallic oxides are immobilized in micro-meter sized biochar granulated with montmorillonite. The structure of the modified biochar was systematically characterized. The adsorption process of phosphate from wastewater by LaFe/MB was described by mathematical models, including adsorption kinetics and isotherms, and the possible adsorption mechanisms were proposed. Furthermore, site energy distribution (SED) is a useful method in treating complex adsorption issues. SED analysis provides direct and detailed information on the adsorption behaviour between adsorbate and adsorbent (Li et al., 2021). Site energy modelling also reveals the distribution of valid adsorption sites, and it is essential for determining why a good performance can be achieved by some adsorbents (Shen et al., 2015). We

comprehensively analysed adsorption mechanism via a combination of SED and characterization analysis, and proposed the foremost adsorption mechanism for the adsorbent. The use of LaFe/MB not only effectively enhances the relief of P eutrophication, but also realizes the efficient immobilization recovery of P resources. Therefore, analysing and mining such kind of data is of great significance for advancing many scientific problems and real engineering applications.

3.2 Materials and Methods

3.2.1 Materials

Rice straw residue was provided by Jiangsu Academy of Agricultural Sciences (Nanjing, China) (34°15′29.99″ N, 108°55′43″ E). Before use, it was air-dried, crushed, and sieved to 2~5 mm mesh size. Dried straw samples were placed in a porcelain crucible and pyrolyzed for 2 h at 550°C in a rotating tube furnace (RTL 1200, Nanjing Boyuntong Instrument Technology CO., LTD.) under N_2 atmosphere (Fletcher et al., 2013; Yang et al., 2016). Straw biochar (B) was crushed and passed through a 0.42 mm stainless steel sieve. Nano-montmorillonite particles (M) were obtained from Huzhou New Material Co., Ltd., China. Iron(III) chloride hexahydrate ($FeCl_3 \cdot 6H_2O$, 97%) and lanthanum(III) chloride heptahydrate ($LaCl_3 \cdot 7H_2O$, 64.5-70.0%, $LaCl_3$ basis) were supplied by Sigma-Aldrich (Shanghai, China). All reagents used in this study are of analytical grade, including KH_2PO_4, HCl, and NaOH, and were purchased from Nanjing Chemical Reagent CO., LTD (Nanjing, China). All solutions required for the test were prepared with deionized water.

3.2.2 Preparation of formable porous granulated biochar adsorbents

A series of formable porous granulated adsorbents was prepared using the coprecipitation method. Different amounts of lanthanum chloride were added during preparation to obtain Fe^{3+}: La^{3+} molar ratios of 0.4:0, 0.3:0.1, 0.2:0.2, 0.1:0.3, and 0:0.4. Preparation conditions for all adsorbents are summarized in Table S3.1.

Briefly, finely crushed rice straw biochar was mixed with montmorillonite in a mass ratio of 2:1 using a mortar. Series of iron/lanthanum chloride solutions were prepared by dissolving $FeCl_3 \cdot 6H_2O/LaCl_3 \cdot 7H_2O$ in 850 mL of deionized water to achieve molar ratios for Fe^{3+} and

La^{3+} that were in the range 0.4:0 ~ 0:0.4 as indicated above. The total moles for each metal ion combination was maintained at 0.4. Subsequently, stable mud mixtures were prepared by adding 150 g of montmorillonite/biochar composites to the series of iron/lanthanum chloride solution with pH adjusted to 9.5~10 by adding NaOH. Afterward, the mixtures were vigorously stirred for 30 min of impregnation in an impregnating tank (HATLAB, Shanghai Huotong Experimental Instrument CO., LTD.), and transferred into an icing machine (BY-400, Changsha Zhuocheng Medical Equipment CO., LTD.), with a rotation angle of 60° and rotating speed at 75 rpm for 30 min. Subsequently, 1~4 mm spherical composite precursors were obtained via a semi-wet granulation process, then oven-dried (60℃) for 10 h. Finally, the precursors were calcined in a tube furnace at 450℃ for 2 h under the protection of N$_2$ atmosphere. The washed modified biochars were dried at 80℃ for 1 d to obtain the formable porous granulated biochar (LaFe/MB), which were labelled respectively as Fe$_{0.4}$/MB, La$_{0.1}$Fe$_{0.3}$/MB, La$_{0.2}$Fe$_{0.2}$/MB, La$_{0.3}$Fe$_{0.1}$/MB, and La$_{0.4}$/MB (the number denoted the molar ratios of Fe^{3+} and La^{3+}).

3.2.3 Macroscopic phosphate adsorption experiments

To determine the phosphate adsorption performance, batch adsorption tests were conducted by mixing 0.2 g adsorbent with 100 mL phosphate solution (100 mg P L^{-1}) in a 250 mL conical flask (Qiu et al., 2017). The flasks were shaken at 28°C in an oscillating incubator (THZ-98C, Shanghai Yiheng Scientific Instrument Co., Ltd., Shanghai, China) for 6 h at 180 rpm. Suspensions were then filtered through a 0.45 μm membrane filter and the residual concentration of phosphate in aqueous solution was determined by the ascorbic acid method using a UV-Vis Lightwave II spectrophotometer (Delaney et al., 2011). All experiments were performed three times for data analysis.

Kinetic tests were performed using 2 g L^{-1} of LaFe/MB with 100 mg P L^{-1} solution with shaking at 28°C and 180 rpm for 6 h. At predetermined time intervals (0 min, 1 min, 2 min, 3 min, 5 min, 15 min, 30 min, 1 h, 2 h, 4 h, 6 h), 1 mL of the suspension was taken out to analyse the phosphate concentration, as described above. The adsorption rate was evaluated by fitting kinetic data using the pseudo-first-order model, pseudo-second-order model, and the intra-particle diffusion models (supplementary information, Text S3.1) (Haris et al., 2022).

Isotherm tests were performed by adding 0.2 g LaFe/MB to 100 mL of phosphate solutions with varying initial concentrations (1.75–300 mg P L^{-1}). The adsorption capacity was determined and the equilibrium data were fitted to Langmuir and Freundlich isotherm models (supplementary information, Text S3.2) as described in the literature (Qiu et al., 2017). Meanwhile, we further studied the site energy distribution deduced from the Langmuir model based on an assumption of the distribution of site energies (Reguyal and Sarmah, 2018; Wang et al., 2022). See the support material Text S3.3 for details.

The effect of solution pH was assessed at pH values varying between 2 and 10 adjusted with 0.2 mol L^{-1} NaOH or HCl solution. The initial phosphate concentration was 100 mg P L^{-1} with the adsorbent dosage of 2 g L^{-1}. Experiments were conducted at 28°C for 24 h.

The influence of competitive ions on phosphate adsorption experiment was investigated using sulphate (SO_4^{2-}), bicarbonate (HCO_3^-), chlorine (Cl^-), and nitrate (NO_3^-) at concentrations of 50 and 100 mg L^{-1}, respectively. The experiment conditions were similar to those of the above isothermal adsorption process, except that the pH of the system was normalized to 7.4±0.2.

3.2.4 Regeneration and recyclability experiments

The recyclability of the adsorbent was tested by four successive phosphate adsorption/desorption cycles. Phosphate desorption tests were carried out by soaking LaFe/MB in 0.1 mol L^{-1} NaOH aqueous solution. After phosphate adsorption and desorption, the adsorbent was separated from the mixture. Then, it was washed to neutral with deionized water and dried at 60°C before the start of the next cycle.

3.2.5 Strength retention rate and pressure resistance tests

The damage to the skeleton and surface of adsorbents after the mechanical wear was analysed. The grain percentage was used as the sample strength indicator according to GB/T 12496.6-1999. The adsorbents with the same diameter were placed on the mold. A microcomputer-controlled electronic universal testing machine (HY-0580, Shanghai Hengyi Precision Instrument CO., LTD., Shanghai) was adopted. The pressure resistance was measured at 28°C and the speed of applied loading was set at 10 mm min^{-1}.

3.2.6 Analysis methods

The specific surface area and pore structure of the adsorbents were determined using an automatic adsorption instrument (USA, ASAP2020) and calculated using the BET adsorption isotherm of nitrogen (77 K). The functional groups of adsorbents were assessed using Fourier transform infrared spectroscopy (Tensor27, Bruker, Germany). X-ray diffraction (XRD, DX-2000, Darmstadt, Germany) with Cu Kα radiation (40 kV, 20 mA) was used to detect the crystallographic phases of the adsorbent before and after adsorption. Micromorphological characteristics and surface elemental composition of adsorbents were characterized using scanning electron microscopy (SEM, FEIQUANTA200, Hillsboro, USA) coupled with energy dispersive X-ray spectroscopy (EDS, Oxford Instruments Link ISIS). The pH was determined using a PHS-3C precision pH meter (China, Changzhou). Zeta potentials were measured at different pH values to determine the zero-charge point (pH_{PZC}) of the adsorbents. Raman imaging (DXR2xi, Thermo Scientific, USA) was performed to analyse the structure and composition of the adsorbent. Surface chemistry of LaFe/MB before and after phosphate adsorption was analysed by X-ray photoelectron spectroscopy (XPS, PHI 5000 VersaProbe ESCA).

The amount of phosphate adsorbed is expressed as mean $\pm$ standard error. Experimental data were analysed with SPSS software (SPSS, 26.0, IBM, USA), and Origin 8.5 (Origin, OriginLab, USA) was used for graphing.

3.3 Results and discussion

Surface modification with La^{3+} and Fe^{3+} significantly improved the phosphate removal performance of modified biochar. The phosphate adsorption capacities of the different adsorbents are presented in Fig. S3.1. The adsorption of phosphate increased with increase in the La^{3+}: Fe^{3+} molar ratio. However, when the molar ratio was more than 0.3:0.1, the adsorption capacity began to decrease. As shown in Fig. S3.1, $La_{0.3}Fe_{0.1}$/MB showed the best phosphate uptake of 39.45 mg P g^{-1}, while $La_{0.2}Fe_{0.2}$/MB and $La_{0.4}$/MB exhibited weaker adsorption capacities of 30.23 and 36.38 mg P g^{-1}, respectively. This may be due to the effect of Fe^{3+} doping on the formation of lanthanum oxide, which can not only promote the dispersion of lanthanum oxide but can also enhance the surface charge of the adsorbent (Shi et al., 2019). Thus, $La_{0.3}Fe_{0.1}$/MB was selected for the following in depth studies.

Table 3.1 Physicochemical properties of biochar (B), biochar/montmorillonite (MB), and $La_{0.3}Fe_{0.1}$/MB.

Characteristics	B	MB	$La_{0.3}Fe_{0.1}$/MB
Particle size (mm)	＜0.3~0.45	0.3~0.45	1~45
Packing density (g mL^{-1})	0.386	0.413	0.518
S_{ssa}[a] (m^2 g^{-1})	227.77	192.19	63.54
V_{tpv}[b] (cm^3 g^{-1})	0.1251	0.1143	0.0861
d_{apz}[c] (nm)	2.20	2.38	6.16
Fe (wt.%)	0.52	2.09	8.02
La (wt.%)	BDL[d]	BDL	19.49

Note: calculated using the BET adsorption isotherm of nitrogen (77 K). [a] specific surface area. [b] total pore volume. [c] average pore size. [d] below detection limit.

3.3.1 Characterization of adsorbents

The physicochemical properties of biochar (B), biochar/montmorillonite (MB), and $La_{0.3}Fe_{0.1}$/MB are summarized in Table 3.1. Compared with the original B, the contents of Mg, Al, Ca, Fe, and La in MB and $La_{0.3}Fe_{0.1}$/MB were significantly increased with the introduction of binary metal, while the relative content of carbon on the surface of $La_{0.3}Fe_{0.1}$/MB was decreased, indicating that Fe and La were successfully anchored in $La_{0.3}Fe_{0.1}$/MB (Table S3.2). The total La and Fe contents in $La_{0.3}Fe_{0.1}$/MB were 19.49% and 8.02%, respectively, which were lower than that of many La/Fe-based materials reported in the literature (Table 3.2). A previous study has shown that composites with lower La content may result in higher La utilization efficiency due to the uniform distribution of La and higher accessibility to phosphorus (Shi et al., 2019). Furthermore, the specific surface area of $La_{0.3}Fe_{0.1}$/MB decreased from 192.19–227.22 m^2 g^{-1} to 63.54 m^2 g^{-1}, which was attributed to the loading of the impregnated iron and lanthanum on the surface of the material, as indicated by SEM-EDS result (Fig. S3.2c and Fig. 3.1). A similar trend was also observed by Li et al. (2015) and Wang et al. (2016). Besides, the total pore volume of $La_{0.3}Fe_{0.1}$/MB decreased from 0.1143 ~ 0.1251 to 0.0861 cm^3 g^{-1}, which was mainly due to the presence of iron/lanthanum adsorption sites on the surface or pores of MB and the filling of loaded particles inside (Xu et al., 2019). It has been reported by Yang et al. (2016) that the combined action of mineral and metal chlorides can improve the average pore diameter of biochar. However, a slight increase in nanoparticle size was observed, and the adsorption average pore size potentially enhanced up to 2.20 ~ 2.38 nm

to 6.16 nm for $La_{0.3}Fe_{0.1}$/MB indicating that $La_{0.3}Fe_{0.1}$/MB possesses a lesser surface area and pore space percent, except the higher pore size as compared with B and MB.

Table 3.2 Comparison of $La_{0.3}Fe_{0.1}$/MB with other newly developed adsorbents in the simultaneous of adsorption of phosphate.

Adsorbent	Adsorption conditions				q_{max} (mg P g^{-1})	References
	P concentration (mg L^{-1})	Dosage (g L^{-1})	pH	T (°C)		
La-BC-5	2-50	2.0	3.0	25	23.52	(Xu et al., 2020b)
La-MB	1~500	2.5	7.0	25	48.40	(Zhong et al., 2020)
LMZ	25~400	2.0	n.a.	25	52.52	(Li et al., 2020)
La-doped magnetic rGO naocomposites	10~200	1.0	4-8	25~30	37.85	(Rashidi Nodeh et al., 2017)
Fe_3O_4@SiO_2@La_2O_3	0~200	1.0	5~9	25	27.8	(Lai et al., 2016)
La/Al pillaraed montmorillonite	5~50	2.5	5	25	13.02	(Tian et al., 2009)
Magnetic biochar (fungal)	4~90	2.0	n.a.	25	23.86	(Jack et al., 2019)
La_2O_3/oak biochar	1~400	2.0	3~9	n.a.	46.37	(Wang et al., 2016)
$La_{0.3}Fe_{0.1}$/MB	1.75~300	2.0	7.4	28	52.12	This work

The morphologies of adsorbents were analysed by SEM images, as shown in Fig. S3.2. The raw B presented a relatively smooth and clean surface with mesoporous structure (Fig. S3.2a), while M doping on the surface of biochar resulted in lamellar or bundled structures (Fig. S3.2b). The EDS mapping confirmed that the immobilized Fe/La mainly resides in the cavities of the composite material.

Finally, the pore diameter of $La_{0.3}Fe_{0.1}$/MB showed a certain increase compared with B or MB. Particulate matter formation was observed and the material surface became rough and uneven (Fig. S3.2c, d). In particular, a more irregular surface was observed for $La_{0.3}Fe_{0.1}$/MB, which can effectively improve the unit size of adsorbent (Fig. 3.1a). This appearance supports the lower specific surface area of $La_{0.3}Fe_{0.1}$/MB well (Table 3.1). As exhibited in the typical TEM images (Fig. 3.1b), the synthesized Lanthanum/iron oxide has a uniform size distribution.

The EDS spectra of all samples displayed prominent peaks for carbon, silicon, and oxygen (Fig. S3.3). Furthermore, small amounts of Fe were present in the MB sample, confirming the

M doping. More importantly, both iron and lanthanide were detected in LaFe/MB, and the corresponding peaks showed higher responsiveness. Peaks for Fe and La were also observed in the $Fe_{0.4}$/MB and $La_{0.4}$/MB adsorbents, respectively, confirming that La and Fe oxide were successfully anchored onto the adsorbents, which was in accordance with the SEM result. The elemental composition (wt.%) of the adsorbents is described in detail in Table S3.2, which indicates strong Fe and La adsorption capacities. Metal oxides were mainly present on the biochar surface as determined by EDS. It is interesting to note that Fe and La loading was synergistic when La/Fe molar ratio was 0.3:0.1, compared with the loading of $La_{0.4}$/MB. The EDS mapping results confirmed that Fe and La were widely and abundantly distributed on the surface of porous granulated materials (Fig. 3.1c), thereby providing active adsorption sites for phosphate.
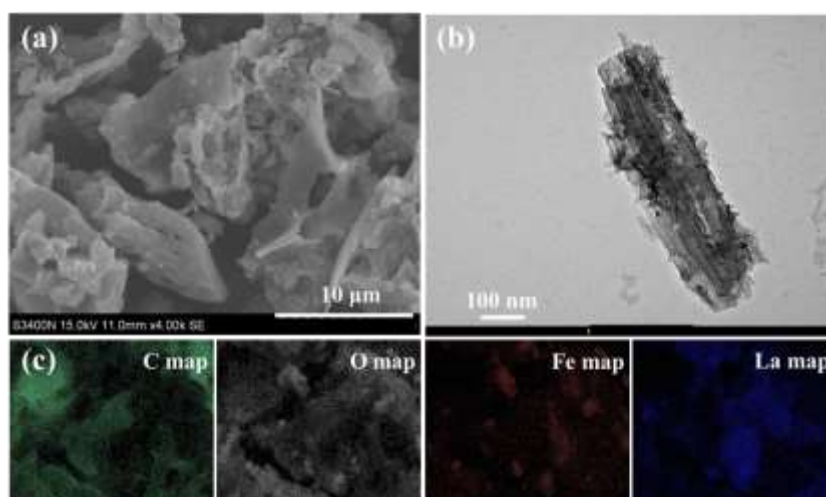
Figure 3.1 SEM (a), TEM (b), EDS elemental mapping images (c) of $La_{0.3}Fe_{0.1}$/MB.

The chemical structure and functional groups of the samples were characterized by FTIR (Fig. 3.2a). The peaks observed at 3416–3441 cm^{-1} belonged to O–H stretching vibrations, the peak for C=O stretching vibrations of carbonyl or carboxyl groups was observed at around 1614–1634 cm^{-1}, while the peak at 1400 cm^{-1} was assigned to C=C stretching vibrations, respectively (Pezoti et al., 2016). The peak for Si–O–Mg bending vibrations, present in all the adsorbent spectra, appeared at 693-664 cm^{-1}. The peak at 796-798 cm^{-1} can be attributed to Si–O stretching, which was significantly enhanced in MB, M, $Fe_{0.4}$/MB, $La_{0.3}Fe_{0.1}$/MB, and $La_{0.4}$/MB adsorbents, reflecting the effect of M on biochar substrate. Correspondingly, the C–O stretching vibration peak at around 1033-1049 cm^{-1} decreased when biochar was modified with both iron and lanthanum oxides. This may be due to the binding of iron/lanthanide to

oxygen-containing groups in biochar (Chen et al., 2017). The peak at 530-536 cm^{-1} corresponded to the Fe–OH stretching vibration in Fe$_{0.4}$/MB and La$_{0.3}$Fe$_{0.1}$/MB (Li et al., 2008; Sun et al., 2019). Moreover, the La–O or La–OH stretching vibration at 674-664 cm^{-1} was more intense in La$_{0.4}$/MB and La$_{0.3}$Fe$_{0.1}$/MB (Fu et al., 2018; Zhang et al., 2011), showing that MB was successfully impregnated with Fe and La (Yin et al., 2017).
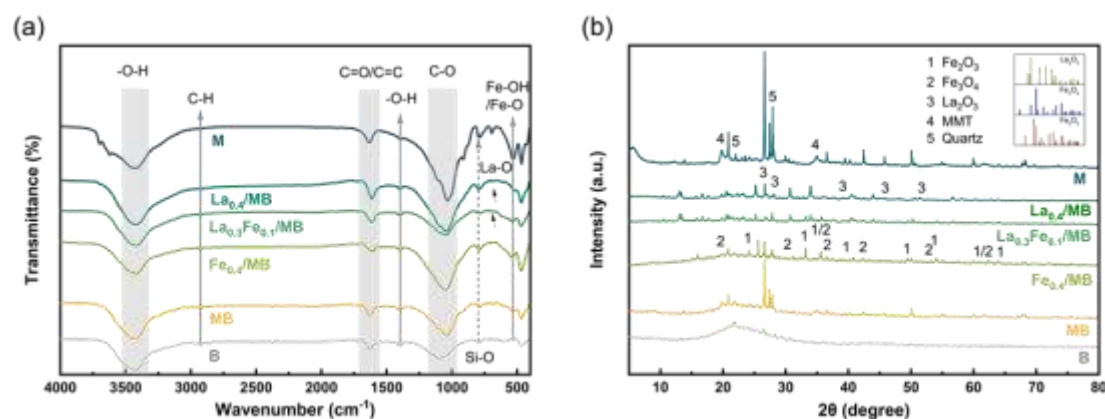
Figure 3.2 FTIR spectra (a), and XRD patterns (b) of B, MB, M, Fe$_{0.4}$/MB, La$_{0.3}$Fe$_{0.1}$/MB, and La$_{0.4}$/MB.

Fig. 3.2b shows the XRD patterns of B, MB, M, Fe$_{0.4}$/MB, La$_{0.3}$Fe$_{0.1}$/MB, and La$_{0.4}$/MB. In the XRD patterns of samples containing MB, peak 4 (M, 2θ=19.6°, 35.2°), peak 5 (quartz, 2θ=22.1°, 27.9°), and a peak at 2θ=26.69° due to graphite were observed, suggesting that M was present in the formable porous granulated adsorbents and that the biochar structure was still retained (Zhu et al., 2020). Interestingly, the intensity of biochar peak decreased upon doping with iron and lanthanum oxides, indicating that the addition of metallic oxides decreased the relative amount of the main component of straw biochar. The XRD pattern of Fe$_{0.4}$/MB showed peaks corresponding to the typical XRD pattern of iron oxide. In particular, the diffraction peaks 1 and 2 observed at 2θ=20.88°, 24.17°, 33.15°, 35.61°, 40.26°, 42.55°, 49.41°, 53.81°, and 62.52° can be ascribed to Fe$_3$O$_4$ and Fe$_2$O$_3$. This suggests that Fe can formed iron oxide nanoparticles. The peaks that appeared at 2θ=26.63°, 28.08°, 39.07°, and 51.43° for La$_{0.4}$/MB can be attributed to crystalline La$_2$O$_3$ (Goscianska et al., 2018; Qiu et al., 2017), which is consistent with the FTIR results. Comparing these diffraction patterns to that of La$_{0.3}$Fe$_{0.1}$/MB, similar characteristic diffraction peaks were observed for Fe$_3$O$_4$, Fe$_2$O$_3$, and La$_2$O$_3$, which suggests that iron and lanthanum oxides were successfully doped into MB. This was also confirmed by the EDS elemental mappings (Fig. 3.1c).

3.3.2 Macroscopic P adsorption performance and energy distribution

3.3.2.1 Adsorption kinetics

The rapid and effective removal of phosphate from wastewater is the key effect of adsorbents in practical applications. Initially, pseudo-first-order and pseudo-second-order kinetic models were employed to estimate the adsorption kinetics of phosphate onto $La_{0.3}Fe_{0.1}$/MB (Fig. 3.3a). The removal process of phosphate in aqueous solution was rapid within 30 min, and the adsorption capacity gradually reached equilibrium after approximately 5 h, indicating a fast kinetic process suitable for column-based practical phosphate removal. Associated sorption parameters are summarized in the table of Fig. 3.3a, which were obtained using the two model equations (details in Text S3.1). Pseudo-second order model provided the best fit with the highest correlation coefficient (R^2) values for $La_{0.3}Fe_{0.1}$/MB (0.9751) compared to pseudo-first-order model (0.9158), suggesting chemi-sorption as the rate-controlling step for phosphate adsorption. Moreover, the adsorption data fitted ($q_{e, second}$ value was 40.41 mg g^{-1}) by the pseudo-second-order kinetic model were closer to the experimental values, indicating that the adsorption corresponded to monolayer chemisorption (Wang et al., 2020b). This result also confirmed the conclusion reported in the literature that there existed a strong chelation and complexation between phosphate and active sites of $La_{0.3}Fe_{0.1}$/MB (Chen et al., 2015; Shi et al., 2019).

In addition, the collected experimental data were fitted into the intra-particle diffusion model to further explain the adsorption mechanism and rate-limiting step. The plot of the intra-particle diffusion model of $La_{0.3}Fe_{0.1}$/MB for phosphate removal is shown in Fig. S3.4, which was composed of three linear sections with distinct slopes, as also confirmed by some previous studies (Haris et al., 2022). The result implied that the adsorption mechanism entailed three nonlinear processes, including external diffusion which was related to surface diffusion, intra-particle diffusion where phosphate intercalated among the internal structure of the adsorbent layer, and adsorption on binding sites with chemical reaction. The adsorption rate constant (k_{pi}) values of the intra-particle diffusion models are listed in Table 3.3. The values of k_{p1} were larger than that of k_{p2} and k_{p3} (4.36, 1.00, and 0.06, respectively), indicating that intra-particle diffusion was the rate-controlling process (Shi et al., 2019). On the other hand, the line did not pass through the origin, instead, it had an intercept. This is in agreement with the findings of the pseudo-second- order model.
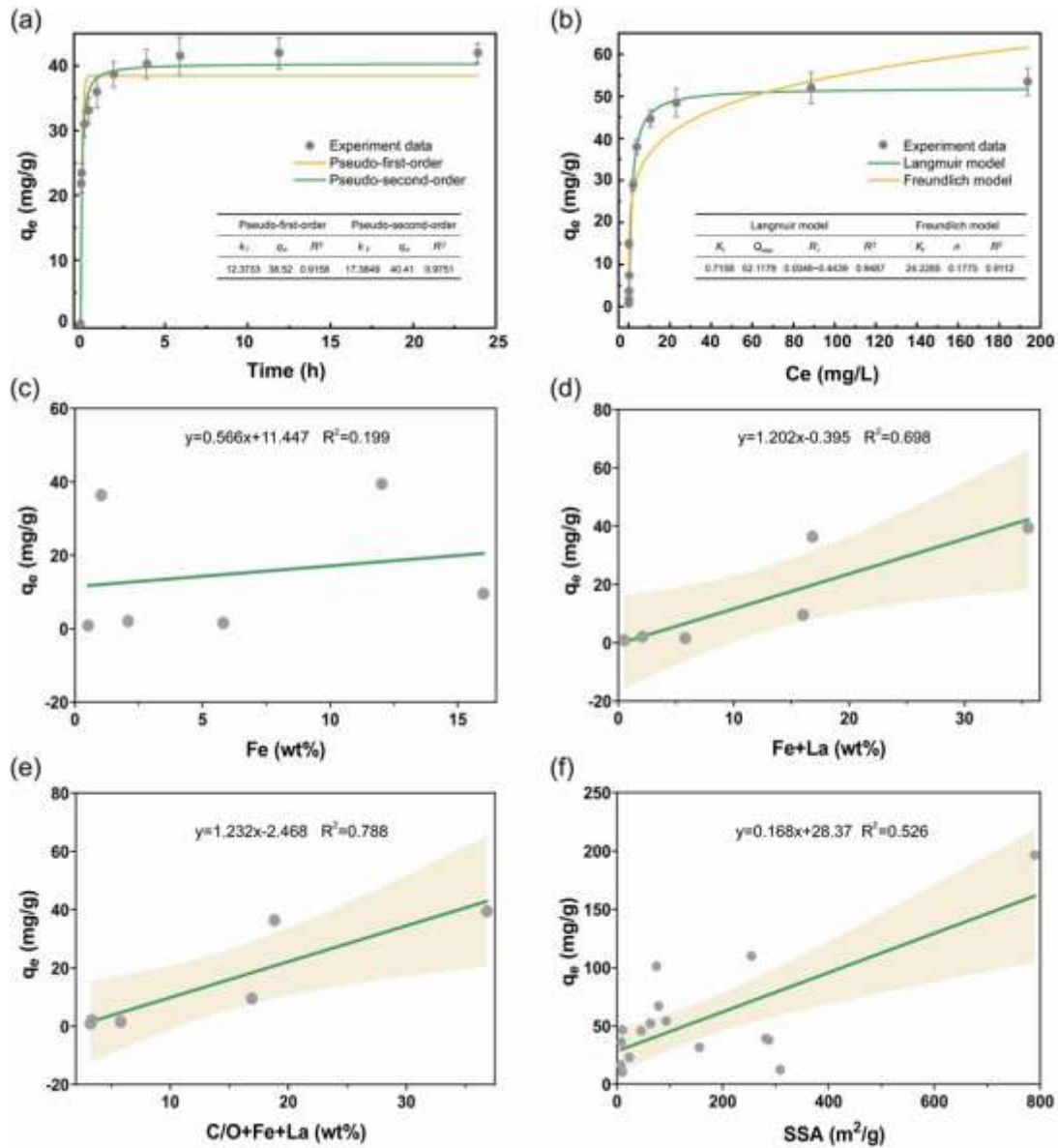
Figure 3.3 Phosphate adsorption kinetics for La$_{0.3}$Fe$_{0.1}$/MB. Time dependence of the phosphate removal by La$_{0.3}$Fe$_{0.1}$/MB, using 50 mL of a 100 mg P L^{-1} solution, pH=7.41, T=298 K, 0.1 g adsorbent, and a total contact time of 6 h (a). Langmuir and Freundlich isotherms for La$_{0.3}$Fe$_{0.1}$/MB (b). Correlation between phosphate removal capacity and Fe, Fe+La, C/O+ Fe+La (c-e), and specific surface area (SSA) of previous references (f).

Table 3.3 Intra-particle diffusion parameters for phosphate adsorption on La$_{0.3}$Fe$_{0.1}$/MB.

	k_{p1}	C_1	R^2	k_{p2}	C_2	R^2	k_{p3}	C_3	R^2
La$_{0.3}$Fe$_{0.1}$/MB	4.36	14.05	0.9967	1.00	27.87	0.9868	0.06	39.97	0.5925

Note: the unit of k_{pi} and C_i are g/(mg min$^{0.5}$), and mg g^{-1}, respectively.

3.3.2.2 Isotherms and thermodynamic investigations

The adsorption isotherms of La$_{0.3}$Fe$_{0.1}$/MB at different phosphate concentrations are presented in Fig. 3.3b. La$_{0.3}$Fe$_{0.1}$/MB exhibited high phosphate adsorption capacity at low equilibrium concentration, suggesting a high affinity to phosphate that meet the requirement of advanced phosphate removal. Two commonly used models, the Langmuir and Freundlich models, were further used to fit the phosphate sorption data for La$_{0.3}$Fe$_{0.1}$/MB (details in Text S3.2). The resulting best-fit parameters are listed in Fig. 3.3b. It can be concluded that the Langmuir model (R^2=0.9487) was more consistent with the adsorption isotherm data than the Freundlich model (R^2=0.9112). The better fit provided by the nonlinear Langmuir model indicated that phosphate adsorption was likely a monolayer molecular adsorption process, and the adsorption process likely involved chemisorption rather than physisorption (Yu et al., 2009). According to the Langmuir equation, the maximum amount of phosphorus uptake by the La$_{0.3}$Fe$_{0.1}$/MB material was estimated to be 52.12 mg P g^{-1}, which was higher than most previously reported adsorbents (Table 3.2), indicating that La$_{0.3}$Fe$_{0.1}$/MB is a promising material for application as phosphate scavenger.

In addition, according to the Langmuir equation, the dimensionless separation factor R$_l$ was calculated to be in the range of 0.0046 ~ 0.4439, indicating that the adsorption of phosphate ions on the surface of the adsorbent was favourable. Moreover, a larger value of R$_l$ is more conducive to pollutant removal, which was confirmed by further studies. For further thermodynamic exploration, energy changes and spontaneity of the phosphate adsorption process (such as, entropy change (ΔS^0), free enthalpy change (ΔH^0), and energy change (ΔG^0)) were examined using Eqs. (1)-(3) (Tran et al., 2017):

$$\ln(K_d^0) = \frac{\Delta S^0}{R} - \frac{\Delta H^0}{RT} \qquad (10)$$

$$\Delta G^0 = -RT ln(K_d^0) \qquad (11)$$

$$K_d = \frac{q_e}{C_e} \qquad (12)$$

where ΔS^0, ΔH^0, and ΔG^0 are the standard entropy, enthalpy, and Gibbs free energy for the adsorption process, R is the ideal gas constant, T is the temperature (K), q_e is the adsorption uptake capacity of adsorbent for phosphate (mg/g), and C_e is the equilibrium concentration of phosphate (mg/L).

Using the plots of ln (q_e/C_e) versus q_e, the values of thermodynamic parameters were obtained. The values of ΔS^0 and ΔH^0 during the adsorption of phosphate were found to be 57.5454 J (mol·K)$^{-1}$, and 1.1340 kJ mol^{-1}, respectively. The positive value of entropy and free enthalpy, affirming the endothermic nature with the rise in randomness at the solid-liquid interface during the phosphate adsorption process, implied an excellent binding affinity for phosphate ions (Zhang et al., 2021a). Furthermore, the value of ΔG^0 (-17.32 KJ mol^{-1}) was found to be negative, indicating a spontaneous process in which the adsorption forces were strong enough to pass the energy barrier for phosphate uptake onto La$_{0.3}$Fe$_{0.1}$/MB.

3.3.2.3 Approximate site energy distribution analysis

Due to the complex surface topography of biochar, the adsorption sites on the surface of biochar are uneven, and the location energy of these adsorption sites is different (Wang et al., 2022). The area with high surface energy becomes the adsorption centre of environmental pollutants, playing an important role in the adsorption process (Li et al., 2021).

Identifying site energy distribution (SED) of P sorption to La$_{0.3}$Fe$_{0.1}$/MB can provide useful information on sorption mechanisms (Wu et al., 2022). The site energy E^* of P sorption on La$_{0.3}$Fe$_{0.1}$/MB calculated from isotherm modelling and Eq. (7) of Text S3.3. As can be seen from Fig. S3.5a, the E^* value decreased with increasing P phase sorption concentration Q_e. This indicates that P was preferentially adsorbed to the high-energy sorption site and then gradually diffused to low-energy sorption site due to the energy distribution on the surface of La$_{0.3}$Fe$_{0.1}$/MB unevenly. As reported in the previous literature (Li et al., 2021), the highly efficient phosphorus removal by a novel sludge-based magnetic gel bead (MCB13) was analysed based on approximate SED. The corresponding E^* value was 24.87~25.80 KJ mol^{-1}, but lower than La$_{0.3}$Fe$_{0.1}$/MB, which implied that a heterogeneous surface was detrimental to a higher value of E^* (Li et al., 2021). Additionally, under the same Q_e value, E^* on La$_{0.3}$Fe$_{0.1}$/MB was significantly higher than that of MCB13, indicating it has much more high-energy adsorption sites (Liao et al., 2020). According to Eqs. (8) and (9) of Text S3.3, the average site energies (E^*) was calculated in the range of the experimental concentrations. The average value of $E^*/\mu(E^*)$ of P to La$_{0.3}$Fe$_{0.1}$/MB was 30.64 KJ mol^{-1} based on Eq. (4). The $F(E^*)$ of La$_{0.3}$Fe$_{0.1}$/MB was much higher than MCB13, indicating more high-energy and low-energy sites for P sorption to La$_{0.3}$Fe$_{0.1}$/MB, resulting in more available binding sites for P sorption.

The SED depicted in Fig. S3.5b, characterizes site energy heterogeneity based on standard deviation σ_e^* of SED. The σ_e^* of SED was able to describe the adsorption site energy inhomogeneity (Shen et al., 2015), which could be quantified by Eq. (5) and Eq. (6). According to Eq. (6), the σ_e^* of SED for P to La$_{0.3}$Fe$_{0.1}$/MB was 4.32 KJ mol^{-1}. In contrast, the σ_e^* was comparable between La$_{0.3}$Fe$_{0.1}$/MB and MCB13 (Li et al., 2021). The heterogeneous sorption sites originate from the defect structure, disordered arrangement, and grafting functional groups of carbonaceous materials, described with σ_e^* (Shen et al., 2015; Wang et al., 2022). Overall, the Fe/La(hydr)oxides-loaded biochar would introduce more high-energy sorption sites, thereby strengthening the interaction between P and La$_{0.3}$Fe$_{0.1}$/MB and increasing its capacity for P removal.

$$\mu(E^*) = \frac{\int_a^b E^* F(E^*) dE^*}{\int_a^b F(E^*) dE^*} = \frac{\int_a^b E^* Q_{max} \frac{K_L C_s \exp\left(\frac{E^*}{RT}\right)}{RT(K_L C_s \exp\left(\frac{E^*}{RT}\right)+1)^2} dE^*}{\int_a^b Q_{max} \frac{K_L C_s \exp\left(\frac{E^*}{RT}\right)}{RT(K_L C_s \exp\left(\frac{E^*}{RT}\right)+1)^2} dE^*} \tag{13}$$

$$\mu(E^{*2}) = \frac{\int_a^b E^{*2} F(E^*) dE^*}{\int_a^b F(E^*) dE^*} = \frac{\int_a^b E^{*2} Q_{max} \frac{K_L C_s \exp\left(\frac{E^*}{RT}\right)}{RT(K_L C_s \exp\left(\frac{E^*}{RT}\right)+1)^2} dE^*}{\int_a^b Q_{max} \frac{K_L C_s \exp\left(\frac{E^*}{RT}\right)}{RT(K_L C_s \exp\left(\frac{E^*}{RT}\right)+1)^2} dE^*} \tag{14}$$

$$\sigma_e^* = \sqrt{\mu(E^{*2}) - \mu(E^*)^2} \tag{15}$$

3.3.2.4 Correlation between adsorbent properties and P adsorption

The correlations between the adsorption capacity and contents of Fe, Fe+La, and (C/O+Fe+La) in the adsorbents were analysed. It was found that there was no correlation between the adsorption capacity and iron content, while the correlation increased significantly with the increase in La content (R^2=0.698), indicating that the loading of La greatly improved the adsorption capacity of the adsorbent. In addition, the loading of (C/O+Fe+La) further improved the correlation (R^2=0.788) which demonstrates that the C/O ratio also promoted the adsorption effect of adsorbents. Also, previous studies suggested that the introduction of iron can promote the uniform distribution of La/Fe bimetallic oxides in the composite's matrix. Subsequently, they can form colloidal or nanoscale oxides on the surface of the adsorbent, and

then form mononuclear and polynuclear complexes with P through precipitation (Wang et al., 2016; Yao et al., 2013).

Given that the specific surface area (SSA) of adsorbents also affects the adsorption performance, a linear correlation was employed to estimate the relationship model (Fig. 3.3f). Although it has been widely reported that the specific surface area of the adsorbent contributes significantly to its adsorption performance (Mosa et al., 2018), the overall correlation between SSA and adsorption performance of $La_{0.3}Fe_{0.1}$/MB was found to be moderate (R^2=0.5261). Thus, combined with experimental conditions and results, it can be inferred that the uptake of phosphate by $La_{0.3}Fe_{0.1}$/MB was not mainly due to the high SSA of the adsorbent.

As can be seen from the data, $La_{0.3}Fe_{0.1}$/MB exhibited good phosphate removal performance with relatively low La content (Table 3.1), compared to other adsorbents doped with La or Fe reported in the literature (Table 3.2). Even at a lower concentration of adsorbent, the adsorption performance was maintained stably under the interference of co-existing competitive anions (Fig. 3.6a). Moreover, powder adsorbents or adsorbents with small-size particles are difficult to separate from aqueous solution, which affects their subsequent recovery and reuse in actual applications. Hence, it was found that there was no significant decrease in content of $La_{0.3}Fe_{0.1}$/MB for phosphate uptake, even compared with La modified zeolite (LMZ) reported by Li et al. (2020). More importantly, $La_{0.3}Fe_{0.1}$/MB adsorbent has formable porous spherical particles, which is conducive to its recovery and reuse.

3.3.3 Proposed adsorption mechanism

3.3.3.1 Influence of pH and Zeta potential

pH also affects the protonation of phosphate in wastewater, the charge and stability of adsorbent, and especially, in the potential loss of metal oxide into solution (Xu et al., 2019). The relationship between solution pH and phosphate removal at pH 2-10 was studied (Fig. 3.4a). At pH 2-6, the amount of phosphate adsorbed by $La_{0.3}Fe_{0.1}$/MB first increased rapidly with the increase in pH and then decreased slowly until pH ~6. At pH values greater than ~6, phosphate adsorption decreased slightly with increase in pH. On the whole, $La_{0.3}Fe_{0.1}$/MB showed a good tolerance to initial pH changes. In general, phosphate species (H_3PO_4, $H_2PO_4^-$, HPO_4^{2-}, and PO_4^{3-}) present in solution vary from acidic to basic with pH (Krishnan and Haridas, 2008). When pH < pH_{pzc} (8.56) (Fig. 3.4b), the $La_{0.3}Fe_{0.1}$/MB surface can be

protonated ($\equiv$Fe/La—OH + H$^+$ $\leftrightarrow$ Fe/La—OH$_2^+$). This leads to a strong electrostatic attraction between phosphate species present in solution and the relatively positively charged surface of the adsorbent, likely due to the formation of metal oxides on the surface. In addition, the amount of adsorbed phosphate decreased when pH exceeded pH$_{pzc}$, due to negative surface charges resulting from the release of hydroxyl groups during ligand exchange (Shi et al., 2019). Therefore, La$_{0.3}$Fe$_{0.1}$/MB can capture phosphate effectively over a wide pH range (3~10) without significant decrease in adsorption capacity.

Metal-loaded adsorbents can attract negatively charged phosphate anions (such as H$_2$PO$_4^-$ and HPO$_4^{2-}$) present in solution through electrostatic attraction at low pH value (Fig. 3.4b). At environmental pH values close to pH$_{pzc}$, the adsorption sites become weak, and the protonation of the surface decreases, leading to a charge that is close to zero. The positive values of ΔpH reflect the gradual increase in hydroxide content (Fig. 3.4a), which is mainly dependent on ligand exchange (Awual et al., 2011). When the solution pH continued to rise above 8.56, fierce repulsion occurred between negatively charged La$_{0.3}$Fe$_{0.1}$/MB and HPO$_4^{2-}$, resulting in a sharp decrease in P adsorption capacity. A high concentration of OH$^-$ was unfavourable to ligand exchange and electrostatic attraction of phosphate by La$_{0.3}$Fe$_{0.1}$/MB, resulting in a downward trend of phosphate adsorption. Nevertheless, the adsorption capacity remained elevated over a range of pH of 9-10, mainly due to the complexation, which is another important mechanism in the adsorption process (Xu et al., 2019).
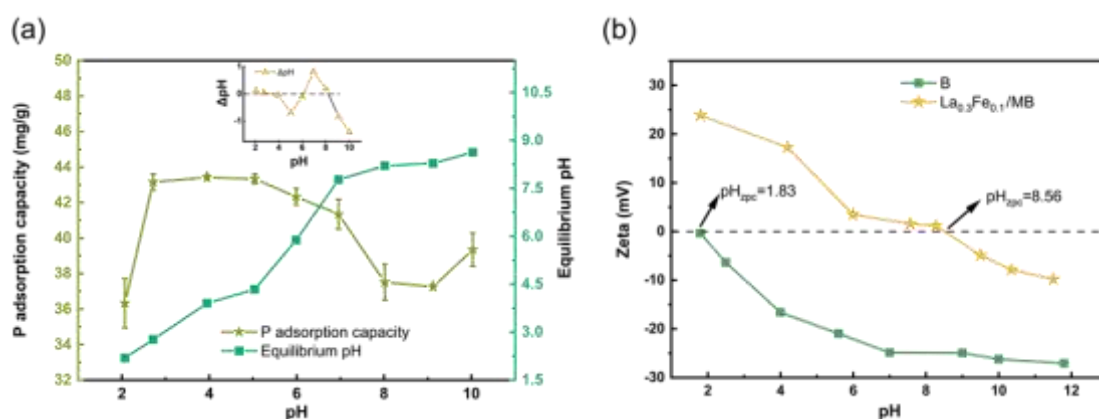
Figure 3.4 Effects of pH and pH equilibria on phosphate adsorption (a), Zeta potential of La$_{0.3}$Fe$_{0.1}$/MB at different pH values (b).

3.3.3.2 Raman, XPS, and XRD analyses

Furthermore, the phosphate adsorption mechanisms of $La_{0.3}Fe_{0.1}$/MB were investigated using a combination of Raman, XPS, and XRD analyses. Fig. 3.5a and b show the Raman spectra of $La_{0.3}Fe_{0.1}$/MB pre and post P adsorption. The characteristic peaks belonging to the D and G bands appeared around 1588 cm^{-1} and 1363 cm^{-1}, respectively. The strong G-peak of the in-plane vibration mode confirmed the graphite carbon in $La_{0.3}Fe_{0.1}$/MB, while the strong D-peak of the ring breathing vibration reflected the existence of a large number of pores and edge defects (Yap et al., 2019). The D/G intensity ratio (obtained by taking the ratio of the total peak areas in the 1300-1400 cm^{-1} and 1500-1600 cm^{-1} ranges) of $La_{0.3}Fe_{0.1}$/MB decreased from 11427/3819 to 7996/2890 after phosphate adsorption (Fig. 3.5a, b). Based on a two-peak fitting model, the peak intensity ratio (I_D/I_G) of the D and G bands declined by 6.54% (from 1.0096 to 0.9436), suggesting that the graphitization of $La_{0.3}Fe_{0.1}$/MB was enhanced and the ordered sp^2 carbon content in the structure increased after phosphate adsorption. This may contribute to the improvement of the strength of $La_{0.3}Fe_{0.1}$/MB after phosphate adsorption (Fig. 3.6c). The formation of a more ordered interface structure after phosphate uptake further implies that precipitation might also be an important mechanism of $La_{0.3}Fe_{0.1}$/MB for phosphate removal.

From the total survey scans of $La_{0.3}Fe_{0.1}$/MB (Fig. 3.5), the O 1s spectra could be separated into three overlapping peaks at 531.2, 532.26, and 533.23 eV, corresponding to M—O (oxygen bonded to a metal), M—OH (hydroxyl bonded to a metal), and adsorbed water (H_2O), respectively. After phosphate adsorption, the relative areas of M—O peaks increased from 23.41% to 49.48%, confirming that $La_{0.3}Fe_{0.1}$/MB can replace hydroxyl groups with P through ligand exchange, which plays a key role in phosphate absorption (Shi et al., 2019). This result may be due to the combination of P with O—La and O—Fe to form La—O—P and Fe—O—P (Fu et al., 2018). Since this value (1.48) lies between 0.5 and 2, monodentate, bidentate mononuclear, and bidentate binuclear inner-complexes may be formed during the adsorption process (He et al., 2016). The relative content of M—OH decreased from 47.42% to 31.97% after P adsorption demonstrating the possible exchange of –OH with P to form inner-complex (Fang et al., 2018; Xu et al., 2020b). The P 2p spectra contained an obvious peak at ~ 133.35 eV, while similar to the reference samples of $LaPO_4 \cdot xH_2O$ (132.85 eV) and $FePO_4 \cdot 2H_2O$ (133.68 eV), which further confirmed the assumption that M—O—P bonds were formed (Fu et al., 2018; He et al., 2017). This finding was consistent with the work of Wang et al (2016). As can be seen, some H_3PO_4 analog was observed which caused by the adsorption of P by $LaPO_4$

through hydrogen bonding. This phenomenon was also been observed in other reports (Yao et al., 2013). It is, therefore, demonstrated that precipitation was the mechanism for P removal using $La_{0.3}Fe_{0.1}/MB$.
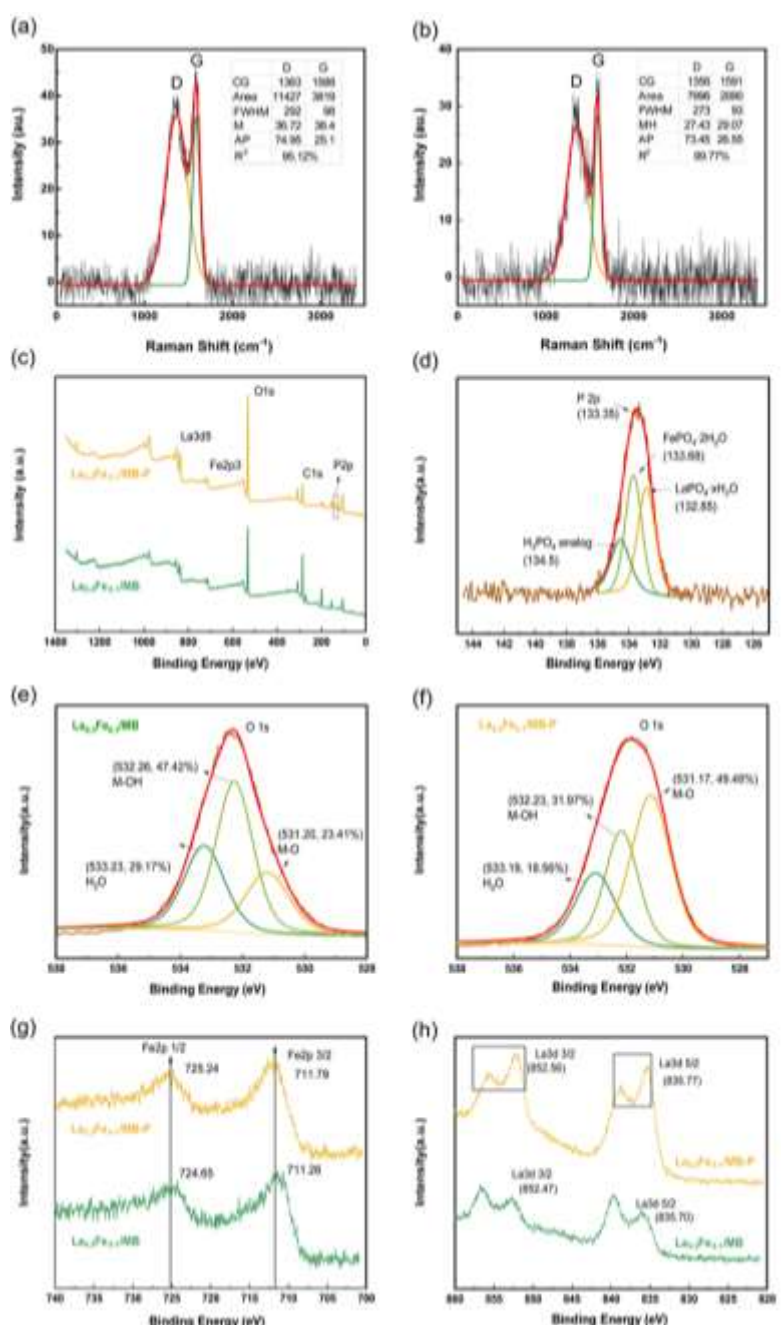
Figure 3.5 Raman mapping analysis of $La_{0.3}Fe_{0.1}/MB$ before (a) and after P adsorption (b); X-ray photoelectron spectra of $La_{0.3}Fe_{0.1}/MB$ before and after P adsorption: survey scan (c); P $_{2p}$ region (d); O $_{1s}$ region (e and f); Fe $_{2p}$ region (g) and La $_{3d}$ region (h).

In addition, the Fe $_{2p1/2}$, and Fe $_{2p3/2}$ spectra showed a slight shift in peaks from 724.65 and 711.26 eV to 725.24 and 711.79 eV, and this shift agreed well with the formation of Fe—O—

P bonding (Fang et al., 2018), implying the possible involvement of iron during phosphate uptake. Moreover, the peaks associated with La $_{3d5/2}$ and La $_{3d3/2}$ located at 835.70 eV/839.46, 852.47 eV/856.46 eV were found for La$_{0.3}$Fe$_{0.1}$/MB in the XPS spectra, while the binding energies shifted to 835.77 eV (La $_{3d5/2}$) and 852.56 eV (La $_{3d3/2}$) after the capture of P, which was likely due to a possible transfer of electrons leading to the formation of LaPO$_4$·xH$_2$O after adsorption (Wu et al., 2017; Xu et al., 2019). The XRD pattern of La$_{0.3}$Fe$_{0.1}$/MB further successfully verified the formation of La—P with weak typical peaks of LaPO$_4$ (JCPDS 04-0635), based on previous investigation (Shi et al., 2019), as shown in Fig. S3.6. These results demonstrated that phosphate was removed via the precipitation of Fe/La and phosphate ions (Li et al., 2016), which confirmed that Fe and La were involved in phosphate adsorption.

To summarize, electrostatic attraction, ligand exchange, and surface precipitation were collectively involved in the removal of P by La$_{0.3}$Fe$_{0.1}$/MB. Moreover, the adsorption of phosphate ions on the surface of the adsorbent was favourable and exhibited an excellent binding affinity according to the isotherms and thermodynamic investigations.

3.3.5 Practical application potential

3.3.5.1 Effect of co-existing ions on phosphate adsorption

There is a variety of co-existing ions such as Cl$^-$, NO$_3^-$, SO$_4^{2-}$, and HCO$_3^-$ in actual wastewater, which may affect the P removal efficiency of adsorbent through Coulomb force (Chen et al., 2016), but also due to other mechanisms (Chen et al., 2015; Shi et al., 2019). It has previously been reported that HCO$_3^-$ anion can compete with phosphate by forming inner-sphere complexes reducing P removal efficiency (Chen et al., 2015; Shi et al., 2019). In a further set of experiments, the effects of interfering co-existing ions on phosphate adsorption onto La$_{0.3}$Fe$_{0.1}$/MB at the concentrations of 50 and 100 mg P L^{-1} were assessed with the result shown in Fig. 3.6a. As observed, NO$_3^-$ was found to possess a negligible effect on P adsorption by La$_{0.3}$Fe$_{0.1}$/MB, closely followed by SO$_4^{2-}$, and Cl$^-$ which exhibited insignificant effects on P uptake with above 97.64% and 96.15% of phosphate removal occurring at both co-existing ions concentrations, respectively. In relative terms, the adsorption capacity decreased in the range examined, with 94.22% and 91.53% of P uptake in the presence of HCO$_3^-$ at 50 and 100 mg L^{-1}, respectively. It was evident that HCO$_3^-$ had some influence on P binding onto La$_{0.3}$Fe$_{0.1}$/MB, especially at a relatively higher concentration. Maybe due to the affinity of La-based adsorbents

for HCO_3^- is higher than that for PO_4^{3-} (Qiu et al., 2017). Overall, data analysis shows that common anions in water have an insignificant influence on the adsorption capacity of $La_{0.3}Fe_{0.1}$/MB for P removal. In other words, these results suggested $La_{0.3}Fe_{0.1}$/MB be suitable for real wastewater implementation owing to its outstanding attraction for P in the case of ions interference.
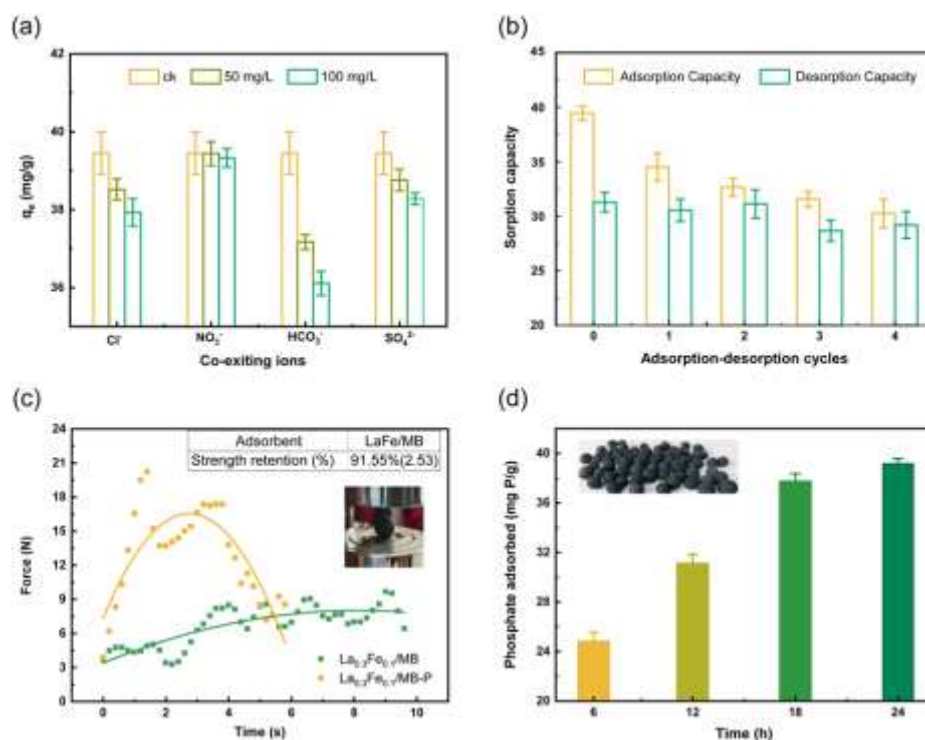
Figure 3.6 Effects of co-existing ions on phosphate adsorption by $La_{0.3}Fe_{0.1}$/MB at pH=7.05 (a), adsorption-desorption cycle experiments of phosphate (b), Force changes of adsorbent before and after adsorption (4 mm in diameter) (c), and Phosphate adsorption capacity of wastewater (d).

3.3.5.2 Consecutive regeneration

Reusability of adsorbent is important for evaluating the practicability and cost-effectiveness of wastewater treatment processes and materials. The regeneration test was then carried out to evaluate the applicability of $La_{0.3}Fe_{0.1}$/MB from an economical perspective. As seen from Fig. 3.4a, the decrease in adsorption capacity at higher pH region indicated that highly alkaline pH may cause the desorption of P from $La_{0.3}Fe_{0.1}$/MB. The adsorbent after P saturation was subjected to regeneration with 0.1 mol L^{-1} NaOH solution. The results showed that after four adsorption-desorption cycles, $La_{0.3}Fe_{0.1}$/MB experienced 87.48% bind of P during the 1st cycle and more than 76.23% of adsorption efficiency was maintained after four cycles as shown in Fig. 3.6b. The slight decrease in phosphorus adsorption may be due to permanent filling of the

active site by subsequent uptake cycles (Zhang et al., 2021a). In addition, the desorption capacity was maintained at 29.21 mg g^{-1} after four cycles confirming the La$_{0.3}$Fe$_{0.1}$/MB P-recovery potential even after reuse. These results further emphasize the outstanding practical applicability of La$_{0.3}$Fe$_{0.1}$/MB in the field of adsorption, making it suitable for the purification of phosphate-containing wastewater.

3.3.5.3 Actual river water phosphorus adsorption and strength retention

The pond water of Jiangsu Academy of Agricultural Sciences was taken as the test sample to evaluate the actual application potential of the adsorbent (basic parameters, as well as the specific sampling point and time, are detailed in Text S3.4). To this sample, a certain amount of phosphate was added to adjust the concentration of phosphate to 30 mg P L^{-1}. The strength retention rate, pressure resistance, and phosphorus adsorption capacity of La$_{0.3}$Fe$_{0.1}$/MB were measured, respectively, at the end of 24 h of adsorption (Fig. 3.6c and d). It can be seen that after the practical wastewater treatment operation, the adsorbent still showed a high strength retention rate up to 91.55%, and its resistance to pressure change increased from 6.21 N to 16.54 N. This was due to the complexation reaction and crystallization, which can be beneficial to the efficient recovery of phosphorus resources. Compared with simulated water, the phosphorus adsorption equilibrium of adsorbent in actual wastewater was delayed from 3 h to 18 h, but the adsorption capacity did not change much, indicating that it has excellent potential in practical engineering application.

Meanwhile, metal leaching of La$_{0.3}$Fe$_{0.1}$/MB in actual wastewater was tracked (Text S3.5), which was adapted according to Shen et al. (2022). From Supplementary data Table S3.3, it could be seen that given actual wastewater contains a high amount of Fe, while La was not detectable. When La$_{0.3}$Fe$_{0.1}$/MB was added, the concentration of La was increased with the prolonged leaching time until equilibrium after the third day, reaching a maximum of 0.006 mg L^{-1}, which was below the standard limit of European Union. It is worth noting that, due to the rich specific surface area and functional groups of La$_{0.3}$Fe$_{0.1}$/MB, which has a certain adsorption capacity for Fe, and little Fe leached, the trial group had slightly lower Fe concentration than the control group on day 0. However, the Fe concentration of the control group was generally balanced on day 5, mainly because the suspended particles in the water settled. The Fe concentration increased from 0.0613 mg L^{-1} to 0.0807 mg L^{-1} on the first day, indicating partial iron leaching from La$_{0.3}$Fe$_{0.1}$/MB. It then tended to balance and the concentration decreased to

0.0440 mg L^{-1}, which was still slightly larger than the control group, indicating that partial Fe leaching from La$_{0.3}$Fe$_{0.1}$/MB into wastewater occurred. By the seventh day, the Fe concentration had increased by 0.0023 mg L^{-1} (Δ_{Fe}), with Fe values still being far lower than the standard limit value (0.03 mg L^{-1}) required of supplementary items found in centralized drinking water or surface water sources, as specified by Chinese National Standard GB 3838-2002 (Environmental Quality Standards for Surface Water). These results demonstrate that the presence of metal (Fe and La) oxides in biochar has a low potential environmental risk to water bodies.

3.4 Conclusions

Herein, a formable porous biochar (LaFe/MB) was synthesized via in situ preloading of lanthanide/iron oxide and montmorillonite nanoparticles on the biochar surface, followed by co-pyrolysis. Phosphate adsorption performance of this composite was then evaluated. The results showed that the molar ratio of Fe and La significantly influenced the phosphate adsorption performance. The adsorption kinetic data could be fitted well by the pseudo-second-order model and Langmuir isotherm, indicating that LaFe/MB had a high adsorption efficiency for phosphate. The presence of most co-existing ions had little impact on phosphate adsorption. LaFe/MB was characterized by FTIR, XRD, SEM/EDX, zeta potential measurements, and XPS analyses. The results demonstrated that electrostatic attraction, ligand exchange, and surface precipitation played major roles in phosphate removal with maximum equilibrium adsorption capacity (Langmuir model) of 52.12 mg P g^{-1}. Negative ΔG^0, positive ΔH^0, and ΔS^0 values indicated that the adsorption of phosphate onto LaFe/MB was a spontaneous and endothermic process. The strength retention rate of LaFe/MB was as high as 91.6% in the actual wastewater application, and resistance to pressure of LaFe/MB before and after adsorption increased from 6.21 N to 16.54 N, which is conducive to the recovery of biochar. This work demonstrated that LaFe/MB is a promising adsorbent that being both enhanced the relief of eutrophication and realized the efficient recovery of phosphorus strategic resources. Future experiments will evaluate the LaFe/MB adsorbents' potential for recovering phosphate from multiple actual wastewater scenarios, environmental impact assessment, techno-economic investigation, and life cycle analysis of formable porous biochar are required for future performance validation.

References

Ahmed S, Lo I M C, (2020). Phosphate removal from river water using a highly efficient magnetically recyclable $Fe_3O_4/La(OH)_3$ nanocomposite. Chemosphere 261: 128118.

Ai T, Jiang X J, Liu Q Y, et al. (2019). Daptomycin adsorption on magnetic ultra-fine wood-based biochars from water: Kinetics, isotherms, and mechanism studies. Bioresource Technology 273: 8-15.

An X, Wu Z, Yu J, et al. (2020). High-Efficiency Reclaiming Phosphate from an Aqueous Solution by Bentonite Modified Biochars: A Slow Release Fertilizer with a Precise Rate Regulation. ACS Sustainable Chemistry & Engineering 8: 6090-6099.

Arif M, Liu G, Yousaf B, et al. (2021). Synthesis, characteristics and mechanistic insight into the clays and clay minerals-biochar surface interactions for contaminants removal-A review. Journal of Cleaner Production 310: 127548.

Arola K, Mänttäri M, Kallioinen M, (2021). Two-stage nanofiltration for purification of membrane bioreactor treated municipal wastewater – Minimization of concentrate volume and simultaneous recovery of phosphorus. Separation and Purification Technology 256: 117255.

Awual M R, Jyo A, Ihara T, et al. (2011). Enhanced trace phosphate removal from water by zirconium(IV) loaded fibrous adsorbent. Water Research 45: 4592-4600.

Bacelo H, Pintor A M A, Santos S C R, et al. (2020). Performance and prospects of different adsorbents for phosphorus uptake and recovery from water. Chemical Engineering Journal 381:122566.

Banu H T, Karthikeyan P, Meenakshi S, (2018). Lanthanum (III) encapsulated chitosan-montmorillonite composite for the adsorptive removal of phosphate ions from aqueous solution. International Journal of Biological Macromolecules 112: 284-293.

Cakmak E K, Hartl M, Kisser J, et al. (2022). Phosphorus mining from eutrophic marine environment towards a blue economy: The role of bio-based applications. Water Research 219: 118505.

Caravelli A H, De Gregorio C, Zaritzky N E, (2012). Effect of operating conditions on the chemical phosphorus removal using ferric chloride by evaluating orthophosphate precipitation and sedimentation of formed precipitates in batch and continuous systems. Chemical Engineering Journal 209: 469-477.

Carter M C, Kilduff J, WEBER JR W J, (1995). Site energy distribution analysis of preloaded adsorbents. Environment Science & Technology 29: 1773–1780.

Cerofoline G F, (1974). Localized adsorption on heterogeneous surfaces. Thin Solid Films 23: 129–152.

Chen L, Chen X L, Zhou C H, et al. (2017). Environmental-friendly montmorillonite-biochar composites: Facile production and tuneable adsorption-release of ammonium and phosphate. Journal of Cleaner Production 156: 648-659.

Chen L, Zhao X, Pan B C, et al. (2015). Preferable removal of phosphate from water using hydrous zirconium oxide-based nanocomposite of high stability. Journal of Hazardous Materials 284: 35-42.

Chen M, Huo C, Li Y, et al. (2016). Selective Adsorption and Efficient Removal of Phosphate from Aqueous Medium with Graphene–Lanthanum Composite. ACS Sustainable Chemistry & Engineering 4: 1296-1302.

Chen W, Meng J, Han X, et al. (2019). Past, present, and future of biochar. Biochar 1: 75-87.

Delaney P, McManamon C, Hanrahan J P, et al, (2011), Development of chemically engineered porous metal oxides for phosphate removal. Journal of Hazardous Materials 185: 382-391.

Fang L, Liu R, Li J, et al. (2018). Magnetite/Lanthanum hydroxide for phosphate sequestration and recovery from lake and the attenuation effects of sediment particles. Water Research 130: 243-254.

Feng Y, Lu H, Liu Y, et al. (2017). Nano-cerium oxide functionalized biochar for phosphate retention: preparation, optimization and rice paddy application. Chemosphere 185: 816-825.

Fletcher A J, Smith M A, Heinemeyer A, et al. (2013). Production factors controlling the physical characteristics of biochar derived from phytoremediation willow for agricultural applications. BioEnergy Research 7: 371-380.

Fu H Y, Yang Y X, Zhu R L, et al. (2018). Superior adsorption of phosphate by ferrihydrite-coated and lanthanum decorated magnetite. Journal of Colloid and Interface Science 530: 704-713.

Goscianska J, Ptaszkowska-Koniarz M, Frankowski M, et al. (2018). Removal of phosphate from water by lanthanum-modified zeolites obtained from fly ash. Journal of Colloid and Interface Science 513: 72-81.

Haris M, Usman M, Su F, et al. (2022). Programmable synthesis of exfoliated biochar nanosheets for selective and highly efficient adsorption of thallium. Chemical Engineering Journal 434: 134842.

He Y H, Lin H, Dong Y B, et al, (2016). Simultaneous removal of ammonium and phosphate by alkaline-activated and lanthanum-impregnated zeolite. Chemosphere 164: 387-395.

He Y H, Lin H, Dong Y B, et al. (2017). Preferable adsorption of phosphate using lanthanum-incorporated porous zeolite: Characteristics and mechanism. Applied Surface Science 426: 995-1004.

Huang X, Wei D, Zhang X W, et al. (2019). Synthesis of amino-functionalized magnetic aerobic granular sludge-biochar for Pb(II) removal: Adsorption performance and mechanism studies. Science of the Total Environment 685: 681-689.

Huang Y, He Y, Zhang H, et al. (2022). Selective adsorption behaviour and mechanism of phosphate in water by different lanthanum modified biochar. Journal of Environmental Chemical Engineering 10: 107476.

Islam M S, Zhang Y, Dong S, et al. (2017). Dynamics of microbial community structure and nutrient removal from an innovative side-stream enhanced biological phosphorus removal process. Journal of Environmental Management 198: 300-307.

Jack J, Huggins T M, Huang Y P, et al. (2019). Production of magnetic biochar from waste-derived fungal biomass for phosphorus removal and recovery. Journal of Cleaner Production 224: 100-106.

Jung K W, Ahn K H, (2016). Fabrication of porosity-enhanced MgO/biochar for removal of phosphate from aqueous solution: Application of a novel combined electrochemical modification method. Bioresource Technology 200: 1029-1032.

Jung K W, Jeong T U, Kang H J, et al. (2016). Characteristics of biochar derived from marine macroalgae and fabrication of granular biochar by entrapment in calcium-alginate beads for phosphate removal from aqueous solution. Bioresource Technology 211: 108-116.

Krishnan K A, Haridas A, (2008). Removal of phosphate from aqueous solutions and sewage using natural and surface modified coir pith. Journal of Hazardous Materials 152: 527-535.

Kumar M, Xiong X, Wan Z, et al. (2020a). Ball milling as a mechanochemical technology for fabrication of novel biochar nanomaterials. Bioresource Technology 312: 123613.

Kumar M, Xiong X N, Wan Z H, et al. (2020b). Ball milling as a mechanochemical technology for fabrication of novel biochar nanomaterials. Bioresource Technology 312:123613.

Lai L, Xie Q, Chi L, et al. (2016). Adsorption of phosphate from water by easily separable $Fe_3O_4@SiO_2$ core/shell magnetic nanoparticles functionalized with hydrous lanthanum oxide. J Colloid Interface Sci 465: 76-82.

Lazaratou C V, Vayenas D V, Papoulis D, (2020). The role of clays, clay minerals and clay-based materials for nitrate removal from water systems: A review. Applied Clay Science 185: 105377.

Le Corre K S, Valsami-Jones E, Hobbs P, et al. (2009). Phosphorus Recovery from Wastewater by Struvite Crystallization: A Review. Critical Reviews in Environmental Science and Technology 39: 433-477.

Li G, Shen B, Li F, et al. (2015). Elemental mercury removal using biochar pyrolyzed from municipal solid waste. Fuel Processing Technology 133: 43-50.

Li G Y, Jiang Y R, Huang K L, et al. (2008). Preparation and properties of magnetic Fe_3O_4-chitosan nanoparticles. Journal of Alloys and Compounds 466: 451-456.

Li H, Zhao Y, Xiao Z, et al. (2021). Analysis on approximate site energy distribution and adsorption behaviours unveils reasons for highly efficient phosphorus removal by a novel sludge-based magnetic gel bead. Chemical Engineering Journal 422: 130028.

Li R H, Wang J J, Zhou B Y, et al. (2016). Recovery of phosphate from aqueous solution by magnesium oxide decorated magnetic biochar and its potential as phosphate-based fertilizer substitute. Bioresource Technology 215: 209-214.

Li X, Kuang Y, Chen J, et al. (2020). Competitive adsorption of phosphate and dissolved organic carbon on lanthanum modified zeolite. Journal of Colloid and Interface Science 574: 197-206.

Liao P, Li B, Xie L, et al. (2020). Immobilization of Cr(VI) on engineered silicate nanoparticles: Microscopic mechanisms and site energy distribution. Journal of Hazardous Materials 383: 121145.

Liu L, Zhang C, Chen S, et al. (2022). Phosphate adsorption characteristics of $La(OH)_3$-modified, canna-derived biochar. Chemosphere 286: 131773.

Melia P M, Busquets R, Hooda P S, et al. (2019). Driving forces and barriers in the removal of phosphorus from water using crop residue, wood and sewage sludge derived biochars. Science of the Total Environment 675: 623-631.

Mohan D, Sarswat A, Ok Y S, et al. (2014). Organic and inorganic contaminants removal from water with biochar, a renewable, low cost and sustainable adsorbent - A critical review. Bioresource Technology 160: 191-202.

Mosa A, El-Ghamry A, Tolba M, (2018). Functionalized biochar derived from heavy metal rich feedstock: Phosphate recovery and reusing the exhausted biochar as an enriched soil amendment. Chemosphere 198: 351-363.

Ngatia L W, Hsieh Y P, Nemours D, et al. (2017). Potential phosphorus eutrophication mitigation strategy: Biochar carbon composition, thermal stability and pH influence phosphorus sorption. Chemosphere 180: 201-211.

Panahi H K S, Dehhaghi M, Ok Y S, et al. (2020). A comprehensive review of engineered biochar: Production, characteristics, and environmental applications. Journal of Cleaner Production 270:122462.

Pezoti O, Cazetta A L, Bedin K C, et al. (2016). NaOH-activated carbon of high surface area produced from guava seeds as a high-efficiency adsorbent for amoxicillin removal: Kinetic, isotherm and thermodynamic studies. Chemical Engineering Journal 288: 778-788.

Qiu H, Liang C, Yu J H, et al. (2017). Preferable phosphate sequestration by nano-La(III) (hydr)oxides modified wheat straw with excellent properties in regeneration. Chemical Engineering Journal 315: 345-354.

Rajapaksha A U, Chen S S, Tsang D C W, et al. (2016). Engineered/designer biochar for contaminant removal/immobilization from soil and water: Potential and implication of biochar modification. Chemosphere 148: 276-291.

Rashidi Nodeh H, Sereshti H, Zamiri Afsharian E, et al. (2017). Enhanced removal of phosphate and nitrate ions from aqueous media using nanosized lanthanum hydrous doped on magnetic graphene nanocomposite. Journal of Environmental Management 197: 265-274.

Reguyal F, Sarmah A K, (2018). Site energy distribution analysis and influence of Fe_3O_4 nanoparticles on sulfamethoxazole sorption in aqueous solution by magnetic pine sawdust biochar. Environ Pollut 233: 510-519.

Rong X, Xie M, Kong L S, et al. (2019). The magnetic biochar derived from banana peels as a persulfate activator for organic contaminants degradation. Chemical Engineering Journal 372: 294-303.

Shen X, Guo X, Zhang M, et al. (2015). Sorption mechanisms of organic compounds by carbonaceous materials: site energy distribution consideration. Environmental Science & Technology 49: 4894-4902.

Shen X, Meng H, Shen Y, et al. (2022). A comprehensive assessment on bioavailability, leaching characteristics and potential risk of polycyclic aromatic hydrocarbons in biochars produced by a continuous pyrolysis system. Chemosphere 287: 132116.

Shi W M, Fu Y W, Jiang W, et al. (2019). Enhanced phosphate removal by zeolite loaded with Mg-Al-La ternary (hydr)oxides from aqueous solutions: Performance and mechanism. Chemical Engineering Journal 357: 33-44.

Song B Q, Chen M, Zhao L, et al. (2019). Physicochemical property and colloidal stability of micron- and nano-particle biochar derived from a variety of feedstock sources. Science of the Total Environment 661: 685-695.

Su Y, Cui H, Li Q, et al. (2013). Strong adsorption of phosphate by amorphous zirconium oxide nanoparticles. Water Research 47: 5018-5026.

Sun Y Q, Yu I K M, Tsang D C W, et al. (2019). Multifunctional iron-biochar composites for the removal of potentially toxic elements, inherent cations, and hetero-chloride from hydraulic fracturing wastewater. Environment International 124: 521-532.

Tian S, Jiang P, Ning P, et al. (2009). Enhanced adsorption removal of phosphate from water by mixed lanthanum/aluminium pillared montmorillonite. Chemical Engineering Journal 151: 141-148.

Tomczyk A, Sokolowska Z, Boguta P, (2020). Biochar physicochemical properties: pyrolysis temperature and feedstock kind effects. Reviews in Environmental Science and Bio-Technology 19: 191-215.

Tran H N, You S J, Hosseini-Bandegharaei A, et al. (2017). Mistakes and inconsistencies regarding adsorption of contaminants from aqueous solutions: A critical review. Water Research 120: 88-116.

Vieira R M, Vilela P B, Becegato V A, et al. (2018). Chitosan-based hydrogel and chitosan/acid-activated montmorillonite composite hydrogel for the adsorption and removal of Pb^{+2} and Ni^{+2} ions accommodated in aqueous solutions. Journal of Environmental Chemical Engineering 6: 2713-2723.

Viglasova E, Galambos M, Dankova Z, et al. (2018). Production, characterization and adsorption studies of bamboo-based biochar/montmorillonite composite for nitrate removal. Waste Management 79: 385-394.

Wang B, Gao B, Fang J, (2017). Recent advances in engineered biochar productions and applications. Critical Reviews in Environmental Science and Technology 47: 2158-2207.

Wang B, Shang C, Xie H, et al. (2022). Unravelling natural aging-induced properties change of sludge-derived hydrochar and enhanced cadmium sorption site heterogeneity. Biochar 4:34.

Wang K, Sun Y B, Tang J C, et al. (2020a). Aqueous Cr(VI) removal by a novel ball milled Fe^0-biochar composite: Role of biochar electron transfer capacity under high pyrolysis temperature. Chemosphere 241: 125044.

Wang L, Wang J Y, Yan W, et al. (2020b). $MgFe_2O_4$-biochar based lanthanum alginate beads for advanced phosphate removal. Chemical Engineering Journal 387: 123305.

Wang Z H, Shen D K, Shen F, et al, (2016), Phosphate adsorption on lanthanum loaded biochar. Chemosphere 150: 1-7.

Weber K, Quicker P, (2018). Properties of biochar. Fuel 217: 240-261.

Wu B L, Fang L P, Fortner J D, et al. (2017). Highly efficient and selective phosphate removal from wastewater by magnetically recoverable $La(OH)_3/Fe_3O_4$ nanocomposites. Water Research 126: 179-188.

Wu L, Zhao X, Bi E, (2022). Predicting the effect of dissolved humic acid on sorption of benzotriazole to biochar. Biochar 4: 15.

Wu P, Ata-Ul-Karim S T, Singh B P, et al. (2019). A scientometric review of biochar research in the past 20 years (1998–2018). Biochar 1: 23-43.

Wu P, Wang Z, Wang H, et al. (2020). Visualizing the emerging trends of biochar research and applications in 2019: a scientometric analysis and review. Biochar 2: 135-150.

Xu C Y, Li Q R, Geng Z C, et al. (2020a). Surface properties and suspension stability of low-temperature pyrolyzed biochar nanoparticles: Effects of solution chemistry and feedstock sources. Chemosphere 259:127510.

Xu Q, Chen Z, Wu Z, et al. (2019). Novel lanthanum doped biochars derived from lignocellulosic wastes for efficient phosphate removal and regeneration. Bioresour Technol 289: 121600.

Xu X, Cheng Y, Wu X, et al. (2020b). La(III)-bentonite/chitosan composite: A new type adsorbent for rapid removal of phosphate from water bodies. Applied Clay Science 190: 105547.

Yang F, Zhao L, Gao B, et al. (2016). The Interfacial Behaviour between Biochar and Soil Minerals and Its Effect on Biochar Stability. Environmental Science & Technology 50: 2264-2271.

Yao Y, Gao B, Chen J J, et al. (2013). Engineered Biochar Reclaiming Phosphate from Aqueous Solutions: Mechanisms and Potential Application as a Slow-Release Fertilizer. Environmental Science & Technology 47: 8700-8708.

Yao Y, Gao B, Fang J, et al. (2014). Characterization and environmental applications of clay–biochar composites. Chemical Engineering Journal 242: 136-143.

Yap P L, Kabiri S, Tran D N H, et al. (2019). Multifunctional binding chemistry on modified graphene composite for selective and highly efficient adsorption of mercury. ACS Appl Mater Interfaces 11: 6350-6362.

Yin H B, Kong M, Gu X H, et al. (2017). Removal of arsenic from water by porous charred granulated attapulgite-supported hydrated iron oxide in bath and column modes. Journal of Cleaner Production 166: 88-97.

Yu Q, Zhang R Q, Deng S B, et al. (2009). Sorption of perfluorooctane sulfonate and perfluorooctanoate on activated carbons and resin: Kinetic and isotherm study. Water Research 43: 1150-1158.

Zhang L, Wan L H, Chang N, et al. (2011). Removal of phosphate from water by activated carbon fibre loaded with lanthanum oxide. Journal of Hazardous Materials 190: 848-855.

Zhang M, Song G, Gelardi D L, et al. (2020). Evaluating biochar and its modifications for the removal of ammonium, nitrate, and phosphate in water. Water Research 186:116303.

Zhang Y, Akindolie M S, Tian X, et al. (2021a). Enhanced phosphate scavenging with effective recovery by magnetic porous biochar supported La(OH)$_3$: Kinetics, isotherms, mechanisms and applications for water and real wastewater. Bioresour Technol 319: 124232.

Zhang Y Y, Ahmed S, Zheng Z X, et al. (2021b). Validation of pilot-scale phosphate polishing removal from surface water by lanthanum-based polymeric nanocomposite. Chemical Engineering Journal 412:128630.

Zhong Z, Lu X, Yan R, et al. (2020). Phosphate sequestration by magnetic La-impregnated bentonite granules: A combined experimental and DFT study. Science of the Total Environment 738: 139636.

Zhu S H, Wang S, Yang X, et al. (2020). Green sustainable and highly efficient hematite nanoparticles modified biochar-clay granular composite for Cr(VI) removal and related mechanism. Journal of Cleaner Production 276:123009.

APPENDIX

Supplementary Information

CHAPTER 3: FORMABLE POROUS BIOCHAR LOADED WITH LA-FE(HYDR)OXIDES/MONTMORILLONITE FOR EFFICIENT REMOVAL OF PHOSPHORUS IN WASTEWATER: PROCESS AND MECHANISMS

Summary

Text S3.1 Mathematical equations and corresponding curve fitting model formulas of adsorption kinetics.

Text S3.2 Langmuir and Freundlich isotherm models of adsorption isotherms.

Text S3.3 Adsorption site energy distribution.

Text S3.4 Basic parameters of the pond water, as well as the specific sampling point and time.

Text S3.5 Leaching experiment of Fe and La from $La_{0.3}Fe_{0.1}/MB$ in actual water.

Figure S3.1 Phosphate adsorption capacities of different adsorbents in a solution with an initial concentration of 100 mg P L^{-1}.

Figure S3.2 Scanning electron microscopy (SEM) images of (a) B, (b) MB, (c) $Fe_{0.4}/MB$, (d) $La_{0.4}/MB$.

Figure S3.3 Energy-dispersive spectra (EDS) of B, MB, M, $Fe_{0.4}/MB$, $La_{0.3}Fe_{0.1}/MB$, and $La_{0.4}/MB$.

Figure S3.4 Phosphate adsorption fitted data of $La_{0.3}Fe_{0.1}/MB$ conducted by intra-particle diffusion model results.

Figure S3.5 Langmuir model based-site energy on phosphate solid-phase sorption (a), Langmuir model based-site energy distribution of phosphate sorption on $La_{0.3}Fe_{0.1}/MB$ (b).

Figure S3.6 XRD patterns of $La_{0.3}Fe_{0.1}/MB$ after phosphate adsorption.

Table S3.1 Preparation conditions used to obtain the different formable porous granulated LaFe/MB adsorbents.

Table S3.2 Surface elemental composition (wt.%) of adsorbents.

Table S3.3 Leaching concentration of Fe and La from $La_{0.3}Fe_{0.1}/MB$ in actual water.

Note: Biochar (B), Montmorillonite (M), Biochar/montmorillonite (MB), respectively.

Text S3.1 Mathematical equations and corresponding curve fitting model formulas of adsorption kinetics.

To better understand the mechanism that controls the adsorption kinetics and the phosphate adsorption process on adsorbent, a pseudo-first-order model, pseudo-second-order model, and intra-particle diffusion models were employed to fit the sorption kinetic data (Tang et al., 2018). The mathematical equations for these models are given in Eqs. (1) to (3).

Pseudo-first-order equation [1]:

$$\ln (q_e - q_t) = \ln q_e - k_1 t$$

Pseudo-second-order equation [2]:

$$t/q_t = 1/k_2 q^2_e + t/q_e$$

Intra-particle diffusion equation [3]:

$$q_t = k_{di} t^{1/2} + C_i$$

where q_t and q_e (mg P g^{-1}) are the amounts adsorbed at time t and at equilibrium, respectively; t (min) is the sorption time; and k_1 (min) and k_2 (g/(mg min)) are the rate constants for the pseudo-first-order model and the pseudo-second-order model, respectively, which can be determined from the experimental data by regression analysis; k_{di} [g/(mg·min$^{0.5}$)] is the adsorption rate constant of the intra-particle diffusion models, and C_i (mg g^{-1}) is a constant of the intra-particle diffusion model, which is related to the thickness of the boundary layer.

Text S3.2 Langmuir and Freundlich isotherm models of adsorption isotherms.

And their equations were presented using the following equations, respectively.

Langmuir model [4]:

$$q_e = k_L q_m C_e / (1 + k_L C_e)$$

Freundlich model [5]:

$$q_e = k_F C_e^{1/n}$$

Where k_L (L·mg^{-1}) and k_F (mg·g^{-1}) are constants related to the Langmuir adsorption and Freundlich affinity, respectively. q_m represents the Langmuir maximum capacity (mg P g^{-1}), n is the Freundlich empirical constant and C_e is the solution concentration at equilibrium (mg P L^{-1}).

Text S3.3 Adsorption site energy distribution.

The site energy distribution of LaFe/MB can be deduced from the Langmuir model based on an assumption of the distribution of site energies, expressed as Eq. (6).

$$Q_e(C_e) = \int_0^{+\infty} Q_h(E, C_e)F(E)\mathrm{d}E \qquad (6)$$

where C_e is the equilibrium aqueous-phase concentration (mg L^{-1}), Q_e (C_e) is the total sorbed solid-phase concentration (mg g^{-1}), Q_h (E, C_e) is energetically homogeneous isotherm with sorption energy E (mg g^{-1}), and $F(E)$ is the site energy frequency function of homogeneous sorption site energies (mol-mg/J-g). The range of the energies is assumed to be from 0 to infinity (∞) since the value of negative infinity (-∞) will not have any physical meaning (Reguyal and Sarmah, 2018).

Based on the condensation approximation or asymptotically correct approximation proposed by Wang (Wang et al., 2022), the equilibrium aqueous-phase concentration (C_e) of P is related to the sorption site energy (E) given by Eq. (7).

$$C_e = C_s \exp\left(-\frac{E-E_s}{RT}\right) = C_s \exp\left(-\frac{E^*}{RT}\right) \qquad (7)$$

where C_s is the maximum solubility of phosphate solution (KH$_2$PO$_4$) at 28°C (mg L^{-1}), E_s is the lowest physically realizable sorption energy when $C_e = C_s$, (J mol^{-1}), R is the universal gas constant (J/mol-K), T is the absolute temperature (K), and calculated E^* is the divergence of sorption energies between the sorbent surface in the solvent and the sorbate (J mol^{-1}), determined by substituting the C_e and C_s into Eq. (7).

Incorporating Eq. (7) into the Langmuir model, Q_e (E^*) was expressed by Eq. (8).

$$Q_e = Q_{max} \frac{K_L C_s \exp\left(\frac{E^*}{RT}\right)}{K_L C_s \exp\left(\frac{E^*}{RT}\right) + 1} \qquad (8)$$

where K_L is the Langmuir affinity coefficient (L kg^{-1}), Qmax is the maximum sorption capacity (mg g^{-1}), and C_e is the equilibrium aqueous-phase concentration (mg L^{-1}).

The approximate site energy distribution $F(E^*)$ can be obtained by differentiating the isotherm Q_e (E^*) with respect to E^* as shown by Eq. (9) (Wang et al., 2022).

$$F(E^*) = Q_{max} \frac{K_L C_s \exp\left(\frac{E^*}{RT}\right)}{RT\left(K_L C_s \exp\left(\frac{E^*}{RT}\right)+1\right)^2} \qquad (9)$$

Text S3.4 Basic parameters of the pond water, as well as the specific sampling point and time.

The pond water of Jiangsu Academy of Agricultural Sciences was taken as the test sample to evaluate the actual application potential of the adsorbent, the basic parameters of the pond water, with total nitrogen content (4.94 ± 0.24) mg L^{-1} and total phosphorus content (0.58 ± 0.04) mg L^{-1}. The sampling time was September 2021, and the sampling site was pond water 10 cm above the surface.

Text S3.5 Leaching experiment of Fe and La from $La_{0.3}Fe_{0.1}/MB$ in actual water.

To determine the leachability of Fe and La from $La_{0.3}Fe_{0.1}/MB$. The leaching test was adapted according to Shen (2022). Briefly, approximately 2 g of $La_{0.3}Fe_{0.1}/MB$ was mixed with 1000 mL of the ditch water (pH, 8.21; EC, 301 us cm^{-1}; TOC, 8.07mg L^{-1}; TN, 2.65 mg L^{-1}; TP, 0.376 mg L^{-1}.) in a 2000-mL polyethylene vessel. The mixture was tumbled at a speed of 30 rpm for 7 days at 25°C. Supernatants were taken on days 0, 1, 3, 5, and 7 d and filtered through 0.45 μm membrane filters, then the concentration of Fe and La were measured by inductively coupled plasma mass spectrometry (ICP-MS, Thermo Fisher Scientific, USA). Among them, the day 0 represents the sample on the sampling day and just after the corresponding materials were added. And ditch water + $La_{0.3}Fe_{0.1}/MB$ was marked as trial group, while the ditch water was control group, respectively.

Figure S3.1 Phosphate adsorption capacities of different adsorbents in a solution with an initial concentration of 100 mg P L^{-1}.

Figure S3.2 Scanning electron microscopy (SEM) images of (a) B, (b) MB, (c) Fe$_{0.4}$/MB, (d) La$_{0.4}$/MB.

Figure S3.3 Energy-dispersive spectra (EDS) of B, MB, M, $Fe_{0.4}/MB$, $La_{0.3}Fe_{0.1}/MB$, and $La_{0.4}/MB$.
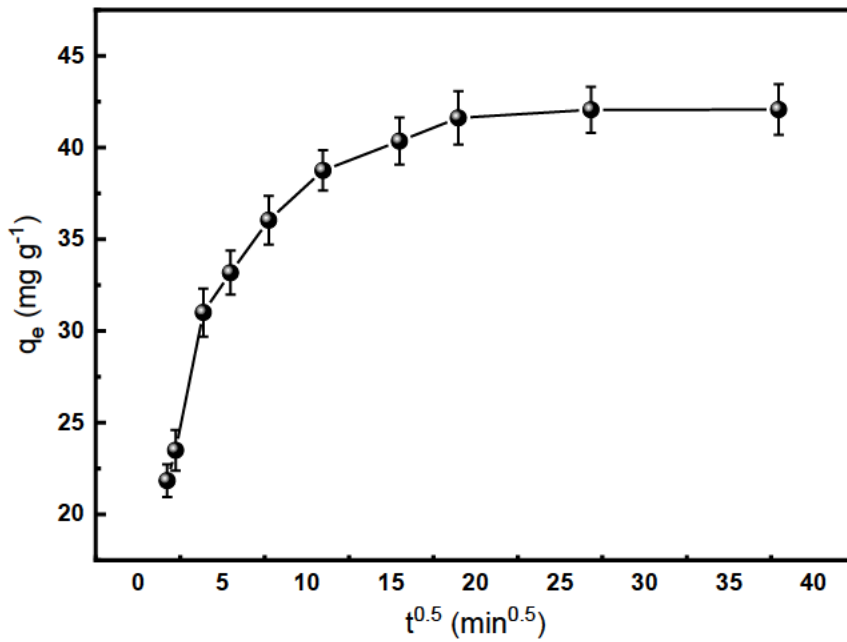
Figure S3.4 Phosphate adsorption fitted data of $La_{0.3}Fe_{0.1}/MB$ conducted by intra-particle diffusion model results.

Figure S3.5 Langmuir model based-site energy on phosphate solid-phase sorption (a), Langmuir model based-site energy distribution of phosphate sorption on $La_{0.3}Fe_{0.1}/MB$ (b).

Figure S3.6 XRD patterns of $La_{0.3}Fe_{0.1}/MB$ after phosphate adsorption. The marks of $LaPO_4$ (JCPDS 04-0635) were referenced from the reported earlier (Shi et al., 2019).

Table S3.1 Preparation conditions used to obtain the different formable porous granulated LaFe/MB adsorbents

Abbreviation	B (g)	M (g)	n Fe^{3+} (mol)	n La^{3+} (mol)
B	100	-	-	-
MB	100	50	-	-
$Fe_{0.4}$/MB	100	50	0.4	-
$La_{0.1}Fe_{0.3}$/MB	100	50	0.3	0.1
$La_{0.2}Fe_{0.2}$/MB	100	50	0.2	0.2
$La_{0.3}Fe_{0.1}$/MB	100	50	0.1	0.3
$La_{0.4}$/MB	100	50	-	0.4

Table S3.2 Surface elemental composition (wt.%) of adsorbents

Adsorbents	Elements wt.% (calculated based on EDS spectrum)							
	C	O	Mg	Al	Si	Ca	Fe	La
B	67.06	24.55	0.12	0.24	7.22	0.30	0.52	BDL
MB	46.17	35.88	0.42	3.77	10.69	0.98	2.09	BDL
$Fe_{0.4}$/MB	31.29	34.81	0.48	3.87	12.68	0.85	14.01	BDL
$La_{0.3}Fe_{0.1}$/MB	30.22	23.12	0.26	1.96	8.54	0.40	8.02	19.49
$La_{0.4}$/MB	49.05	24.58	0.12	1.14	7.76	0.52	1.03	15.80
M	BDL	53.93	0.90	9.73	28.74	0.88	5.81	BDL

Note: B, M and BDL means straw biochar, montmorillonite particles, and below detection limit, respectively.

Table S3.3 Leaching concentration of Fe and La of $La_{0.3}Fe_{0.1}$/MB in actual water

d	Control group		Trial group		Δ_{Fe}
	La (mg L^{-1})	Fe (mg L^{-1})	La (mg L^{-1})	Fe (mg L^{-1})	(mg L^{-1})
0	BDL	0.094	BDL	0.0613	-0.0327
1	BDL	0.076	0.004	0.0807	0.0047
3	BDL	0.053	0.005	0.0565	0.0035
5	BDL	0.0457	0.005	0.0463	0.0006
7	BDL	0.0417	0.006	0.0440	0.0023

Note: BDL means below detection limit; Δ_{Fe} means the difference between trial and control groups.

References

Reguyal F, Sarmah A K, (2018). Site energy distribution analysis and influence of Fe_3O_4 nanoparticles on sulfamethoxazole sorption in aqueous solution by magnetic pine sawdust biochar. Environmental Pollution 233: 510-519.

Shen X, Meng H, Shen Y, et al. (2022). A comprehensive assessment on bioavailability, leaching characteristics and potential risk of polycyclic aromatic hydrocarbons in biochars produced by a continuous pyrolysis system. Chemosphere 287: 132116.

Shi W M, Fu Y W, Jiang W, et al. (2019). Enhanced phosphate removal by zeolite loaded with Mg-Al-La ternary (hydr)oxides from aqueous solutions: Performance and mechanism. Chemical Engineering Journal 357: 33-44.

Tang N, Niu C G, Li X T, et al. (2018). Efficient removal of Cd^{2+} and Pb^{2+} from aqueous solution with amino and thiol-functionalized activated carbon: Isotherm and kinetics modelling. Science of the Total Environment 635: 1331-1344.

Wang B, Shang C, Xie H, et al. (2022). Unravelling natural aging-induced properties change of sludge-derived hydrochar and enhanced cadmium sorption site heterogeneity. Biochar 4: 34.

CHAPTER *4*

IMMOBILIZATION OF P-ACCUMULATING BACTERIA ON FORMED-BIOCHAR SUPPORTED LA/FE OXIDE NANOPARTICLES: ENHANCED REMOVAL OF PHOSPHATE

CHAPTER 4: IMMOBILIZATION OF P-ACCUMULATING BACTERIA ON FORMED-BIOCHAR SUPPORTED LA/FE OXIDE NANOPARTICLES: ENHANCED REMOVAL OF PHOSPHATE

This chapter has been submitted for publication in a peer review journal with the title: Immobilization of p-accumulating bacteria on formed-biochar supported lanthanum-iron oxide nanoparticles: Enhanced removal of phosphate in *Colloids and Surfaces A: Physicochemical and Engineering Aspects*. The manuscript is presented in the following pages.

Graphical Abstract
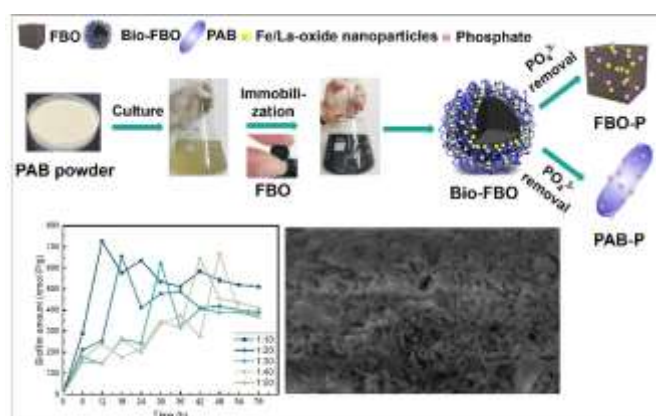
Figure 4.1 Schematic diagram illustrating the immobilization of phosphorus-accumulating bacteria onto a formed biochar and its contribution to synergistic phosphorus removal.

Abstract

Phosphorus (P) pollution levels are a major global challenge, resulting in an urgent need for P remediation. A stable, high-efficiency phosphorus removal system was established using a phosphorus accumulating bacteria (PAB) consortium in conjunction with formable-biochar supported lanthanum-iron oxide nanoparticles (FBO) to form a composite (Bio-FBO). A preliminary colonization study demonstrated that a 1:10 dilution of PAB inoculum resulted in the highest level of biofilm development on FBO nanoparticles. PAB was immobilized on the external and internal surfaces of FBO via physical adsorption. Abundant oxygen-containing

functional groups on the surface of FBO facilitate the attachment of microorganisms. P uptake by Bio-FBO reached ca. 100% after 60 h when an initial P concentration of 10 mg P/L was used. Adsorption kinetics data demonstrated that P removal from wastewater using Bio-FBO fitted well with the Pseudo-second order kinetic model. Microbial analysis showed that *Acinetobacter* was the most dominant genus in the bio-system. Members of this genus are known P accumulators in wastewater systems, and therefore, considered likely contributors to the removal of P. Phosphorous removal from solution was attributed to a combination of biological uptake mechanisms and physicochemical adsorption mechanisms. Hence, the excellent porosity, active group, and microbial attachment of Bio-FBO carbon-based biosorbents make it a promising candidate for P-removal, in P-rich wastewater treatment.

Keywords:

Formable porous biochar, Phosphorus accumulating bacteria, Phosphate removal, Immobilization microorganism; Wastewater treatment

4.1 Introduction

Since the industrial revolution, wastewater management has become one of the primary challenges in balancing the ecosystem. A large amount of wastewater is discharged every year in the world, inevitably causing a series of ecological and environmental problems, such as water pollution, and eutrophication, which adversely affect aquatic organisms (Li et al., 2016). Thus, developing cost-effective methods to remove phosphorus from contaminated wastewater remains a technological challenge.

A variety of wastewater phosphorus removal technologies have been developed and applied, such as adsorption (Xu et al., 2018), precipitation (de-Bashan and Bashan, 2004), and biological removal methods (Hou et al., 2021). Biological methods such as activated sludge (Xie et al., 2011) and biofilm technologies have attracted much attention because of their low cost and simple operation (Chaudhry and Nautiyal, 2011). These methods are advantageous since they are capable of stable performance and can support a high concentration of active biomass, which can achieve the goal of efficient phosphorus removal (Tarjányi-Szikora et al., 2013; Zhao et al., 2019). Phosphate-accumulating organisms (PAOs) are a specific group of microorganisms found in activated sludge and biofilm treatment processes that can convert free

phosphate in wastewater into polyphosphate (Kodera et al., 2013; Tarayre et al., 2016). The characteristics of aerobic phosphorus absorption and anaerobic phosphorus release are the working principle of PAOs (Zhang et al., 2021). By enriching biofilm containing PAOs, the concentration of phosphorus in solution can be significantly increased, and the content of excess sludge produced in activated sludge treatment processes is reduced (Kodera et al., 2013). However, the limitations of using free cells in wastewater treatment include biodegradation rate, cell separation, and substrate inhibition (Lin and Jianlong, 2010). To address these issues, immobilized cell technology can be applied to microbial treatment processes (Halecky et al., 2014). In establishing a biofilm treatment process, the carrier substrate used is core to the process. Fixing microorganisms on suitable carriers before wastewater treatment will help to enhance the adsorption of phosphorus. Microorganisms attached to the carrier can achieve rapid phosphorus enrichment under alternating aerobic and anaerobic conditions (Yin et al., 2015). The existence of carriers can improve the stability and activity of microorganisms, shorten the formation time of biofilm, and improve the efficiency of wastewater treatment (Zhang et al., 2016). The range of biofilm carriers that are relevant to wastewater treatment has been summarized comprehensively in the literature (Zhang et al., 2016) and can be divided into inorganic and organic biofilm carriers, and also includes new biofilm carrier materials, such as ceramic balls, zeolites and polyethylene particles (Santos et al., 2017). The application of biofilm carriers on a large-scale face several challenges such as lower levels of adhesion, easy clogging, and increased incidence of tangling (Ding et al., 2011). The specific surface area, surface properties, pore structure, and material of the carrier are all factors that influence biofilm formation (Zhao et al., 2019).

Biochar has been widely used in wastewater treatment processes, where it demonstrates good biocompatibility characteristics and can be used as a carrier for biofilms containing phosphorus-accumulating bacteria (Teng et al., 2020). Previous studies have shown that the addition of biochar can improve biofilm formation, and its pore structure provided a good attachment site for microorganisms (Hu et al., 2021). A recent study showed that the establishment of biofilm on biochar was an effective means to solve the problem of limited adsorption capacity of materials, which could improve the efficiency of wastewater treatment (Siggins et al., 2021). The study further pointed out that in the process of biofilm regeneration, the blocked pores of biochar were exposed, and its adsorption capacity was stimulated (Jayakumar et al., 2021). Yang et al. (2020) have demonstrated the beneficial effect of using biologically modified rice

straw biochar on the biodegradation of chloramphenicol, an antibiotic commonly used in aquaculture, by *P. stutzeri*. The biodegradation efficiency of biologically colonized biochar was also far higher (90%) than unmodified biochar (10%) or free-living cultures of *P. stutzeri* (44%). The results indicated that *P. stutzeri* colonized biochar improved the biodegradation efficiency of antibiotics through the promotion of growth, changing fatty acid composition, and increasing gene expression (Yang et al., 2021). Su et al. (2020) found that microwave pyrolysis biochar was suitable for use as a biological carrier to grow nitrifying bacteria, resulting in higher biofilm mass (14 wt.%) in a catfish aquaponics system. This was mainly because it has micropores (1.803 nm) and a high BET-specific surface area (419 m^2/g). Since most bacteria are $\geq$ 1-4 μm in length and 0.5-1 μm in diameter, they cannot directly enter the micro, meso, and macropores (2~200 nm) that exist in biochar. However, the adsorption of nutrients or pollutants in the micro and mesopores can improve enrichment conditions for microbial colonization on adjacent macropores and intergranular surfaces (Jayakumar et al., 2021). Another advantage of microbial modification is that functional bacteria can degrade wastewater nutrients such as NH_4^+–N, TP, and COD which are adsorbed by the biochar (Liao et al., 2022). Biochar is usually in powder form and, even if it can be biologically regenerated, is easily lost from a treatment system and maybe difficult to recycle. Hence, there is a need to correlate biochar properties (especially the dimensions and specifications) to biofilm development, which can eventually determine adsorption efficiency and sustainability.

In a previous study, we developed novel formed-biochar-supported lanthanum-iron oxide (LaFe/MB) nanoparticle granules that can be used to recover P from wastewater (Sun et al., 2022). These biochar granules demonstrated high compressive strength and had a high maximum adsorption capacity of 52.12 mg P/L. As a carrier, it has the potential to be used for the immobilization of cells. The aim of this study was, therefore, to evaluate the phosphorus removal efficacy of using a biochar-biofilm composite established using a commercial inoculant containing phosphorous accumulating bacteria (PAB). Changes in the structure of the immobilized biofilm community microorganisms in the treatment process were analysed to determine the relationship between microorganisms and carriers. This article focuses mainly on: (1) the immobilization of bacterial on formed-biochar/nanoscale lanthanum-iron oxide composite, (2) phosphorus removal analysis under different treatments, and (3) determining the underlying mechanisms associated with phosphorus removal.

4.2 Materials and Methods

4.2.1 Materials

For the study, a commercial inoculum comprising a lyophilized consortium of phosphorus-accumulating bacteria (PAB) (5×10^9 cells/g) provided by Shanghai Blaqn Bio-Tech CO., LTD (China) was used.

Formed-biochar/nanoscale lanthanum-iron oxide composite (FBO) was prepared according to the method detailed by our previous study (Sun et al., 2022). Briefly, finely crushed straw biochar was mixed with montmorillonite in a mass ratio of 2:1 using a mortar. Iron/lanthanum chloride with a mole ratio of 0.3:0.1 solution was prepared by dissolving $FeCl_3 \cdot 6H_2O/LaCl_3 \cdot 7H_2O$ in 850 mL of deionized water. Then, a stable mud mixture was prepared by adding 150 g of montmorillonite/biochar composites to a series of iron/lanthanum chloride solutions with pH adjusted to 9.5~10. Thereafter, the mixtures were stirred vigorously for 30 min in an impregnating tank (HATLAB, Shanghai Huotong Experimental Instrument CO., LTD.) to allow for impregnation of the metal oxides to occur. Subsequently, the mixture was transferred into an icing machine (BY-400, Changsha Zhuocheng Medical Equipment CO., LTD.) to allow spherical composite precursor granules to be formed. The final step involved calcination of FBO granules in a tubular furnace at 450℃ for 2 h. Characterization of the physicochemical adsorbent properties of the FBO has been described previously, with a specific surface area of 63.54 m^2/g, an average pore size of 6.16 nm, and packing density of 0.518 g/mL being determined (Sun et al., 2022).

4.2.2 Immobilization of PAB on FBO (Bio-FBO)

The PAB was added to a 4% glucose solution (100 mL) at ratios of 1:10/20/30/40/50 and activated for 6 h on a shaker at 30℃ with 180 rpm, before being centrifuged at 2000 rpm for 2 min, and the supernatant was used. To immobilize the PAB on FBO, 0.2 g FBO was added to a 250 mL conical flask and sterilized at 121℃ for 30 min. Thereafter, 75 mL of condensed cell suspension was added to each flask and incubated on a rotary shaker at 30℃ and 160 rpm for culturing for indicated times. The mixture of suspended cells and FBO were sampled every 6 h to assess PAB attachment on FBO. Recovered FBO particles were separated by filtration and rinsed gently with deionized water three times to remove the free cells, and bio-beads were

obtained (Bio-FBO). The amount of microbial biomass adsorbed on the FBO-microbial complex was determined by the lipid-phosphorus method (Moll et al., 1999).

4.2.3 Adsorption kinetics

Phosphate adsorption tests were carried out using treatments comprising 1% PAB suspension (1:10 dilution), 2 g/L FBO, and 2 g/L colonized bio-beads (Bio-FBO) that had been optimized previously (Section 4.2.2). Each treatment was added to 100 mL of phosphate solution in a 250 mL flask and incubated at 30°C with shaking at 180 rpm for 96 h.

Kinetic tests were performed using solutions of KH_2PO_4 with initial concentrations of 10, 20, and 30 mg P/L in a 250 mL flask. At predetermined time intervals (viz. 0 min, 1 min, 2 min, 3 min, 5 min, 10 min, 30 min, 1 h, 2 h, 4 h, 8 h, 16 h, 26 h, 36 h, 46 h, 56 h, 66 h, 76 h, 86 h and 96 h), 1 mL of the suspension was taken out to analyse the phosphate concentration. Samples were filtered (0.2 µm membrane filter) before residual aqueous phosphate concentrations were determined by the ascorbic acid method using a UV-Vis Lightwave II spectrophotometer. All the experiments were performed at room temperature, and three replicates were used to avoid the experimental error. Pseudo-first-order (Eq. (1)), Pseudo-second-order (Eq. (2)), intra-particle diffusion (Eq. (3)), and Elovich models (Eq. (4)) were used to fit experimental data (Sumaraj et al., 2020). Equations describing each of the models assessed are shown as follows:

$$Q_t = Q_e\left(1 - e^{-k_f t}\right) \tag{1}$$

$$Q_t = \frac{Q_e^2 k_s t}{1 + Q_e k_s t} \tag{2}$$

$$Q_t = k_i t^{1/2} + C \tag{3}$$

$$Q_t = \frac{1}{\beta} Ln\,(\alpha\beta) + \frac{1}{\beta} Ln(t) \tag{4}$$

where, C = boundary layer thickness constant, K_f = rate constant (h^{-1}), k_i = rate constant (mg g^{-1} $h^{-0.5}$), K_s = rate constant (g mg^{-1} h^{-1}), Q_e = Amount of adsorbate per mass of adsorbent at equilibrium (mg g^{-1}), Q_t = adsorption of phosphorus at time t (mg g^{-1}), t = adsorption time (h), α = initial adsorption rate (mg h g^{-1}), β = constant for the extent of surface coverage and chemisorption activation energy (g mg^{-1}).

4.2.4 Characterization of Bio-FBO

FBO and Bio-FBO samples were characterized before and after phosphate adsorption. The element content of the biochar samples (viz. C, H, O, N, S) was determined by an element analyser (Thermo Flash 2000 CHNS-O Elemental Analyser). The zeta potential of sample suspensions was determined by measuring the electrophoretic mobilities using a Zeta-sizer analyser (Model: Nano ZS, Malvern, UK) instrument. All the experiments were performed in triplicate. Scanning electron microscopy (SEM) was used to characterize the porous structure and surface morphology. The surface chemistry of biochar samples was analysed by X-ray photoelectroscopy (XPS, PHI 5000 VersaProbe ESCA). The available functional groups on the adsorbent's surface were detected using Fourier transform infrared spectroscopy (FTIR; Nexus 670, Nicolet).

4.2.5 DNA extraction and pyrosequencing

Bio-FBO samples were collected from flasks used in the 30 mg P/L adsorption kinetics determination (described in Section 4.2.3) to detect changes in the phosphorous-accumulating bacteria community associated with Bio-FBO biofilms. Samples were taken at different time points (viz., 1, 6, 24, 48, and 96 h) and subsequently frozen in liquid nitrogen and kept at −80°C until DNA extraction could be performed.

The total genomic DNA was extracted from Bio-FBO samples using the TruSeq^{TM} DNA Sample Prep Kit (Omega Bio-Tek, USA) following the manufacturer's instructions. The final DNA concentration and purification were measured on a NanoDrop 2000 UV-Vis spectrophotometer (NanoDrop Technologies, Wilmington, DE, USA). The V3-V4 hypervariable regions of bacterial 16S rRNA gene were amplified using primers 338F (5'-ACTCCTACGGGAGGCAGCAG-3') and 806R (5'-GGACTACHVGGGTWTCTAAT-3') according to the method of Wu et al. (2021).

The PCR amplification was conducted as previously described in Fang et al. (2018). Purified amplified gene products were sequenced at Majorbio Bio-pharm Technology Co., Ltd. (Shanghai, China) using the Illumina MiSeq platform (Illumina, San Diego, USA) according to standard protocols. Amplicon sequencing was performed on the HiSeq 2500 platform (Illumina, San Diego, USA). The quality control of raw data was performed in QIIME 1.9.1 software. Operational taxonomic units (OTUs) were generated by clustering high-quality sequences at a

similarity level of 97% using UPARSE (version 7.0). The beta diversity of each treatment was determined by principal coordinate analysis (PCoA), which was analysed using QIIME 1.9.1.

4.2.6 Statistical and bioinformatics analysis

The amount of phosphate adsorbed is expressed as mean ± standard error. Experimental data were analysed with SPSS software (SPSS, 26.0, IBM, USA), and Origin 8.5 (Origin, OriginLab, USA) was used for graphing. Differences in microbial community structures between treatment groups were determined by β-Diversity analysis. The significance of differences between groups was determined using the Kruskal-Wallis H test.

4.3 Results and discussion

4.3.1 Amount of membrane hanging of Bio-FBO

Fig. 4.2a shows a suspension of PAB culture when incubated with FBO nano-particles. SEM examination revealed the establishment of biofilm formation on the surface of FBO after 6 h co-incubation with a PAB suspension (Fig. 4.2e). The effect of PAB starting concentration on the level of biomass accumulation on FBO is shown in Fig. 4.2b. The rate and amount of biofilm biomass that accumulated on FBO particles were directly related to the initial starting concentration of PAB. Starting dilutions of 1:10 and 1:20 yielded significantly higher amounts of biofilm biomass than the lower concentrations used. A maximum level of biomass (ca. 700 nmol P/g) attachment to FBO was achieved after 12 h of incubation. Over time, biomass levels associated with the 1:10 PAB treated FBO tapered off until a final yield of ca. 500 nmol P/g was recorded at the end of the incubation period. When lower starting concentrations of PAB were used (viz. 1:30 ~ 1:50 dilutions), the rate of biomass accumulation was slower, and lower overall biomass yields peaked after significantly longer incubation periods. Overall, the amount of immobilized microbial biofilm increased and then decreased to equilibrium, indicating that at high initial concentrations of PAB (ie 1:10), available surfaces are rapidly colonized. Once fully colonized, further biomass accumulation on FBO appears to be limited, whereas, at low biomass concentrations (1:30 ~ 1:50) the increase in biofilm increases over time at a slower rate – this probably reflects biofilm growth over time until surface/particle colonization is saturated.

Elemental analysis was performed to determine and compare the adsorption characteristics of FBO and Bio-FBO. The H/C and O/C values can be used to describe the aromaticity of FBO, that is, smaller H/C and larger O/C values are indicative of higher aromaticity, stronger hydrophilicity, and greater polarity. The colonization of FBO by PAB biomass was found to increase its aromaticity which could further facilitate the adsorption capacity of Bio-FBO (Liu et al., 2012).
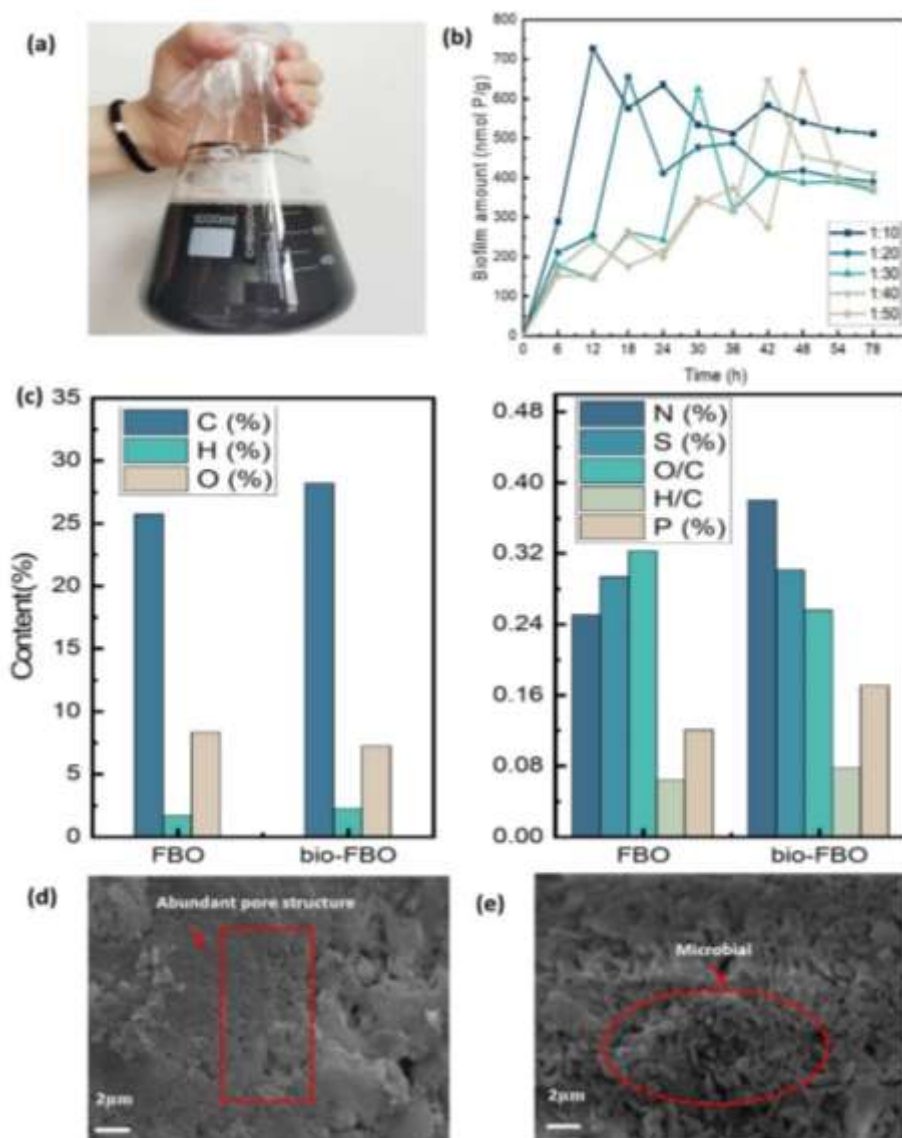
Figure 4.2 Relationship between biofilm development and time for FBO nanoparticles co-incubated with PAB: (a) Suspension of PAB culture mixed with FBO; (b) Establishment of biofilm biomass associated with FBO biochar nanoparticles over time; (c) Element content comparison of FBO and Bio-FBO; (d) SEM of FBO; (e) SEM of microbial cell aggregate on the surface of Bio-FBO.

SEM micrographs presented in Fig.4.2 (d and e) highlight the potential for FBO biochar particles to be colonized by bacteria due to an abundance of favourable surface and/or pore structures for the attachment of PAB. FBO, as a carrier, furthermore, provided enough space for PAB growth to generate high cell density and protected cells (Ha et al., 2009; Lin et al., 2010). Fig.4.2e showed that large quantities of bacteria had successfully aggregated on, or colonized, the surface of FBO after exposure to a PAB suspension (Zhang et al., 2013). These results indicated that the biochar particles provided favourable adhesion sites for biofilm development. Further, it is likely that the abundant pore structures present in FBO particles also facilitate the delivery of oxygen and substrates through to immobilized cells. The gradual increase of surface microorganisms also intuitively indicates that the surface of the biochar has been effectively colonized (Zeng et al., 2021), which enables the biomass present to be in contact with the P in suspension and this allows for mechanisms of P adsorption and/or uptake to occur (Zhang et al., 2013).

4.3.2 Phosphate removal by PAB, FBO, and Bio-FBO

All treatments exhibited a capacity to remove phosphorous from the solution at each concentration evaluated (Fig. 4.3). The highest levels of phosphorous removal occurred with PAB immobilized on FBO, followed by FBO and PAB treatments. Moreover, with an initial phosphorus concentration of 10 mg P/L, the removal efficiency of phosphorus increased with incubation time, reaching approximately 100% after 60 h, whereas, at starting concentrations of 20 and 30 mg P/L phosphorus removal efficiencies of ca. 80% and 60% respectively, were achieved. The initial rates of P removal associated with the FBO and Bio-FBO treatments were very similar for each of the P concentrations tested. Subsequently, P removal rates decreased over time, eventually plateauing, which might be attributable to the limited availability of adsorption sites.

During the initial phases of the experiment, the FBO treatment appeared to be more efficient than the Bio-FBO at removing P. The results also demonstrated an interesting synergic effect between the formed-biochar-supported lanthanum-iron oxide nanoparticles and functional bacteria found in the combined process. By the end of the incubation period, the phosphorus removal efficiency of Bio-FBO was significantly higher than that of FBO and PAB. The PAB component of the Bio-FBO appeared to be responsible for the increase in P removal efficiency.

This may be attributed to biological uptake mechanisms, or, due to an increase in sites for P adsorption associated with PAB biomass.
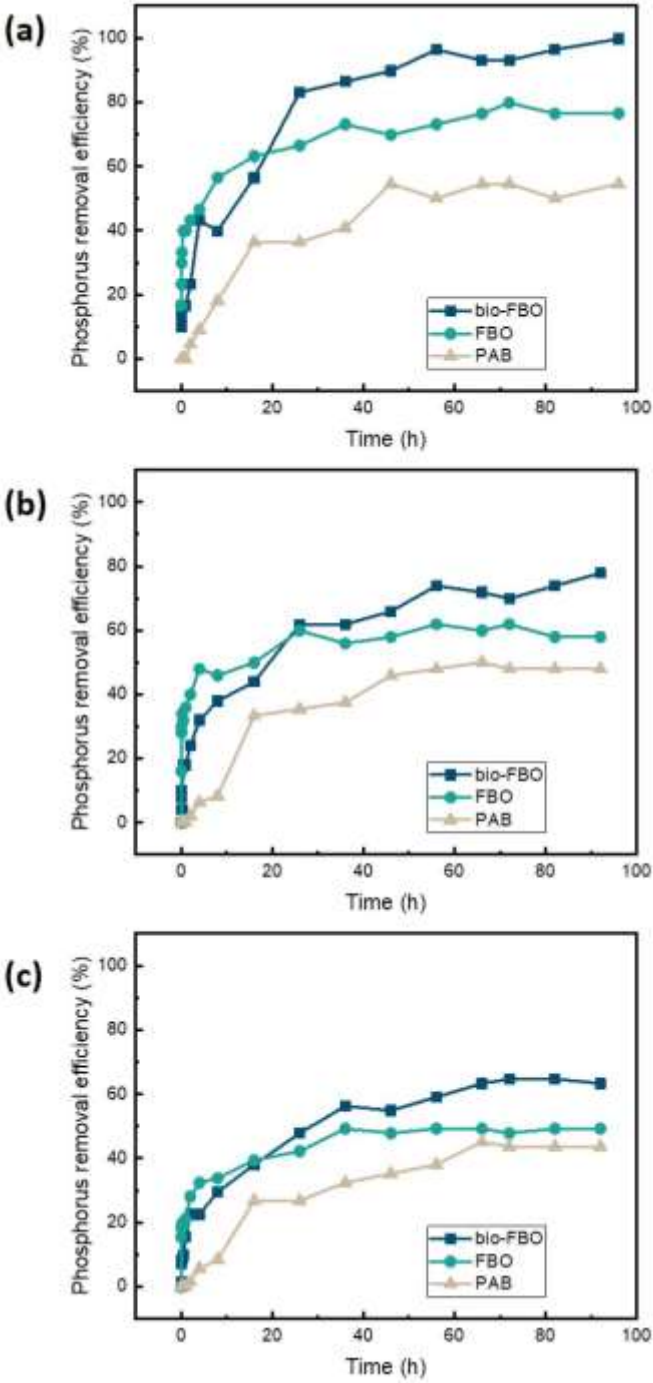
Figure 4.3 The phosphorus removal efficiency of PAB, FBO, and Bio-FBO treatments at initial phosphorus concentrations of (a) 10 mg P/L; (b) 20 mg P/L, and (c) 30 mg P/L. (agitation speed: 180 rpm; pH 7; temperature: 28℃; contact time 96 h).

4.3.3 Phosphate removal kinetics

To compare the adsorption effect between Bio-FBO and FBO treatments, the kinetics of P-removal efficiency were described according to the widely accepted Pseudo-first order kinetic, Pseudo-second order kinetic, Elovich, and Intra-Diffusion models (Fig. 4.4). The kinetic constants for P-removal efficiency derived from these models is presented in Table 4.1.

In all instances, the adsorption rates and P-removal capacity of Bio-FBO were always higher than that of FBO. The kinetics of phosphorus removal efficiency according to the first-order reaction model ($R^2 \leq 0.708$) and the Elovich model ($R^2 \leq 0.974$) exhibited, in relative terms, the poorest fits. Whereas, the second-order reaction model was well expressed, for both the FBO ($R^2 > 0.987$) and Bio-FBO ($R^2 \geq 0.988$) treatments under different P concentrations. The $q_{e, cal}$ (theoretical calculation of adsorption capacity) of Bio-FBO were 30.46% and 28.53% higher than that of FBO at 10 and 20 mg P/L concentration, whereas, the adsorption rate constants (k_2) were lower. These results show that the adsorption process was dominated by chemisorption, however, biological adsorption can also be expected to play a role for Bio-FBO. At an initial concentration of 30 mg P/L the adsorption rate constant for Bio-FBO ($k_2 = 0.019$) immobilized cells was slightly higher than the FBO adsorbent ($k_2 = 0.018$).

When the Intra-particle diffusion model was run the q_t and $t^{1/2}$ of FBO and Bio-FBO were found to exhibit multi-segmented linear relationships (Fig. 4.4d) indicating that both liquid film diffusion and particle internal diffusion mechanisms exist in the adsorption process (Bolbol et al., 2019). The first stage represents the rapid adsorption process to the outer surface through membrane diffusion driven by the difference in solution concentration (Jia et al., 2020). In the second stage, internal diffusion rate constants (k_{p2}) of 0.861 and 1.274 were achieved for Bio-FBO when initial phosphorus concentrations of 10 and 20 mg P/L were used, compared to 0.484 and 0.827 for FBO, respectively. The results indicate that PAB immobilization increases the internal diffusion mechanism of P adsorption by Bio-FBO. Furthermore, the fitted line in the second stage does not pass through the origin, indicating that intra-particle diffusion is not the only rate-limiting step and that the speed rate may be controlled jointly by surface adsorption and intra-particle diffusion mechanisms (Jung et al., 2017).

In the Bio-FBO immobilized systems, the carriers could act as a protective shelter against the influence of the external environment. Additionally, metal nanoparticles would affect the physiological responses of cells to phosphate metabolism. Under aerobic conditions PAOs can

generate energy from the oxidative metabolism of stored poly-β-hydroxybutyrate (PHB), resulting in the uptake of orthophosphate and its conversion to insoluble poly-P. Peng et al. (2020) have shown that iron oxide nanoparticles can enhance membrane permeability, thereby strengthening both bio- and chem-dephosphorization (Peng et al., 2020). Therefore, the enhanced removal of P occurring on Bio-FBO immobilized cells could be attributed to increased cell permeability, enhanced enzyme activity, and protection of the cells by FBO acting as a barrier.
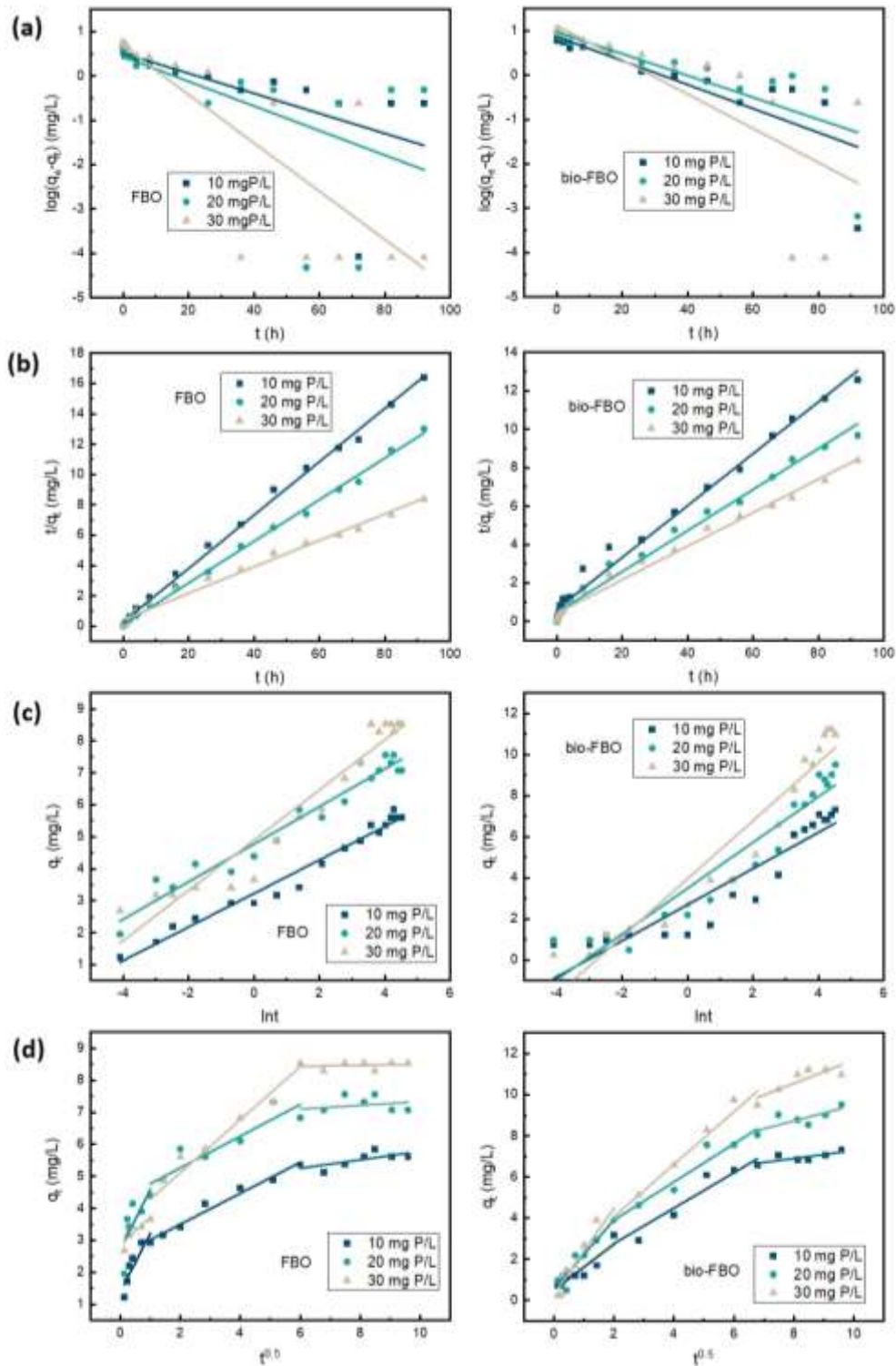
Figure 4.4 Adsorption kinetics results of P adsorption on FBO and Bio-FBO according to: (a) pseudo-first order kinetics; (b) pseudo-second order kinetics; (c) Elovich model; and d) Intra-particle diffusion model.

Table 4.1 The kinetic constants of P-removal efficiency by FBO and Bio-FBO.

Model	Indicators	Unit	FBO			Bio-FBO		
			10 mg/L	20 mg/L	30 mg/L	10 mg/L	20 mg/L	30 mg/L
	q_e	mg/g	5.85	7.56	8.54	7.32	9.51	11.22
Pseudo-first-order	$q_{e, cal}$	mg/g	3.26	2.72	4.68	7.43	9.57	13.21
	k_1	L/min	0.052	0.064	0.125	0.062	0.057	0.089
	R^2	-	0.427	0.317	0.692	0.708	0.657	0.594
Pseudo-second-order	$q_{e, cal}$	mg/g	5.68	7.29	11.48	7.41	9.37	11.48
	k_2	mg/g × min	0.111	0.190	0.018	0.029	0.024	0.019
	R^2	-	0.997	0.998	0.987	0.988	0.988	0.988
Elovich	α	mg/g × min	245.44	1957.87	397.96	18.85	25.77	23.14
	β	g/mg	1.907	1.701	1.273	1.138	0.899	0.707
	R^2	-	0.974	0.949	0.930	0.867	0.904	0.918
Intra-particle diffusion	K_{p1}	mg/g × min	1.820	1.884	0.859	1.115	1.672	2.092
	C_1	mg/g	1.399	2.711	2.857	0.512	0.570	0.306
	R_1^2	-	0.737	0.398	0.665	0.843	0.895	0.888
	K_{p2}	mg/g × min	0.484	4.270	0.827	0.861	0.927	1.274
	C_2	mg/g	2.532	0.496	3.456	1.046	2.052	1.522
	R_2^2	-	0.971	0.815	0.935	0.897	0.931	0.962
	K_{p3}	mg/g × min	0.133	0.059	0.015	0.194	0.381	0.564
	C_3	mg/g	4.452	6.742	8.345	5.351	5.672	6.033
	R_3^2	-	0.398	-0.112	-0.169	0.504	0.522	0.656

4.3.4 Dynamics of microbial community abundances and succession of the bacterial community composition

The diversity of the microbiota associated with the PAB consortium is presented in Fig. 4.5. The pie chart shows the composition of the bacteria community at a genus level. These genera belong to the *Proteobacteria* and *Firmicutes* phyla and included representatives of *Acinetobacter* (36.68%), *Enterobacter* (7.24%), *Pantoea* (12.66%), an Unclassified_Enterobacteriaceae (11.33%), *Bacillus* (6.73%), *Paenibacillus* (5.56%), and *Brevundimonas* (5.49%) as the main groups of bacteria associated with Bio-PAB.

Fig. 4.6 shows the changes in the microbial community structure of Bio-FBO samples over time. *Acinetobacter* was the most abundant group of bacteria found in all treatments, although its relative abundance fluctuated with time. *Acinetobacter* species are commonly associated with phosphorus removal processes in wastewater and be a dominant group in wastewater bioreactors (Ji et al., 2015). Members of this genus are referred to as phosphorus-accumulating organisms (PAO), due to their ability to take up phosphate from the aqueous environment and convert it into insoluble polyphosphate which is stored in cells as storage granules (Kim et al., 1997; Streichan et al., 1990). Bacteria belonging to the genus Acinetobacter occur in a wide variety of activated sludges in which enhanced biological phosphate removal was observed (Korstee et al., 1994).

Enterobacter spp. were also prominent representatives associated with the Bio-FBO biofilm microbiota throughout the phosphorus adsorption experiment. Members of this genus are associated with wastewater microbiota and are known to contribute toward denitrification and phosphorus accumulation processes (Zheng et al., 2019). The simultaneous removal of nitrogen and phosphorus is attractive since this can contribute to improving wastewater treatment efficiencies (Wan et al., 2017; Zhang et al., 2019). Representatives of the genus *Pantoea* were also significant contributors to the biofilm community structure throughout the experiment. Strains of *Pantoea* have been identified as phosphate-solubilizing bacteria, which can release insoluble phosphate by secreting phosphatase (Lv et al., 2022; Rasul et al., 2021). *Pantoea* sp. can release soluble phosphate to the culture broth with concentrations of 28 mg/L $FePO_4$ without being affected by the pH (Son et al., 2006).
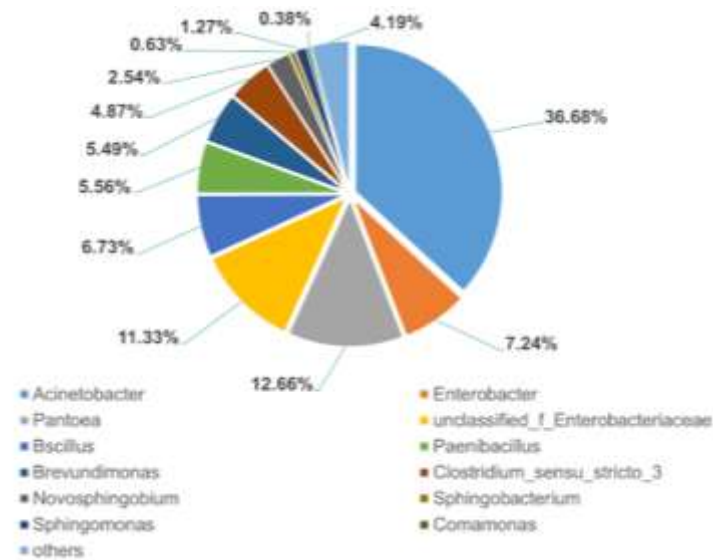
Figure 4.5 Pie chart of PAB microbial genera were drawn based on community analysis at genus level.
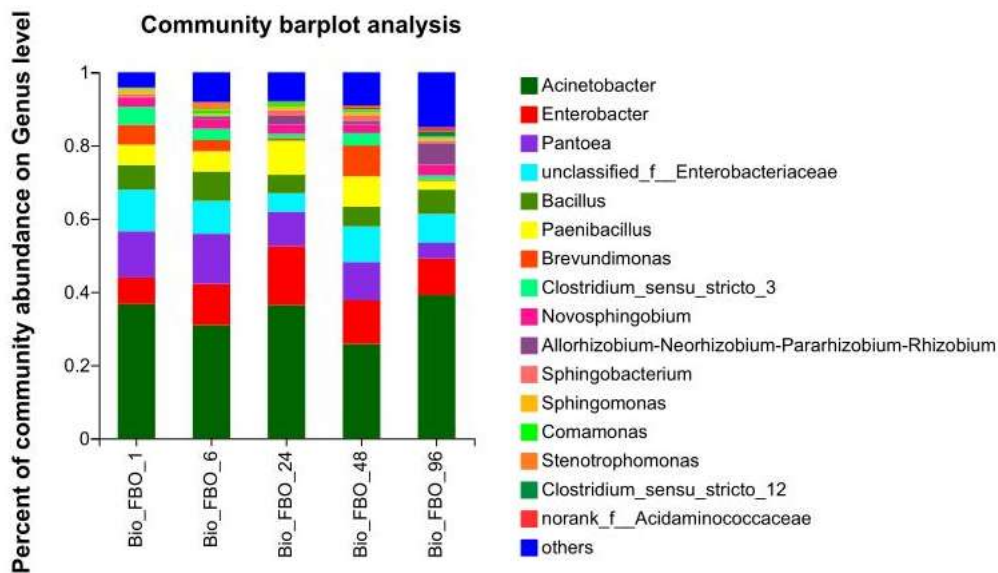
Figure 4.6 Variations in bacterial community structure in biofilm microbiota associated with Bio-FBO during removal of phosphate.

In addition, *Bacillus* and *Paenibacillus* representatives have also been shown to play an important role in removing nitrogen and phosphorus (Kim et al., 2005; Postma et al., 2010; Wang et al., 2018). Previous studies have reported that *Bacillus* sp. can be used as bioflocculants and have industrial potential in water purification processes (Giri et al., 2015; Tang et al., 2021; Su et al., 2021; Vijayaraghavan et al., 2021). In a recent study, Dong et al. (2022) demonstrated that the phosphate-solubilizing bacteria *Paenibacillus xylanexedens* promoted the biomass growth of *Chlorella pyrenoidosa* in an algae-bacteria co-culture, leading to enhanced removal rates of COD, NH_4^+-N, and PO_4^{3-} during wastewater treatment.

To illustrate the effect of culture time on bacterial communities, principal co-ordinates analysis (PCoA) was used (Fig. 4.7). The PC1 axis and PC2 axis explained 42.03% and 20.04% of the results, respectively. It could be seen from the figure that different treatment groups were separated from each other, which indicated the differences in community composition and abundance occurring over time. The result showed that the culture time had a significant effect on the microbial community structure, and the differences between samples increased with the passage of time.
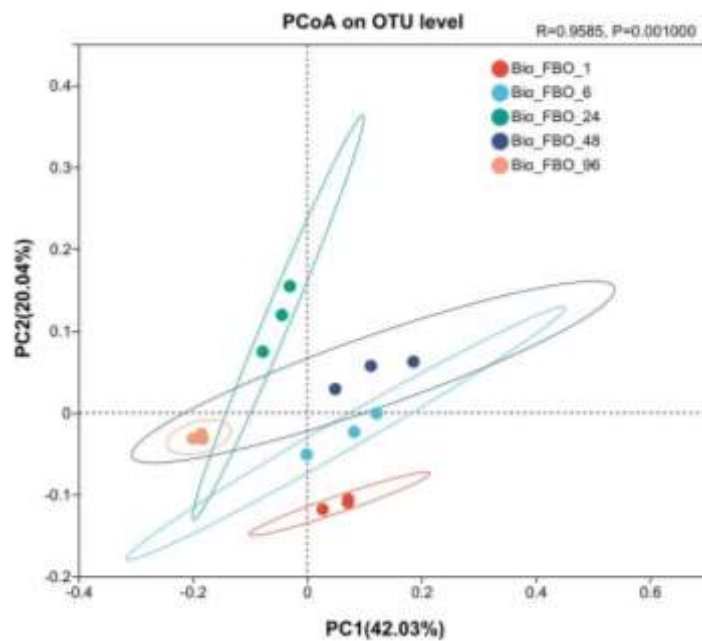
Figure 4.7 Variations of ß diversity during Bio-FBO removal of P in wastewater. Note: The X-axis and Y-axis represent the two selected principal axes, and the percentage represents the explanatory value of the principal axes for the difference in sample composition; The scale of X axis and the Y-axis is relative distance, which has no practical significance; Points of different colours or shapes represent samples of different groups. The closer the two sample points are, the more similar the species composition of the two samples is.

Based on the abundance data of the microbial communities present in each sample, the Kruskal-Wallis H test statistical method was applied to detect and evaluate significant differences in abundance for genera in the microbial communities of different groups (Fig. 4.8). It was noted that *Enterobacter* and *Pantoea* were the predominant strains among the significantly different strains. Specifically, *Enterobacter* was dominant in Bio_FBO_24, Bio_FBO_48, and Bio_FBO_96 treatment groups, while *Pantoea* was significantly more

abundant in Bio_FBO_1 and Bio_FBO_6 treatment groups than *Enterobacter*. Despite the large proportion of *Acinetobacter*, there was no significant difference in its content over time.
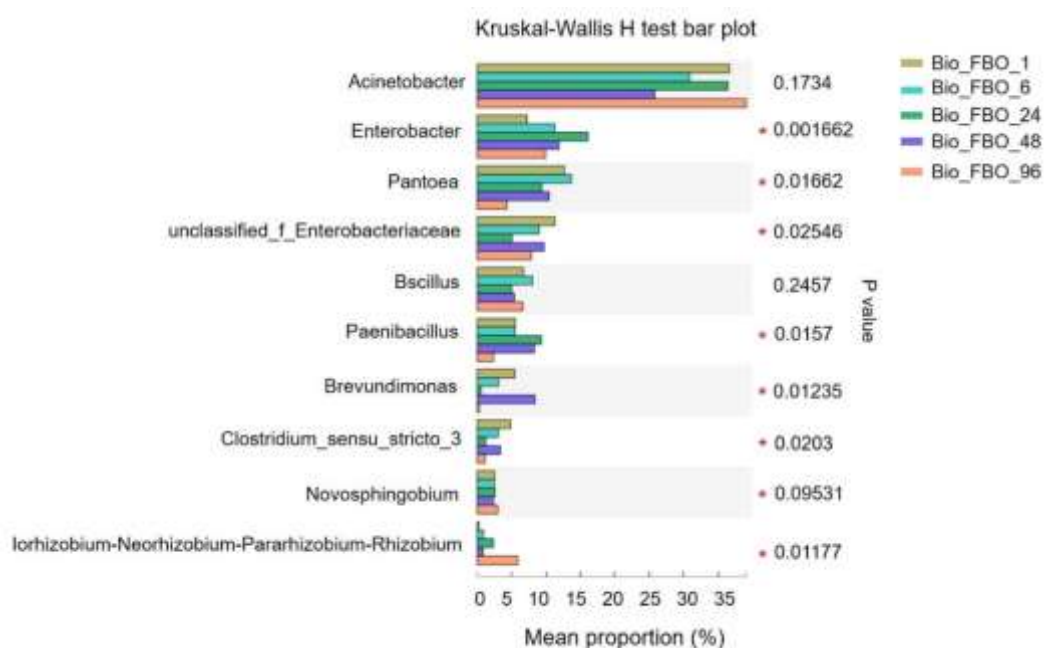
Figure 4.8 Statistical comparison of the relative abundance of the dominant genus in different stages of Bio-FBO for removal of P. Note: The Y axis represents the taxonomic groups differentiated at the genus level, the X axis represents the average relative abundance in different groups of species, and the columns with different colours represent different groups. On the far right is the P value, [*] 0.01, $P \leq 0.05$.

4.3.5 Possibility of enhanced phosphorus removal by Bio-FBO

A schematic illustration of the preparation of PAB immobilized on Bio-FBO and its application for enhanced removal of P is presented in Fig. 4.9. As shown previously, the establishment of PAB-derived biofilms on FBO enhanced the P-removal capacities of the biochar (Fig. 4.3). Three variants of the FBO biochar were analysed by FTIR to further evaluate the effect of microbial loading on biochar surface functional groups before and after P adsorption (Fig. 4.10). The intensity changes of functional groups mainly focused on the 3400-2800 cm^{-1} and 1750-550 cm^{-1} bands. The broad peaks at approximately 3280 cm^{-1} are ascribed to the stretching vibrations of hydroxyl groups (–OH) found in carboxylic groups and phenol groups, or N–H bonds (Miretzky et al., 2008). The sharp peaks at approximately 1611 cm^{-1} are attributed to the C=C double bonds found in aromatic rings or C=O stretching vibration of carbonyl or carboxyl groups (Vu et al., 2018). The peak at 565 cm^{-1} corresponding to the Fe–

OH stretching vibration, while 675 cm^{-1} belonged to La–O or La–OH stretching vibration (Fu et al., 2018; Zhang et al., 2011). The peak intensity at 565 and 675 cm^{-1} in Bio-FBO and Bio-FBO-P were higher than those in FBO, indicating that a new characteristic spectral peak was formed, which was attributed to surface-bound O–P–O bonds (Li et al., 2020). The reasons for this may be attributed to the presence of P in the phospholipids of bacterial membranes or that PABs produce linear or ring polymers formed by orthophosphate monomers bonded to ester bonds (Pereira et al., 1996). The characteristic peak of 3280 cm^{-1} associated with FBO nanoparticles decreased due to the attachment of PABs on the surface of FBO and the exchange of ligands between the hydroxyl group and phosphate group on the surface of the adsorbent after adsorption of P (Sun et al., 2022). The absorption peaks at 1477, 1450 and 1401 cm^{-1} were characteristic of the protein amide I band (C=O double bond stretching vibration), amide II band (N–H bond stretching vibration), and amide III bands, respectively (Zhang and Wang, 2021), representing the presence of microbial biomass and extracellular materials secreted during biofilm formation. FBO showed a C=C stretching vibration peak around 1400-1600 cm^{-1}, indicating that the biochar surface contains a stable aromatic skeleton, which facilitates cell adhesion and proliferation (Goh et al., 2019). Overall, the infrared spectrogram shows that successful microbial colonization of the FBO was achieved and that the biochar-biofilm complex integrates all functional groups of FBO and PAB, which improves the stability and improves the removal ability of the Bio-FBO (Goh et al., 2019).
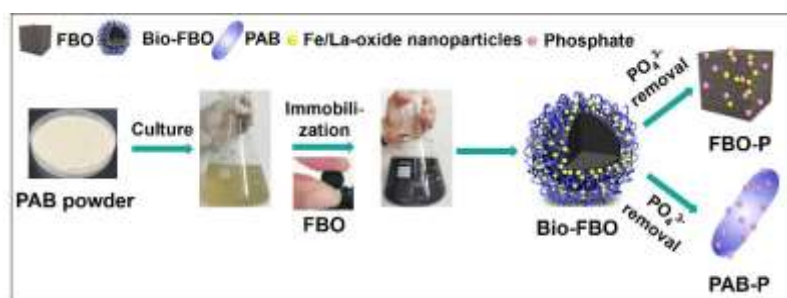
Figure 4.9 Schematics of the preparation of immobilization of PAB on formed-biochar/nanoscale lanthanum-iron oxide composite (Bio-FBO).

Microbial loading on biochar has a significant impact on the surface morphology and structure of FBO, which can be shown by SEM, FTIR, and microbial community structure analysis data. XPS was used to analyse the changes in element content and chemical bond before and after the adsorption of P to clarify the adsorption mechanism of P on Bio-FBO (Fig. 4.11). The full XPS spectra of Bio-FBO before and after P adsorption are shown in Fig. 4.11(a).

It was evident that P had been successfully adsorbed on the Bio-FBO surface according to the full spectrum after FBO adsorption. Simultaneously, characteristic peaks of Fe and La elements appeared in the full range, which can promote the increase of phosphorus adsorption. Combined with the previous analysis results, it can be seen that the removal of P was mainly the result of the synergistic action of FBO and microorganisms. The mechanism of P removal by FBO has been attributed to the adsorption effect of lanthanum-iron oxide nanoparticles loaded on biochar surfaces (Sun et al., 2022). The fine spectrum of P $_{2p}$ could be divided into three peaks of 133.75 (59.73%), 132.68 (5.44%), and 134.46 (34.83%), corresponding to $FePO_4$, $LaPO_4$, and H_3PO_4, respectively (Fig. 4.11b). This indicated that P could combine with Fe and La metal on the Bio-FBO adsorbent. The existence of interlayer phosphate was also confirmed, which could be associated with the PABs biofilms layer on the surface of Bio-FBO (Zhang et al., 2021).
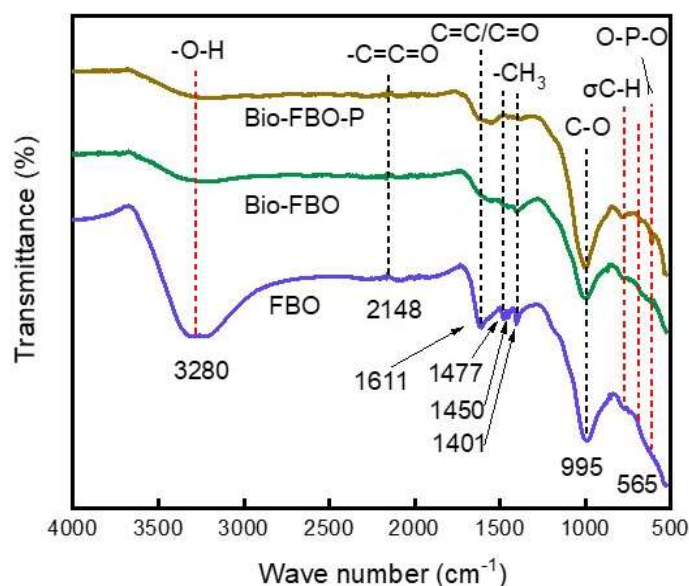
Figure 4.10 Fourier transform infrared spectrum (FTIR) of FBO, Bio-FBO, and Bio-FBO-P materials.

The findings of this study indicate that FBO is a suitable carrier for PABs, offering them a protected niche for biofilm development and phosphate adsorption. PABs have the potential to absorb orthophosphate directly from wastewater and synthesize polyphosphate within the cell, which accumulates as a storage material thereby reducing the P content in the wastewater (Hou et al., 2021; Zhang et al., 2021). A large number of bacterial cells associated with surface biofilms were observed by SEM, which further supported this result (Fig. 4.3e).

The C $_{1s}$ of Bio-FBO could be subdivided into three peaks, i.e., C–C, C–OH, and O–C=O (Fig. 4.11e). After P uptake, the intensity of the C–OH peak of Bio-FBO decreased from

43.59% to 30.34% for Bio-FBO-P (Fig. 4.11f). This decrease in intensity is attributed to ligand exchange of the C–OH from the surface of Bio-FBO. The adsorption of P by carbonyl, hydroxyl, and other oxygen-containing functional groups on the surface of Bio-FBO-P was confirmed by FTIR. In addition, the O–C=O peak area increased significantly, indicating that a small part of C–O–C or C–O=C participated in the adsorption reaction. Decarboxylation may also occur during the adsorption process leading to an increase in C–O groups (Miretzky and Cirelli, 2010).
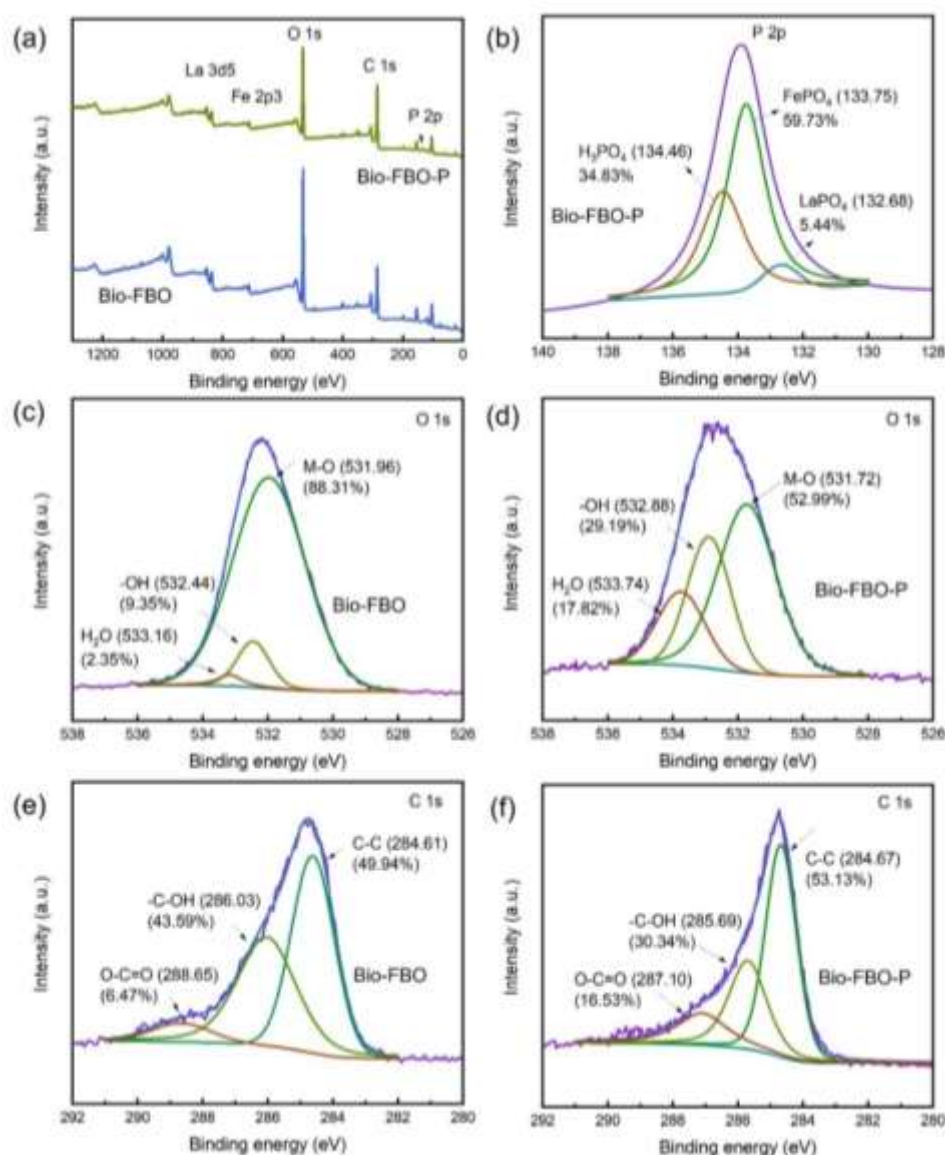
Figure 4.11 The full scan XPS spectra of Bio-FBO before and after P adsorption (a), the P $_{2p}$ fine spectrum of Bio-FBO after P adsorption (b), the O $_{1s}$ fine spectrum of Bio-FBO before and after P adsorption (c) and (d), the C $_{1s}$ fine spectrum of Bio-FBO before and after P adsorption (e) and (f).

Furthermore, the high-resolution XPS spectrum of O $_{1s}$ included three components at 531.96 eV, 532.44 eV, and 533.16 eV, which can be attributed to metal oxides (M–O, M=Fe or La) (Gou et al., 2009), hydroxyl groups bound to a metal (M–OH), and adsorbed H_2O, respectively (Fig. 4.11c and d) (Kong et al., 2020). After the P adsorption reaction, the ratio of the M–O bond decreased from 88.31% to 52.99%, while the ratio of –OH increased from 9.35% to 29.19%. This was mainly attributed to the rehydration reaction of the Fe/La of the Bio-FBO in the process of conversion. Some M–O bonds in metal oxides were converted into M–OH, which led to the increase of hydroxyl functional groups (Mallet et al., 2013). This transformation of functional group ratio when P adsorption occurs not only further facilitates microbial fixation to the surface of the biochar but can also promote the ligand exchange between surface hydroxyl groups and phosphorus.

4.4 Conclusions

In this research, a unique approach was proposed for the efficient treatment of phosphorus (P) contaminated wastewater using a novel formed-biochar carrier incorporating lanthanum-iron oxide nanoparticles (FBO) and colonized by immobilized phosphorous-accumulating bacteria (PAB). Optimal conditions for immobilizing PAB onto FBO composites (Bio-FBO) were achieved when 0.2 g FBO was combined with 75 mL PAB cell suspension and shaker incubated at 30℃ at 160 rpm for 12 -18 h.

Bio-FBO demonstrated enhanced P-removal efficiency compared to free-living PAB cultures or unamended FBO. This was attributed to a possible increase in the surface area of biofilm on the surface of FBO which supported higher levels of P adsorption or uptake. The FBO carrier proved to be a suitable substrate for PAB attachment due to its physicochemical properties, which included available surface area (including its abundant pore structure), and suitable functional groups/attachment sites for PAB to colonize and form biofilm layers. PAB development on the surface of FBO particles was positively influenced by the aromaticity, hydrophilicity, and polarity properties of the biochar. SEM confirmed that biofilms consisting of PAB microorganisms readily attached to the surface of the FBO. Adsorption kinetics data demonstrated that P removal from wastewater using Bio-FBO fitted well with the Pseudo-second order kinetic model. The PAB colonized FBO composites (Bio-FBO) demonstrated a favourable remediation efficiency and were able to remove 100% of an initial P concentration of 10 mg P/L within 60 h. Overall, the adsorption capacity of Bio-FBO was attributed to the

following factors: (1) A large number of La-Fe active sites and oxygen-containing groups on the surface of Bio-FBO that can bind to P; (2) Adsorption of P by PAB biomass from the wastewater directly; and, (3) uptake of P by PAB immobilized on FBO adsorbent, which promotes the activation of active sites of FBO to continue to adsorb P, thereby achieving synergistic P-removal. Based on the results obtained from application experiments, Bio-FBO adsorbent demonstrates much potential as an enhanced technique for biological-chemical adsorption removing P from wastewater.

References

Bolbol H, Fekri M, Hejazi-Mehrizi M, (2019). Layered double hydroxide–loaded biochar as a sorbent for the removal of aquatic phosphorus: behaviour and mechanism insights. Arabian Journal of Geosciences 12: 503.

Chaudhry V, Nautiyal C S, (2011). A high throughput method and culture medium for rapid screening of phosphate accumulating microorganisms. Bioresource Technology 102: 8057-8062.

de-Bashan L E, Bashan Y, (2004). Recent advances in removing phosphorus from wastewater and its future use as fertilizer (1997-2003). Water Research 38: 4222-4246.

Ding D, Feng C P, Jin Y X, et al. (2011). Domestic sewage treatment in a sequencing batch biofilm reactor (SBBR) with an intelligent controlling system. Desalination 276: 260-265.

Dong H W, Liu W, Zhang H, et al. (2022). Improvement of phosphate solubilizing bacteria Paenibacillus xylanexedens on the growth of Chlorella pyrenoidosa and wastewater treatment in attached cultivation. Chemosphere 306: 135604.

Fang D X, Zhao G, Xu X Y, et al. (2018). Microbial community structures and functions of wastewater treatment systems in plateau and cold regions. Bioresource Technology 249: 684–693.

Fu H Y, Yang Y X, Zhu R L, et al. (2018). Superior adsorption of phosphate by ferrihydrite-coated and lanthanum-decorated magnetite. Journal of Colloid and Interface Science 530: 704-713.

Giri S S, Harshiny M, Sen S S, et al. (2015). Production and characterization of a thermostable bioflocculant from Bacillus subtilis F9, isolated from wastewater sludge. Ecotoxicology and Environmental Safety 121: 45-50.

Goh C L, Sethupathi S, Bashir M J, et al. (2019). Adsorptive behaviour of palm oil mill sludge biochar pyrolyzed at low temperature for copper and cadmium removal. Journal of Environmental Management 237: 281-288.

Gou K H, Lim T T, Dong Z L, (2009). Enhanced arsenic removal by hydrothermally treated nanocrystalline Mg/Al layered double hydroxide with nitrate intercalation. Environment Science & Technology 43: 2537-2543.

Ha J, Engler C R, Wild J R, (2009). Biodegradation of coumaphos, chlorferon, and diethylthiophosphate using bacteria immobilized in Ca-alginate gel beads. Bioresource Technology 100: 1138-1142.

Halecky M, Spackova R, Paca J, et al. (2014). Biodegradation of nitro-glycerine and ethylene glycol dinitrate by free and immobilized mixed cultures. Water Research 48: 529-537.

Hou P F, Sun X L, Fang Z M, et al. (2021). Simultaneous removal of phosphorous and nitrogen by ammonium assimilation and aerobic denitrification of novel phosphate-accumulating organism Pseudomonas chloritidismutans K14. Bioresource Technology 340: 125621.

Hu Y, Shi C, Ma H Y, et al. (2021). Biofilm formation enhancement in anaerobic treatment of high salinity wastewater: Effect of biochar/Fe addition. Journal of Environmental Chemical Engineering 9: 105603.

Jayakumar A, Wurzer C, Soldatou S, et al. (2021). New directions and challenges in engineering biologically-enhanced biochar for biological water treatment. Science of the Total Environment 796: 148977.

Ji B, Wei L, Chen D, et al. (2015). Domestic wastewater treatment in a novel sequencing batch biofilm filter. Applied Microbiology and Biotechnology 99: 5731-5738.

Jia Z Y, Zeng W, Xu H H, et al. (2020). Adsorption removal and reuse of phosphate from wastewater using a novel adsorbent of lanthanum-modified platanus biochar. Process Safety and Environmental Protection 140: 221-232.

Jung K W, Lee S, Lee Y J, (2017). Synthesis of novel magnesium ferrite ($MgFe_2O_4$)/biochar magnetic composites and its adsorption behaviour for phosphate in aqueous solutions. Bioresource Technology 245: 751-759.

Kim J K, Park K J, Cho K S, et al. (2005). Aerobic nitrification-denitrification by heterotrophic Bacillus strains. Bioresource Technology 96: 1897-1906.

Kim M H, Hao O J, Wang N S, (1997). Acinetobacter isolates from different activated sludge processes: characteristics and neural network identification. FEMS Microbiology Ecology 23: 217-227.

Kodera H, Hatamoto M, Abe K, et al. (2013). Phosphate recovery as concentrated solution from treated wastewater by a PAO-enriched biofilm reactor. Water Research 47: 2025-2032.

Kong L C, Tian Y, Pang Z, et al. (2020). Needle-like Mg-La bimetal oxide nanocomposites derived from periclase and lanthanum for cost-effective phosphate and fluoride removal: Characterization, performance and mechanism. Chemical Engineering Journal 382: 122963.

Kortstee G J, Appeldoorn K J, Bonting C F C, et al. (1994). Biology of polyphosphate-accumulating bacteria involved in enhanced biological phosphorus removal. FEMS Microbiology Reviews 15: 137-153.

Li R H, Wang J J, Zhou B Y, et al. (2016). Recovery of phosphate from aqueous solution by magnesium oxide decorated magnetic biochar and its potential as phosphate-based fertilizer substitute. Bioresource Technology 215: 209-214.

Li S Y, Huang X F, Wan Z Y, et al. (2020). Green synthesis of ultrapure $La(OH)_3$ nanoparticles by one-step method through spark ablation and electrospinning and its application to phosphate removal. Chemical Engineering Journal 388: 124373.

Liao Y, Jiang L, Cao X K, et al. (2022). Efficient removal mechanism and microbial characteristics of tidal flow constructed wetland based on in-situ biochar regeneration (BR-TFCW) for rural grey water. Chemical Engineering Journal 431: 134185.

Qiao L, Wen D H, Wang J L, (2010). Biodegradation of pyridine by Paracoccus sp. KT-5 immobilized on bamboo-based activated carbon. Bioresource Technology 101: 5229-5234.

Qiao L, Wang J L, (2010). Biodegradation characteristics of quinoline by Pseudomonas putida. Bioresource Technology 101: 7683-7686.

Liu Y, Gan L, Chen Z L, et al. (2012). Removal of nitrate using Paracoccus sp. YF1 immobilized on bamboo carbon. Journal of Hazardous Materials 229-230: 419-425.

Lv Y, Tang C Y, Liu X Y, et al. (2022). Stabilization and mechanism of uranium sequestration by a mixed culture consortium of sulphate-reducing and phosphate-solubilizing bacteria. Science of the Total Environment 827: 154216.

Mallet M, Barthelemy K, Ruby C, et al. (2013). Investigation of phosphate adsorption onto ferrihydrite by X-ray photoelectron spectroscopy. Journal of Colloid and Interface Science 407: 95-101.

Miretzky P, Cirelli A F, (2010). Cr(VI) and Cr(III) removal from aqueous solution by raw and modified lignocellulosic materials: A review. Journal of Hazardous Materials 180: 1-19.

Miretzky P, Munoz C, Carrillo-Chavez A, (2008). Experimental binding of lead to a low cost on biosorbent: Nopal (Opuntia streptacantha). Bioresource Technology 99: 1211-1217.

Moll D M, Summers R S, Matheis W, (1999). Impact of temperature on drinking water biofilter performance and microbial community structure. Environmental Science & Technology 33: 2377-2382.

Peng S, Deng S H, Li D S, et al. (2020). Iron-carbon galvanic cells strengthened anaerobic/anoxic/oxic process (Fe/C-A2O) for high-nitrogen/phosphorus and low-carbon sewage treatment. Science of the Total Environment 722: 137657.

Pereira H, Lemos P C, Reis M A M, et al. (1996). Model for carbon metabolism in biological phosphorus removal processes based on in vivo [13] C-NMR labelling experiments. Water Research 30: 2128-2138.

Tang P, Xiang Z X, Ma P H, et al. (2021). Laboratory investigation on Bacillus subtilis addition to alleviate bio-clogging for constructed wetlands. Environmental Research 194: 110642.

Postma J, Nijhuis E H, Someus E, (2010). Selection of phosphorus solubilizing bacteria with biocontrol potential for growth in phosphorus rich animal bone charcoal. Applied Soil Ecology 46: 464-469.

Rasul M, Yasmin S, Yahya M, et al. (2021). The wheat growth-promoting traits of Ochrobactrum and Pantoea species, responsible for solubilization of different P sources, are ensured by genes encoding enzymes of multiple P-releasing pathways. Microbiological Research 246: 126703.

Santos A B, Cervantes F J, Lier J B, (2007). Review paper on current technologies for decolourisation of textile wastewaters: Perspectives for anaerobic biotechnology. Bioresource Technology 98: 2369-2385.

Siggins A, Thorn C, Healy M G, et al. (2021). Simultaneous adsorption and biodegradation of trichloroethylene occurs in a biochar packed column treating contaminated landfill leachate. Journal of Hazardous Materials 403: 123676.

Son H J, Park G T, Cha M S, et al. (2006). Solubilization of insoluble inorganic phosphates by a novel salt- and pH- tolerant *Pantoea agglomerans* R42 isolated from soybean rhizosphere. Bioresource Technology 97: 204-210.

Su C, Sun X J, Mu Y Z, et al. (2021). Multilayer calcium alginate beads containing diatom biosilica and bacillus subtilis as microecologics for sewage treatment. Carbohydrate Polymers 256: 117603.

Su M H, Azwar E, Yang Y F, et al. (2020). Simultaneous removal of toxic ammonia and lettuce cultivation in aquaponic system using microwave pyrolysis biochar. Journal of Hazardous Materials 396: 122610.

Sumaraj, Xiong Z X, Sarmah A K, et al. (2020). Acidic surface functional groups control chemisorption of ammonium onto carbon materials in aqueous media. Science of the Total Environment 698: 134193.

Sun E H, Zhang Y, Xiao Q B, et al. (2022). Formable porous biochar loaded with La-Fe(hydr)oxides/montmorillonite for efficient removal of phosphorus in wastewater: process and mechanisms. Biochar 4: 53.

Streichan M, Golecki J R, Schön G, (1990). Polyphosphate-accumulating bacteria from sewage plants with different processes for biological phosphorus removal. FEMS Microbiology Ecology 6: 113-124.

Tarayre C, Nguyen H T, Brognaux A, et al. (2016). Characterisation of Phosphate Accumulating Organisms and Techniques for Polyphosphate Detection: A Review. Sensors 16: 797.

Tarjányi-Szikora S, Oláh J, Makó M, et al. (2013). Comparison of different granular solids as biofilm carriers. Microchemical Journal 107: 101-107.

Teng Z D, Shao W, Zhang K Y, et al. (2020). Enhanced passivation of lead with immobilized phosphate solubilizing bacteria beads loaded with biochar/ nanoscale zero valent iron composite. Journal of Hazardous Materials 384: 121505.

Vu M T, Chao H P, Van Trinh T, et al. (2018). Removal of ammonium from groundwater using NaOH-treated activated carbon derived from corncob wastes: Batch and column experiments. Journal of Cleaner Production 180: 560-570.

Wan W J, He D L, Xue Z J, (2017). Removal of nitrogen and phosphorus by heterotrophic nitrification-aerobic denitrification of a denitrifying phosphorus-accumulating bacterium Enterobacter cloacae HW-15. Ecological Engineering 99: 199-208.

Wang Q B, Yao R D, Yuan Q, et al. (2018). Aerobic granules cultivated with simultaneous feeding/draw mode and low-strength wastewater: Performance and bacterial community analysis. Bioresource Technology 261: 232-239.

Wu D, Xia T Y, Zhang Y X, et al. (2021). Identifying driving factors of humic acid formation during rice straw composting based on Fenton pre-treatment with bacterial inoculation. Bioresource Technology 337: 125403.

Xie C S, Zhao J, Tang J, et al. (2011). The phosphorus fractions and alkaline phosphatase activities in sludge. Bioresource Technology 102: 2455-2461.

Xu K N, Lin F Y, Dou X M, et al. (2018). Recovery of ammonium and phosphate from urine as value-added fertilizer using wood waste biochar loaded with magnesium oxides. Journal of Cleaner Production 187: 205-214.

Yang F, Jian H X, Wang C P, et al. (2021). Effects of biochar on biodegradation of sulfamethoxazole and chloramphenicol by Pseudomonas stutzeri and Shewanella putrefaciens: Microbial growth, fatty acids, and the expression quantity of genes. Journal of Hazardous Materials 406: 124311.

Yin J, Zhang P Y, Li F, et al. (2015). Simultaneous biological nitrogen and phosphorus removal with a sequencing batch reactor–biofilm system. International Biodeterioration & Biodegradation 103: 221-226.

Zeng X, Huang J J, Hua B, (2021). Efficient phosphorus removal by a novel halotolerant fungus *Aureobasidium* sp. MSP8 and the application potential in saline industrial wastewater treatment. Bioresource Technology 334: 125237.

Zhang H L, Fang W, Wang Y P, et al. (2013). Phosphorus removal in an enhanced biological phosphorus removal process: roles of extracellular polymeric substances. Environmental Science & Technology 47: 11482-11489.

Zhang L, Wan L H, Chang N, et al. (2011). Removal of phosphate from water by activated carbon fibre loaded with lanthanum oxide. Journal of Hazardous Materials 190: 848-855.

Zhang M Y, Pan L Q, Su C, et al. (2021). Simultaneous aerobic removal of phosphorus and nitrogen by a novel salt-tolerant phosphate-accumulating organism and the application potential in treatment of domestic sewage and aquaculture sewage. Science of the Total Environment 758: 143580.

Zhang M L, Wang H X, Han X M, 2016. Preparation of metal-resistant immobilized sulphate reducing bacteria beads for acid mine drainage treatment. Chemosphere 154, 215-223.

Zhang S N, Wang J H, (2021). Removal of chlortetracycline from water by Bacillus cereus immobilized on Chinese medicine residues biochar. Environmental Technology & Innovation 24: 101930.

Zhang Y X, Xu Z X, Li J X, et al. (2019). Cooperation between two strains of Enterobacter and Klebsiella in the simultaneous nitrogen removal and phosphate accumulation processes. Bioresource Technology 291, 121854.

Zhao Y X, Liu D, Huang W L, et al. (2019). Insights into biofilm carriers for biological wastewater treatment processes: Current state-of-the-art, challenges, and opportunities. Bioresource Technology 288: 121619.

Zheng L, Ren M, Xie E, et al. (2019). Roles of phosphorus sources in microbial community assembly for the removal of organic matters and ammonia in activated sludge. Frontiers in Microbiology 10: 1023.

CHAPTER 5

COMBINED IMPACT OF FUNCTIONALIZED FORMED-BIOCHAR AND UREASE INHIBITOR ON N/P FORM AND AMMONIA EMISSION DURING URINE STORAGE

CHAPTER 5: UREASE INHIBITOR-MEDIATED POROUS FORMED-BIOCHAR DOPED WITH METAL OXIDE REDUCES AMMONIA VOLATILIZATION AND PROMOTES PRESERVATION OF N/P NUTRIENTS DURING SOURCE-SEPARATED URINE STORAGE

This chapter has been submitted for publication in a peer review journal with the title: Urease inhibitor-mediated porous formed-biochar doped with metal oxide reduces ammonia volatilization and promotes effective preservation of N/P nutrients during source-separated urine storage in *Journal of Environment Management (02/23/2023)*. The manuscript is presented in the following pages.

Graphical Abstract
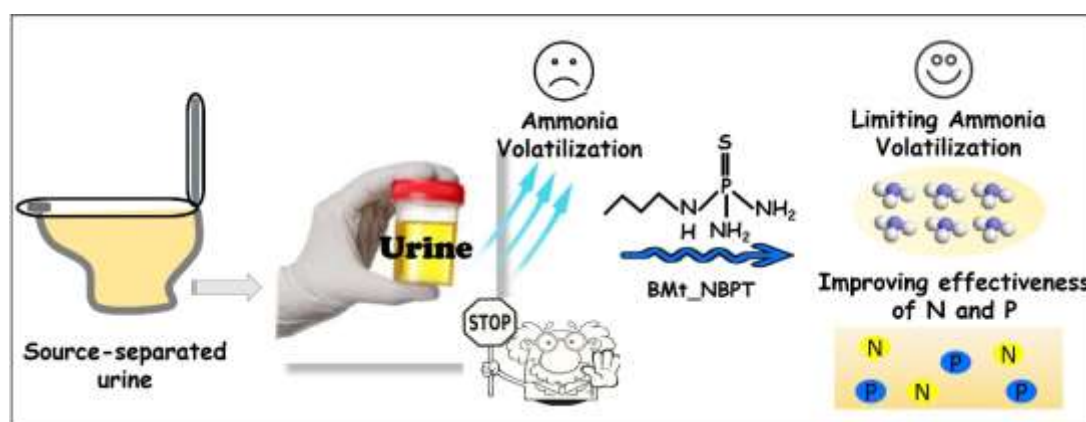
Figure 5.1 Summary diagram of the combined effect of formed-biochar (BMt) and urease inhibitors (NBPT) on nitrogen transformation during urine storage.

Highlights

✪ Beneficial for recovery of concentrated N and P from urine resources.

✪ The conversion of urea to ammonia nitrogen was significantly inhibited, with an 89.7% reduction of NH_3 emission being achieved.

○ Development of an effective preservation technology of N/P nutrients in human urine.

Abstract

Ammonia volatilization is the main N-loss pathway in the process of urine storage and transportation. Acidification can only temporarily reduce ammonia emissions. Therefore, it is necessary to add other nitrogen retention materials, such as biochar-based materials and urease inhibitors, to achieve a lasting reduction in ammonia volatilization emissions. Hence, the contribution of using functionalized formed-biochar (BMt) and urease inhibitor (NBPT) on nitrogen loss, nutrient transformation, and bacterial community composition during urine storage, was explored using urine collected from non-water urinals. Results showed that BMt can limit the conversion of total nitrogen to ammonia during the early stages of storage and was also able to immobilize ammonium ions from solution by adsorption. The addition of 2 g/L BMt to urine samples reduced gaseous NH_3 emission by 40.7%. When BMt was combined with NBPT (0.1% w/w), the conversion of urea to ammonia nitrogen was significantly inhibited, with an 89.7% reduction of NH_3 emission being achieved. The BMt_NBPT treatment was also found to reduce the level of phosphorous precipitation. Additionally, alpha analysis of 16s rRNA gene sequence data from each treatment revealed that the BMt and BMT_NBPT treatments both supported greater levels of microbial diversity compared to the untreated control. The inhibitory effect of acidification on ammonia formation in urine was found to be transitory, that is, after ca. 13-15 d, the physicochemical data starts to show similarities to the control. Whereas, the BMt and BMt_NBPT treatments retained their effectiveness for longer. The current study demonstrates that a BMt_NBPT treatment of urine has the potential as a novel alternative to the traditional acidification method used to inhibit urea hydrolysis.

5.1 Introduction

Treatment of source-separated urine has promoted wastewater management and resource reuse, which is very important in reducing environmental pollution (Paepe et al., 2020).

Nitrogen is an essential growth-limiting-nutrient in terrestrial ecosystems; its incorporation into fertilizers is an important driver of agricultural productivity and improving crop yields (Zaman et al., 2009; Pradhan et al., 2009; Heinonen-Tanski et al., 2007). The recovery of phosphorus in urine has also been proposed as an effective way of alleviating the shortage of phosphorus-containing mineral fertilizer resources (Guadie et al., 2020).

Direct utilization of urine as a fertilizer is not recommended since it may contain pathogens that are harmful to humans (Schönning et al., 2002; Bonvin et al., 2015). Storage and processing of urine are considered to be viable ways to turn urine into safe fertilizers (Hu et al., 2016). Nitrogen and phosphorus resources can be recovered and utilized in a variety of ways (Wald 2022); the current technologies include precipitation (Etter et al., 2011), air stripping/acid scrubbing (Wei et al., 2018), ion exchange (Simha et al., 2018), membrane (Courtney et al., 2021), electrochemical (Tarpeh et al., 2018), and biological treatment (Badeti et al., 2022; Behera et al., 2020). The treatment technologies associated with source-separated urine have been comprehensively reviewed in the literature (Maurer et al., 2006). It is important to note that the composition of urine changes during storage, which can compromise the nutrient value of urea-based fertilizers (Karak et al., 2011). The urea component of urine is prone to hydrolysis, which is driven by microbially associated urease activity leading to ammonia production, elevated pHs, scaling, and resulting in nitrogen loss. The specific chemical reactions are listed as follows:

$$CO(NH_2)_2 + 3H_2O \rightarrow NH_3 + NH_4HCO_3 \qquad (1)$$

$$Mg^{2+} + NH_4^+ + PO_4^{3-} + 6H_2O \rightarrow Mg(NH_4)PO_4 \cdot 6H_2O\downarrow \qquad (2)$$

$$5Ca^{2+} + 3PO_4^{3-} + OH^- \rightarrow Ca_5(PO_4)_3OH \qquad (3)$$

Ammonia volatilization is one of the forms of nitrogen loss, which can adversely impact the environment and human health (Lahr et al., 2016; Lelieveld et al., 2015; Van Damme et al., 2018). Thus, urine pre-treatment is critical for preventing ammonia volatilization and maintaining its stability during storage.

Acidification is often used to prevent urea degradation by microorganisms and ammonia volatilization (Charteris et al., 2021). Previous studies have demonstrated the effectiveness of

sulfuric acid treatment, which has a significant impact on the mitigation of nitrous oxide and ammonia emissions (Sommer et al., 2017). Similarly, acetic acid has also been shown to inhibit urea hydrolysis at the laboratory scale (Saetta et al., 2020). It was found by Saetta (2020) that the coefficient of change of ammonia concentration decreased significantly after the addition of acid, indicating that urea hydrolysis was inhibited. Urine acidification was also found to reduce bacterial diversity. Further, Saetta et al. (2017) demonstrated that the addition of acetic acid also improved the recovery rate of phosphate (struvite) from urine. However, Hoglund et al. (1998) found that some bacteria, such as *Escherichia coli* died off rapidly during hydrolysis, while others, such as faecal streptococci, persisted during storage.

Another mitigation strategy used to reduce nitrogen loss and improve the nutritional value of fertilizer is to add a urease inhibitor, such as N- (n-butyl) thiotriamide phosphate (NBPT) (Kawakami et al., 2012). NBPT inhibits urea hydrolysis by competing with urea molecules for urease binding sites (Kawakami et al., 2012). The addition of NBPT has been found to reduce cumulative NH_3 emissions by about 48% (Pereira et al., 2013). In another study, NBPT delayed the onset of urea hydrolysis by 1-2 weeks (Zaman et al., 2009). Similarly, recent studies have reported that urea-based fertilizer treated with NBPT resulted in a 5.3% increase in crop yield (Silva et al., 2017).

In addition to the inhibition of urea hydrolysis, the recovery of nitrogen and phosphorus directly from urine is considered a promising approach that can be used to realize the full potential and value of urine as a renewable fertilizer resource. Biochar has been used as an effective adsorbent for the recovery of nutrients in urine (Pathy et al., 2021). From the available, conventional adsorbents, the focus on choosing biochar for recovering the nutrients has several advantages. Unlike other adsorbents such as zeolite, activated carbon, and alumina, biochar is produced from waste. Biochar adds value to the management of waste products and at the same time, makes it comparatively more economical (Pathy et al., 2021). In recent years, a large number of studies on the recovery of nitrogen in urine by biochar have been published (Otieno et al., 2021). The adsorption characteristics of biochar depend mainly on its porous structure, high specific surface area, and abundant functional groups on particle surfaces (Masrura et al., 2020). High cation exchange capacity can also endow biochar with good NH_4^+-N adsorption capacity (Gai et al., 2014). Tarpeh et al. (2017) observed that although cations such as NH_4^+, Na^+, and K^+ in urine compete for adsorption sites, biochar tended to adsorb NH_4^+ preferentially.

After treatment, recovered biochar could also be used directly as a fertilizer to improve soil fertility.

To improve the adsorption properties of biochar materials, surface modification with metal oxides has been implemented. A recent study confirmed that metal oxide-modified biochar could simultaneously recover ammonium and phosphate from urine (Xu et al., 2018). Ammonium adsorption was attributed primarily to negatively charged functional groups present on particle surfaces with an adsorption capacity of up to 47.5 mg N/g (Xu et al., 2018). Recent studies have further recommended that the introduction of metals would lead to more reaction sites (Xu et al., 2017). Various metallic oxides, such as MgO, CaO, AlOOH, Fe_2O_3, and La_2O_3, can result in higher adsorption capacity for phosphate since phosphate ions make surface deposition or precipitation with the metallic oxides by hydrogen bonding (weak bonds) or strong chemical bonds, respectively (Shakoor et al., 2021; Vikrant et al., 2018). On the other hand, increasing the negatively charged functional groups (such as carboxyl) in biochar can also improve the ammonium adsorption capacity (Liang et al., 2006). Engineered biochar, which was functionalized with metal salt impregnation, possesses abundant surface functional groups that improved adsorption capacity (Shakoor et al., 2021). In addition, the microporous structure of biochar can also provide a suitable place for microorganisms to grow (Liu et al., 2017). The inhibition of ammonia volatilization by adding an exogenous substance has received much attention in previous studies (He et al., 2018; Kavanagh et al., 2021; Taghizadeh-Toosi et al., 2012). We have previously reported that La/Fe-MB can be obtained via a simple one-step co-precipitation, then fabricated via a granulation and pyrolysis process method (Sun et al., 2022). La/Fe-MB was stable under the acidic conditions investigated (pH 3 ~ 6) and displayed a high compressive strength with an excellent ability to uptake P (52.12 mg P/g), which enables the rapid separation of the adsorbent from water for repeated use.

The separation of urine at the source for phosphorus (P) recovery is attractive considering the high P concentration relative to volume (Xu et al., 2015). In order to retain nitrogen within the system, an important goal is to achieve a lasting reduction in ammonia volatilization during urine storage. Therefore, the purpose of this study was to investigate a new strategy to recover P and inhibit nitrogen volatilization. To the best of our knowledge, no previous study has investigated the application of a urease inhibitor in conjunction with biochar treatment to inhibit ammonia volatilization in source-separated urine. Hence, it is also interesting to investigate the

changes in bacterial community structure after BMt and NBPT addition to determine their impact on the incidence of harmful or pathogenic bacteria. Thus, physicochemical changes in the urine were measured over the course of a 70-day storage period, and differences in the microbiota associated with different treatments were assessed after the experiment. The main objectives of this study were to 1) determine the effects of different treatments on ammonia emission during storage of source-separated urine; 2) determine changes in physical and chemical properties of urine over time; 3) reduce the loss of nitrogen from urine by the conversion of urea to ammonium, and ammonia volatilization; and, 4) determine the effects of different treatments on the composition and richness of bacterial communities within stored urine. The motivation for controlling urea hydrolysis in these experiments was to maximize nutrient content in the storage tanks at the end of the experiment for subsequent nutrient recovery.

5.2 Materials and methods

5.2.1 Materials

The fresh urine for the storage experiment was collected directly from a male public toilet in Nanjing vegetable market (32°02′46″N, 118°53′33″E), Jiangsu province, China, and stored in a sealed plastic tank for 2 days at 4°C until incubation. The initial pH, EC, TN, NH_4^+-N, TP, PO_4^{3-} were 6.21, 34.30 mS/cm, 9.40 g/L, 3.2545 g/L, 386.15 mg/L, and 207.96 mg/L, respectively. Functionalized formed-biochar granules were prepared according to the method detailed in our previous study (Sun et al., 2022). Characterization of the physicochemical adsorbent properties of the formed biochar have been described previously (Sun et al., 2022), with a specific surface area of 63.54 m^2/g, the average pore size of 6.16 nm, and packing density of 0.518 g/mL. All chemicals used in this study were analytical grade, including sulfuric acid (H_2SO_4) and urease inhibitor N-(n-butyl) thiophosphoric triamide (NBPT) supplied by Sigma Aldrich (United States).

5.2.2 Experimental setup

Three treatments were evaluated as management regimes to control nitrogen transformation in urine, each with two replicates and arranged in a randomized complete block design.

Treatments included: (i) a urine control ('CK') without additives; (ii) urine acidified with sulfuric acid to reduce the pH to 4.0 ('pH4'); (iii) urine amended with functionalized formed-biochar ('BMt'); and, (iv) urine amended with BMt and a urease inhibitor N-(n-butyl) thiophosphoric triamide ('BMt_NBPT').

For each treatment, 500 mL urine was first added to a 2 L sealed glass vessel, before the exogenous substances (viz., H_2SO_4, BMt, NBPT) were added, with mixing, to meet the conditions required for the experiment. BMt and NBPT were applied to the urine at concentrations of 2 g/L (w/v) and 0.1% NBPT (w/w), respectively. The test was conducted from July 2021 to September 2021. All treatments were operated on the laboratory test bench at room temperature, and the glass vessels used were plugged with rubber stoppers. Samples (4 mL) were taken from each vessel via a tube inserted into the liquid for the determination of physical and chemical indexes. Samples were taken on days 1, 3, 7, 15, 30, 45, and 70, and analysed for pH, EC, and concentrations of total nitrogen (TN), NH_4^+-N, total phosphorous (TP), and PO_4^{3-}. From day 1 onwards, the urine solution was shaken intermittently and was allowed to stand before each sampling. Ammonia (NH_3) emissions for all treatments were monitored periodically using a dynamic chamber system. The monitoring was performed on days 10, 14, 15, 30, 32, 35, 45, 50, 52, 60, and 70, each time the test instrument was placed in the glassware for 1-2 minutes. When the data was stable, the ammonia concentration was recorded. The sampling site and test device were depicted in Fig.5.2.

5.2.3 Analytical methods

Urine solution pH and EC were determined with a pH meter (pHS-3C, Shanghai Lei Ci Instrument Factory, Shanghai, China), and a conductivity meter (DDSJ-308A, Shanghai Lei Ci Instrument Factory, Shanghai, China), respectively. NH_4^+-N was analysed according to the Nashi reagent spectrophotometry method (Huang et al., 2019). TN and TP were determined by the potassium persulfate oxidation-UV spectrophotometric method and the molybdenum-antimony anti-spectrophotometric method, respectively (Cao et al., 2019). Phosphate concentration was measured colorimetrically at a wavelength of 700 nm according to the ascorbic acid method, whereas that of ammonium was analysed at a wavelength of 697 nm with a spectrophotometer (Lianhua Technology 5B-3B, China) (Cao et al., 2022).

Real-time dynamic ammonia concentrations were analysed with a photoacoustic INNOVA 1412 field gas-monitor (LumaSense Technologies, Denmark).
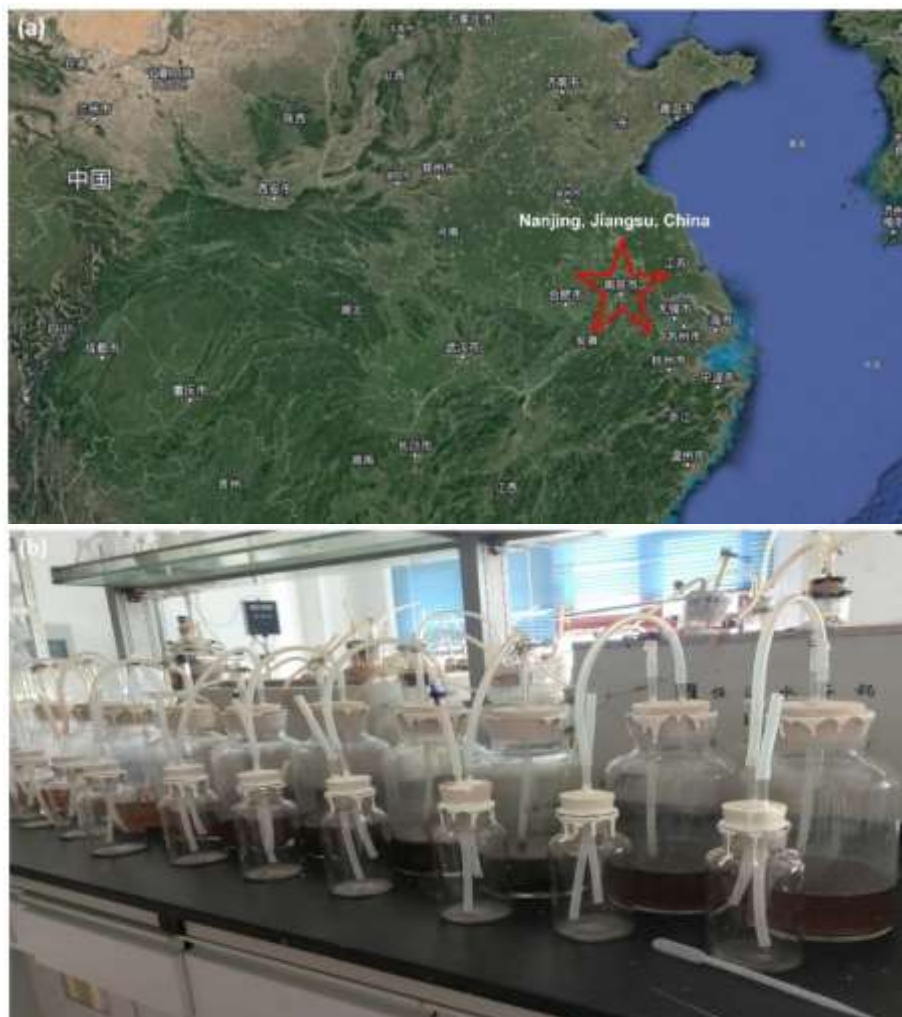
Figure 5.2 Sample sampling site from Nanjing, Jiangsu, China (a) and test device (b). Note, the small bottle next to the 2 L sealed glass vessel are used to balance the air pressure.

5.2.4 Microbiological analysis

Sediment samples were collected from the bottom of each treatment container at the end of the experiment, and kept at -80°C until processed. DNA was extracted from each sample using an E.Z.N.A. ® soil DNA Kit (Omega Bio-Tek, Norcross, GA, U.S.) following the manufacturer's recommended protocol. Agarose gel electrophoresis (1% w/v) was performed to check DNA quality and DNA concentration and purity were determined by UV-vis spectrophotometry (NanoDrop 2000, Thermo Scientific, Wilmington, USA). The V3-V4 hypervariable regions of bacterial 16S rRNA gene were amplified using primers 338F (5'-

ACTCCTACGGGAGGCAGCAG-3') and 806R (5'-GGACTACHVGGGTWTCTAAT-3')
according to the method of Li et al. (2022) and Wu et al. (2021). PCR reactions (20 μL) were
conducted in triplicate using a thermocycler PCR system (GeneAmp 9700, ABI, USA) with the
following reaction cycle: initial denaturation at 95°C for 3 min; 27 cycles of 30 s at 95°C, 30 s
for annealing at 55°C, and 45 s for elongation at 72°C; and, a final extension at 72°C for 10
min. Purified amplified gene products were sequenced at Majorbio Bio-pharm Technology Co.,
Ltd. (Shanghai, China) using the Illumina MiSeq platform (Illumina, San Diego, USA)
according to standard protocols.

5.2.5 Statistical and bioinformatics analysis

SPSS 19.0 software was used for one-way analysis of variance (ANOVA) to evaluate the
differences in physical and chemical properties of different treatment groups. Sequence data
were analysed using pre-configured bioinformatic pipelines available on the online Majorbio
Cloud Platform (www.majorbio.com). Processing of raw sequencing data (fastq files) involved
demultiplexing, quality-filtering (Trimmomatic), and merging using FLASH according to the
following criteria: (i) Sequence reads were truncated at any site receiving an average quality
score <20 over a 50 bp sliding window; (ii) Primers were exactly matched allowing 2 nucleotide
mismatching, and reads containing ambiguous bases were removed; (iii) Sequences with
overlaps longer than 10 bp were merged according to their overlap sequence. UPARSE（
version 7.1, http://drive5.com/uparse/) was used to cluster operational taxonomic units (OTUs)
based on a 97% similarity cut-off limit and chimeric sequences were identified and removed
using UCHIME. Taxonomic classification of the 16S rRNA gene sequence data was undertaken
using the RDP Classifier algorithm (http://rdp.cme.msu.edu/) against the Silva (SSU123) 16S
rRNA database using a confidence threshold of 70%. Differences in microbial community
structures between treatment groups were determined by α-Diversity analysis. Redundancy
analysis (RDA) was used to analyse the relationships between bacterial community structure
and physio-chemical parameters (Canoco 4.5 software package, Microcomputer Power, Ithaca,
NY, USA). Ecological interpretation of 16S marker gene data was performed using the
Functional Annotation of Prokaryotic Taxa (FAPROTAX) database to map prokaryotic clades
to established ecologically relevant functions. The direct and indirect relationships between
environmental factors (pH, EC, TN, NH_4^+, TP, and PO_4^{3-}) and the NH_3 process were performed

by Partial least squares path modelling (PLS-PM) using the plspm package in R (Cao et al., 2022).

5.3 Results and discussion

5.3.1 Analysis of physio-chemical parameters during storage

5.3.1.1 Evolution of pH, and EC

pH and conductivity can be used as a proxy for evaluating the progression of urea hydrolysis (Ray et al., 2018). We focused specifically on pH as this parameter was deemed the most useful for evaluating different technologies for limiting nitrogen loss via urea hydrolysis (Chipako et al., 2020). The pH changes of urine associated with different treatments over a 70-d incubation period are shown in Fig. 5.3a.

Except for the 'pH4' treatment, the pH changes followed a similar trend. Initially, pH levels rose rapidly over the first five days and this was attributed to the release of bicarbonate ions associated with urea hydrolysis (Zaman et al., 2009). Additionally, ammonia produced from this reaction may also react with water producing ammonium hydroxide, which contributes to pH increases. Urea hydrolysis is attributed mainly to the action of urease active bacteria or free urease (Kai et al., 2003). Since porous biochar is acidic, the initial pH of the BMt and BMt_NBPT treatment groups was lower than the unamended 'CK' control. By the 5th day, the pH of the 'CK' control had increased to 9.0, which is consistent with the pH changes associated with stored urine reported in the literature previously (Almeida et al., 2019).

The pH of the BMt and BMt_NBPT treatments only increased to 7.76 and 6.91, respectively, suggesting that these treatments reduced the levels of hydrolysis of urea. On day seven a notable decrease in pH was evident for each treatment; this was ascribed to precipitation and the resultant consumption of phosphate ions and partial ammonia concentration, resulting in a relative decrease in pH. For the 'pH4' acidification treatment, the pH of urine remained relatively stable during the early phases of storage (0-7 days); this was attributed to the negative impact that acidic pH had on urease enzymes and bacterial activity in general (Saetta et al., 2019). The pH of the CK, pH4, and BMt treatments increased to about 9.0 at 15 days, and remained at that pH range for the duration of the experiment, whereas the BMt_NBPT treatment

only increased to 7.58. The precipitation in the early stage broke the balance of the conversion of nitrogen to ammonia nitrogen, thus increasing the pH of the solution. As storage time increased, a gradual increase in pH of the BMT_NBPT treated urine occurred; by day 60 pH levels similar to the remaining treatments were recorded. Overall, the BMT_NBPT treatment was found to be the most effective modulator of the pH of stored urine, indicating its effectiveness in delaying the ammonification process of urine over extended periods.
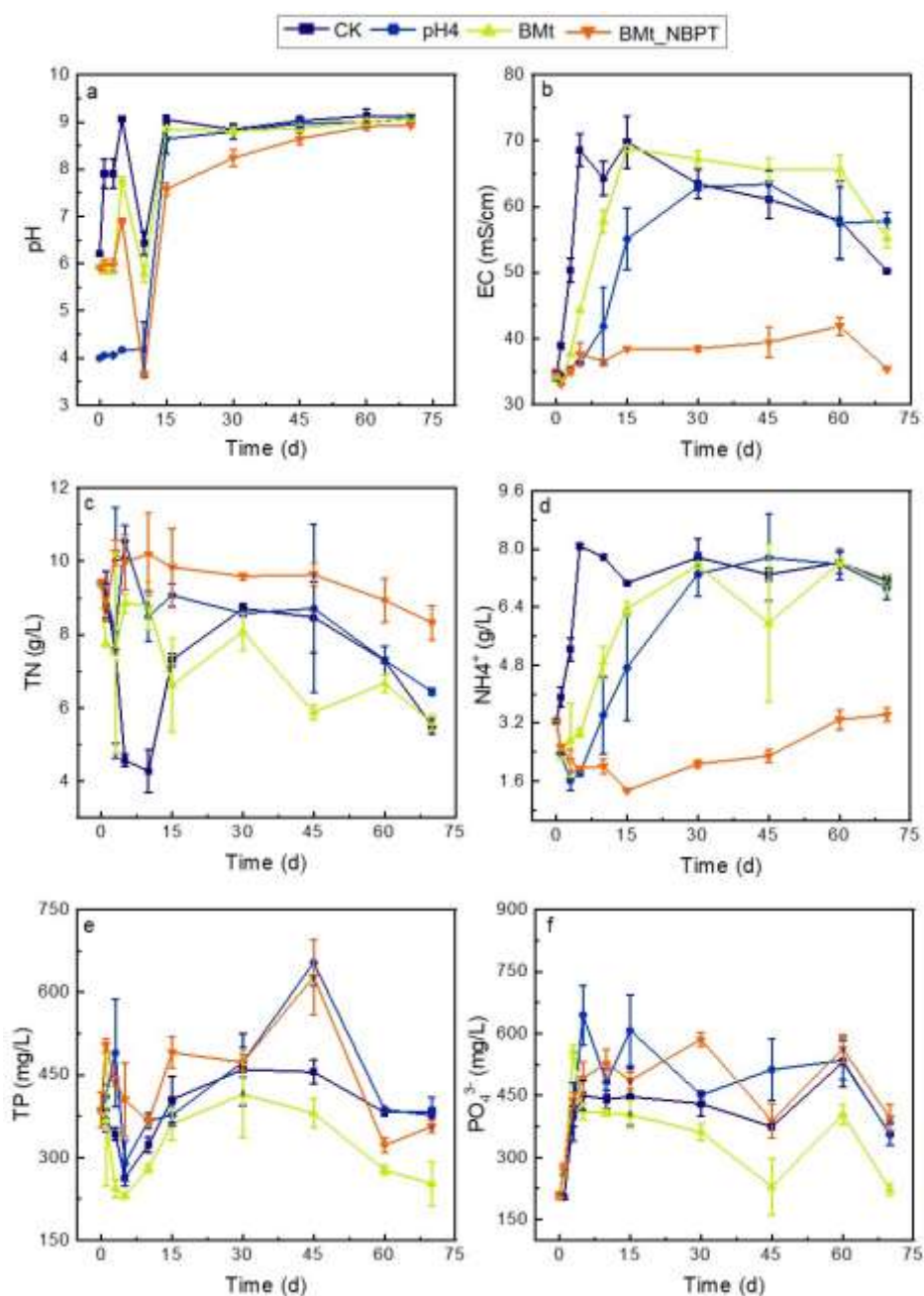
Figure 5.3 Changes in physicochemical indices over time for different treatment groups. (a) pH, (b) EC, (c) TN, (d) NH_4^+, (e) TP, (f) PO_4^{3-}.

EC determination was used to observe changes in soluble ion concentration in urine (Fig. 5.3b). As seen for the 'CK' control, during the storage of urine, the ion concentration increases due to urea hydrolysis and an accumulation of NH_4^+ with a concomitant increase in pH. This can lead to struvite ($MgNH_4PO_4 \cdot 6H_2O$) precipitation, resulting in a decrease of aqueous phosphate concentration in urine (Kai et al., 2003). Struvite is a common sediment in the urine, which can be recycled and used as a slow-release fertilizer (De Boer et al., 2018). Therefore, the presence of precipitation during urine storage does not adversely affect the nutrient value of urine.

Under acidic conditions (pH4), during the early stage of storage, EC values increase slowly, indicating that urea hydrolysis is effectively suppressed. Over time, EC values increase, which is consistent with rising pH values (Fig. 5.3a) resulting from urea hydrolysis (Fig. 5.3b). It appeared that the 'pH4' acidification treatment was temporary and that the changes in pH that occurred may have resulted from the metabolic activity of microbial populations that were able to tolerate/survive the acidified conditions. BMt-treated urine appeared to reduce the rate of urea hydrolysis during the initial stages of the study (0-15 days), as indicated by a lower rate of EC increase compared to the CK control. Adsorption interactions between NH_4^+ and negatively charged functional groups on the surface of biochar may account for this observation (Wang et al., 2015). Further, the addition of a urease inhibitor in the BMt_NBPT treatment resulted in significantly lower EC levels for the duration of the study compared to the other treatments. This result indicated the effectiveness of NBPT in inhibiting urea hydrolysis in urine when added in combination with BMt.

5.3.1.2 Transformation of nitrogen form

Fig. 5.3c and d shows the changes of total nitrogen and ammonium nitrogen concentrations in different urine treatments. The duration and progress of naturally occurring urea hydrolysis are dependent on the prevailing environmental conditions and will vary in different environments. In the process of urine storage, the total nitrogen content of all treatments was found to fluctuate over time and this was attributed to various factors such as NH_3 volatilization, nitrogen assimilation by microbial biomass, and nitrogen adsorption to biochar.

The 'CK' control treatment exhibited a major decline in TN at day five, which coincided with a significant increase in pH value, and this was attributed to nitrogen loss caused by

microbially mediated urea hydrolysis and NH_3 volatilization. Subsequently, TN concentrations increased to levels similar to the other treatments by day 30. This observation was ascribed to the reabsorption of the ammonia gas present in the sealed headspace of the treatment vessel. The TN concentration for the 'CK' control decreased by 54.52% from day 0 to day 10, whereas the TN of the pH4 and BMt treatments decreased by 9.59% and 6.54% respectively over the same period.

Comparatively, the initial TN of BMt_NBPT treatment was slightly higher than the control value, mainly because of the influence of the nitrogen element in the NBPT inhibitor itself. During days 8 ~ 30 days, there was a small relative upward trend in TN for all treatments, which may also reflect the reabsorption of NH_3 into the solution from the chamber headspace.

There are three main reactions that nitrogen transformation occurs during urine storage (eq. (4) ~ (6)).

$$CO(NH_2)_2 + 3HO \rightarrow 2NH_4^+ + HCO_3^- + OH^- \tag{4}$$
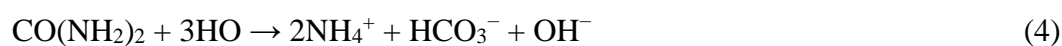
Ammonium is in equilibrium with dissolved ammonia.

$$NH_4^+ + OH^- \leftrightarrow NH_3 \text{ (aq)} + H_2O \tag{5}$$

The pKa value for the equilibrium is 9.3 at 25°C (Snoeyink and Jenkins, 1980). Dissolved ammonia is in equilibrium with gaseous ammonia.

$$NH_3 \text{ (aq)} \leftrightarrow NH_3 \text{ (g)} \tag{6}$$

Therefore, the decomposition of urea will lead to an increase in the concentration of ammonia nitrogen, and an increase in pH, resulting in an increased risk of nitrogen loss through ammonia volatilization. Reaction (6) also shows that the partial pressure of ammonia above the liquid level has an important effect on the volatilization of ammonia. This means that there is a gas exchange in the tank to balance the nitrogen loss during urine storage and diffusion of solute in the liquid phase (Hellström et al., 1999).

Overall, there was a downward trend in total N content over time (Fig. 5.3c), with CK, pH4, BMt, and BMt_NBPT treatments decreasing by 41.42%, 31.47%, 40.41%, and 11.48%, respectively at the end of the storage period. These results reflect, indirectly, the impacts of the urea hydrolysis reaction on TN values and can be used as an indicator of the extent of urea hydrolysis (Ray et al., 2018). The TN of the BMt treatment was lower than that of CK after 15 days, which may indicate adsorption in the BMt material. Meanwhile, the concentration of NH_4^+-N in the urine of all treatments showed an overall upward trend with time (Fig. 5.3d). The increase of NH_4^+ was attributed to the hydrolysis of urea. On the 5th day, the content of NH_4^+-N in the CK group increased from 3.25 g/L to the maximum value of 8.09 g/L, then decreased to 7.78 g/L and remained essentially unchanged for the remainder of the storage period. The NH_4^+-N concentrations increased slightly in the pH4 and BMt treatments, increasing to 7.31 and 7.55 g/L respectively, by the 30th day.

In contrast, the BMt_NBPT treatment showed significantly lower levels of NH_4^+-N accumulation. NH_4^+-N concentrations declined from 3.26 g/L to a low of 1.5 g/L on day 15 and were followed by a subsequent increase to 3.43 g/L by the end of the study period. These data indicate that the BMt_NBPT treatment was able to significantly inhibit the conversion of urea to NH_4^+-N compared to the other treatments. In addition, during 30 - 45 days of storage, BMt showed a downward trend in NH_4^+-N concentration, which may be because the ammonia volatilization of the treatment was maintained at a high level, resulting in the reduction of NH_4^+-N concentration, thereby affecting TN. The NH_4^+-N of BMt_NBPT showed a relatively slow upward trend after 15 days, this may be linked to the degradation of NBPT, which would allow urease to be reactivated and react with urea (Xu et al., 2021). The NH_4^+-N content for CK peaked on day 5, whereas for the pH4 and BMt treatments this only occurred at days 45 and 30, respectively. The BMt_NBPT treatment demonstrated the lowest levels of NH_4^+-N during urine storage, indicating that the addition of NBPT was effective in delaying the conversion of total nitrogen to ammonia nitrogen.

In previous studies, Takaya et al. (2016) pointed out that the surface area of biochar is not the main factor affecting the ammonium adsorption capacity, while the availability of acid functional groups was. Cai et al. (2016) discussed the mechanism of adsorption of NH_4^+-N by biochar and found it to be attributable to hydrogen bonds and electrostatic interactions between biochar and NH_4^+-N. In addition, the biochar had a better adsorption effect on NH_4^+-N, which

could reach 114.71 mg/g (Yu et al., 2022). Specifically, the oxygen-containing functional groups on biochar, including C−O, −COC− and −COOH, play an important role, providing a large number of negative potential points for NH_4^+−N adsorption (Yu et al., 2022). Hence, adding BMt to urine can inhibit the conversion of TN in an early stage of storage, and can adsorb a certain amount of ammonia nitrogen during the later stages. Additionally, simultaneous treatment of BMt with NBPT was found to further inhibit urea hydrolysis.

5.3.1.3 Evolution of phosphorus form

Fig. 5.3e and f show the change in total phosphorus (TP) and orthophosphate (PO_4^{3-}) concentrations in urine affected by different treatments over time. The addition of NBPT in the BMt_NBPT treatment resulted in a TP concentration that was higher than the initial value in urine. This observation was attributed to the P component of NBPT increasing the overall phosphorus content in urine for this treatment. It was noted in all treatments that phosphorus combines with urea hydrolysate to form struvite and hydroxyl calcium phosphate precipitate during the early stages of urine storage, resulting in the reduction of initial TP.

The TP content of urine in CK, pH4, and BMt_NBPT groups before and after storage was not significantly different. However, the TP content of BMt decreased with time, due to electrostatic attraction, surface precipitation, and inner-sphere complexation via ligand exchange to selective P removal (Liu et al., 2021). This work demonstrated that BMt was a promising adsorbent suitable for enhanced relief of eutrophication, and the efficient recovery of phosphorus as a strategic resource from urine (Sun et al., 2022). Similar conclusions have been made by Masrura (2020).

pH will have a significant impact on the distribution of various orthophosphate species in the solution. pH will also impact whether phosphates will precipitate with calcium and/or ammonium/magnesium. The change of PO_4^{3-} is closely related to precipitation in the early stage of acid treatment, urea hydrolysis and PO_4^{3-} precipitation were inhibited, so the concentration of PO_4^{3-} in urine remained at a high level.

However, we found that at 30 days, the TP of the CK and pH4 treatments were slightly higher than the initial value, possibly due to a concentration effect caused by the evaporation of water during the storage period (Tian et al., 2021). Alternatively, this observation may have

resulted from the presence of insoluble P present at the beginning of the experiment, which was subsequently solubilized throughout the storage period. This phenomenon also existed in the BMt and BMt_NBPT groups, but due to the efficient adsorption of phosphorus to BMt, the TP of BMt's was less than that of other treatments at 30 days.

The optimum pH range for struvite precipitation is 8.0-10.0 (Liu et al., 2013). Within 30 - 45 days, the pH value of BMt_NBPT gradually increased from pH 8.81 to 8.88. An increase in pH coincided with a decrease in PO_4^{3-} concentration (Fig. 5.3f), suggesting that struvite precipitation occurred during this period. In addition to this, likely, phosphate radicals may also precipitate with Ca^{2+} to produce calcium phosphate (mainly hydroxyapatite, $Ca_{10}(PO_4)_6OH_2$) during prolonged periods of urine storage (Kannan et al., 2017; Grases et al., 1996), which was also one of the possible reasons for the reduction of phosphate concentration. In addition, PO_4^{3-} adsorption by BMt could also explain the reduction of PO_4^{3-} concentration.

In previous work, we explored the adsorption effect of biochar materials on phosphorus and found that $PO_4^{3-}-P$ adsorption could reach about 50 mg P/g (Sun et al., 2022). At 70 days, the $PO_4^{3-}-P$ contents of CK, pH4, and BMt were 358.22, 355.71, and 222.76 mg/L, respectively. This observation supports the notion that BMt was able to adsorb phosphate, resulting in significantly lower levels of phosphorus in urine after 70 days of storage. Results similar to our findings have been reported by Yu et al. (2022). The maximum $PO_4^{3-}-P$ adsorption capacity of the prepared sludge-derived biochar was 30.29 mg/g. Another study found that biochar with a net positive charge tended to adsorb phosphorus (Jiang et al., 2019; Liu et al., 2021). In this study, changes in PO_4^{3-} concentration in urine were attributed mainly to removal caused by precipitation, and the biochar effect was mainly reflected in NH_4^+ adsorption.

5.3.2 NH$_3$ emissions

Another potential drawback to urine handling systems is the risk of ammonia evaporation during collection, storage, transport, and utilization (Hellström et al., 1999). One method to reduce this risk is to prevent the decomposition of urea to ammoniacal nitrogen (i.e. the sum of NH_4^+-N, and NH_3). Since urea is hydrolysed into ammonia by urease activity, the influence of different treatment conditions on the process is evaluated by monitoring the change of gaseous ammonia concentrations during storage (Fig. 5.4a). The ammonia content of the CK treatment

was maintained in the range of 800 -1200 ppm for the duration of the experiment, with the maximum value of 1125 ppm gaseous ammonia being recorded. In comparison, the gaseous ammonia concentration of pH4 and BMt treatments decreased by 57.51% and 62.76%, respectively, at this initial stage. For the BMt_NBPT treatment, ammonia levels were consistently lower than all of the other treatments for the duration of the experiment and at several sampling intervals (viz., day 15, 32, 35, and 52) no ammonia was detected.

During the initial stages of urine storage, the pH4 and BMt treatments had reduced ammonia emission compared to the untreated control. In both instances, the inhibitory effects of these treatments on ammonia emission were temporary with ammonia concentrations increasing from day 15 onwards. The pH4 treatment was able to limit ammonia levels to the 424 – 656.5 ppm range for the first 30 days, thereafter, the ammonia concentration increased reaching levels that were not significantly different to the CK control treatment. BMt was able to limit ammonia volatilization during the initial phase of the study (days 0-15) at levels consistent with the pH4 treatment. This observation was attributed to the ability of acidic functional groups on biochar to adsorb NH_3 (Taghizadeh-Toosi et al., 2012). Subsequently, ammonia level increased with fluctuating levels of ammonia being recorded for the remainder of the storage period. The final ammonia detection values of CK, pH4, and BMt treatments of urine storage tanks were 1125.00, 1125.00, and 711.50 ppm, respectively.

The BMt_NBPT treatment proved to be the most effective at suppressing ammonia volatilization throughout storage. Ammonia levels below the initial starting concentration of 455.5 ppm were maintained for the duration of the study with a final concentration of 124 ppm being determined on the 70th day. This was attributed to the action of NBPT as a urease inhibitor, which prevents the enzymatic conversion of urea to NH_3. Overall, the BMt_NBPT treatment achieved an 89.7% reduction in NH_3 volatilization (124 ppm) compared with the CK control (1200 ppm). The BMt treatment only reduced NH_3 levels by 40.7%, whereas, the acidification (pH4) treatment was only effective at limiting ammonia emissions for the first 15 days of the study, thereafter, an increase in pH was linked to an increase in ammonia emissions for the remainder of the 70-day storage period. In contrast, Sommer et al. (2017) achieved a 62% reduction in NH_3 emissions over 47 days using sulfuric acid treatment.

In this study, the acidification treatment was only found to be suitable for inhibiting urea hydrolysis over relatively short storage periods of 30 days. In a previous study, He et al. (2018) confirmed the effectiveness of biochar combined with urease inhibitors in reducing soil ammonia emissions during rice growth. Similarly, the findings of the current study demonstrate the efficacy of this combined treatment approach for reducing ammonia emissions in source-separated urine that is stored for a prolonged period.
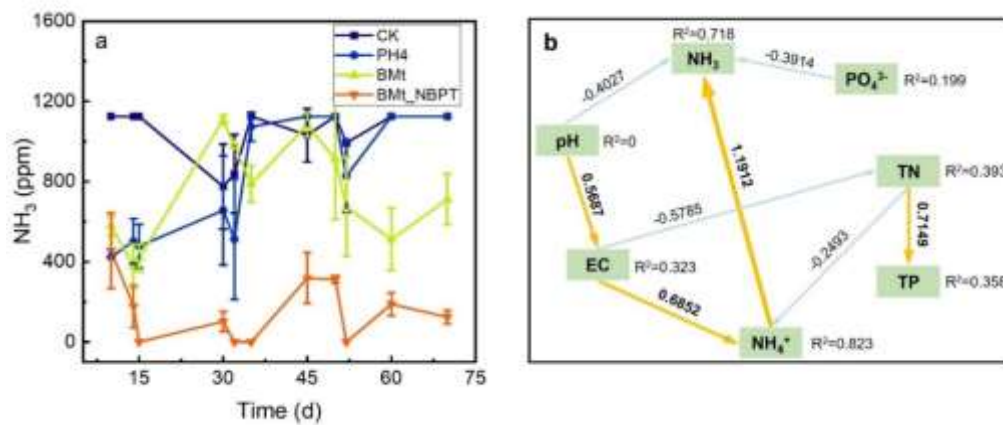
Figure 5.4 The emission of NH_3 in stored urine over time in different treatment groups (a); Partial least squares path modelling showing the direct and indirect effects of various factors on the ammonia emissions during the urine storage period (b).

The effects of pH, EC, TN, NH_4^+, TP, and PO_4^{3-} on ammonia volatilization during urine storage were evaluated using a partial least squares path modelling approach (Fig. 5.4b). In general, pH is positively correlated with EC, ammonium ion is positively correlated with EC, and ammonia gas is positively correlated with ammonium ion. It can be seen that these parameters are the key factors driving volatilization (Fig. 5.4b). Phosphoric acid is negatively correlated with ammonia volatilization, and total nitrogen is negatively correlated with ammonium ions. These observations indicate that the change of physical and chemical properties, especially pH, plays a more important and direct role in the improvement of ammonia volatilization. There is a positive correlation between total nitrogen and total phosphorus, which may be the reason why nitrogen and phosphorus co-produce struvite in proportion during urine storage (Krishnamoorthy, et al., 2020).

Table 5.1 summarizes the effects of different treatment methods on urea hydrolysis inhibition. It can be seen that acidification treatments can effectively inhibit urea hydrolysis and reduce ammonia volatilization under long-term storage conditions; however, the amount of acid

required to achieve this is often large, which may lead to higher final costs. Other treatment methods have also shown good results (viz., FeCl$_3$, sugar beet molasses, biochar, NBPT). A variety of exogenous substances have been developed and applied to minimize ammonia volatilization thereby realizing the recycling potential of nutrients in urine.

The BMt_NBPT treatment method adopted in this study proved to be more effective than a traditional acidification approach and was found to be easy to implement. The purpose of this study is to develop methods or guidelines, for minimizing nitrogen losses from source-separated urine to ensure that its resource potential is optimized. This technology offers a relatively simple and cost-effective method for harnessing the fertilizer potential of toilet resources in rural areas. The addition of biochar was shown to reduce the level of urea hydrolysis and adsorb the NH$_4^+$ and PO$_4^{3-}$ nutrient elements in urine. After recovery, the biochar can potentially be reused as fertilizer. Further, combined with a urease inhibitor, the biochar treatment proved to be even more beneficial having a more significant effect on nitrogen capture by adsorption and ammonia volatilization inhibition. In future studies, additional control experiments should be included in order to determine whether or not the effect observed for the BMt_NBPT treatment, could be attributed to NBPT alone, or whether it is a synergistic effect.

5.3.3 Microbiological analysis

5.3.3.1 Composition and relative abundance of microbial community

To better understand the impact of different treatments on urine-associated microbiota, bacterial community structure was carried out on the sediment samples collected at the end of the storage period. Fig. 5.5 shows the community structure and relative abundance, at the genus level, of the bacteria present within each treatment. Overall, a total of 15 genera with species richness >1.5% were differentiated. Significant differences in terms of microbial community composition and relative abundance of microorganisms in each treatment group were apparent.

The dominant genera associated with the control (CK) and acidified (pH4) treatments were similar, which were *Pseudomonas* (32.51%, 19.05%) and *Tissierella* (18.96%, 9.57%) belonging to Proteobacteria and Firmicutes, respectively. The addition of BMt to urine resulted in an increase in species richness and significant changes in the composition of the dominant

genera present. The BMt community is mainly composed of the following genera *Koukoulia* (24.34%), *Gallicola* (11.80%), *Pseudographilibacillus* (9.22%), unassigned OTU W5053

Table 5.1 Inhibition of urea hydrolysis by different methods reported in the literature.

Additives	Days	The initial pH	Type	Results	Reference
Acetic acid	84	5.5	Cattle slurry	73% reduction of NH_3	Kavanagh et al., 2019
Hydrochloric acid	2	5.3	Swine manure	Ammonia volatilization was inhibited.	Panetta et al., 2005
Sulfuric acid	47	5.5	Cattle faeces	62% reduction of NH_3	Sommer et al., 2017
Sulfuric acid	>100	<5	Human urine	Urea hydrolysis was inhibited.	Hellström et al., 1999
$FeCl_3$	117	ND		20%-68% reduction of NH_3	Kavanagh et al., 2021
5% sugar beet molasses	70	ND		67% reduction of NH_3	
7% apple pulp	70	ND		49% reduction of NH_3	
7% grass silage	70	ND		38% reduction of NH_3	
A wood based low-temperature biochar	ND	ND	ruminant urine	45% reduction of NH_3	Taghizadeh-Toosi et al., 2012
urease inhibitor	ND	ND	urea	50% reduction of NH_3	Wang et al., 2020
NBPT	ND	ND	urine	62.5% reduction of NH_3 peak emissions	Singh et al., 2013
NBPT	ND	ND	urea	Ammonia emissions were reduced with increasing NBPT concentrations.	Mira et al., 2017
sauerkraut juice and sugar beet molasses	36	3.8-4.7 (after storage)	Human urine	The ammonium content decreased by 22-30%.	Andreev et al., 2017
BMt_NBPT	66		Human urine	89.7% reduction of NH_3	This study

Note: ND - not determined.

(8.34%), *Enteractinococcus* (8.17%) and *Tissierella* (5.25%) representatives. The dominant genera of the BMt_NBPT treatment were similar to BMt, but with varying relative abundances being evident. For example, the abundance of *Gallicola* and *Koukoulia* decreased to 7.06% and 8.30% respectively. BMt_NBPT also had increased *Pseudochrobactrum* (4.80%), unassigned OTU_ MBA03 (3.59%), and *Brevundimonas* (3.94%) over BMt.
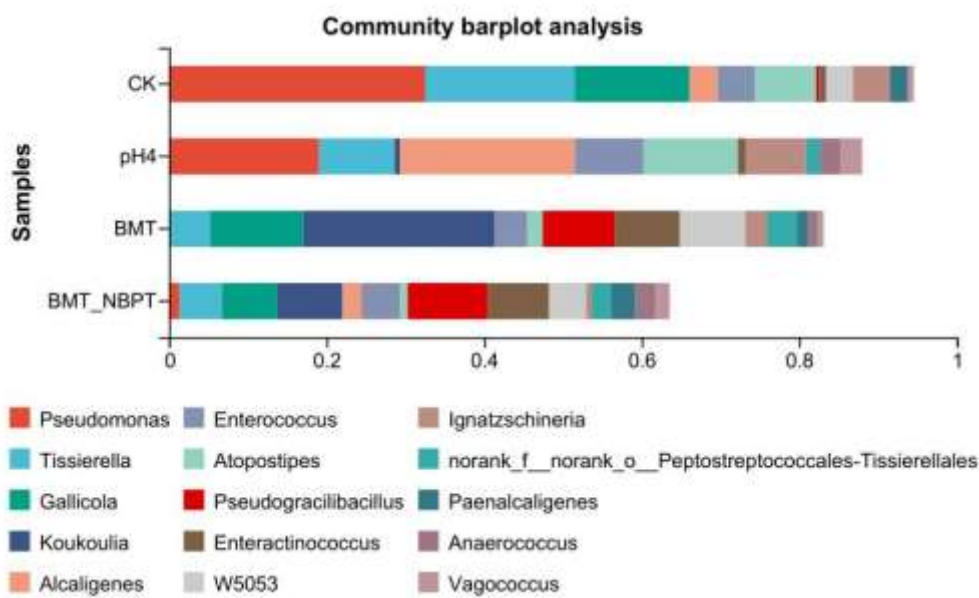
Figure 5.5 Composition and relative abundance of bacterial taxa at the genus level with different treatments used to inhibit urea hydrolysis in urine.

Gallicola is an anaerobic bacterium that can grow under the conditions of uric acid, organic acid, ammonia, and carbon dioxide (Ziganshina et al., 2017; Cyab et al., 2022). Members of the genus *Pseudomonas* contain a gene encoding urease, which is very important for the hydrolysis of urea (Zhu et al., 2019). *Pseudomonas aeruginosa*, a common pathogen associated with urinary tract infections, promotes urea hydrolysis via urease secretion, thereby providing a nitrogen source for biological growth (Bai et al., 2015). *Tissierella* species are strict anaerobes and include members that can use creatinine as a carbon and energy source converting to acetate with an accompanying release of ammonia and carbon dioxide (Harms et al., 1998; Barbosa et al., 2017). Representatives of the *Alcaligenes* genus were present in the highest relative abundance (22.18) in the pH4 acidification treatment at the end of the 70-day storage period (Wang et al., 2021). *Alcaligenes faecalis*, a member of the genus Alcaligenes, is also a pathogen causing human infection (Huang et al., 2020). By the end of the storage period, the conditions have reverted to urea degradation and increase in pH – the microbiota reflects those organisms

that survived the acidification steps and then proceeded to degrade urea and other organic compounds present. Acidification may have been selected for/or given a selective advantage to those microorganisms that can survive or tolerate lowered pH values.

5.3.3.2 Evolution of microbial community

Based on the results of difference analysis between treatment groups, changes in community structure can be seen more intuitively with predominant genera for each treatment being discerned (Fig. 5.6). The relative abundance of each genus present varied depending on the treatment groups. The genera with the highest relative abundance in CK, pH4, BMt, and BMt_NBPT were *Pseudomonas*, *Alcaligenes*, *Koukoulia,* and *Pseudographilibacillus*, respectively.

Figure 5.6 Statistical comparison of the relative abundance of differences between groups. Note: The Y axis represents the OUT designations at the genus level, the X axis represents the average relative

abundance in different groups of genera, and the columns with different colours represent different treatment groups. On the far right is the P value, * 0.01, P ≤ 0.05, ** 0.001, P ≤ 0.01, *** P ≤ 0.001.

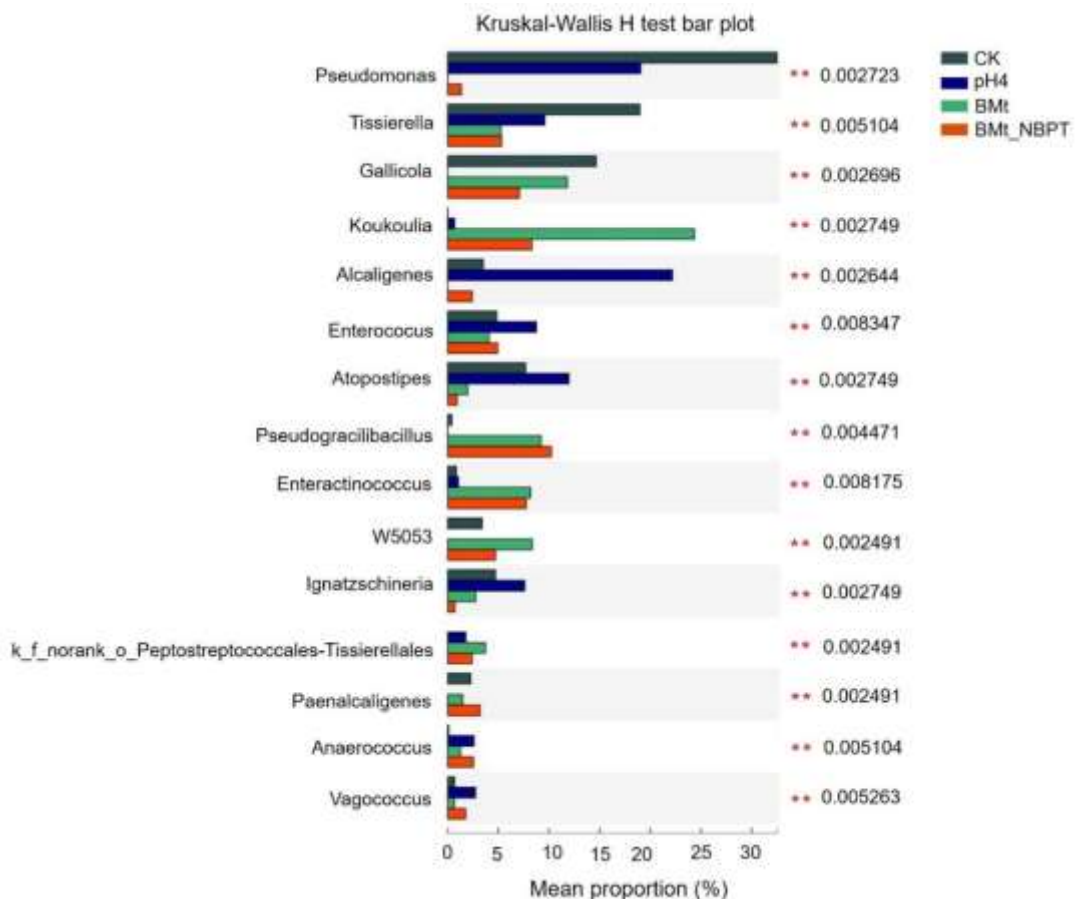All of the taxa representatives in the 'CK' control were also detected in the other treatments at varying levels, with the exception of OTU W5053 and *Paenalcaligenes*, which were absent from the 'pH4' treatment, suggesting their sensitivity to the acidic conditions established therein at the beginning of the treatment. A norank-o-Peptostreptococccales-Tissierellales OTU was detected in the 'pH4', BMt, and BMt_NBPT treatment groups but not in the 'CK' control treatment. Since this taxon is phylogenetically very similar to *Tissierella* (Fig. 5.8), it is possible that it was present at levels that were below the detection threshold or it was competitively excluded due to PCR amplification bias of *Tissierella* sequences.

To further investigate differences in microbial flora associated with each urine treatment, α Diversity-indices were compared (Table 5.2). Alpha diversity indexes are composite indexes that reflect abundance and consistency within a microbial community. The Sobs, Ace, and Chao1 indices all reflect OTU abundance within a sample and indicate species richness. The Shannon and Simpson indices both indicate OTU diversity. Ace and Shannon indexes of BMt/BMt_NBPT treatment group were significantly higher than 'CK', indicating that these treatments increased the richness and diversity of microorganisms, possibly because the pore structure of biochar provided a suitable growth place for microorganisms. Further, inhibition of urease activity may have also selected for bacterial populations that are not reliant on this mechanism to secure nitrogen for growth; thereby increasing species richness and diversity levels.

Table 5.2 α-diversity indices of the bacterial communities in different treatment groups. Values are means of four replicates.

Treatment	Sobs	Shannon	Simpson	Ace	Chao	Coverage
CK	83(2.45)	2.56(0.05)	0.15(0.02)	90.01(4.70)	88.38(5.17)	1.00
pH4	75.75(1.50)	2.77(0.05)	0.11(0.01)	86.15(5.06)	85.01(7.16)	1.00
BMt	146(0.82)	3.03(0.05）	0.10(0.01)	170.33(3.00)	175.04(3.94)	1.00
BMt_NBPT	227.25(4.86)	3.83(0.02）	0.04(0.00)	240.77(4.89)	241.94(1.97)	1.00

Note: The greater the Sobs, Chao, or Ace index value, the higher the expected species richness of the microbiota; the greater the Shannon index, the higher the diversity of the microbiota, whereas, the

smaller the Simpson index, the higher the diversity of the microbiota (Xu et al., 2018). The values shown in brackets represent - the standard deviation.

5.3.3.3 RDA and phylogenetic tree analysis

It is worth noting that physical and chemical parameters affect the succession of microbial communities (Mellendorf et al., 2010). RDA was used to evaluate the relationship between physical and chemical properties, bacterial communities, and samples at the genus level (Fig. 5.7). The interaction between bacterial community and environmental factors was found to be a key factor affecting urine transformation. pH, EC, TN, NH_4^+–N, and NH_3 were significantly correlated with bacterial community composition and were selected in RDA.
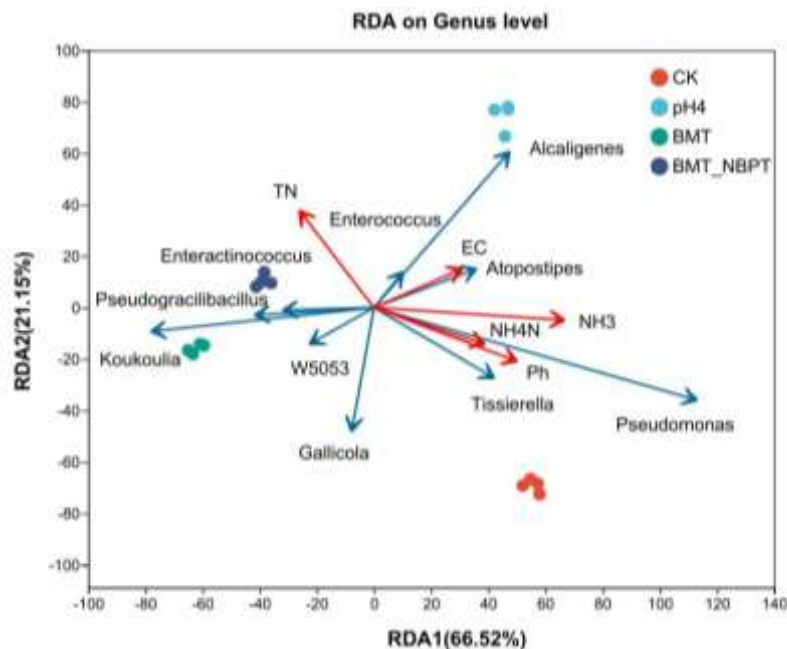
Figure 5.7 RDA analysis of the relationship between physicochemical parameters and bacterial community with different treatments used to inhibit urea hydrolysis in urine. The physicochemical parameters are depicted in arrows. pH, pH value; EC, electric conductivity; TN, total nitrogen; NH_4^+, ammonia nitrogen; NH_3, ammonia (a). Note: Dots with different colours or shapes in the figure represent sample groups under different environments or conditions; Species in RDA are represented by blue arrows; The red arrows represent quantitative environmental factors, and the length of the environmental factor arrow can represent the impact degree (interpretation quantity) of environmental factors on species data. The Angle between the arrows of environmental factors represents positive and negative correlations (acute Angle: positive correlation; Obtuse Angle: negative correlation; Right Angle: no correlation); From the sample point to the arrow of quantitative environmental factors, the distance of

the projection point from the origin represents the relative influence of environmental factors on the distribution of sample communities.

RDA showed that axis 1 and axis 2 explained 66.52% and 21.15% of the total variation in bacterial community structure, respectively. Except for TN, which was negatively correlated, there were positive correlations among the other environmental factors, EC, NH_3, pH, and NH_4^+–N. NH_3 and pH had the greatest effects on bacterial community structure along the first axis. *Pseudomonas* and *Tissierella* were positively correlated with NH_3 and negatively correlated with TN ratio, which was consistent with the above analysis results. The correlation between pH and NH_4^+–N showed that urea hydrolysis was affected by pH. With the increase of pH, NH_3 volatilized, resulting in the decrease of TN. The microbiota associated with the 'CK' control and 'pH4' treatment were distinct from the other treatments, whereas the BMt and BMt_NBPT treatments were closely aggregated indicating similarities in the response matrix. These results showed that the urine treatments and physio-chemical parameters had significant effects on microbial community structure.
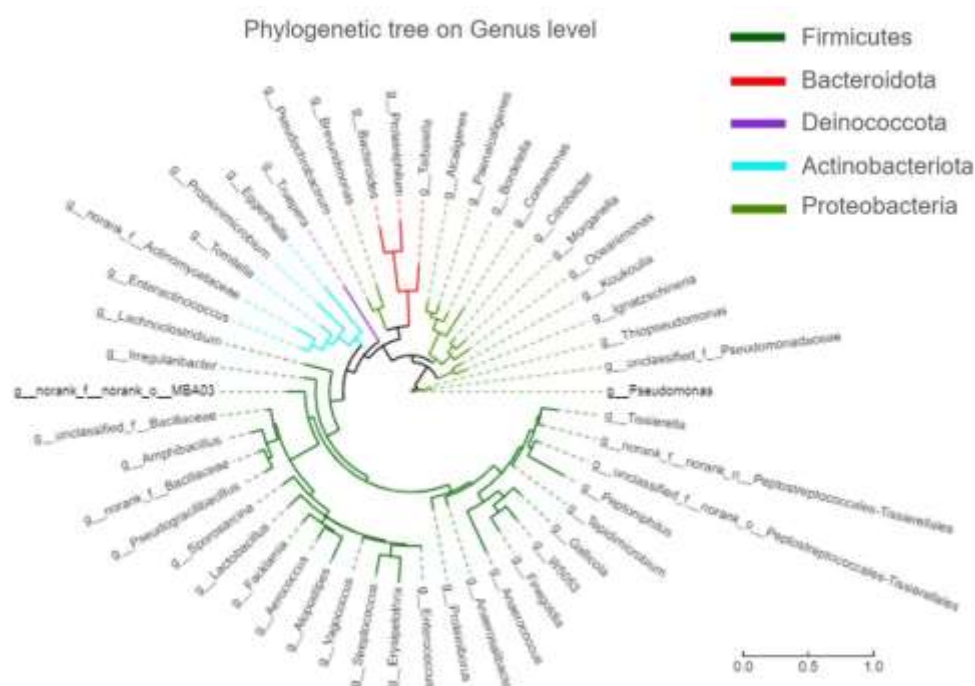
Figure 5.8 A phylogenetic tree showing the relationship between the sedimentary microbiota in the differences between groups. The phylogenetic tree was constructed based on the 16S rRNA sequences associated with the V3-V4 region using the Neighbour-Joining method with the maximum composite likelihood substitution model.

Fig. 5.8 shows the phylogenetic tree of relevant strains depicting their evolutionary relatedness. It can be seen that *Koukoulia* and *Ignatzschineria* have high homology. Although *Ignatzschineria* strains are routinely isolated in the intestines of diptera insects (Iancu et al., 2018), members of this genus are considered to be opportunistic human pathogens (Difranza et al., 2021). It was interesting to note that, at the end of the BMt_NBPT treatment, the abundance representatives of this genus decreased significantly compared to the 'CK' control, indicating that this treatment method could contribute towards decreasing the incidence of certain pathogens in urine thereby increasing the safety of urine use after long term storage.
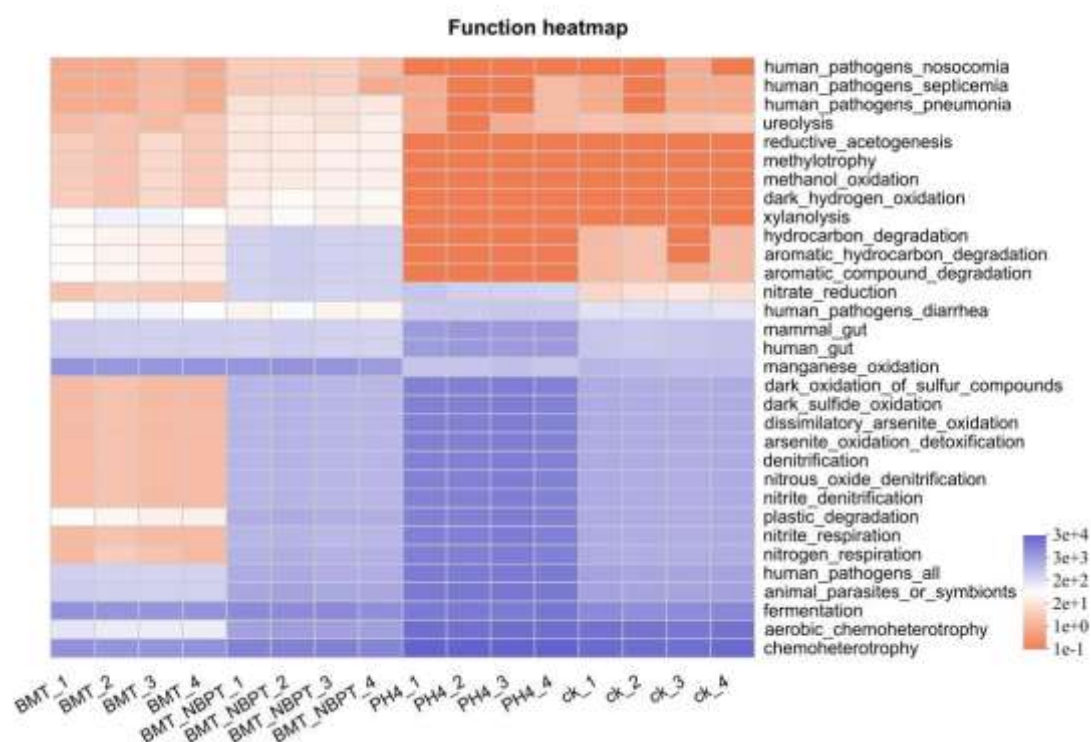
Figure 5.9 Function heatmap of the top 32 functional groups with the highest cumulative OTU relative sequence abundance in different samples based on analysis of FAPROTAX. Note: The abscissa is the name of the sample or group, and the ordinate is the name of the function. The colour gradient of the colour block is used to show the variation in the abundance of different functions in each sample. The value represented by the colour gradient is on the right of the figure.

The microbial transformation of urine requires multiple genes, which can be further studied through gene function assignment and annotation based on the FAPROTAX database. Fig. 5.9 shows the functional gene profile and relative abundance of bacterial communities associated with each treatment group evaluated. For each urine treatment, the functional attributes of the bacterial community changed. The sequence was divided into 32 functional groups. Among

them, the two functions of fermentation and chemoheterotrophy showed high abundance in all treatment groups, which is not unexpected. Chemoheterotrophy is prevalent under conditions where a source of organic carbon is available as an energy source and fermentation typically involves the anaerobic degradation of organic nutrients (Zhu et al., 2019; Smbr et al., 2020). In the BMt_NBPT group, the abundance of human pathogen diarrhoea-related sequences decreased, indicating the potential effectiveness of BMt_NBPT treatment in reducing pathogen loading.

5.4 Implication for P and N recovery from source-separated urine

Nutrients such as nitrogen and phosphorus are the main culprits of eutrophication in water bodies. If nitrogen and phosphorus in urine can be recycled, it will make a significant contribution to mitigating eutrophication. Nitrogen and phosphorus resources that can be effectively recovered, or recycled will also greatly reduce the loading of sewage treatment plants. Since urine contributes significant nutrients such as nitrogen and phosphorus to domestic sewage, it would be desirable and of great importance to treat and utilize urine directly. Studies have shown that the total pollutant discharge of the wastewater without faeces and urine after further treatment is significantly smaller than that of the traditional drainage mode (Zhang et al., 2008).

This study puts forward a method that can reduce nitrogen loss from urine by inhibiting urine hydrolysis, thereby preventing gaseous ammonia volatilization. Added to this partial ammonium nitrogen in urine can be fixed on the BMt adsorbent and recovered from urine. During the operation of the urine storage process, phosphorus mainly existed in the form of phosphate, and in the storage process, phosphorus mostly existed in the form of soluble, not easy to form struvite precipitation. BMt can adsorb phosphate, which can be collected and used as biochar-based nitrogen and phosphorus slow-release fertilizer (Jena et al., 2021). It not only offers a possible solution to the recycling problem of nitrogen and phosphorus resources but could also reduce eutrophication caused by sewage load.

After a prolonged storage period, it was found that the prevalence of taxonomic groups associated with pathogenic traits (viz., human pathogen diarrhoea) was reduced in the BMt_NBPT group, indicating that this treatment may not be conducive to the survival and

proliferation of pathogens associated with urine. This finding is significant in practical terms because processing stored urine and recovering urine-derived products involves staff contact. Future work should focus on a detailed economic and life-cycle assessment of the urine treatment sequence for maximum resource recovery (Chipako et al., 2020).

5.5 Conclusions

Urease inhibitor-mediated porous formed-biochar doped with metal oxide was found to reduce ammonia volatilization and promote effective preservation of N/P nutrients during source-separated urine storage. BMt_NBPT reduced ammonia emission by 89.7%, thereby improving the content of nutrient elements in urine, and was conducive to stabilizing the value of urea fertilizer under long-term storage conditions. However, compared with traditional acidification treatment, BMt_NBPT treatment needs further optimization to consider the effects of application amount, the adsorption capacity of biochar materials, and other factors on reducing nitrogen loss. Finally, BMt and NBPT addition to urine impacts the rate of urea hydrolysis in storage tanks and can be used to select urea or ammonia-nitrogen depending on the nutrient recovery technology available or the targeted nutrient product of interest. BMt treatment increased the richness and diversity of microorganisms, possibly due to the pore structure of biochar providing a suitable growth environment for microorganisms. Compared to the other treatments, the abundance of OTU sequences associated with human pathogen traits (viz., diarrhoea) decreased, indicating the potential of BMt_NBPT treatment in improving the safety of urine utilization.

References

Almeida J, Azevedo A L, Brett M, et al. (2019). Urine recovery at the building level. Building and Environment 156:110-116.

Andreev N, Ronteltap M, Boincean B, et al. (2017). Lactic acid fermentation of human urine to improve its fertilizing value and reduce odour emissions. Journal of Environmental Management 198: 63.

Badeti U, Jiang J X, Almuntashiri A, et al. (2022). Impact of source-separation of urine on treatment capacity, process design, and capital expenditure of a decentralised wastewater treatment plant. Chemosphere 300: 134489.

Bai S, Bharti P, Seasotiya L, et al. (2015). In vitro screening and evaluation of some Indian medicinal plants for their potential to inhibit Jack bean and bacterial ureases causing urinary infections. Pharmaceutical Biology 53: 326.

Barbosa S G, Peixoto L, Ter Heijne A, et al. (2017). Investigating bacterial community changes and organic substrate degradation in microbial fuel cells operating on real human urine. Environmental Science: Water Research & Technology 3: 897-904.

Behera B, Patra S, Balasubramanian P, (2020). Biological nutrient recovery from human urine by enriching mixed microalgal consortium for biodiesel production. Journal of Environmental Management 260: 110111.

Bonvin C, Etter B, Udert K M, et al. (2015). Plant uptake of phosphorus and nitrogen recycled from synthetic source-separated urine. Ambio 44: 217-227.

Cai Y, Qi H, Liu Y J, et al. (2016). Sorption/desorption behaviour and mechanism of NH_4^+ by biochar as a nitrogen fertilizer sustained-release material. Journal of Agricultural & Food Chemistry 64: 4958-4964.

Cao Y, Gu J Y, Zhang J, et al. (2022). Reduced pH is the primary factor promoting humic acid formation during hyperthermophilic pre-treatment composting. Journal of Environmental Management 316: 115215.

Cao Y, Wang J D, Huang H Y, et al. (2019). Spectroscopic evidence for hyperthermophilic pre-treatment intensifying humification during pig manure and rice straw composting. Bioresource Technology 294: 122131.

Charteris A F, Marsden K A, Evans J R, et al. (2021). Optimising storage conditions and processing of sheep urine for nitrogen cycle and gaseous emission measurements from urine patches. Scientific Reports 11: 12116.

Chipako T L, Randall D G, (2020). Urine treatment technologies and the importance of pH. Journal of Environmental Chemical Engineering 8: 103622.

Courtney C, Randall D G, (2021). Concentrating stabilized urine with reverse osmosis: how does stabilization method and pre-treatment affect nutrient recovery, flux, and scaling?. Water Research 209: 117970.

Cyab C, Mla B, Bz C, et al. (2022). Hydrothermal pre-treatment contributes to accelerate maturity during the composting of lignocellulosic solid wastes. Bioresource Technology 346: 126587.

De Boer M A, Hammerton M, Slootweg J C, (2018). Uptake of pharmaceuticals by sorbent-amended struvite fertilisers recovered from human urine and their bioaccumulation in tomato fruit. Water Research 133: 19.

Difranza L T, Annavajhala M K, Uhlemann A C, et al. (2021). Closing the brief case: A maggot mystery— ignatzschineria larvae sepsis secondary to an infested wound. Journal of Clinical Microbiology 59.

Etter B, Tilley E, Khadka R, et al. (2011) Low-cost struvite production using source-separated urine in Nepal. Water Research, 45: 852.

Gai X P, Wang H Y, Jian L, et al. (2014). Effects of feedstock and pyrolysis temperature on biochar adsorption of ammonium and nitrate. Plos One 9: e113888.

Guadie A, Belay A, Liu W Z, et al. (2020). Rift valley lake as a potential magnesium source to recover phosphorus from urine. Environmental Research 184: 109363.

Grases F, Söhnel O, Vilacampa A I, et al. (1996). Phosphates precipitating from artificial urine and fine structure of phosphate renal calculi. Clinica chimica acta 244: 45.

Harms C, Schleicher A, Collins M D, et al. (1998). Tissierella creatinophila sp. nov., a Gram-positive, anaerobic, non-spore-forming, creatinine-fermenting organism. International Journal of Systematic Bacteriology 48: 983.

He T h, Liu D Y, Yuan J J, et al. (2018). A two years study on the combined effects of biochar and inhibitors on ammonia volatilization in an intensively managed rice field. Agriculture Ecosystems & Environment 264: 44.

Heinonen-Tanski H, Sjöblom A, Fabritius H, et al. (2007). Pure human urine is a good fertiliser for cucumbers. Bioresource Technology 98: 214.

Hellström D, Johansson E, Grennberg K. (1999). Storage of human urine: acidification as a method to inhibit decomposition of urea. Ecological Engineering 12: 253.

Hu M, Fan B, Wang H L, et al. (2016). Constructing the ecological sanitation: a review on technology and methods. Journal of Cleaner Production 125: 1.

Huang C. (2020). Extensively drug-resistant *Alcaligenes faecalis* infection. BMC Infectious Diseases 20: 833.

Huang Y, Li D Y, Wang L, et al. (2019). Decreased enzyme activities, ammonification rate and ammonifiers contribute to higher nitrogen retention in hyperthermophilic pre-treatment composting. Bioresource Technology 272: 521.

Höglund C, Stenström T A, Jönsson H, et al. (1998). Evaluation of faecal contamination and microbial die-off in urine separating sewage systems. Water Science and Technology 38: 17.

Iancu L, Junkins E N, Purcarea C, (2018). Characterization and microbial analysis of first recorded observation of *Conicera similis* Haliday (Diptera: Phoridae) in forensic decomposition study in Romania. Journal of Forensic and Legal Medicine 58: 50.

Jena J, Das T, Sarkar U. (2021). Explicating proficiency of waste biomass-derived biochar for reclaiming phosphate from source-separated urine and its application as a phosphate biofertilizer. Journal of Environmental Chemical Engineering 9: 104648.

Jiang Y H, Li A Y, Deng H, et al. (2019). Characteristics of nitrogen and phosphorus adsorption by Mg-loaded biochar from different feedstocks. Bioresource Technology 276: 183.

Kai M U, Larsen T A, Biebow M, et al. (2003). Urea hydrolysis and precipitation dynamics in a urine-collecting system. Water Research 37: 2571.

Kai M U, Larsen T A, Gujer W. (2003). Estimating the precipitation potential in urine-collecting systems. Water Research 37: 2667.

Kannan M B, Ronan K. (2017). Conversion of biowastes to biomaterial: An innovative waste management approach. Waste Management 67: 67.

Karak T, Bhattacharyya P. (2011). Human urine as a source of alternative natural fertilizer in agriculture: A flight of fancy or an achievable reality. Resources Conservation & Recycling 55: 400.

Kavanagh I, Burchill W, Healy M G, et al. (2019). Mitigation of ammonia and greenhouse gas emissions from stored cattle slurry using acidifiers and chemical amendments. Journal of Cleaner Production 237: 117822.

Kavanagh I, Fenton O, Healy M G, et al. (2021). Mitigating ammonia and greenhouse gas emissions from stored cattle slurry using agricultural waste, commercially available products and a chemical acidifier. Journal of Cleaner Production 294: 126251.

Kawakami E M, Oosterhuis D M, Snider J L, et al. (2012). Physiological and yield responses of field-grown cotton to application of urea with the urease inhibitor NBPT and the nitrification inhibitor DCD. European Journal of Agronomy 43:147.

Krishnamoorthy N, Dey B, Arunachalam T, et al. (2020). Effect of storage on physicochemical characteristics of urine for phosphate and ammonium recovery as struvite. International Biodeterioration & Biodegradation 153: 105053.

Lelieveld J, Evans J, Fnais M et al. (2015). The contribution of outdoor air pollution sources to premature mortality on a global scale. Nature 525: 367.

Liang B, Lehmann J, Solomon D, et al. (2006). Black carbon increases cation exchange capacity in soils. Soil Science Society of America Journal 70: 1719.

Li Y X, Hao W J, Peng S J, et al. (2022). Composition and potential functions of bacterial communities associated with aurelia polyps. Frontiers in Marine Science.

Liu B X, Giannis A, Zhang J F, et al. (2013). Characterization of induced struvite formation from source-separated urine using seawater and brine as magnesium sources. Chemosphere 93: 2738.

Liu H B, Shan J H, Chen Z B, et al. (2021). Efficient recovery of phosphate from simulated urine by Mg/Fe bimetallic oxide modified biochar as a potential resource. Science of the Total Environment 784: 147546.

Liu Y L, He P J, Shao L M, et al. (2017). Significant enhancement by biochar of caproate production via chain elongation. Water Research 119: 150.

Masrura S U, Dissanayake P, Sun Y Q, et al. (2020). Sustainable use of biochar for resource recovery and pharmaceutical removal from human urine: A critical review. Critical Reviews in Environmental Science and Technology 51: 3016.

Maurer M, Pronk W, Larsen T A, (2006). Treatment processes for source-separated urine. Water Research 40: 3151.

Mellendorf M, Huber-Humer M, Gamperling O, et al. (2010). Characterisation of microbial communities in relation to physical–chemical parameters during in situ aeration of waste material. Waste Management 30: 2177.

Mira A B, Cantarella H, Souza-Netto G, et al. (2017). Optimizing urease inhibitor usage to reduce ammonia emission following urea application over crop residues. Agriculture, Ecosystems & Environment 248: 105.

Otieno A O, Home P G, Raude J M, et al. (2021). Pineapple peel biochar and lateritic soil as adsorbents for recovery of ammonium nitrogen from human urine. Journal of Environmental Management 293: 112794.

Paepe J D, Paepe K D, Gòdia F, et al. (2020). Bio-electrochemical COD removal for energy-efficient, maximum and robust nitrogen recovery from urine through membrane aerated nitrification. Water Research 185: 116223.

Panetta D M, Powers W J, Lorimor J C. (2005). Management strategy impacts on ammonia volatilization from swine manure. Journal of Environmental Quality 34: 1119.

Pathy A, Ray J, Paramasivan B, (2021). Challenges and opportunities of nutrient recovery from human urine using biochar for fertilizer applications. Journal of Cleaner Production 304: 127019.

Pereira J, Barneze A S, Misselbrook T H, et al. (2013). Effects of a urease inhibitor and aluminium chloride alone or combined with a nitrification inhibitor on gaseous N emissions following soil application of cattle urine. Biosystems Engineering 115: 396.

Pradhan S K, Holopainen J K, Heinonen-Tanski H, (2009). Stored human urine supplemented with wood ash as fertilizer in tomato (Solanum lycopersicum) cultivation and its impacts on fruit yield and quality. Journal of Agricultural and Food Chemistry 57: 7612.

Ray H, Saetta D, Boyer T H. (2018). Characterization of urea hydrolysis in fresh human urine and inhibition by chemical addition. Environmental Science: Water Research & Technology 4: 87.

Saetta D, Boyer T H, (2017). Mimicking and inhibiting urea hydrolysis in non-water urinals. Environmental Science and Technology 51: 13850.

Saetta D, Padda A, Li X, et al. (2019). Real-time monitoring and control of urea hydrolysis in cyber-enabled non-water urinal system. Environmental Science and Technology 53: 3187.

Saetta D, Zheng C, Leyva C, et al. (2020). Impact of acetic acid addition on nitrogen speciation and bacterial communities during urine collection and storage. Science of the Total Environment 745: 141010.

Schönning C, Leeming R, Stenström T A, (2002). Faecal contamination of source-separated human urine based on the content of faecal sterols. Water Research 36: 1965.

Shakoor M B, Ye Z L, Chen S H, (2021). Engineered biochars for recovering phosphate and ammonium from wastewater: A review. Science of the Total Environment 779:146240.

Silva A G B, Sequeira C H, Sermarini R A, et al. (2017). Urease inhibitor NBPT on ammonia volatilization and crop productivity: A meta-analysis. Agronomy Journal 109: 1.

Simha P, Senecal J, Nordin A, et al. (2018). Alkaline dehydration of anion–exchanged human urine: Volume reduction, nutrient recovery and process optimisation. Water Research 142: 325.

Singh J, Kunhikrishnan A, Bolan N S, et al. (2013). Impact of urease inhibitor on ammonia and nitrous oxide emissions from temperate pasture soil cores receiving urea fertilizer and cattle urine. Science of the Total Environment 465: 56.

Smbr A, Lwm B, Lmdso A, et al. (2020). Nodule microbiome from cowpea and lima bean grown in composted tannery sludge-treated soil. Applied Soil Ecology 151: 103542.

Snoeyink V, Jenkins D. Water Chemistry. John Wiley, New York, 1980.

Sommer S G, Clough T J, Balaine N, et al. (2017). Transformation of organic matter and the emissions of methane and ammonia during storage of liquid manure as affected by acidification. Journal of Environmental Quality 46: 514.

Sun, E H, Zhang, Y, Xiao, Q B, et al. (2022). Formable porous biochar loaded with La-Fe(hydr)oxides/montmorillonite for efficient removal of phosphorus in wastewater: process and mechanisms. Biochar 4: 53.

Taghizadeh-Toosi A, Clough T J, Sherlock R R, et al. (2012). A wood based low-temperature biochar captures NH3-N generated from ruminant urine-N, retaining its bioavailability. Plant and Soil 353: 73.

Takaya C A, Fletcher L A, Singh S, et al. (2016). Phosphate and ammonium sorption capacity of biochar and hydrochar from different wastes. Chemosphere 145: 518.

Tarpeh W A, Barazesh J M, Nelson K L, (2018). Electrochemical stripping to recover nitrogen from source-separated urine. Environmental Science and Technology 52: 1453.

Tarpeh W A, Udert K M, Nelson K L, (2017). Comparing ion exchange adsorbents for nitrogen recovery from source-separated urine. Environmental Science and Technology 51: 2373.

Tian S Y, Kuai X Y, Huang T, et al. (2021). The property of urine in collection and storage process for resource utilization of urine. Environmental Engineering 39: 66.

Van Damme M, Clarisse L, Whitburn S, et al. (2018). Industrial and agricultural ammonia point sources exposed. Nature 564: 99.

Vikrant K, Kim K H, Ok Y S, et al. (2018). Engineered/designer biochar for the removal of phosphate in water and wastewater. Science of the Total Environment 616: 1242.

Wald C. (2022). The urine revolution: how recycling pee could help to save the world. Nature 602: 202.

Wang B, Lehmann J, Hanley K, et al. (2015). Adsorption and desorption of ammonium by maple wood biochar as a function of oxidation and pH. Chemosphere 138: 120.

Wang H, Kbke S, Dittert K. (2020). Use of urease and nitrification inhibitors to reduce gaseous nitrogen emissions from fertilizers containing ammonium nitrate and urea. Global Ecology and Conservation 22: 00933.

Wang Y R, Hosomi K, Shimoyama A, et al. (2021). Lipopolysaccharide derived from the lymphoid-resident commensal bacteria *Alcaligenes faecalis* functions as an effective nasal adjuvant to augment IgA Antibody and Th17 cell responses. Frontiers in Immunology 12: 699349.

Wei S P, Van Rossum F, Jan V D P G, et al. (2018). Recovery of phosphorus and nitrogen from human urine by struvite precipitation, air stripping and acid scrubbing: A pilot study. Chemosphere 12: 1030.

Wu D, Xia T x, Zhang Y X, et al. (2021). Identifying driving factors of humic acid formation during rice straw composting based on Fenton pre-treatment with bacterial inoculation. Bioresource Technology 337: 125403.

Xu J, Liu S J, Song S R, et al. (2018). Arbuscular mycorrhizal fungi influence decomposition and the associated soil microbial community under different soil phosphorus availability. Soil Biology and Biochemistry 120: 181.

Xu K N, Li J Y, Zheng M, et al. (2015). The precipitation of magnesium potassium phosphate hexahydrate for P and K recovery from synthetic urine. Water Research 80: 71.

Xu K N, Lin F Y, Dou X M, et al. (2018). Recovery of ammonium and phosphate from urine as value-added fertilizer using wood waste biochar loaded with magnesium oxides. Journal of Cleaner Production 187: 205.

Xu K N, Zhang C K, Dou X M, et al. (2017). Optimizing the modification of wood waste biochar via metal oxides to remove and recover phosphate from human urine. Environmental Geochemistry and Health 41: 1767.

Xu W, Zheng J, Chu J, et al. (2021). New method for using N-(N-butyl)-thiophosphoric triamide to improve the effect of microbial induced carbonate precipitation. Construction and Building Materials 313: 125490.

Yao Y, Gao B, Inyang M, et al. (2011). Removal of phosphate from aqueous solution by biochar derived from anaerobically digested sugar beet tailings. Journal of Hazardous Materials 190: 501.

Yu C Y, (2022). Recovery of NH_4^+–N and PO_4^{3-}–P from urine using sludge-derived biochar as a fertilizer: performance and mechanism. RSC Advances 12: 4224.

Zaman M, Saggar S, Blennerhassett J D, et al. (2009). Effect of urease and nitrification inhibitors on N transformation, gaseous emissions of ammonia and nitrous oxide, pasture yield and N uptake in grazed pasture system. Soil Biology and Biochemistry 41: 1270.

Zhang J, Gao S B, Zhang J, et al. (2008). Concept and application demonstration for ecological sanitation. China Water and Wastewater 24: 10.

Zhu G R, Liu G H, Liu D L, et al. (2019). Research on the hydrolysis of human urine using biological activated carbon and its application in bioregenerative life support system. Acta Astronautica 155: 191.

Zhu L J, Wei Z M, Yang T X, et al. (2019). Core microorganisms promote the transformation of DOM fractions with different molecular weights to improve the stability during composting. Bioresource Technology 299: 122575.

Ziganshina E E, Ibragimov E M, Vankov P Y, et al. (2017). Comparison of anaerobic digestion strategies of nitrogen-rich substrates: Performance of anaerobic reactors and microbial community diversity. Waste Management 59: 160.

CHAPTER *6*

CONCLUSIONS AND RECOMMENDATIONS

FOR FURTHER RESEARCH

CHAPTER 6. CONCLUSIONS AND RECOMMENDATIONS FOR FURTHER RESEARCH

6.1 Introduction

6.1.1 Brief description

Phosphorus (P) and nitrogen (N) pollution levels are a major global challenge, resulting in an urgent need for N and P emission reduction and remediation (Krishnamoorthy et al., 2022). High concentrations of N and P nutrient salts flow into farmland ditches via rainwater run-off, migrating into downstream waterbodies and driving eutrophication in aquatic environments (Liu et al., 2018, Ngatia et al., 2017). Going further, eutrophication will cause water quality deterioration, water shortage and ecological environment destruction. Determining how to effectively control water environmental pollution has become one of the most important research topics faced by scholars all over the world. Therefore, methods are required to remove N and P during the treatment of wastewater to reduce their impact on receiving water bodies. Further, methods that support the sustainable recovery and reuse of these nutrients have the potential to be used for agricultural fertilizer applications (De-Bashan et al., 2004; Gilbert 2009; Nancharaiah et al., 2016).

Biochar has been shown to address multiple Sustainable Development Goal challenges through its carbon storage capacity and pollution remediation properties (He et al., 2021; He et al., 2022). Due to its poor adsorption capacity for phosphorus and nitrogen, its practical application scope is limited (Cheng et al., 2021; Yang et al., 2021). The functional modification of biochar can greatly improve its adsorption and retention ability. According to bibliometric analysis data, it can be seen that the application of modified biochar in advanced wastewater treatment (nitrogen and phosphorus pollutants) has attracted more and more attention in recent years (Chen et al., 2019). The modification technologies used include physical (steam and gas activation), chemical (acid, alkali, oxide, metal Fe, Ma, La, Al, Zn, Ca, and other salts), biological modification (loaded with microorganisms), ball milling modification, catalytic modification, magnetic modification, and mineral modification (Cheng et Al., 2021; Jiao et al., 2021; Kumar et al., 2020; Yang et al., 2021; Zhang et al., 2022).

Unfortunately, there are relatively few reports on the functional design of formable biochar. The related modified biochar reported in most studies usually exists in the form of powder. Although it has a good removal effect and adsorption characteristics (Zhang et al., 2020), it is difficult to carry out the practical regeneration process. To effectively solve the phosphorus crisis, China and international scientific research institutions have developed numerous phosphorus recovery processes and achieved good phosphorus recovery results (Fang et al., 2018). However, large-scale recycling application is still a technological process bottleneck hindering sustainable development. Therefore, the study of formable biochar has important engineering application significance.

6.1.2 Summary of research objectives

In this study, a novel method was developed for the preparation of porous straw biochar with formable lanthanum iron bimetallic oxide/montmorillonite loading, for the efficient adsorption of wastewater pollutants (N and P). This work provides a new approach for the application of this novel biochar in phosphorus and nitrogen removal from wastewater, which is of great significance for practical engineering applications. The formable material's selective adsorption of N and P is an effective strategy for reducing the challenge posed by fertilizer pollution and run-off water management. The major aims of this study were to 1) develop and characterize a novel formable porous granulated biochar suited to phosphorous removal from wastewater; 2) explore the synergistic phosphorus removal effect of microorganisms immobilized on the novel biochar; and, 3) evaluate the ability of this novel biochar to treat actual high nitrogen and phosphorus concentration wastewater and determine the impact on associated microbiota.

6.2 Major findings in summary

6.2.1 Practical application of functionalized adsorbent based on formable porous granulated biochar formulated for phosphorus removal from wastewater

Phosphorus emission reduction and resource utilization are of great significance. Functional modification of biochar can greatly improve its adsorption and fixation capacity. However, large-scale recycling is still a technical bottleneck hindering sustainable development, and

reports on biochar functional moulding design are still very rare. In this study, a new method for the preparation of porous straw biochar (LaFe/MB) with formable lanthanum iron bimetallic oxide/montmorillonite loading was developed, which is suitable for the efficient adsorption of phosphorus from industrial wastewater. The major findings were:

✪ A new formable porous particle biochar adsorbent (LaFe/MB) with high efficiency for P removal from wastewater was prepared by in-situ impregnation and granulation of lanthanum/ferric oxide (hydroxide) on the surface of biochar/nano-montmorillonite. The surface-loaded lanthanum iron bimetallic oxide provides abundant adsorption sites for porous biochar, and almost no lanthanum and iron leaching are found in the adsorbent.

✪ LaFe/MB has a high adsorption capacity (52.12 mg P/g), and the adsorption efficiency is maintained at 76.7% after four sorption-desorption processes, the adsorption of phosphorus by LaFe/MB is a spontaneous endothermic process.

✪ The porous structure of the biochar material is beneficial to the impregnation of bimetallic iron lanthanide (hydroxide) and improves the adsorbent solid strength and stability.

✪ Under actual wastewater operation conditions, LaFe/MB demonstrated excellent hydraulic endurance strength (up to 91.6%) and compressive resistance increased by 1.66 times, showing good engineering application potential.

✪ LaFe/MB not only effectively enhances the relief of P eutrophication, but also realizes the efficient immobilization recovery of P resources. In terms of a possible shortage of phosphate ore, immobilizing by the formable porous granulated biochar from the wastewater systems can be a promising way to supply secondary sourced phosphorus to the market and thereby promote the blue economy. This work provides a new design for LaFe/MB regeneration and phosphorus recovery and a new strategy for effectively alleviating water eutrophication and realizing phosphorus resource recycling.

6.2.2 Effect of phosphorus accumulating bacteria on the synergistic phosphate removal by formed-biochar supported metal oxide nanoparticles

Formed-biochar-supported metal oxide nanoparticles (FBO) were used as carriers for microbial attachment to study the immobilization and attachment effects of phosphorus-accumulating bacteria (PAB) under different conditions. The synergistic phosphorus removal effect and mechanism of the composite (Bio-FBO) were investigated. The major findings were:

✪ Abundant oxygen-containing functional groups on the surface of FBO are conducive to the attachment of microorganisms.

✪ PAB can be well fixed on the internal and external surfaces of large particle biochar by physical adsorption.

✪ Phosphorus-accumulating bacteria are capable of forming biofilms on biochar in a short time under the condition of a low dilution ratio, and a P removal efficiency of up to 100% could be achieved at a concentration of 10 mg P/L.

✪ The excellent porosity, active groups, and microbial attachment of Bio-FBO biosorbent make it a promising candidate for phosphorus removal, especially in the treatment of phosphorus-rich wastewater.

6.2.3 Effect of urease inhibitor-mediated porous formed-biochar on nitrogen and phosphorus form transformation in source-separated urine under long-term storage conditions

Urine is a nutrient resource with high N and P content (Ajiboye et al., 2022). During storage, nitrogen can be lost from urine through ammonification and gaseous ammonia volatilization (Dilshani et al., 2022). If untreated, or not recovered, N and P from urine serve as pollutants that can cause eutrophication (Zhang et al., 2023). A urease inhibitor combined with formed-biochar (BMt_NBPT) can inhibit the transformation of nitrogen into an unstable form in urine and was found to have good adsorption capacity for nitrogen and phosphorus. Some major findings were:

✪ Urease inhibitor-mediated porous formed-biochar doped with metal oxide reduced ammonia volatilization, and promoted the retention of N/P nutrients during source-separated urine storage. In terms of treatments evaluated, the introduction of a urease inhibitor demonstrated the greatest influence on inhibiting ammonia volatilization.

✪ BMt_NBPT treatment was found to promote greater levels of microbial diversity within stored urine compared to untreated control. A consequence of this is that the incidence of bacteria with associated pathogenic traits was reduced during the urine storage process. Urease inhibitor-mediated porous formed-biochar doped with metal oxide, which was introduced to urine storage technology has the potential to replace the traditional acidification treatment and provides theoretical and technical support for the effective utilization of urine source separation.

✪ On the whole, recovery of nutrients from source-isolated urine is of great significance for establishing a sustainable and closed nutrient loop.

6.3 General conclusions

In this study, metal oxide amended formable biochar adsorbent for phosphorus removal from wastewater was prepared by in situ impregnation and granulation. Montmorillonite was used as a binder in the process, which increased the size of the granular biochar. Iron effectively enhanced the surface charge and promoted the uniform dispersion of lanthanum, which was the key to the selective removal of phosphate. Here, the surface-loaded lanthanum iron bimetallic oxide provides abundant adsorption sites for granular biochar, and almost no lanthanum or iron leaching was found from the adsorbent. The novel biochar demonstrated rapid phosphorus adsorption kinetics and a high adsorption capacity that was superior to similar biochar-based adsorbents. Moreover, it showed a superior adsorption capacity and hydraulic compressive strength in actual wastewater. After the four cycles of the adsorption-desorption process, the novel biochar could be recycled, and 76.7% of the initial adsorption capacity could be maintained. The retention rate of hydraulic lasting strength of the material is 91.6%, which has high practicability in actual wastewater treatment. Over a wide pH range of 3 to 9; electrostatic attraction, surface precipitation, ligand exchange, and inner sphere complexation are the main mechanisms of phosphate adsorption. Thermodynamic analysis revealed the feasibility and

spontaneity of biochar adsorption. Based on the analysis of approximate spectral energy distribution, high distribution frequency is conducive to efficient phosphorus removal, and metal oxide will introduce more energetic adsorption sites, thus strengthening the interaction between phosphorus and novel biochar. This study provides a new idea for the application of metal oxide-amended formable biochar in the deep phosphorus removal of wastewater, which is of great significance for advancing scientific problems and practical engineering applications.

Based on this, we used the metal oxide amended formable biochar as a microbial carrier, and the phosphorus-accumulating bacteria were attached to the surface of the material through an immobilization process. Studies have found that metal oxide amended formable biochar with microorganisms has a significant removal effect on phosphorus, which is due to the adsorption of biochar containing surface-active groups and the absorption of phosphorus in wastewater by phosphorous-accumulating bacteria, achieving the synergistic effect of reducing phosphorus content.

To further verify the effect of this novel material on the two elements that contribute most directly to the eutrophication of wastewater, we applied it directly to wastewater sources (source-separated urine) with high concentrations of nitrogen and phosphorus. Results showed that the material had an adsorption effect on nitrogen and phosphorus, and the coupling of the composite with a urease inhibitor could further reduce the transformation and volatilization of nitrogen in urine. In addition, this material promoted the maintenance of phosphorus in the dissolved form. The benefits of this effect are that it cannot only lock the nitrogen and phosphorus nutrients in the solution, and improve the large-scale resource utilization of the nitrogen and phosphorus-containing liquid, but also reduce the possibility that the improper treatment may further aggravate the eutrophication of the wastewater. Therefore, we say that our study not only clarifies the basic theory of biochar adsorption but also takes the practical engineering application as an example, which has important guiding significance for future related research.

6.4 Future research and the way forward

The literature review reported on current research trends using bibliometric analysis and identifies recent developments that contribute to the current understanding of biochar

adsorption of pollutants and other emerging contaminants from wastewater. The analysis suggests some potential research and directions for future studies of biochar for pollutant removal from contaminated water.

In fact, the best method to save the eutrophication of the wastewater environment is to "Stop pollution". However, it is impossible in today's climate. What needs to be done is develop the "tools" to speed up the repairing process or recycle nitrogen and phosphorus, then minimize the impacts of pollution using suitable materials.

6.4.1 Scale-up and field-testing considerations for evaluating modified biochar adsorbents

Many low-cost adsorbents have been proposed (Zhang et al., 2022; Pal et al., 2021), but the efficiencies of many sorbents have only been measured in the laboratory (Qiu et al., 2021). Field-level testing and pilot-scale application are required for the implementation of strategies using biochar as an economical adsorbent for field application (Gupta et al., 2022). Subsequently, engineering applications of biochar should be compared to verify adsorption capacity with consideration of costs of recycling and regeneration. Advances in the methodology and equipment used for the preparation of biochar and strategies developed to optimize energy use and reduce emissions during the production process are important priorities of current studies.

6.4.2 Cost and economic feasibility of large-scale production of formable‑biochar materials

According to the author's preliminary investigation, Phoslock, a lanthanum-modified montmorillonite adsorbent developed by CSIRO (Australia), has a high phosphate adsorption capacity of 10 mg P/g (Funes et al., 2021; Spears et al., 2013). This product retails in China with a selling price in the range of 10,000 to 18,000 ¥/ton (2022). The formable LaFe/MB biochar adsorbent detailed in this dissertation demonstrated a phosphorous adsorption capacity that is three times that of Phoslock, and based on preliminary calculations, has production costs of about 6000~8000 ¥/ton. Added costs associated with subsequent large-scale production still need to be calculated. In general, the adsorbent developed in this study was considered to have good market competitiveness in terms of its adsorption capacity and cost-effectiveness.

6.4.3 Key points of future research

Due to natural resource exploitation, economic instability, and poor farming practices, ever-growing constraints are being placed on agriculture. As the demand for chemical fertilizers grows, technologies that seek to provide alternative methods to recover and recycle phosphorus nutrients from sustainable waste streams become increasingly attractive (Vasa et al., 2021). The development of adsorbent materials that play a dual role in mitigating environmental pollution and harvesting nutrients from wastewater, therefore, have an important contribution to make in future studies aimed at reducing pollutant loading and maintaining the fertility and productivity of agricultural soil. This approach is desirable since it integrates sustainable development concepts that link sanitation, water security, human health, and agriculture.

Based on the promising findings of this study, further investigation of formable LaFe/MB granulated biochar material is warranted in future studies. Questions that still need to be addressed include determining its environmental effect, cost analysis, renewability, and life-cycle within 'real-world' wastewater treatment systems. Since this biochar composite material readily adsorbs nitrogen and phosphorus, its suitability as a soil amendment/carbon-based fertilizer needs to be investigated. Its influence on crop growth, soil pore structure, and microbial diversity are all factors that need to be considered. However, the risk level of spent biochar should be fully considered before possible reuse (He et al., 2022). Ultimately, such studies can contribute to Sustainable Development Goals (SDG) 2 (zero hunger; SDG2.3 and SDG2.4) by improvement of soil health for higher crop yield and food security (He et al., 2022). The practical application and feasibility of using formable porous granulated biochar, in terms of potential applications need to be fully explored and systematically evaluated, which is of great significance to the practical application and market promotion of biochar materials.

6.4.4 Future challenges

At present, there are many studies on the application of nano-biochar engineering (Ai et al., 2022; Rajput et al., 2022; Song et al., 2022), however, the negative effects of nanomaterials on the environment remains an area of concern for scientists (Chen et al., 2017; Guggenberger et al., 2008; Wang et al., 2020). Although biochar nanoparticles represent a relatively small proportion of biochar populations, these small biochar particles are active and can leach into

surface waters through runoff, drainage, or irrigation levels, causing negative environmental impacts (Godlewska et al., 2021; He et al., 2022; Zhang et al., 2010). The formable porous granulated biochar prepared in this study demonstrated a high adsorption capacity and good hydraulic load potential (Sun et al., 2022), which suggests its potential as a suitable replacement for nano-adsorption materials. Future studies are required to verify this hypothesis.

References

Ai D, Wei T Q, Meng Y, et al. (2022). Ball milling sulphur-doped nano zero-valent iron @biochar composite for the efficient removal of phosphorus from water: Performance and mechanisms. Bioresource Technology 357: 127316.

Ajiboye T O, Ogunbiyi O D, Omotola E O, et al. (2022). Urine: Useless or useful "waste"?. Results in Engineering 16: 100522.

Cakmak E K, Hartl M, Kisser J, et al. (2022). Phosphorus mining from eutrophic marine environment towards a blue economy: The role of bio-based applications. Water Research 219: 118505.

Chen M, Wang D J, Yang F, et al. (2017). Transport and retention of biochar nanoparticles in a paddy soil under environmentally-relevant solution chemistry conditions. Environmental Pollution 230: 540.

Chen W F, Meng J, Han X R, et al. (2019). Past, present, and future of biochar. Biochar 1: 75.

Cheng N, Wang B, Feng Q W, et al. (2021). Co-adsorption performance and mechanism of nitrogen and phosphorus onto *Eupatorium adenophorum* biochar in water. Bioresource Technology 340: 125696.

Cheng N, Wang B, Wu P, et al. (2021). Adsorption of emerging contaminants from water and wastewater by modified biochar: A review. Environ Pollut 273: 116448.

De-Bashan, L E, Bashan Y, 2004. Recent advances in removing phosphorus from wastewater and its future use as fertilizer (1997-2003). Water Research 38: 4222

Dilshani A, Wijayananda A, Rathnayake M, (2022). Life cycle net energy and global warming impact assessment for hydrogen production via decomposition of ammonia recovered from source-separated human urine. International Journal of Hydrogen Energy 47: 24093.

Fang L P, Liu R, Li J, et al. (2018). Magnetite/Lanthanum hydroxide for phosphate sequestration and recovery from lake and the attenuation effects of sediment particles. Water Research 130: 243.

Funesm A, Álvarez-Manzaneda I, del Arco A, et al. (2021). Evaluating the effect of CFH-12® and Phoslock® on phosphorus dynamics during anoxia and resuspension in shallow eutrophic lakes. Environmental Pollution 269: 11693.

Gilbert N, (2009). The disappearing nutrient. Nature 461: 716.

Godlewska P, Ok Y S, Oleszczuk P, (2021). The dark side of black gold: Ecotoxicological aspects of biochar and biochar-amended soils. Journal of Hazardous Materials 403: 123833.

Guggenberger G, Rodionov A, Shibistova O, et al. (2008). Storage and mobility of black carbon in permafrost soils of the forest tundra ecotone in northern Siberia. Global Change Biology 14: 1367.

Gupta M, Savla N, Pandit C, et al. (2022). Use of biomass-derived biochar in wastewater treatment and power production: A promising solution for a sustainable environment. Science of The Total Environment 825: 153892.

He M J, Xu Z B, Hou D Y, et al. (2022). Waste-derived biochar for water pollution control and sustainable development. Nature Reviews Earth & Environment 3: 444.

He M J, Xu Z B, Sun Y Q, et al. (2021). Critical impacts of pyrolysis conditions and activation methods on application-oriented production of wood waste-derived biochar. Bioresource Technology 341: 125811.

Jiao Y X, Li D Y, Wang M, et al. (2021). A scientometric review of biochar preparation research from 2006 to 2019. Biochar 3: 283.

Kumar M, Xiong X N, Wan Z H, et al. (2020). Ball milling as a mechanochemical technology for fabrication of novel biochar nanomaterials. Bioresource Technology 312: 123613.

Krishnamoorthy N, Paramasivan B, (2022). Evolution of struvite research and the way forward in resource recovery of phosphates through scientometric analysis, Journal of Cleaner Production. doi: https://doi.org/10.1016/j.jclepro.2022.131737.

Liu F, Zhang S N, Luo P, et al. (2018). Purification and reuse of non-point source wastewater via Myriophyllum-based integrative biotechnology: A review. Bioresour Technol 248: 3.

Nancharaiah Y V, Venkata Mohan S, Lens P N L. (2016). Recent advances in nutrient removal and recovery in biological and bioelectrochemical systems. Bioresource Technology 215: 173.

Ngatia L W, Hsieh Y P, Nemours D, et al. (2017). Potential phosphorus eutrophication mitigation strategy: Biochar carbon composition, thermal stability and pH influence phosphorus sorption. Chemosphere 180: 201.

Pal D B, Singh A, Jha J M, et al. (2021). Low-cost biochar adsorbents prepared from date and delonix regia seeds for heavy metal sorption. Bioresource Technology 339: 125606.

Qiu B B, Tao X D, Wang H, et al. (2021). Biochar as a low-cost adsorbent for aqueous heavy metal removal: A review. Journal of Analytical and Applied Pyrolysis 155: 105081.

Rajput V D, Minkina T, Ahmed B, et al. (2022). Nano-biochar: A novel solution for sustainable agriculture and environmental remediation. Environmental Research 210: 112891.

Song B, Cao X W, Gao W R, et al. (2022). Preparation of nano-biochar from conventional biorefineries for high-value applications. Renewable and Sustainable Energy Reviews 157: 112057.

Spears B M, Lürling M, Yasseri S, et al. (2013). Lake responses following lanthanum-modified bentonite clay (Phoslock®) application: An analysis of water column lanthanum data from 16 case study lakes. Water Research 47: 5930.

Sun E H, Zhang Y, Xiao Q B, et al. (2022). Formable porous biochar loaded with La-Fe(hydr)oxides/montmorillonite for efficient removal of phosphorus in wastewater: process and mechanisms. Biochar 4: 53.

Vasa T N, Chacko S P, (2021). Recovery of struvite from wastewaters as an eco-friendly fertilizer: Review of the art and perspective for a sustainable agriculture practice in India. Sustainable Energy Technologies and Assessments 48: 101573.

Wang Y, Bradford S A, Shang J Y, (2020). Release of colloidal biochar during transient chemical conditions: The humic acid effect. Environmental Pollution 260: 114068.

Yang F, Chen Y C, Nan H Y, et al. (2021). Metal chloride-loaded biochar for phosphorus recovery: Noteworthy roles of inherent minerals in precursor. Chemosphere 266: 128991.

Zhang B, Tian S Y, Wu D L, (2023). An integrated strategy for nutrient harvesting from hydrolysed human urine as high-purity products: Tracking of precipitation transformation and precise regulation. Science of The Total Environment 854: 158721.

Zhang M D, He M Z, Chen Q P, et al. (2022). Feasible synthesis of a novel and low-cost seawater-modified biochar and its potential application in phosphate removal/recovery from wastewater. Science of The Total Environment 824: 153833.

Zhang M, Lin K, Li X D, et al. (2022). Removal of phosphate from water by paper mill sludge biochar. Environmental Pollution 293: 118521.

Zhang W, Niu J Z, Morales V L, et al. (2010). Transport and retention of biochar particles in porous media: effect of pH, ionic strength, and particle size. Ecohydrology 3: 497.